Hydrodynamics Modeling to Study the Impacts of Hurricanes without and with NNBFs in the Coastal Region of Mobile Bay

By

Susan Poudel

A thesis submitted to the Graduate Faculty of

Auburn University

in partial fulfillment of the

requirements for the Degree of

Masters of Science

Auburn, Alabama

December 9, 2023

Keywords: Mobile Bay, Hydrodynamics, EFDC+, Hurricane, Flooding, NNBFs.

Approved by

Dr. Xing Fang, Arthur H. Feagin Chair Professor of Civil Engineering, Auburn University

Dr. Jeffrey J. LaMondia, Professor of Civil Engineering, Auburn University

Dr. Luke Marzen, Professor of Geosciences, Auburn University

ABSTRACT

The coastal communities of Mobile Bay, AL, are facing a serious problem of flooding due to storm surges. With the increasing economic and social activities along with the increasing frequency as well as the intensity of the hurricanes, the coastal regions are at greater risk than before. This short- and long-term flooding due to frequent storms, could result in substantial harm to properties and roadways, decline in tourism, increase traffic for both commercial and personal purposes, and negatively impacting the quality of life for the residents. A three-dimensional hydrodynamic model using Environmental Fluid Dynamics Code Plus (EFDC+) was developed to study the impacts of different intensities of Hurricane without and with the implementation of Natural and Nature-Based Features (NNBFS) in the coastal regions of the bay. The external driving forces for the model include the inflows from two major rivers (Mobile River and Tensaw River), atmospheric winds, tropical cyclones, and the harmonics tides or water level at the open boundaries, on the south where flow exchange takes place. Hurricane Ivan (2004) and Hurricane Sally (2020) were used for model calibration and verification. The simulated water surface elevations (WSEL) were compared against the observed data at different monitoring stations within the bay with good agreement (coefficient of determination, $R^2 = 0.96$ and 0.92 between the observed WSEL and the modeled results at Dauphin Island station for 2004 and 2020 respectively). The calibrated EFDC+ model was used to study the response of the bay under two different hurricane scenarios, one was based on the storm events with seven different return period, provided by Hazus application, and another was based on hypothetical worst-case approach with three different hurricane track directions.

The northern coastal area in Baldwin County sits at relatively higher elevation as compared to the other coastal regions in Mobile and Baldwin Counties which is why this was the least impacted region for all the scenarios. Hurricanes were modeled in such a way that the peak windspeed was achieved along the top half of the bay, which was the reason low lying northern coastal region of Mobile County was mostly flooded for all major hurricanes (Categories 3 and above). For Hurricane categories 2 and below, the flooding occurred along the track of the hurricanes whereas for major hurricanes (Categories 3 and above), the flooding occurred along the path as well as other low-lying areas away from the track. The area near the Mobile regional airport, which was the most impacted region in different scenario runs, was selected to test different NNBFs:

Vegetations with three different plant densities (#/m^2), Artificial Reefs modeled as partially blocking fixed masks, Artificial Sand Dunes modeled by increasing the bottom elevation, and also artificial sand dunes with vegetation. One storm event from each modeling scenario was used for the evaluation of the NNBFs – 100-year storm event from modeling scenario 1 and category 4 hurricane moving North from modeling scenario 2. Both of these storm events fall under the category of major hurricanes. Four different parameters: water depth, velocity, flow, and bed shear, were compared before and after the implementation of NNBFs. Among the three different NNBFs, the results for all four parameters were similar without and with the use of artificial reefs modeled as masks. Also, the water depths, before and after the implementation of vegetation, were almost similar for all three plant densities. However, there was reduction in velocity, flow, and bed shear after the installation of vegetation with increasing plant density. The installation of artificial sand dunes provided greater reduction in water depths, velocities, flows, and bed shear as compared to other tested NNBFs. The results were even better for the combined use of sand dunes along with the vegetations.

This study compared the impact of hurricane events with different tracks and intensities to identify the vulnerable regions, in terms of flooding, on the coastal areas of the Mobile Bay. The coastal region of the Daphne-Fairhope cities of Baldwin County is at the least risk of flooding being at higher elevations. All other coastal areas are at relatively lower elevations which are vulnerable to flooding from extreme events depending on the storm track and intensity. The NNBFs test results showed the ability of different NNBFs to reduce storm impacts. Among the three tested NNBFs, construction of artificial sand dunes was seen to be much more effective, and the use of combination of NNBFs such as sand dunes with high density vegetations was even more effective at reducing the storm impacts.

ACKNOWLEDGEMENT

The author would like to express special gratitude to the academic advisor, Professor Dr. Xing Fang for the devotion, guidance, mentorship, and support provided throughout this research. The amount of work and professionalism he showed during this time will always be carried as motivation in any future work. The author would also like to thank Prof. Dr. Jeffrey LaMondia for the time and supervision he provided during the whole course of the project. The author would like to thank Prof. Dr. Luke Marzen for the knowledge the author gained about Geographical Information System which was utilized in the course of the project. The author would also like to thank the Mississippi-Alabama Sea Grant Consortium (MASGC) who funded the project and fellow research group members who put in their precious time for suggestions and feedback.

The author would like to especially thank his parents Bishnu Prasad Poudel and Devaki Poudel, his sister Sumpa Poudel, and brother-in-law Sunder Adhikari who through love, hard work, and a lot of sacrifices provided the author support throughout his educational endeavor.

Finally, the author would like to thank Auburn University and the Department of Civil Engineering for providing the author an opportunity to pursue Master's in Water Resources Engineering with financial support and an assistantship opportunity.

Table of Contents

LIST OF FIGURES

LIST OF TABLES

CHAPTER 1. INTRODUCTION

1.1 BACKGROUND

A storm surge is a rapid and unusual rise in sea level that occurs during storm events like hurricanes. The changes in atmospheric pressure, strong winds, and low-pressure center of a storm are the major factors causing the storm surge (Ji, 2008). During the storm events, the low atmospheric pressure causes the sea level to be higher (~1 cm/millibar) because of the "inverse barometer effect" (Ji, 2008) and the strong wind pushes the water towards the shore, flooding the coastal regions. In the event of a severe storm, the combined effect of storm surge, wind waves, and tides, can cause disastrous damage hundreds of meters inland from the coast, where buildings and roadways may be entirely flooded or even completely destroyed (Darayi et al., 2019; Ji, 2008; Smith et al., 2016). This is getting a serious problem as the frequency as well as the intensity of a tropical storms are projected to significantly increase due to climate change in near future (Knutson et al., 2010; Sweet et al., 2018; Webster et al., 2005; Woodruff et al., 2013). A study conducted on the city of Corpus Christi, Texas, to analyze the potential impact of climate change on hurricane flooding inundation, people affected, and economic damages indicated a destructive consequences even for the relatively short time frame of 80 years (Frey et al., 2010). Although the storm surges are temporary, the damage it causes to coastal communities and businesses are devastating, thus there is a strong need for focusing on the sustainable eco-friendly solutions to preserve and protect coastal communities and ecosystem.

Floodings are one of the costliest and most destructive natural calamities all around the world killing many lives and causing massive economic losses (Bhusal et al., 2022; Parajuli et al., 2023). Coastal communities, all around the world, are always at the serious risk of flooding due to storm surges. According to the National Oceanic and Atmospheric Administration (NOAA) Office for Coastal Management, 40 percent of US population lives in coastal counties which is only 10 percent of nation's land excluding Alaska. Population density in coastal areas is around 461 people per square mile whereas the nation's population density is 87 people per square mile. As the human population living in low lying coastal regions is increasing, due to economic development and population growth, the probability of damage and economic loss by the flooding is also increasing

(Abdelhafez et al., 2021; Bouwer, 2019). The coastal region of Alabama is also facing a similar situation.

1.2 STUDY AREA

Mobile Bay, shown in Figure 1.1, is a large estuary situated in the southwest part of the state of Alabama. It is bordered by the Mobile County (East) and Baldwin County (East). Mobile River and Tensaw River are the two major rivers that flow into the bay from the north. Many other small rivers also flow into the bay such as Dog River, Fowl River, and Deer River on the western side, and Fish River on the eastern side. Mobile Bay is the fourth largest estuary in the US in terms of streamflow with an outflow of 62,000 cubic feet (1,800 cu. m) of water per second (Wikipedia contributors, 2023a). On the southern end, it is connected to the Gulf of Mexico by an opening formed by Fort Morgan (on the east) and Dauphin Island (on the west).

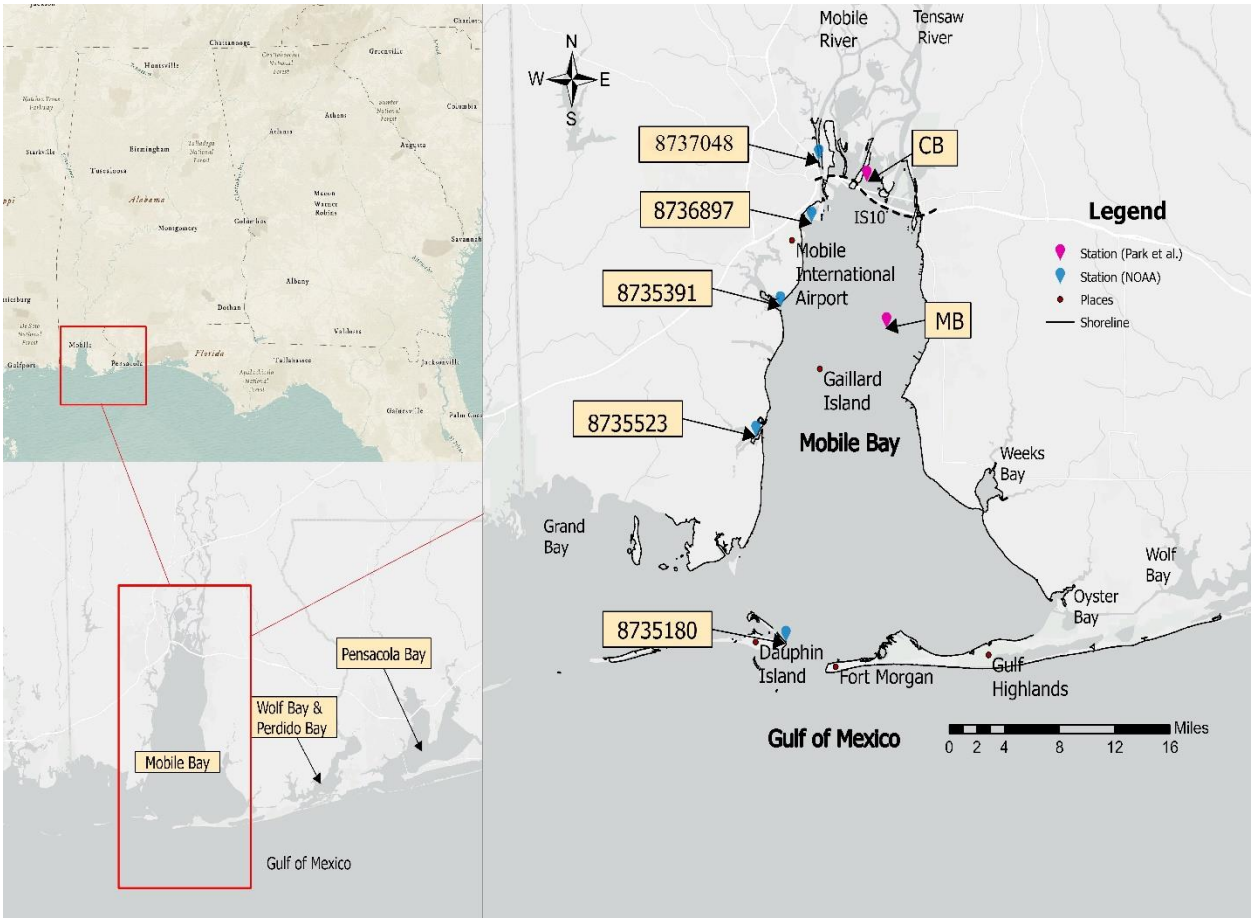

Figure 1.1 Geographic location of Mobile Bay with different monitoring stations (ArcGIS Pro)

Mobile Bay covers an area of around 413 square miles (1070 sq. km) with a length of around 31 miles (50 km) (Wikipedia contributors, 2023a). The width of the bay varies from 8 miles (13 km) at the narrowest point to a maximum width of 24 miles (39 km) near the outlet to the Gulf of Mexico (Misachi, 2021; Wikipedia contributors, 2023a). This bay is connected to the Gulf of Mexico by a narrow shipping channel known as Mobile Ship Channel, which is the deepest part of the bay with a depth of over 75 feet (23 m) (Misachi, 2021). Overall, the average depth of this bay is 10 feet (3 m) (Misachi, 2021).

The major urban area in Mobile and Baldwin Counties are shown in Figure 1.2. With the economic growth and tourism popularity in the coastal counties of Mobile Bay, a large number of populations are attracted to this area. Not only people are migrating to live but also people are travelling to spend their vacations in these coastal communities. From the landcover classification shown in Figure 1.3, it can be seen that medium to high intensity development are along the coastal areas of Mobile city, Dauphin Island, nearby Fort Morgan, and coastal areas of Daphne-Fairhope city. According to the U.S. Census, between the years of 1990 and 2007 Baldwin County experienced a 75% increase in its population, from 98,280, to 171,769. In Mobile County there was a smaller increase of seven percent, from 378,643 to 404,406. It is estimated that by 2025 the combined coastal population of Alabama will exceed 690,000 people, representing a 76.9% increase for Baldwin County and a 10.9% increase for Mobile County (Barnes et al., 2008).

City of Mobile, one of the oldest and largest cities in Alabama, is a major city of this area having great historical significance and many historical sites serving as a tourist attraction. It serves as a major port city on the Gulf Coast and is also home to Mobile International Airport. Even though, the average elevation of this city is 200 ft (61 m) MSL, which is above average for the coastal region of Gulf of Mexico, the average elevation of the downtown region is only around 3 ft (1 m) (Ellis et al., 2011). The coastal region of the Daphne-Fairhope cities in Baldwin County sits at relatively higher elevation, as compared to the coastal region of Mobile city, making these areas relatively less vulnerable to coastal flooding. The Road networks in the coastal regions of Mobile and Baldwin Counties are shown in Figure 1.4. Low lying coastal highways such as Dauphin Island Pkwy 193, Fort Morgan Road, and Scenic Highway 98 are at greater risk of flooding due to storm surge.

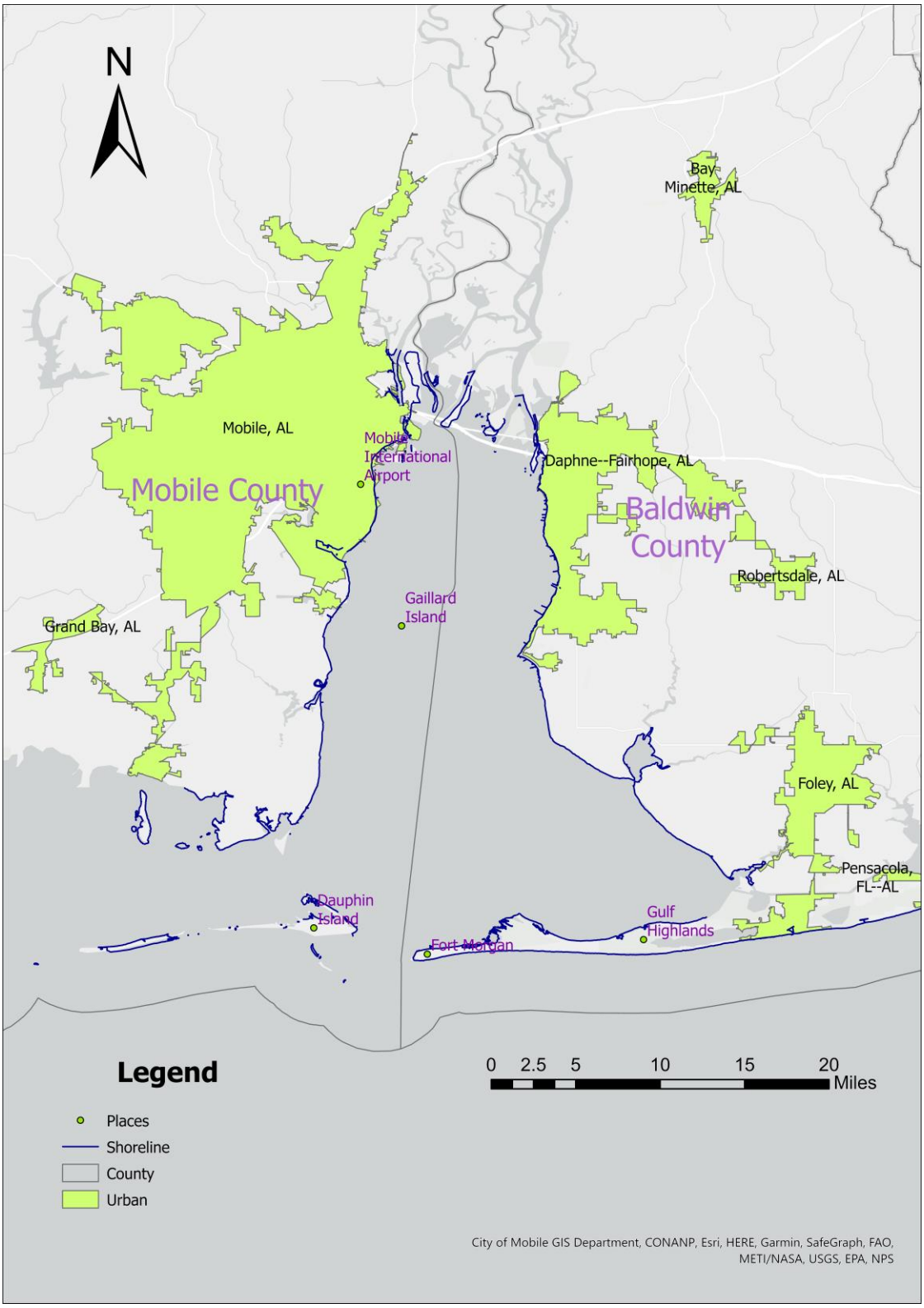

Figure 1.2 Urban areas in Mobile and Baldwin Counties (TIGER line data)

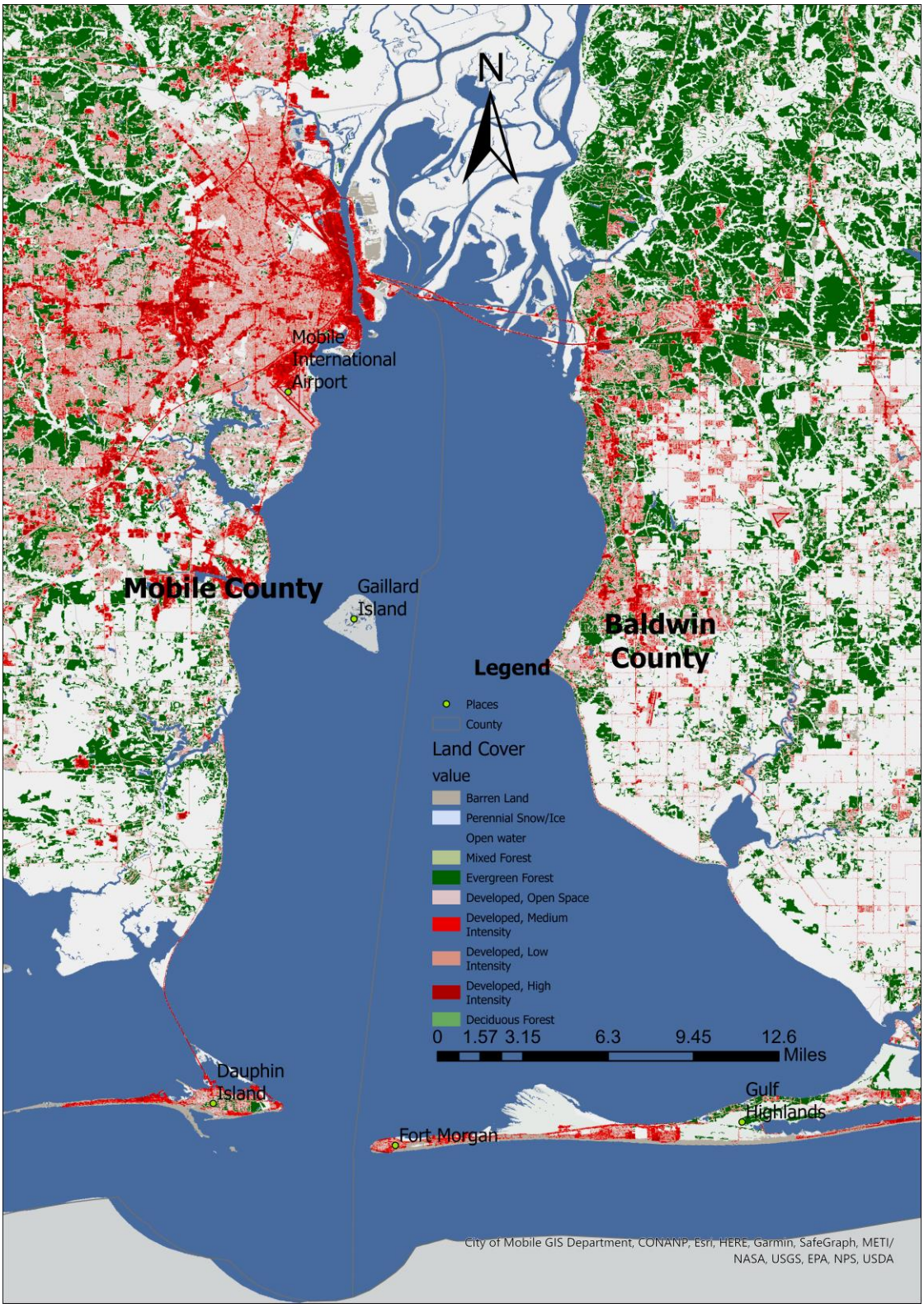

Figure 1.3 Landcover Classification of Mobile Bay region (USGS)

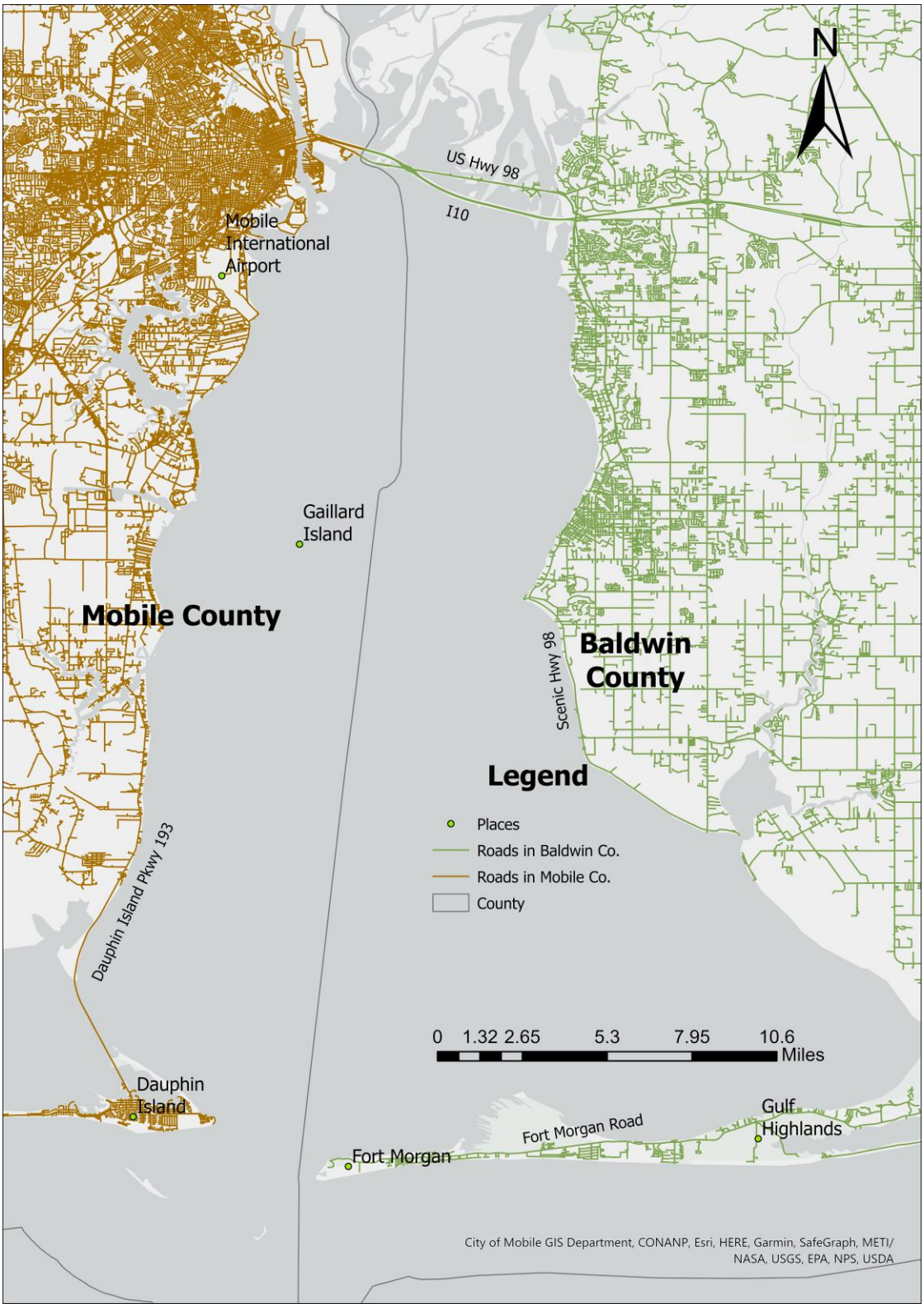

Figure 1.4 Road networks in Mobile and Baldwin Counties (TIGER line data)

1.3 SCOPE AND OBJECTIVES

The coastal region of the Mobile Bay is facing a problem of significant property and roadway damage, lost tourism and other economic loss, traffic congestion, and reduction in quality of life due to the flooding caused by storm events such as hurricanes. Implementation of Natural and Nature-based Features (NNBFs) which is a sustainable and eco-friendly means of absorbing and adapting to floodings is necessary to preserve the coastal communities. To make the coastal communities more resilient against flooding due to storm surge, more detailed flooding models and data are required. This study is conducted to develop a high-resolution hydrodynamic numerical simulation model to study the ability of NNBFs to reduce the impacts of flooding due to storm surge. This is not a laboratory experimental study or field data collection/measurements to study NNBF's capabilities to reduce the flooding impacts.

The simulation model used for the study is Environmental Fluid Dynamics Code (EFDC)."EFDC is a state-of-the-art hydrodynamic model that can be used to simulate aquatic systems in one, two, and three dimensions" (Environmental Fluid Dynamics Code (EFDC) | US EPA, 2023). EFDC is widely used surface water quality modeling system which is capable of modeling hydrodynamic, sediment-contaminant, and eutrophication components of a water body (Environmental Fluid Dynamics Code (EFDC) | US EPA, 2023). EFDC+, developed by DSI, is an enhanced and improved version of the original EFDC with increased performance, stability and accuracy (DSI LLC., 2023).

The objective of this study is to develop, calibrate, and apply a three-dimensional EFDC+ model for Mobile Bay to simulate and determine the flooding potential of its coastal shorelines under various hurricane scenarios without and with NNBFs implemented in proposed shoreline areas. The primary tasks to achieve the objective are given below:

1. To develop a curvilinear grid for the Mobile Bay EFDC+ model in such a way that the grid cells are finer along the coastal regions as the major focus of this study is coastal shoreline areas.
2. Acquisition of bathymetry data of Mobile Bay as well as the elevation data of the coastal landscape.

3. To develop a hydrodynamic model using EFDC+ to determine the flooding areas along the Mobile Bay shorelines due to hurricanes.
4. To calibrate and validate the EFDC+ model using water level data of historical hurricane events.
5. To use the EFDC+ model to run different hypothetical hurricane scenarios to identify the flooding areas with major impacts under different hurricane scenarios.
6. To apply/propose different NNBFs, to the areas identified in task #5, to study the ability of NNBFs in mitigating flooding in coastal areas.

1.4 THESIS ORGANIZATION

This thesis is organized into five different chapters. Chapter one covers the background, study area, scope and objectives, and thesis organization. Chapter two is the literature review which provides information about the hurricanes and their impacts, information on different types of NNBFs, and information about SLOSH model that NOAA uses to the flood inundation maps in coastal areas in USA.

Chapter 3 covers the Mobile Bay EFDC model development which gives information on hydrodynamics, governing equations, initial and boundary conditions, vertical layering approaches, grid development, bathymetry development, and input data, along with the EFDC+ model calibration and verification using the data from two hurricane events in 2004 and 2020.

Chapter four covers the modeling scenarios and results which provides information on two different scenario methods that are adopted in this study. This chapter provides the results and discussion of modeling scenarios, NNBFs tests, slow- and fast-moving hurricanes, and comparison with similar studies. Finally, chapter five contains the summary, conclusions, limitations for this study, and scope for future studies.

CHAPTER 2. LITERATURE REVIEW

2.1 INTRODUCTION

Mobile Bay has great ecological and economic importance but is currently facing higher urbanization rates and unpredicted effects due to climate change (Ellis et al., 2011). Urbanization generally increases impervious areas, reduces rainfall loss, and increases surface runoff. This rapid urbanization is making the low-lying coastal communities more vulnerable to flooding due to gentle land slopes which reduces runoff velocity during storm events. There have been large numbers of studies and investigations going on the US Gulf shore's sustainability, particularly following the significant hurricane landfalls in 2004 (Ivan), 2005 (Dennis, Katrina, and Rita), and 2008 (Gustav and Ike) as such Hurricanes have caused severe impacts to the coastal communities (Ellis et al., 2011).

2.2 ATLANTIC HURRICANE

Atlantic hurricanes are powerful tropical cyclones, that occurs in the Atlantic basin (Atlantic Ocean, Caribbean Sea, and Gulf of Mexico), characterized by low-pressure center, strong winds and heavy rainfall (Wikipedia contributors, 2023c). Due to the complex nature of tropical cyclones, they are very difficult to completely describe and predict, and researchers are focusing on developing and applying various modeling approaches to study the storm induced coastal flooding (Bates et al., 2005; Cheung et al., 2003; Sheng et al., 2010; Woodruff et al., 2013). According to National Hurricane Center (NHC), tropical storms have maximum sustained wind speed of 39 mph to 73 mph whereas hurricanes are characterized as tropical cyclones with maximum sustained wind speed of 74 mph or higher (*Tropical Cyclone Climatology*, n.d.). The impact of a hurricane can be devastating, causing widespread damage to structures and roadways, flooding from storm surges, traffic congestion, reduction in quality of life, and disruption of essential services making them the most dangerous and costliest natural calamities (Adhikari et al., 2021; Darayi et al., 2019; Emanuel, 2005). Preparedness, early warning systems, and evacuation plans are critical in reducing the potential loss of life and property during a hurricane. As coastal population is increasing with the increase in economic activities and coastal infrastructure, there has been a substantial increase in the economic damage in these areas (Bouwer, 2019; Emanuel, 2005; T. R. Knutson et al., 2010). In the period of 1900 to 2017, the United States was hit by around 197

hurricanes resulting in an economic damage of around US$2 trillion in normalized (2018) damage (Weinkle et al., 2018). According to NOAA Office for Coastal Management, of the 310-billion-dollar weather disasters between 1980 and 2021, hurricanes have caused the most damage: over $1.1 trillion total. In 2021 alone, hurricane damage costs were almost $79 billion.

According to the NHC, the Atlantic hurricane season runs from June 1 to November 30 as shown in Figure 2.1, which shows the peak of the Atlantic hurricane season to fall around mid-September (*Tropical Cyclone Climatology*, n.d.).

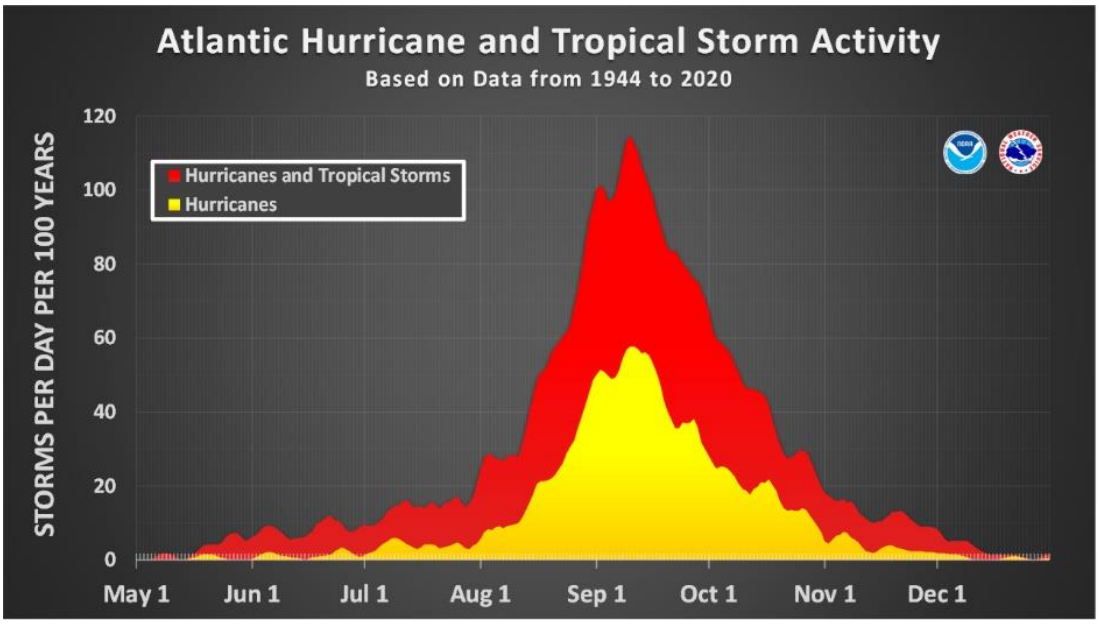

Figure 2.1 Atlantic hurricane seasonal activity based on data from 1944 to 2020 (*Tropical Cyclone Climatology*, n.d.)

The hurricanes are categorized into 5 categories (Category 5 being the strongest) based on the Saffir-Simpson Hurricane Wind Scale as shown in Table 2.1.This scale uses hurricane's maximum sustained wind speed to measure the strength of a hurricane and it does not consider other hazards like storm surge, rainfall flooding, and tornadoes. This wind scale classifies hurricane category 3 and higher as a major hurricane and it also provides information regarding the potential property damage due to different categories of hurricanes. The damage due to a hurricane depends on various other factors such as translation speed or the landfall location. The study conducted within the Tampa Bay indicated that slow moving hurricanes produce larger surges than a fast moving hurricane (Weisberg & Zheng, 2006). The slower moving storms have extended duration of wind

forcing acting on the surface increasing the peak surge while faster moving storms produce lower surge due to relatively short life span (Zhong et al., 2010). Peck et al. (2020) also concluded that slower moving hurricanes have longer duration of strong winds acting on the water surface which makes the storm surge stronger.

Table 2.1 Saffir-Simpson hurricane wind scale (*Saffir-Simpson Hurricane Wind Scale*, n.d.)

Category	Sustained Winds	Types of Damage Due to Hurricane Winds
1	33-42 m/s 74-95 mph 64-82 kt 119-153 km/h	**Very dangerous winds will produce some damage:** Well-constructed frame homes could have damage to roof, shingles, vinyl siding and gutters. Large branches of trees will snap, and shallowly rooted trees may be toppled. Extensive damage to power lines and poles likely will result in power outages that could last a few to several days.
2	43-49 m/s 96-110 mph 83-95 kt 154-177 km/h	**Extremely dangerous winds will cause extensive damage:** Well-constructed frame homes could sustain major roof and siding damage. Many shallowly rooted trees will be snapped or uprooted and block numerous roads. Near-total power loss is expected with outages that could last from several days to weeks.
3 (major)	50-57 m/s 111-129 mph 96-112 kt 178-208 km/h	**Devastating damage will occur:** Well-built framed homes may incur major damage or removal of roof decking and gable ends. Many trees will be snapped or uprooted, blocking numerous roads. Electricity and water will be unavailable for several days to weeks after the storm passes.
4 (major)	58-69 m/s 130-156 mph 113-136 kt 209-251 km/h	**Catastrophic damage will occur:** Well-built framed homes can sustain severe damage with the loss of most of the roof structure and/or some exterior walls. Most trees will be snapped or uprooted, and power poles downed. Fallen trees and power poles will isolate residential areas. Power outages will last weeks to possibly months. Most of the area will be uninhabitable for weeks or months.
5 (major)	70 m/s or higher 157 mph or higher 137 kt or higher 252 km/h or higher	**Catastrophic damage will occur:** A high percentage of framed homes will be destroyed, with total roof failure and wall collapse. Fallen trees and power poles will isolate residential areas. Power outages will last for weeks to possibly months. Most of the area will be uninhabitable for weeks or months.

Mobile Bay is susceptible to hurricanes and tropical storms. This region experienced the greatest effects by Hurricane Frederic, Hurricane Ivan, Hurricane Katrina, and Hurricane Sally in the last 50 years(Berg & Brad, 2021; Q. Chen et al., 2008; Ellis et al., 2011; Parker, 1979; Stewart, 2011). Hurricane Frederic was a category 3 hurricane which made landfall at Dauphin Island on 13th

September 1979 (Ellis et al., 2011). Hurricane Ivan was a Category 3 hurricane which made landfall near Gulf Shores, AL on 16th September 2004 (Sheng et al., 2010). Hurricane Katrina was a category 4 hurricane which made the landfall near Alabama-Mississippi (AL-MS) border on 29th August 2005 with highest storm surge of 11.5 ft (3.5 m) at the Mobile State Docks (Ellis et al., 2011). Hurricane Sally was a Category 2 hurricane which made landfall on 16th September 2020 along the Gulf Shores, AL (Berg & Brad, 2021). Storm surge of 10 to 15 ft (Stewart, 2011) could be seen on the coast of Mobile region during the Hurricane Ivan with an estimated damage of around 14 billion US dollars (NOAA's National Weather Service, n.d.).A complex pattern of storm surge flooding was observed during hurricane Sally rainfall with an estimated damage of around 7.3 billion USD (Berg & Brad, 2021). Hurricane Ivan and Hurricane Sally are used for model calibration and verification in this study as the landfall location of these hurricanes is closest to the Mobile Bay. The track for Hurricane Ivan and Hurricane Sally is shown in Figure 2.2 and Figure 2.3, respectively.

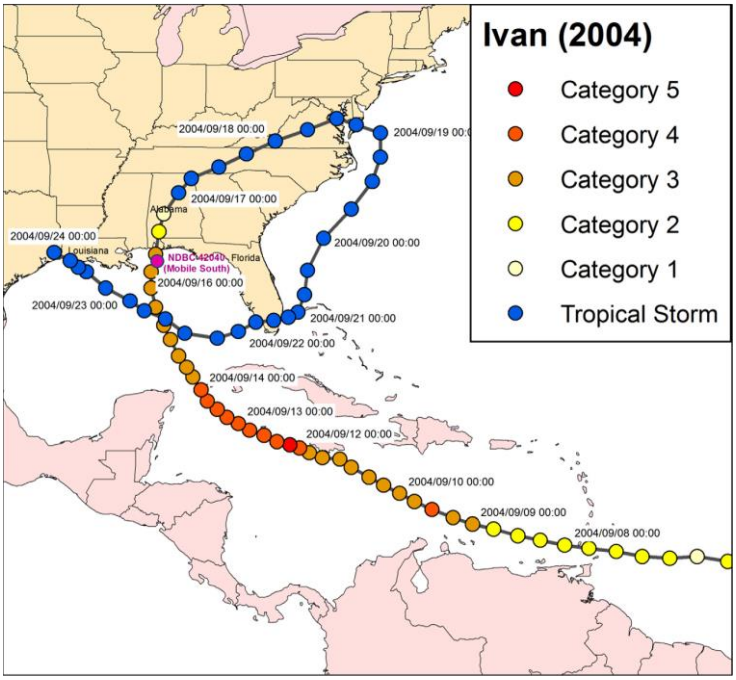

Figure 2.2 Hurricane Ivan track with its intensity, 8-24 September 2004 (NHC) (Sheng et al., 2010)

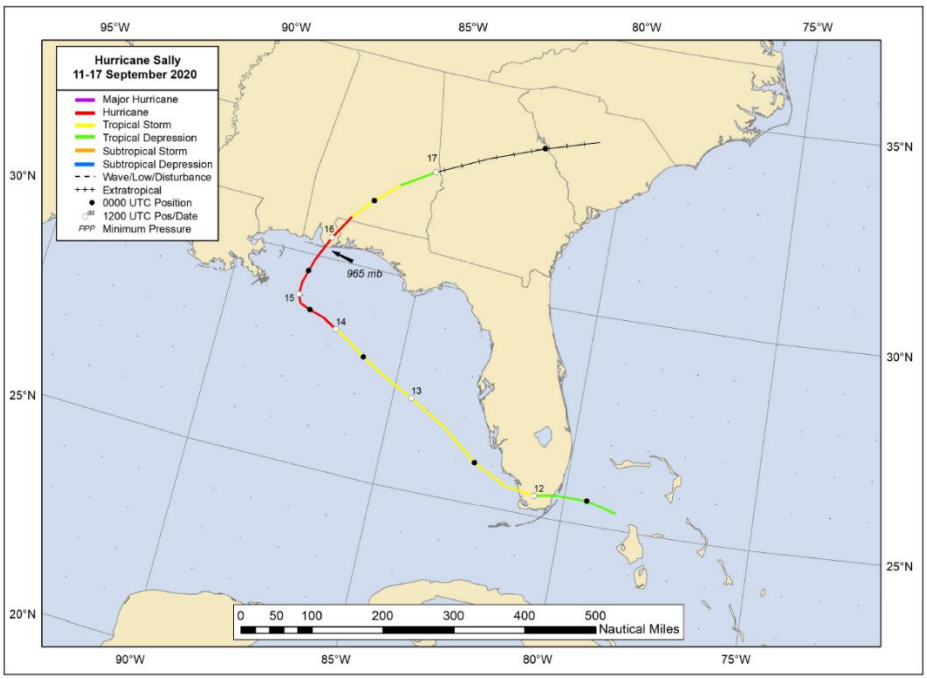

Figure 2.3 Hurricane Sally track with its intensity, 11-17 September 2020 (NHC)

2.3 NATURAL AND NATURE-BASED FEATURES (NNBFS)

The method of protecting the coastal communities from flooding, due to storm events and sea level rise, is generally approached from a conventional engineering point of view which has resulted in negative ecological impacts on surrounding ecosystems (Bilkovic & Mitchell, 2013; Borsje et al., 2011). Traditional engineering solutions, hard concrete structures like sea walls and embankments, can cause various ecological side effects and requires frequent maintenance as well (Temmerman et al., 2013). For example, the Dutch flood defense system are expected to cost €1.6 billion per year and have caused erosion of tidal habitats and occurrence of toxic algal blooms killing aquatic life (Temmerman et al., 2013). These traditional engineering solutions to the coastal flooding are inefficient, unsustainable, and expensive to install and maintain (Temmerman et al., 2013). Therefore, an ecosystem-based practice, which is more sustainable, efficient, and cost-effective approach, is gaining popularity, all over the world, in preserving the coast against the increasing risk of flooding due to storm surges and sea level rise as a substitute traditional engineering approaches (Schrass & Mehta, 2017; Temmerman et al., 2013). This eco-friendly and green engineering practice has given rise to the concepts of Natural and Nature-Based Features (NNBFs) which is beneficial to both environment and human society. The comparison of conventional coastal engineering and eco-system based coastal defence systems for an estuary, delta or lagoon

is shown in Figure 2.4. It can be seen that conventional solution has caused increased surge heights in the land and increased land subsidence whereas ecosystem-based coastal defence system is able to reduce the surge heights and simulate wetland sedimentation resulting in wetland creation (Temmerman et al., 2013).

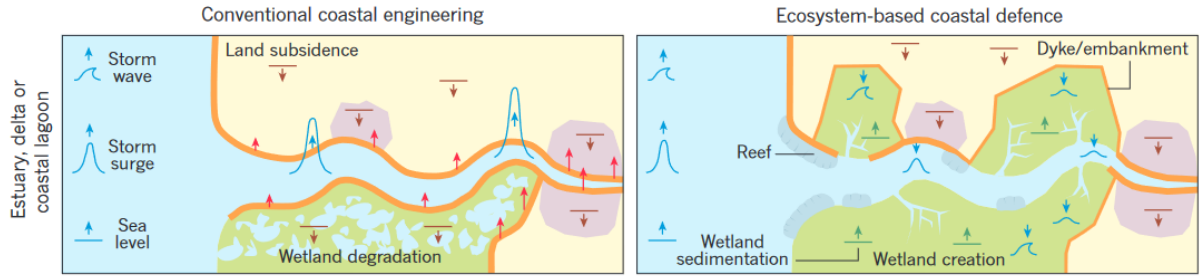

Figure 2.4 Conventional (left) and ecosystem based (right) coastal engineering for estuary, delta or lagoon. Blue arrows indicate an increase or decrease in storm waves intensity and red arrows indicate the need for maintenance. Brown arrows indicate land subsidence (sinking), and green arrows indicate wetland sedimentation (Temmerman et al., 2013).

Natural features (NF) are those features that are occurring naturally and they evolve over time whereas Nature-based features (NBF) are man-made features that mimic the natural conditions (Bridges et al., 2015). Collectively, these features are known as NNBFs. NNBFs are one of the most environmentally friendly and sustainable means of reducing the impact of flooding in coastal regions and also increasing the coastal resilience along with habitat restoration (Palinkas et al., 2022; Sutton-Grier et al., 2015).

Increasing risk of coastal communities to coastal flooding and shoreline erosion from storms and hurricanes have made the coastal engineers to incorporate more sustainable NNBFs to protect and preserve coastal regions (Palinkas et al., 2022; Schrass & Mehta, 2017). NNBF projects go above and beyond coastal restoration as they protect the coastal communities from storms, flooding, and erosion in addition to various other natural benefits such as habitats restoration (Palinkas et al., 2022). The Living Breakwaters project of New York Harbor consisting of around 2500 ft (760 m) of nearshore breakwaters (partially submerged rubble-mound structures) provides wave attenuation, protecting buildings and other infrastructure, along with strengthening the shoreline from erosion enhancing the beach width (Palinkas et al., 2022). The Coastal Texas Protection and Restoration project in the Gulf of Mexico (Texas coast, from the Sabine River to the Rio Grande

River) is using the strategy of multiple line of defense to achieve its goal, which includes restored beach and dune systems (nature-based system) along with a gate system (structural system) to minimize the storm surge impacts along with enhancing the coastal communities and ecosystems (Palinkas et al., 2022). Coastal regions has a great significance from an environmental and socio-economic perspective, which is why NNBFs are getting lots of attention for the coastal protection against storm surges (Smith et al., 2016) due to its eco-friendly and sustainable nature.

2.3.1 ARTIFICIAL REEFS

The Nature Conservancy in Alabama has been implementing various projects to protect and preserve the coast of Mobile Bay through living shoreline, one type of NNBFs. These projects are using the concept of nature-based features where they install different kinds living shoreline such as bagged shells, vegetation, reef blocks, etc. as shown in Figure 2.5. The artificial reefs made of concrete help to withstand the high energy tides and plantation of vegetation along the coast helps to stabilize the shoreline. The Nature Conservancy (TNC) has installed and tested different kinds of living shoreline at different locations as shown in Figure 2.6 (Top). Table 2.2 provides some information regarding the living shoreline projects in Mobile Bay by TNC. They regularly monitor the projects that have been implemented to keep track of progress as well as to understand the effectiveness of different kinds of living shorelines. Figure 2.6 (bottom) shows the progression photos of using living shoreline to retrofit the existing bulkhead with gabion baskets at location C. In this project, TNC coordinated with the private landowner on Fowl River to implement the use of living shoreline to restore the near shore marsh habitat and preserve the ecosystem from bulkheads installation.

Figure 2.5 Precast concrete reefs (left) and bagged shells (right) (TNC, 2023).

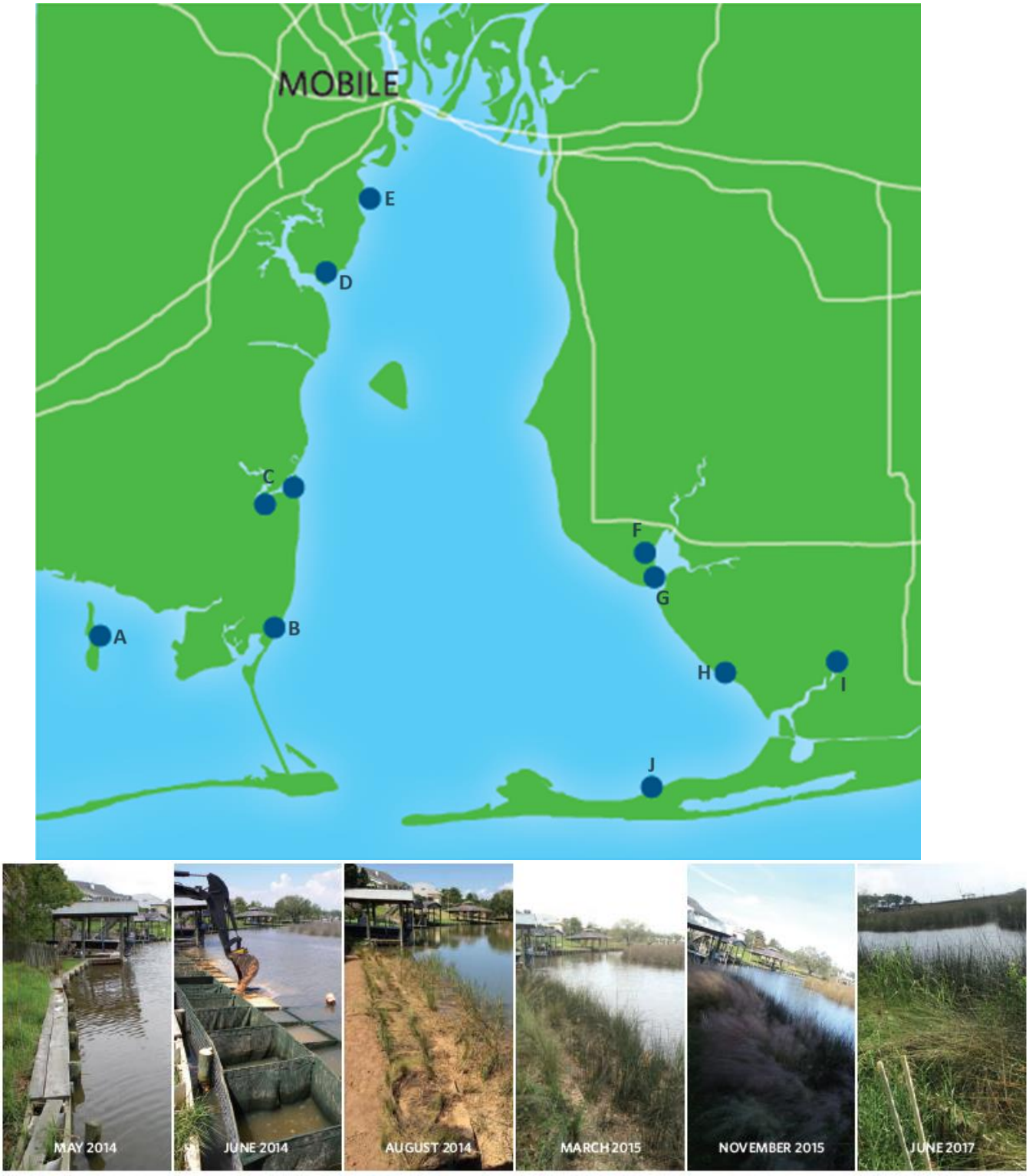

Figure 2.6 Project locations (Top) and progression photos of a living shoreline at location C in Mobile Bay (Bottom) (TNC, 2023)

Table 2.2 Living shorelines projects at various locations by TNC in Mobile Bay (TNC, 2023).

Location	Project	Description
A	Coffee Island	Constructed in 2010 36% improved shoreline protection 1968 Reef Balls, 100,000 Bags of shells, 325 Reef Blocks
B	Alabama Port	Constructed in 2011 32% improved shoreline protection 984 Reef Balls, 50,000 Bags of Shells, 164 Reef Blocks
C	Fowl River Private Shorelines	Constructed in 2014 240 ft of shoreline protected 550 Plants Planted, 0.4 acres of Marsh Restored
D	Helen Wood Park	Constructed in 2011 43% improved shoreline protection 343 Reef Balls, 23,000 Bags of Shells, 12 Reefs
E	Arlington Cove	Constructed in 2015 938 ft of shoreline protected 2,375 Oyster Castles, 36 Marsh Plants, 5 Reefs
F	The Beckwith Camp	Constructed in 2014 2% improved shoreline protection 1,265 Oyster Castles, 36 Marsh Plants, 23 Reefs
G	Pelican Point	Constructed in 2013 99% improved shoreline protection 14,000 Oyster Castles, 150 Marsh Plants, 4 Reefs
H	The Swift Tract	Constructed in 2012 21% improved shoreline protection 1,772 yards Gabion Stone, 172 yards of Shells, 5 Reefs
I	Taylor’s Riverview Park	Constructed in 2014 13% improved shoreline protection 1,922 Oyster Castles, 800 Marsh Plants, 41 Reefs
J	Fort Morgan Private Shorelines	Constructed in 2012 63% improved shoreline protection 162 yards of Shells, 650 yards Rip-Rap Rock 364 Marsh Plants, 11 Reefs

2.3.2 COASTAL VEGETATION

Coastal vegetation are one of the sustainable coastal protection measures, which acts as a buffer zone against severe storm events protecting coastal communities and coastal ecosystems (Athikalam & Karur Vaideeswaran, 2022). In addition to protection against the waves and wind (Mei et al., 2011), coastal vegetation provides many more benefits to the coastal ecosystem such as providing foods and livelihoods for coastal communities as well as providing the habitat for coastal animals and plants (Athikalam & Karur Vaideeswaran, 2022). As the wave approaches the coastal vegetation, the wave energy gets dissipated due to the obstruction created by vegetation (Jadhav et al., 2013). And the coastal vegetation specifically seagrasses are able to withstand strong forces of hurricanes, hence seagrasses are one of the sustainable solution against hurricanes (Byron & Heck, 2006).

- **Spartina alterniflora**

Spartina Alterniflora (shown in Figure 2.7), which is the dominant plant species found along the Gulf Coast, is known to attenuate wave energy (Knutson et al., 1982). Numerous studies have been conducted all over the world to study the ability of Spartina Alterniflora to reduce wave energy. The various laboratory experiments conducted showed the beneficial properties of Spartina Alterniflora to attenuate wave energy (Knutson et al., 1982; Zhao et al., 2023), which was also observed in field experiments conducted in 1981 (Knutson et al., 1982). The study conducted by Zhang et al. (2020), has compared traditional rigid cylinder vegetation against the flexible vegetation on wave damping by using a different drag coefficient approach. This new approach could be applied over wide variety of plant properties along with large range of wave conditions, hence provided better prediction on the drag and wave damping (Zhang et al., 2020). The biomechanical properties of Spartina alterniflora such as dimensions, flexibility, and bending strength were used to test the newly developed vegetation capabilities of Cross-SHORE (CSHORE) program (Chen et al., 2022; Ding et al., 2022). The validation of the model results with laboratory experiments indicated the ability of CSHORE to assess vegetation effectiveness against surges (Chen et al., 2022; Ding et al., 2022). Some of the properties of Spartina Alterniflora, that has been used in different study are mentioned in the Table 2.3.

Table 2.3 Properties of Spartina Alterniflora based on different sources.

Species	Plant Density (#/m^2)	Stem Diameter (cm)	Stem Height (cm)	Source
Spartina Alterniflora	**330 ± 10**	**0.52 ± 0.2**	**84 ± 63**	**(Ysebaert et al., 2011)**
Spartina Alterniflora	346.00	0.62	41.00	(P. L. Knutson et al., 1982)
Spartina Alterniflora	173.00	0.93 ± 0.06	91 ± 10	(Zhang et al., 2020)

Figure 2.7 Spartina Alterniflora (Wikipedia contributors, 2023b)

2.3.3 COASTAL SAND DUNES

Coastal topography, landscape features, and vegetation have been known to attenuate the storm's wave energy as they act as a physical barrier creating resistance for the waves (Wamsley et al., 2009). Coastal sand dunes are the elevated lands, shown in Figure 2.8, which plays a vital role in protecting and preserving the coastal ecosystem as it acts as a barrier against storm surges, wave attack, and erosion while serving as a natural environment for plants and animals (Sigren et al., 2014). Coastal sand dunes occupy relatively small but highly active zone and are very effective in reducing the damage caused by severe storms as it provides resistance for the storm surges and

waves (Sigren et al., 2014; Wamsley et al., 2009). Coastal sand dunes provides a physical buffer attenuating the wave energy and protecting the coast from direct impact of the storm unlike other hard shoreline stabilization structures (seawalls, rock revetments, etc.) reflecting the waves onto nearby beaches or neighboring properties (StormSmart Coasts Program CZM, 2013). The length, height, and width of a dune is determined based on the protection required against the predicted storm activity in the area (StormSmart Coasts Program CZM, 2013).

Figure 2.8 Coastal sand dunes in Mobile Bay, AL.

There was a study conducted, in south of Portugal, to examine the benefits of artificial construction of dunes by increasing the height of an existing sand dunes (from 2.5 meters to around 3.5–5.5 meters above MSL) (Matias et al., 2005). The study demonstrated significant reduction in over washes and erosion from waves ultimately protecting the coastal regions after the construction of an artificial dunes (Matias et al., 2005). The design of an artificial sand dunes should be derived based on the set of storms instead of a single storm especially the crest elevation should consider

the most extreme conditions (Bruun, 1998). The comparison between the dimensions of an artificial sand dunes in five different places in US provides the dune elevation ranging from 4.5 meters to 5.5 meters (Bruun, 1998). Similar dune elevation is considered for this study as well for the implementation of artificial sand dunes. Figure 2.9 shows the implementation of artificial sand dunes on the left and dune nourishment on the right.

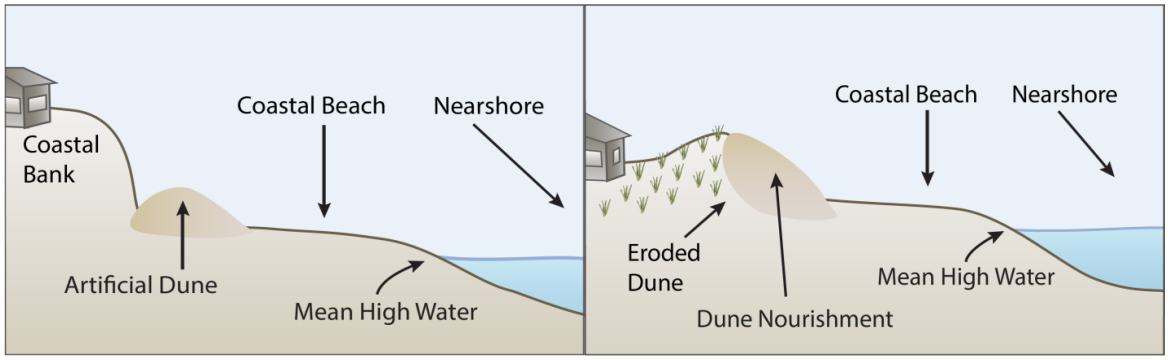

Figure 2.9 Construction of artificial sand dunes (left) and dune nourishment (right) to protect the house (StormSmart Coasts Program CZM, 2013).

2.4 SLOSH MODEL

The Sea, Lake, and Overland Surges from Hurricanes (SLOSH) model is a storm surge model developed by the National Weather Service (NWS) to forecast the storm surge in real-time when a hurricane is approaching (Glahn et al., 2009). SLOSH model has been applied to coastal regions of Gulf and Atlantic basins, 38 specific coastal regions as shown in Figure 2.10, and is run by NHC (Glahn et al., 2009). This model was derived from the earlier hurricane model developed in 1960 and 1970 (Glahn et al., 2009; Jelesnianski, 1972; Jelesnianski et al., 1992). The three important time dependent parameters for a SLOSH model are:

1. Latitude and longitude of storm positions.
2. Radius of maximum winds.
3. Central barometric pressure.

SLOSH model has also been used for variety of purposes such as to predict the flooding of coastal regions of Gulf and Atlantic basins for different hurricane scenarios (Glahn et al., 2009). SLOSH model has been applied in Mobile Bay region as well which is presented in the document "ALABAMA - HAZARDS ANALYSIS AND SLOSH DOCUMENTATION." This document

presents all the hurricane parameters used and all the different hurricane scenarios. The grid used for the Mobile Bay SLOSH model for is shown in Figure 2.11. The grid is a telescoping grid with cells ranging from 0.1 square miles to 1.3 square miles. This type of grid was used to put grid cells in land as well for better visualization of storm surge on land. For this model, 9 different hurricane directions were assumed with 3 different forward speeds and all five categories for each direction were tested. A total of 1815 hypothetical hurricane models were run through Mobile Bay SLOSH model which are summarized in Table 2.4.

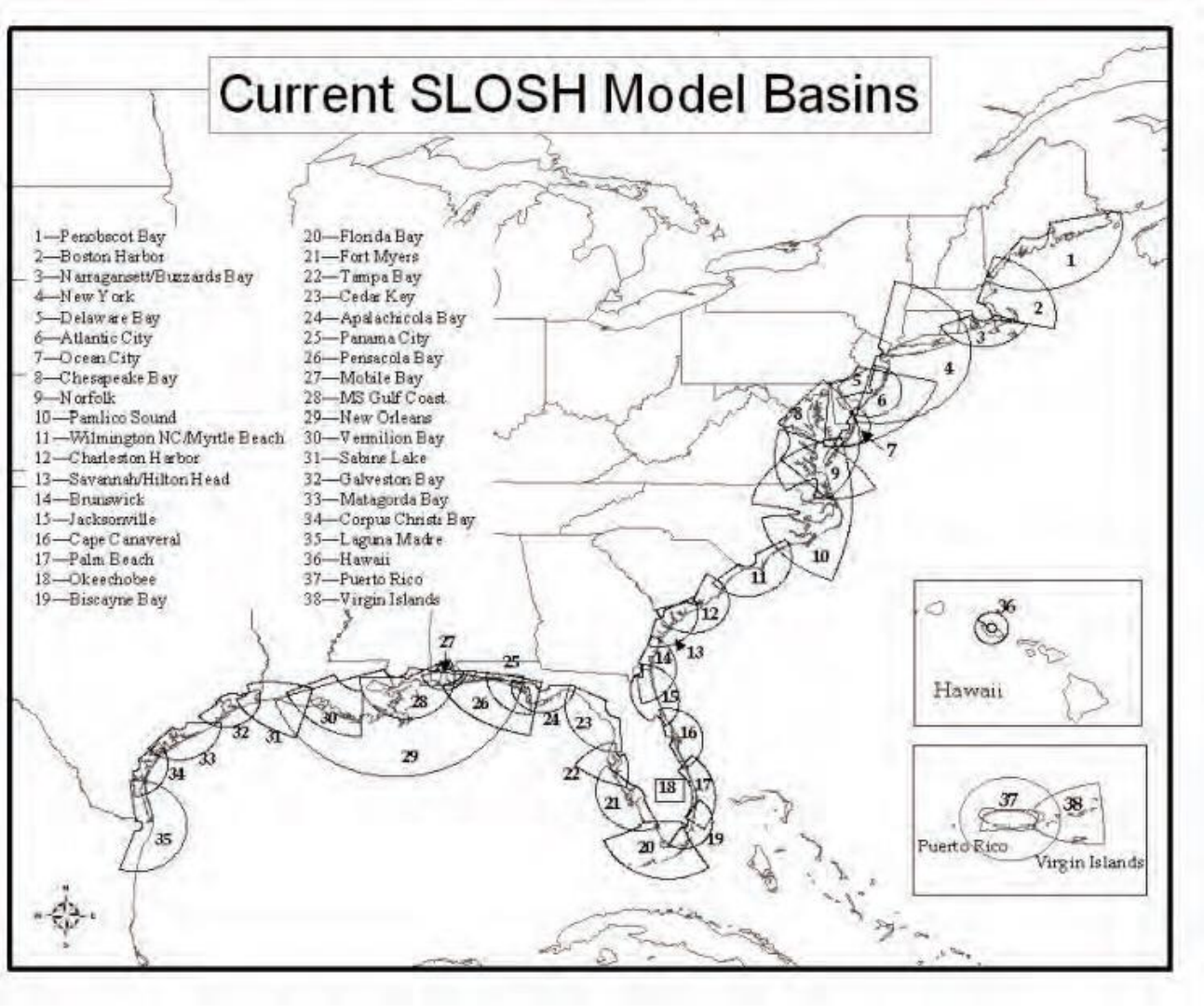

Figure 2.10 Map showing 38 SLOSH model basins (Glahn et al., 2009)

Table 2.4 Hypothetical Hurricane Scenarios for Mobile SLOSH model

Direction	Speed (mph)	Intensities	Tracks	Runs
W	5, 15, 25	Category 1-5	11	165
WNW	5, 15, 25	Category 1-5	15	225
NW	5, 15, 25	Category 1-5	14	210
NNW	5, 15, 25	Category 1-5	17	255
N	5, 15, 25	Category 1-5	17	255
NNE	5, 15, 25	Category 1-5	14	210
NE	5, 15, 25	Category 1-5	13	195
ENE	5, 15, 25	Category 1-5	10	150
E	5, 15, 25	Category 1-5	10	150
			Total	1815

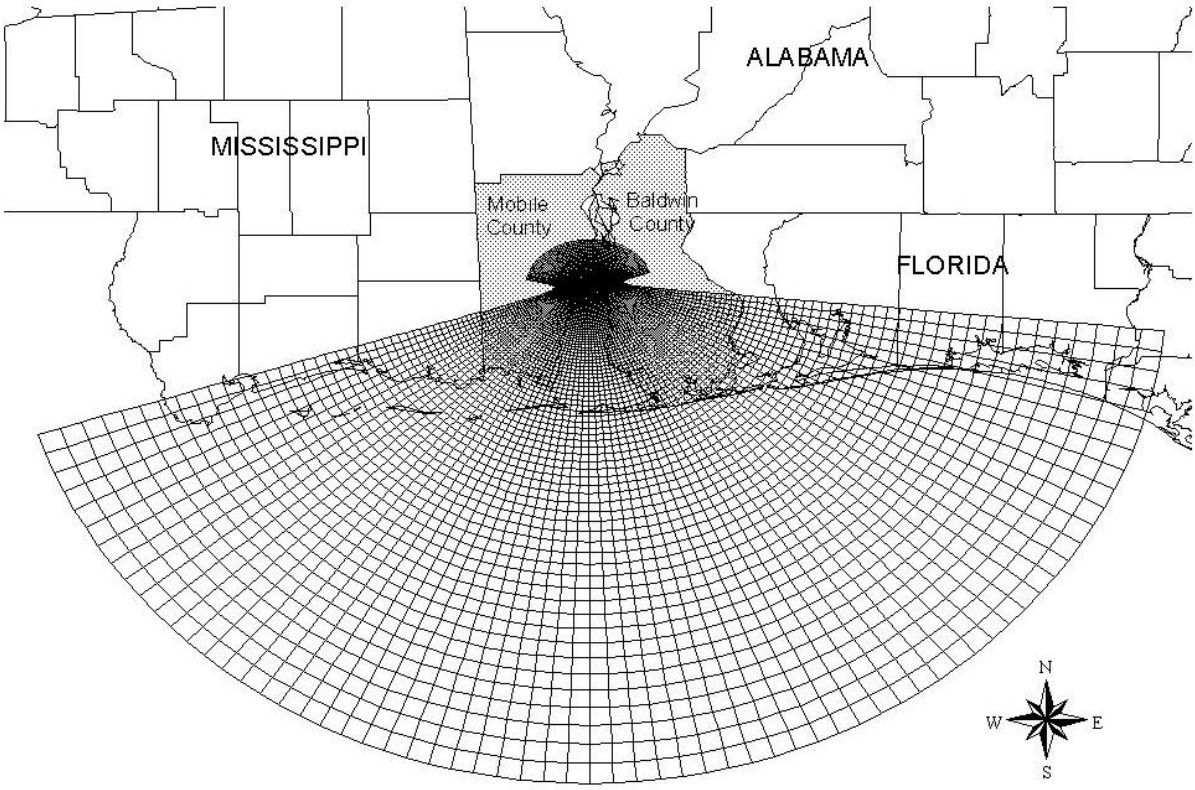

Figure 2.11 Mobile Bay SLOSH grid

The Mobile Bay SLOSH model provides two products known as MEOW and MOM to show the storm surge depths. MEOWs is the maximum water surface elevation in each cell for all the hurricane tracks in one direction for a particular forward speed and storm category (Glahn et al., 2009). MOM is the maximum of the MEOW, which provides the maximum surge for all the simulated hurricane of given category (Glahn et al., 2009). MEOW provides the maximum surge for a particular direction, forward speed, and intensity hurricane for each cell whereas MOM provides the maximum surge for a particular hurricane category. The MOM maps from SLOSH model are available to download in TIF format for different basins on the NHC "National Storm Surge Risk Maps" website. The SLOSH map for Mobile Bay region for hurricane category 3 is shown in Figure 2.12. Different colors are used to show the height of surge from a category 3 hurricane in the coastal regions of the bay. The information from SLOSH maps were later used to

compare the results from the Mobile Bay EFDC Model for all five hurricane categories which is discussed in Chapter 4.6.

There is capabilities and limitations of every model, so it is required to have knowledge of the model capabilities and limitations for better understanding of the model results (Turan et al., 2018). The study conducted by Turan et al. (2018) comparing the storm surge simulation results by ADCIRC (advanced circulation model) and SLOSH model with observed data for hurricane Andrew and Irma near Miami, FL concluded that the grid resolutions plays a major role in storm surge predictions for any models. The study concludes that models with higher resolution grid (finer grid cells) are better at storm surge predictions as compared to the models with lower resolution grid. As SLOSH models have relatively coarser spatial resolution, they may not be able to capture fine-scale variations in storm surge heights due to local bathymetry. The normal river flow, flooding due to rainfall, and impacts of wave on surge is not included in the SLOSH model which is another limitation of the model (*Sea, Lake, and Overland Surges from Hurricanes (SLOSH)*, n.d.). The input parameters are another important component of the SLOSH model such as bathymetric data, storm parameters, and meteorological data. The accuracy of the model results depends on the accuracy of the input data. Despite these limitations, the NWS SLOSH has been a reliable tool for understanding and predicting storm surge.

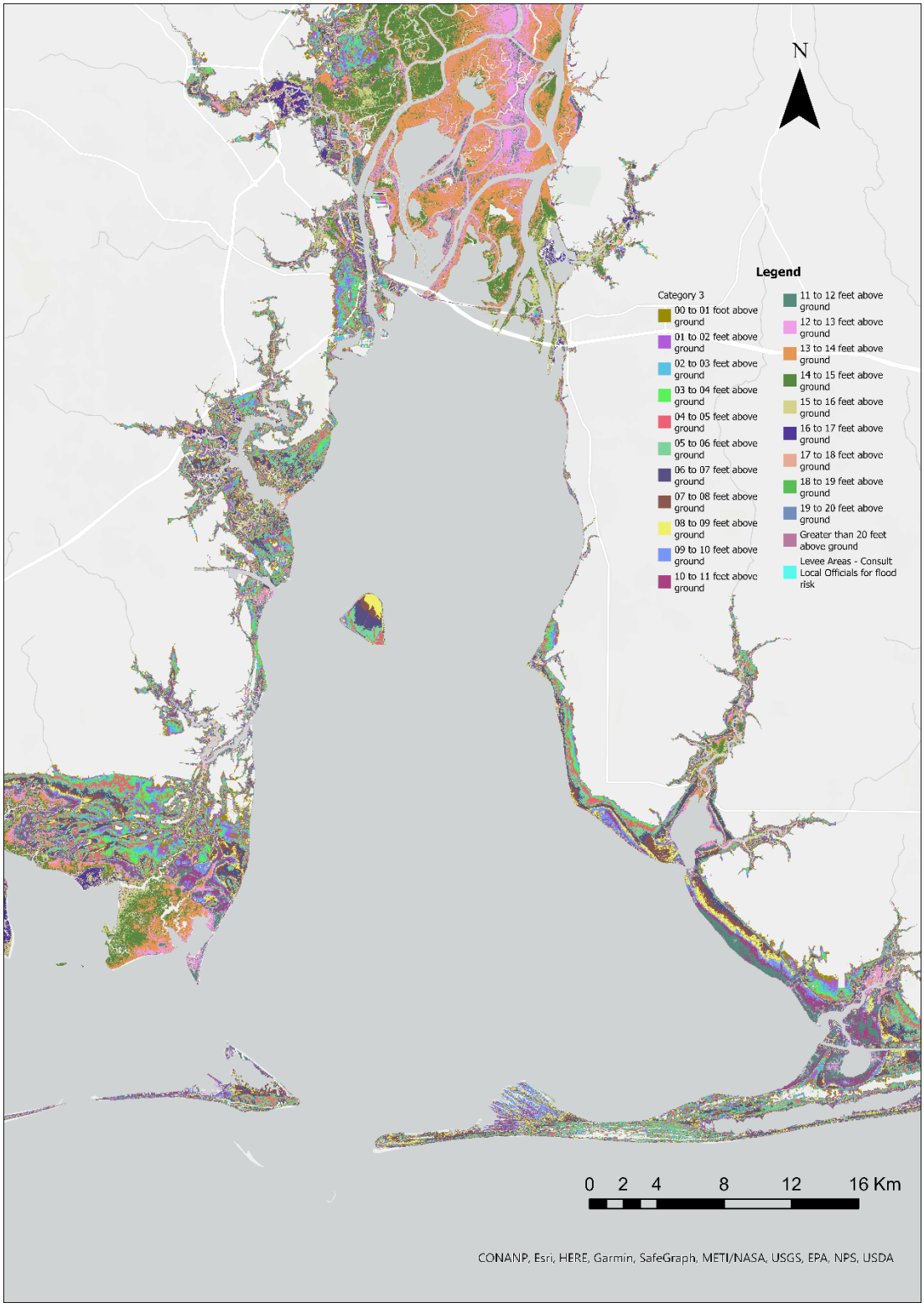

Figure 2.12 Flooding in Mobile Bay due to category 3 hurricane provided by NHC (SLOSH model).

CHAPTER 3. MOBILE BAY EFDC MODEL DEVELOPMENT

3.1 INTRODUCTION AND REVIEW OF EFDC+ HYDODYNAMIC MODELING

Environmental Fluid Dynamics Code Plus (EFDC+) developed by EE Modeling System (EEMS, https://www.eemodelingsystem.com/) is used for the hydrodynamics modeling of the Mobile Bay in this research. EEMS is a product of Dynamic Solutions International (DSI), LLC (https://dsi.llc/). EEMS consists of EFDC+, EFDC+ Explorer, and CVLGrid (Updated version Grid+). EFDC+ is the updated EFDC that is an open-source modeling system and was originally developed by Dr. John M. Hamrick at the Virginia Institute of Marine Science (VIMS) and School of Marine Science of The College of William and Mary in the year 1988 (DSI LLC., 2023). Since EFDC's development, many enhancements have been made and many new features have been added to become the updated version called EFDC+ allowing users to make much more detailed studies of the water bodies (DSI LLC., 2023).EFDC+ is a comprehensive modeling tool which is used by researchers all over the globe and has been widely used for the study of many water bodies such as rivers, lakes, reservoirs, estuaries, wetlands, and coastal regions (Devkota & Fang, 2015; Ji, 2008; Kim & Park, 2012; Xia et al., 2011). The EFDC hydrodynamics model which was developed to estimate the flooding and water depths in Grand Bay, AL, during hurricane Ivan showed good agreement with the observed data, and comparable agreement to SLOSH model estimated data (Alarcon & McAnally, 2012). The hydrodynamics modeling of St. Louis Bay, MS using EFDC indicated fairly good agreement between computed and observed water level, also the computed velocities was within the range of observed data (Liu et al., 2008). Their EFDC model was also used for water quality simulations and the modeled salinity and water temperature indicated good agreement with the observed data (Liu et al., 2008). The EFDC hydrodynamics model of the Perdido and Wolf Bay, AL, also indicated a good agreement between the modeled water surface elevation, temperature, and salinity with the field data at several observation stations (Devkota et al., 2013). This coastal model was used to study the response characteristics of the study area to the different level of inflow and sea level rise under climate change using the concept of age of water (Devkota et al., 2013). EFDC has also been used to study the flow dynamics in rivers such as Mobile River, AL (Devkota & Fang, 2015), Bankhead river-reservoir system, AL (G. Chen et al., 2016), Mispillion and Cedar Creek, DE (Zou et al., 2008), etc.

EFDC+ can simulate the complex hydrodynamics process based on near-field plume, wind-generated, and externally linked wave models along with temperature and salinity as an optional modeling parameters (DSI LLC., 2023). For this study, a hydrodynamic model for Mobile Bay was developed using EFDC+ to study the impacts of various intensity of hurricanes on the coastal region of Mobile Bay along with the study of the ability of NNBFs to change the extent, severity, and probability of flooding during extreme storms.

3.2 HYDRODYNAMICS

Hydrodynamics, the study of the motion of water and the forces acting on the water, is the major driving mechanism for the sediment transports, and pollutants movement in the water body (Ji, 2008). Hydrodynamics are the integral components of complex surface water systems providing critical information to sediment, toxic, and eutrophication models, including water velocities, temperature, and many more (Ji, 2008). Numerical models, which can evaluate the complex relationship of storms surges and NNBFs, provide various important information which is vital in decision making process (Smith et al., 2016). In order to create such complex numerical models, it is required to include the physical features of the coastal regions such as landscape, bathymetry, and landcover which is a very difficult task (Wamsley et al., 2009).

3.2.1 GOVERNING EQUATIONS

The three conservation laws that govern the hydrodynamics process in EFDC+ models are the conservation of mass, the conservation of energy, and the conservation of momentum (DSI LLC., 2023; Ji, 2008). The governing equations of EFDC+ include Navier-Stokes for fluid flow, the advection-diffusion equations for salinity, temperature, dye, toxicants, eutrophication constituents and suspended sediment transport (DSI LLC., 2023; Hamrick, 1992, 1996). The equations are expressed as curvilinear coordinate system in the horizontal direction, and equations are expressed as Standard Sigma (SIG) or Sigma Zed (SGZ) coordinates system for vertical direction (Craig et al., 2014; DSI LLC., 2023). The SGZ coordinate system is more time efficient even with large numbers of vertical layers and is more accurate in representing systems with sharp density gradient when compared to the SIG coordinate system (Craig et al., 2014).

3.2.2 COORDINATE SYSTEMS

The EFDC+ can model the horizontal coordinates, x and y, as curvilinear and orthogonal coordinate systems to make the simulation more realistic and appropriate and a time variable mapping or stretching transformation is adopted to provide uniform resolution in the vertical direction (as shown in Figure 3.1) for the vertical coordinate system which is given by (DSI LLC., 2023; Hamrick, 1992):

$$z = \frac{z^*+h}{\zeta+h} = \frac{z^*+h}{H} \tag{3.1}$$

where,

z is the sigma coordinate (dimensionless) (0 at the bottom and 1 at the water surface),

z^* is the vertical coordinate with respect to the vertical reference level (datum) (m),

h is the water depth below the vertical reference level (m),

ζ is the water surface elevation above the vertical reference level (m), and

H is the total depth of water columns (m), defined as or $\zeta + h$.

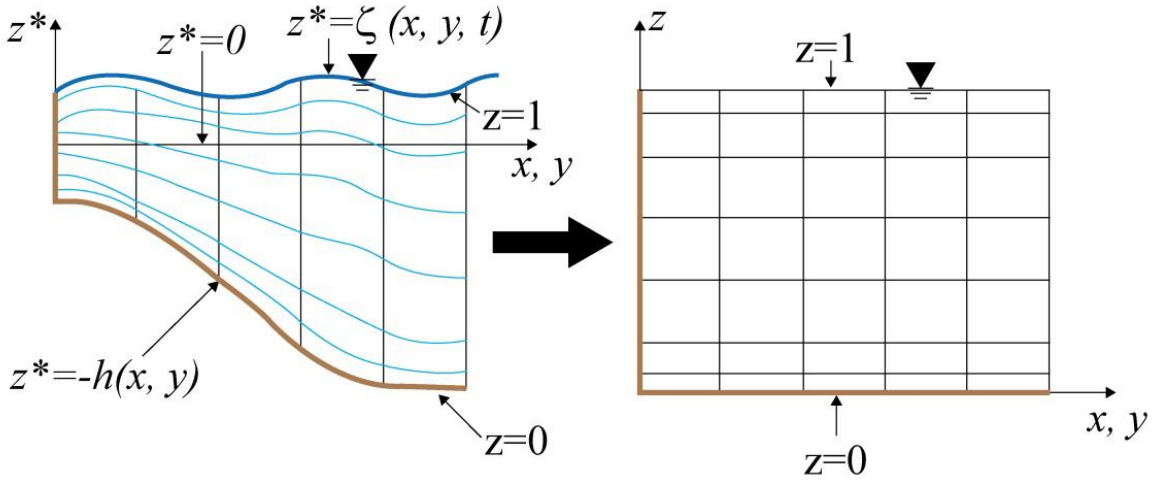

Figure 3.1 Vertical coordinate system in physical space in left and sigma space in right (DSI LLC., 2023)

3.2.3 BASIC HYDRODYNAMIC EQUATIONS

The EFDC+ model solves three-dimensional continuity and momentum equations (Devkota et al., 2013; DSI LLC., 2023; Ji, 2008) utilizing the Boussinesq approximation. According to the Boussinesq approximation, for an incompressible fluid density is not related to pressure except when gravitation force are considered (Ji, 2008).

$$\frac{\partial \rho}{\partial p} = 0 \tag{3.2}$$

The momentum equation in the x-direction:

$$\begin{aligned} &\frac{\partial}{\partial t}\left(m_x m_y H u\right) + \frac{\partial}{\partial x}\left(m_y H u u\right) + \frac{\partial}{\partial y}\left(m_x H v u\right) + \frac{\partial}{\partial z}\left(m_x m_y w u\right) \\ &\quad - m_x m_y f H v - \left(v\frac{\partial m_y}{\partial x} - u\frac{\partial m_x}{\partial y}\right) H v \\ &= -m_y H \frac{\partial}{\partial x}\left(g\zeta + p + P_{atm}\right) - m_y\left(\frac{\partial h}{\partial x} - z\frac{\partial H}{\partial x}\right)\frac{\partial p}{\partial z} + \frac{\partial}{\partial x}\left(\frac{m_y}{m_x} H A_H \frac{\partial u}{\partial x}\right) \\ &\quad + \frac{\partial}{\partial y}\left(\frac{m_x}{m_y} H A_H \frac{\partial u}{\partial y}\right) + \frac{\partial}{\partial z}\left(\frac{m_x m_y}{H} A_v \frac{\partial u}{\partial z}\right) - m_x m_y c_p D_p u\sqrt{u^2 + v^2} + S_u \end{aligned} \tag{3.3}$$

The momentum equation in the y-direction:

$$\begin{aligned} &\frac{\partial}{\partial t}\left(m_x m_y H v\right) + \frac{\partial}{\partial x}\left(m_y H u v\right) \\ &+ \frac{\partial}{\partial y}\left(m_x H v v\right) + \frac{\partial}{\partial z}\left(m_x m_y w v\right) + m_x m_y f H u + \left(v\frac{\partial m_y}{\partial x} - u\frac{\partial m_x}{\partial y}\right) H u \\ &= -m_x H \frac{\partial}{\partial y}\left(g\zeta + p + P_{atm}\right) - m_x\left(\frac{\partial h}{\partial y} - z\frac{\partial H}{\partial y}\right)\frac{\partial p}{\partial z} + \frac{\partial}{\partial x}\left(\frac{m_y}{m_x} H A_H \frac{\partial v}{\partial x}\right) \\ &+ \frac{\partial}{\partial y}\left(\frac{m_x}{m_y} H A_H \frac{\partial v}{\partial y}\right) + \frac{\partial}{\partial z}\left(\frac{m_x m_y}{H} A_v \frac{\partial v}{\partial z}\right) - m_x m_y c_p D_p v\sqrt{u^2 + v^2} + S_v \end{aligned} \tag{3.4}$$

The momentum equation in the z-direction:

$$\frac{\partial p}{\partial z} = -gH\frac{\rho - \rho_0}{\rho_0} = -gHb \tag{3.5}$$

The continuity equations in internal and external nodes:

$$\frac{\partial}{\partial t}\left(m_x m_y \zeta\right) + \frac{\partial}{\partial x}\left(m_y H u\right) + \frac{\partial}{\partial y}\left(m_x H v\right) + \frac{\partial}{\partial z}\left(m_x m_y w\right) = S_h \tag{3.6}$$

$$\frac{\partial}{\partial t}\left(m_x m_y \zeta\right) + \frac{\partial}{\partial x}\left(m_y H U\right) + \frac{\partial}{\partial y}\left(m_x H V\right) = S_h \tag{3.7}$$

where U and V are the depth-integrated horizontal velocities,

$$U = \int_0^1 udz,\ V = \int_0^1 vdz \tag{3.8}$$

where,

u, v are the horizontal velocity components in the curvilinear coordinates (m/s),

x, y are the orthogonal curvilinear coordinates in the horizontal direction (m),

w is the vertical velocity in the stretched vertical coordinate z,

z is the sigma coordinate (dimensionless),

t is time (s),

m_x, m_y are the square roots of the diagonal components of the metric tensor (dimensionless),

m is the Jacobian of the metric tensor determinant (dimensionless), $m = m_x m_y$,

p is the physical pressure in excess of the reference density hydrostatic pressure (m^2/s^2),

P_{atm} is the barotropic pressure normalized by the reference water density (m^2/s^2),

ρ_o is the reference water density (kg/m^3),

b is the buoyancy,

f is the Coriolis parameter (1/s),

A_H is the horizontal momentum and mass diffusivity (m^2/s),

A_v is the vertical turbulent eddy viscosity (m^2/s),

c_p is the vegetation resistance coefficient (dimensionless),

D_p is the projected vegetation area normal to the flow per unit horizontal area (dimensionless),

S_u, S_v are the source/sink terms for the horizontal momentum in the x and y directions (m^2/s^2),

S_h is the source/sink terms for the mass conservation equation (m^3/s),

z_s^* is the free surface elevation,

z_b^* is the bottom or topography elevation,

H is the total water column depth in a grid (z_s^* - z_b^*) and is a function of time and location,

U, V are the depth averaged velocity components in the x and y directions, respectively (m/s),

3.2.4 TURBULENCE MODELS

The random, irregular motion of water creates the turbulence causing the mixing of water table, which is much more greater than molecular diffusion in natural surface waters (Ji, 2008). EFDC+ uses the vertical turbulent viscosity and diffusivity model developed by (Mellor & Yamada, 1982) and modified by (Galperin et al., 1988), described in following vertical turbulent mixing coefficient equations (DSI LLC., 2023).

Vertical turbulent momentum diffusion coefficient:

$$A_v = \phi_A A_0 q l \tag{3.9}$$

$$\phi_A = \frac{(1+R_q/R_1)}{(1+R_q/R_2)(1+R_q/R_3)} \tag{3.10}$$

$$A_0 = A_1\left(1 - 3C_1 - \frac{6A_1}{B_1}\right) = \frac{1}{B_1^{1/3}} \tag{3.11}$$

$$\frac{1}{R_1} = 3A_2\frac{(B_2-3A_2)\left(1-\frac{6A_1}{B_1}\right)-3C_1(B_2+6A_1)}{1-3C_1-\frac{6A_1}{B_1}} \tag{3.12}$$

$$\frac{1}{R_2} = 9A_1A_2 \tag{3.13}$$

$$\frac{1}{R_3} = 3A_2[6A_1 + B_2(1-C_3)] \tag{3.14}$$

Vertical mass diffusion coefficient:

$$A_b = \rho_K K_0 q l \tag{3.15}$$

$$\phi_K = \frac{1}{\left(1+\frac{R_q}{R_3}\right)} \tag{3.16}$$

$$K_0 = A_2\left(1 - \frac{6A_1}{B_1}\right) \tag{3.17}$$

$$R_q = \frac{gH}{q^2}\frac{l^2}{H^2}\frac{\partial b}{\partial z} \tag{3.18}$$

Where,

q^2 is turbulent intensity,

l is turbulent length scale,

R_q is Richardson Number,

$\phi A \phi_A$ is the stability viscosity coefficient,

ϕ_K is the stability diffusivity coefficient,

K_0 is dimensionless coefficient,

All the vertical turbulent options along with all the turbulence closure constants used in EFDC+ model is shown in Figure 3.2 as an example. The turbulence closure constants are typically fixed but can be modified by advance users (activating Modify option).

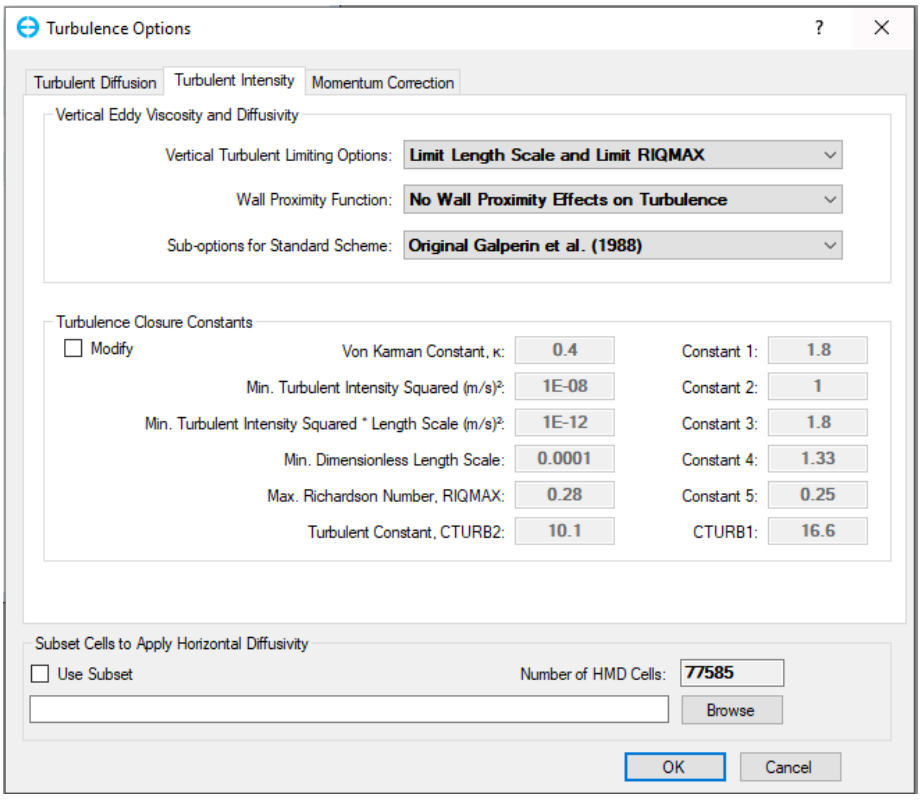

Figure 3.2 Vertical Turbulent options under Turbulence Options windows EFDC+

EFDC+ uses Smagorinsky's sub grid scale closure formulation (Smagorinsky, 1963) for the horizontal turbulent viscosity and diffusivity (A_H) modeling.

$$A_H = C_s \Delta x \Delta y \sqrt{\left(\frac{\partial u}{\partial x}\right)^2 + \left(\frac{\partial v}{\partial y}\right)^2 + \frac{1}{2}\left(\frac{\partial u}{\partial y} + \frac{\partial v}{\partial x}\right)^2} \quad (3.19)$$

where,

C_s is the Smagorinsky coefficient,

$\Delta x\ \Delta y$ are the grid sizes in x and y directions,

All the horizontal turbulent options along with all the turbulence closure constants used in the EFDC+ model is shown in Figure 3.3.

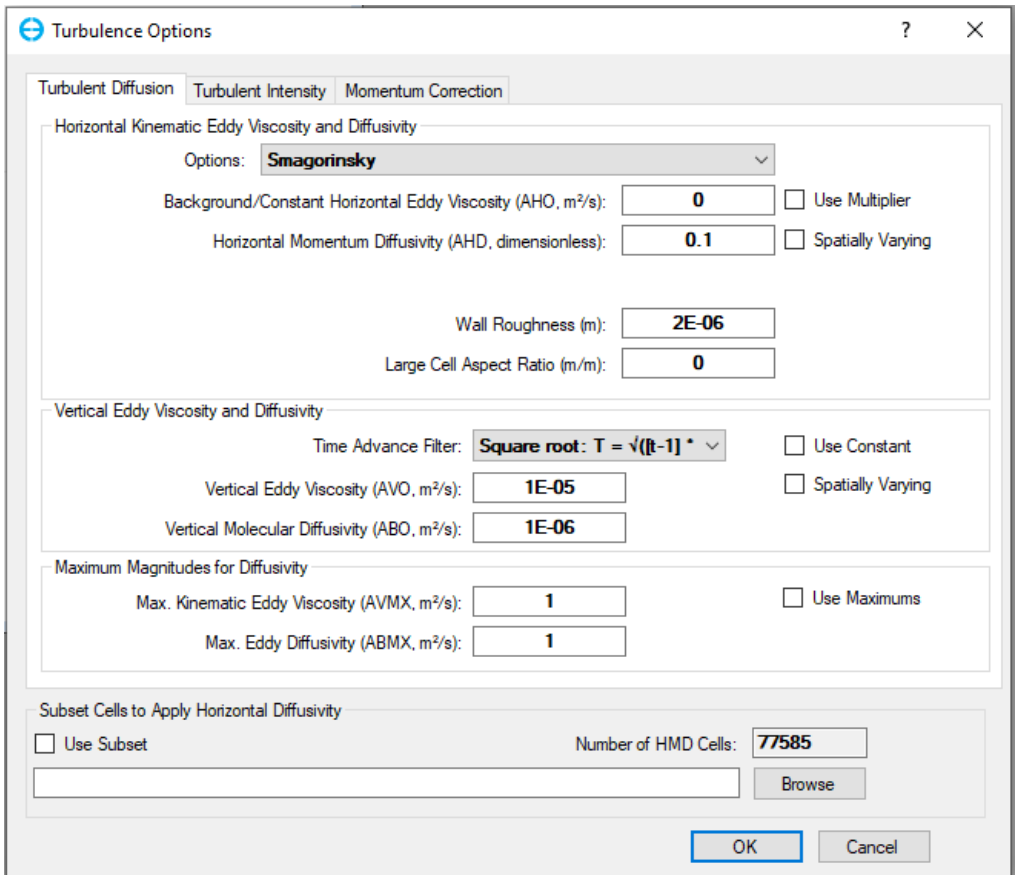

Figure 3.3 Horizontal turbulent options under Turbulence Options windows EFDC+

3.2.5 BOTTOM FRICTION

The stress components at the bottom layer of the model is dependent on bottom layer (layer 1) velocity components given by(DSI LLC., 2023):

$$\frac{1}{\rho_w}\begin{bmatrix}\tau_{bx}\\ \tau_{by}\end{bmatrix} = C_b\sqrt{u_1^2 + v_1^2}\begin{bmatrix}u_1\\ v_1\end{bmatrix} \tag{3.20}$$

where,

ρ_w is the density of water,

τ_{bx}, τ_{by} are the bottom friction drag in x and y directions,

u_1, v_1 are the velocity components in x and y directions for layer 1.

The bottom stress coefficient assuming the logarithmic velocity profile at the bottom is (Nezu, 1993):

$$C_b = \left[\frac{\kappa}{\ln(\Delta_1/2z_0)+(\Pi-1)}\right]^2 \tag{3.21}$$

where,

κ is von Karman constant,

Δ_1 is dimensionless thickness of the bottom layer,

z_0 is dimensionless roughness height ($z_0{}^*$/H),

Π is wake strength parameter (assumed 0).

3.2.6 VEGETATION

Vegetation, EFDC+ framework shown in Figure 3.4, creates a drag affecting the flow, mean velocity, and turbulence within the vegetated areas (DSI LLC., 2023). The effect of vegetation drag on the flow is represented by adding an additional drag term in the momentum equations, and the impacts on turbulent intensity and turbulent length is represented by adding the additional canopy related terms (DSI LLC., 2023) which are given below:

$$\partial_t\left(m_x m_y H q^2\right) + \partial_x\left(m_y H u q^2\right) + \partial_y\left(m_x H v q^2\right) + \partial_z\left(m_x m_y w q^2\right)$$

$$= \partial_z\left(m_x m_y \frac{A_q}{H}\partial_z q^2\right) - 2m_x m_y \frac{Hq^3}{B_1 l} \tag{3.22}$$

$$+2m_x m_y\left(\frac{A_v}{H}\left((\partial_z u)^2 + (\partial_z v)^2\right) + gK_v\,\partial_z b + \partial_p \boldsymbol{c_p D_p}(u^2+v^2)^{\frac{3}{2}}\right) + Q_q$$

$$\partial_t(m_x m_y H q^2 l) + \partial_x(m_y H u q^2 l) + \partial_y(m_x H v q^2 l) + \partial_z(m_x m_y w q^2 l)$$

$$= \partial_z\left(m_x m_y \frac{A_{ql}}{H}\partial_z(q^2 l)\right) - m_x m_y E_2 \frac{H l q^3}{l B_1}\left(1 + E_4\left(\frac{l}{\kappa K z}\right)^2 + E_5\left(\frac{l}{\kappa H(1-z)}\right)^2\right) \quad (3.23)$$

$$+ m_x m_y l\left(E_1 \frac{A_v}{H}((\partial_z u)^2 + (\partial_z v)^2) + E_3 g K_v \partial_z b + E_1 \eta_p \boldsymbol{c_p D_p}(u^2 + v^2)^{3/2}\right) + Q_l$$

where,

D_p is the vegetation drag term,

c_p is the production efficiency factor.

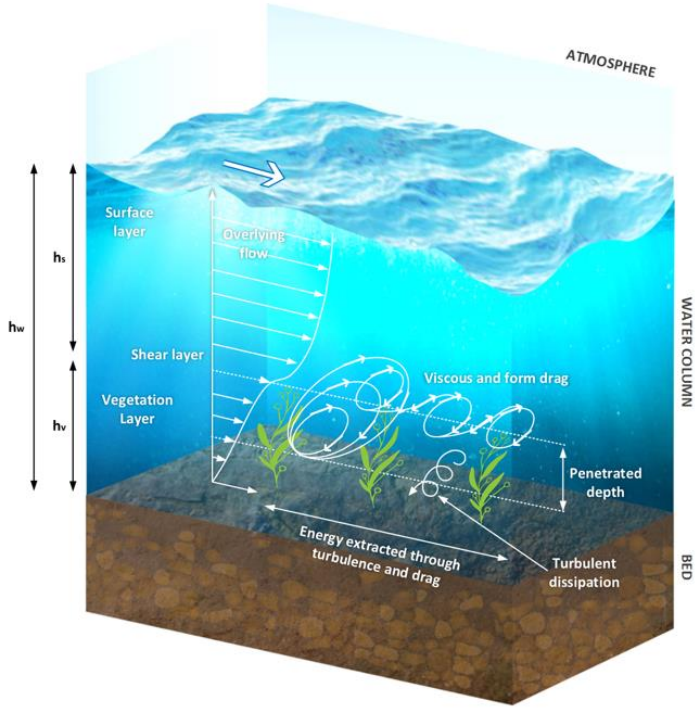

Figure 3.4 EFDC+ vegetation framework (DSI LLC., 2023)

The drag coefficient of the vegetation depends on various factors such as plant density, shape of the plants as well as the flow conditions (DSI LLC., 2023; Ghisalberti & Nepf, 2004). The bulk drag coefficient can be obtained using the following equations (James & O'Donncha, 2019; Plew, 2011):

$$\overline{C_D} = 2.0 - 67ad \quad (3.24)$$

$$C_D(\zeta) = \overline{C_D}(1.2 + 0.8\zeta - 0.5\zeta^2) \quad (3.25)$$

$\overline{C_D}$ is the bulk drag coefficient,

ad is the dimensionless canopy density,

$C_D(\zeta)$ is the depth-varying drag coefficient,

ζ is the distance from the water surface along normalized lengths of the canopy cylinders.

3.2.7 MASK

EFDC+ provides a feature known as mask which can be implemented in the model to provide an obstruction to the flow (DSI LLC., 2023). The schematic of the mask is shown in Figure 3.5. Mask can be added on the west or/and south boundary of the cell as a completely blocking or partially blocking. Fully blocking masks completely prevent the movement of water between adjoining masks from top to bottom whereas partially blocking mask allows the water movement depending upon the clearance thickness.

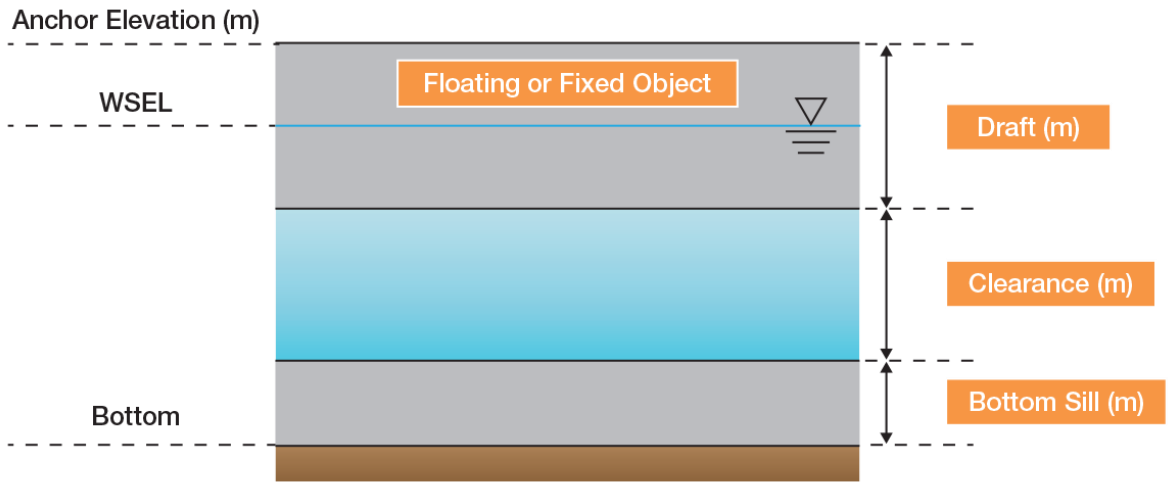

Figure 3.5 EFDC+ schematic of mask

3.3 VERTICAL WATER LAYER

There are three different vertical layering options available in EFDC+. One of them is Standard Sigma (SIG) approach and other two are Sigma-Zed (SGZ) approach: SGZ-Specified Bottom Layer and SGZ-Uniform Layer. SIG is a conventional approach which provides same number of

vertical layers for every cells irrespective of the water depth (DSI LLC., 2023) as shown in Figure 3.6. As the number of layers are kept constant for every cell, this method is not able to mimic the real-world scenario of the water bodies with steep bathymetry and sharp changes in vertical water quality components causing the significant error in density gradient and other vertical components gradient (Mellor et al., 1994).

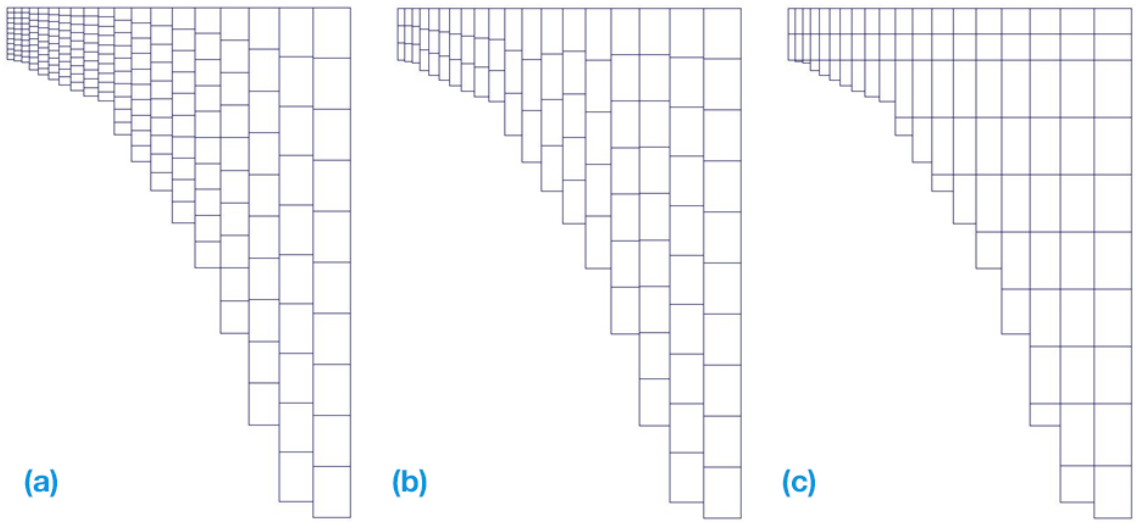

Figure 3.6 EFDC+ layer option with 10 layers a) SIG b) SGZ-Bottom Specified c) SGZ-Uniform Layer (DSI LLC., 2023; Ji, 2008)

SGZ is a new and improved layering approach developed to overcome the weakness of SIG approach (Craig et al., 2014). Depending on the water depth, users can specify cells with different number of layers and the thickness of the layers can also vary. SGZ-Bottom Specified, shown in Figure 3.6b, allows users to use SGZ layering with specified number of bottom layers in each horizontal cell and SGZ-Uniform layer, shown in Figure 3.6c, allows user to use SGZ layering where bottom of each vertical layer are aligned in horizontal direction (DSI LLC., 2023). In both approaches, the user has to provide a minimum number of vertical layers. SGZ approach can significantly reduce the error in density gradient and other vertical components gradient and it produces more efficient and more practical models. SGZ-Uniform layer option has been used in this study.

3.4 GRID DEVELOPMENT

The first step in the process of developing any 3-dimensional hydrodynamics model starts with grid generation for the study area. There are various things to be considered while generating the grid for any study such that there is good balance between the spatial resolution, a site conceptual model, and modeling objectives against the simulation time and resources (Devkota et al., 2013). Even though higher resolution grids can produce better- and high-quality results as compared to the lower resolution grids, it might not be feasible as the higher the grid resolution is, longer will be the model computational time as well as increased input resources required. Therefore, depending on the nature and requirement of the study, reasonable resolution of grid should be developed so that adequate calibration and validation could be performed resulting in better modeling results (Devkota et al., 2013).

CVLGrid is a 2-D grid building tool, developed by the EEMS team, which provides a user friendly and quick grid generation platform. It allows the user to create a normal rectangular grid as well as the curvilinear grid. Since the curvilinear grid does not have uniform cell dimensions like a normal rectangular grid, it can represent the natural water bodies like lakes, rivers, estuaries etc. more accurately. Thus, curvilinear grid was developed for the Mobile Bay region as shown in Figure 3.12. As this study is focused on studying the impacts of hurricanes in terms of flooding in the coastal region of Mobile Bay, the model grid was not only developed for the water body but also for the coastal land of Mobile Bay region. Figure 3.7 shows the different sections on eastern and western coast of the bay, which is used to show the elevation profiles in Figure 3.8, Figure 3.9, and Figure 3.10. From the elevation profiles, it can be seen that around 1 km width of coastal land was able to represent the elevation changes. Thus 1 km width of the coastal land was included in the model grid on both sides of the bay to represent the coastal geography including coastal highways. The curvilinear grid for Mobile Bay was developed in such a way that the grid cells are finer at the coastal regions and coarser in the main water body of the bay. Therefore, we have developed higher resolution (finer grid cell size) grid for the coastal region of the bay and lower resolution (coarser grid cell size) for the water body which can be seen in Figure 3.11 and Figure 3.12. After the development of the curvilinear grid for the Mobile Bay, it was then imported in EFDC+ explorer to assign various modeling parameters required for the development of the "Mobile Bay EFDC Model".

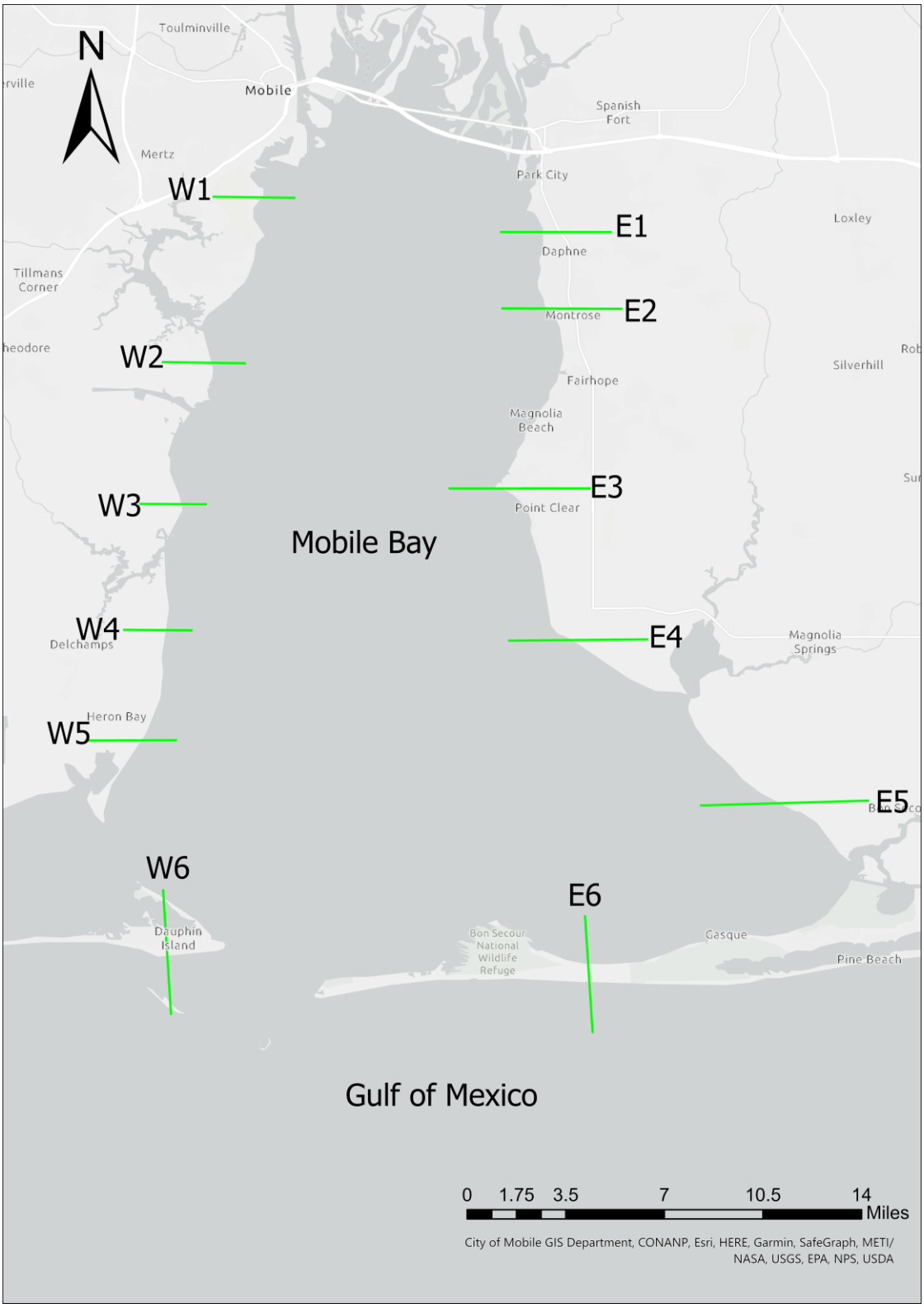

Figure 3.7 Different sections for elevation profile on eastern and western coast of the Mobile Bay (ArcGIS Pro)

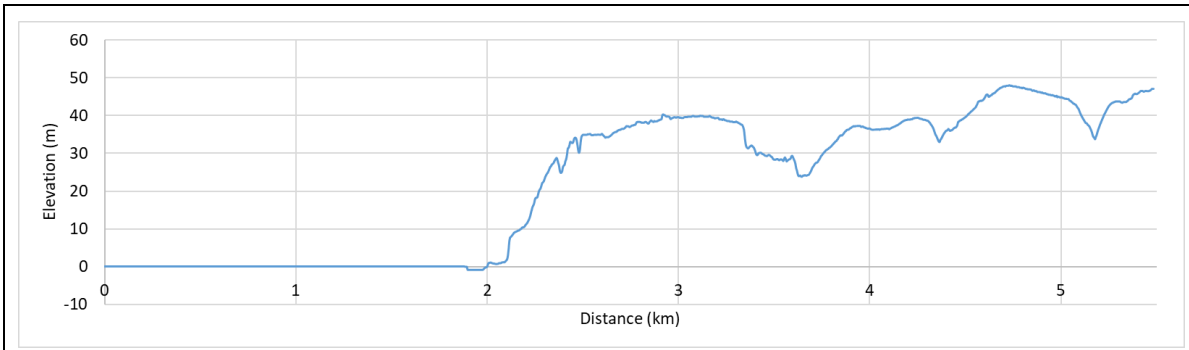

a. E1

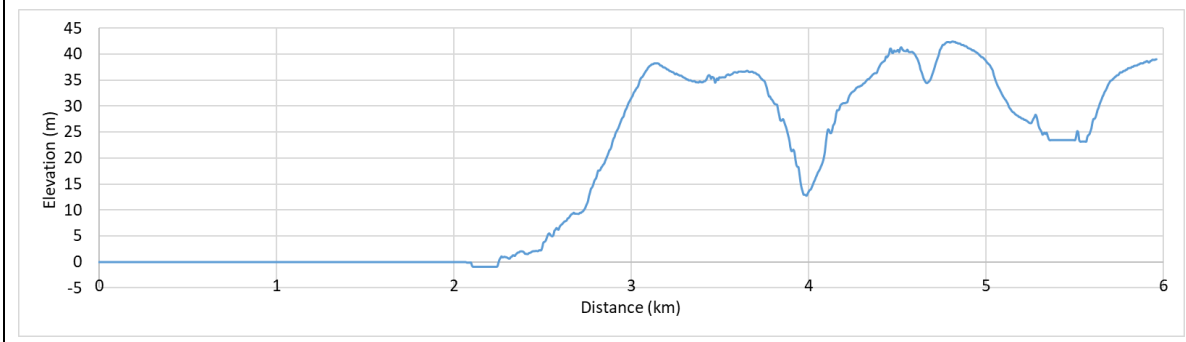

b. E2

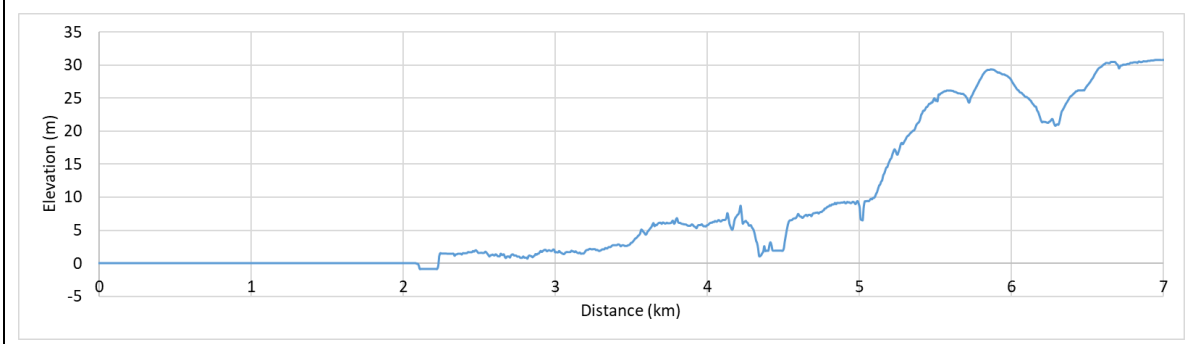

c. E3

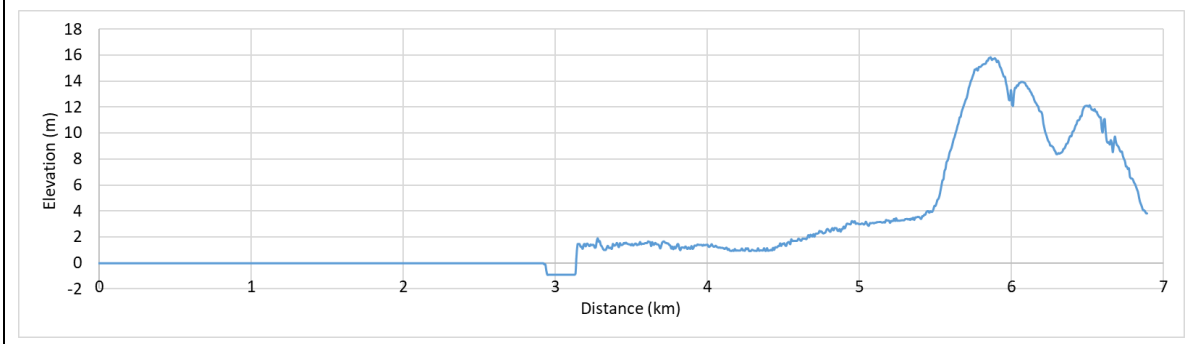

d. E4

Figure 3.8 Elevation profiles at different sections of the bay a. E1 b. E2 c. E3 d. E4 with respective to Figure 3.7

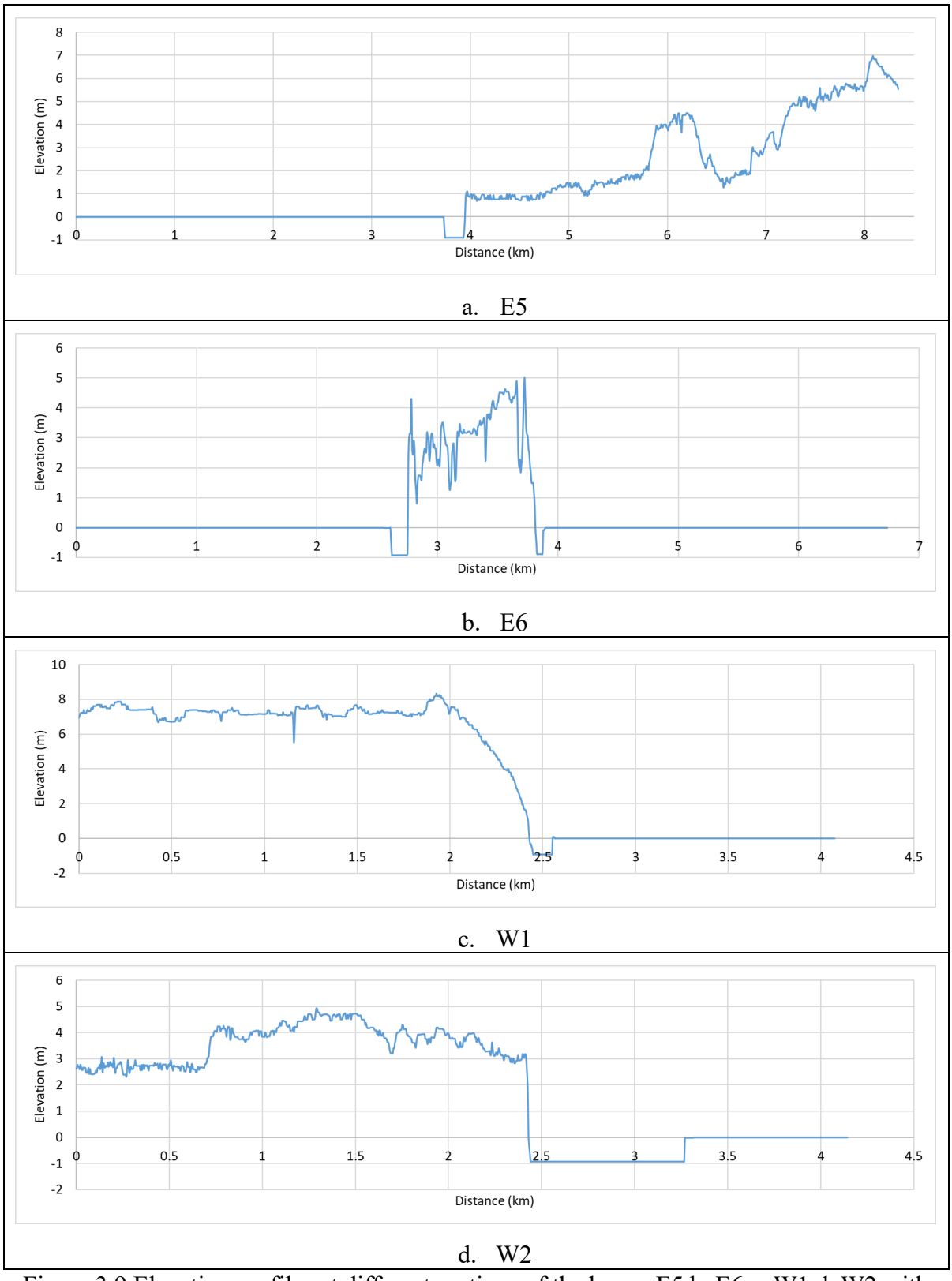

Figure 3.9 Elevation profiles at different sections of the bay a. E5 b. E6 c. W1 d. W2 with respective to Figure 3.7

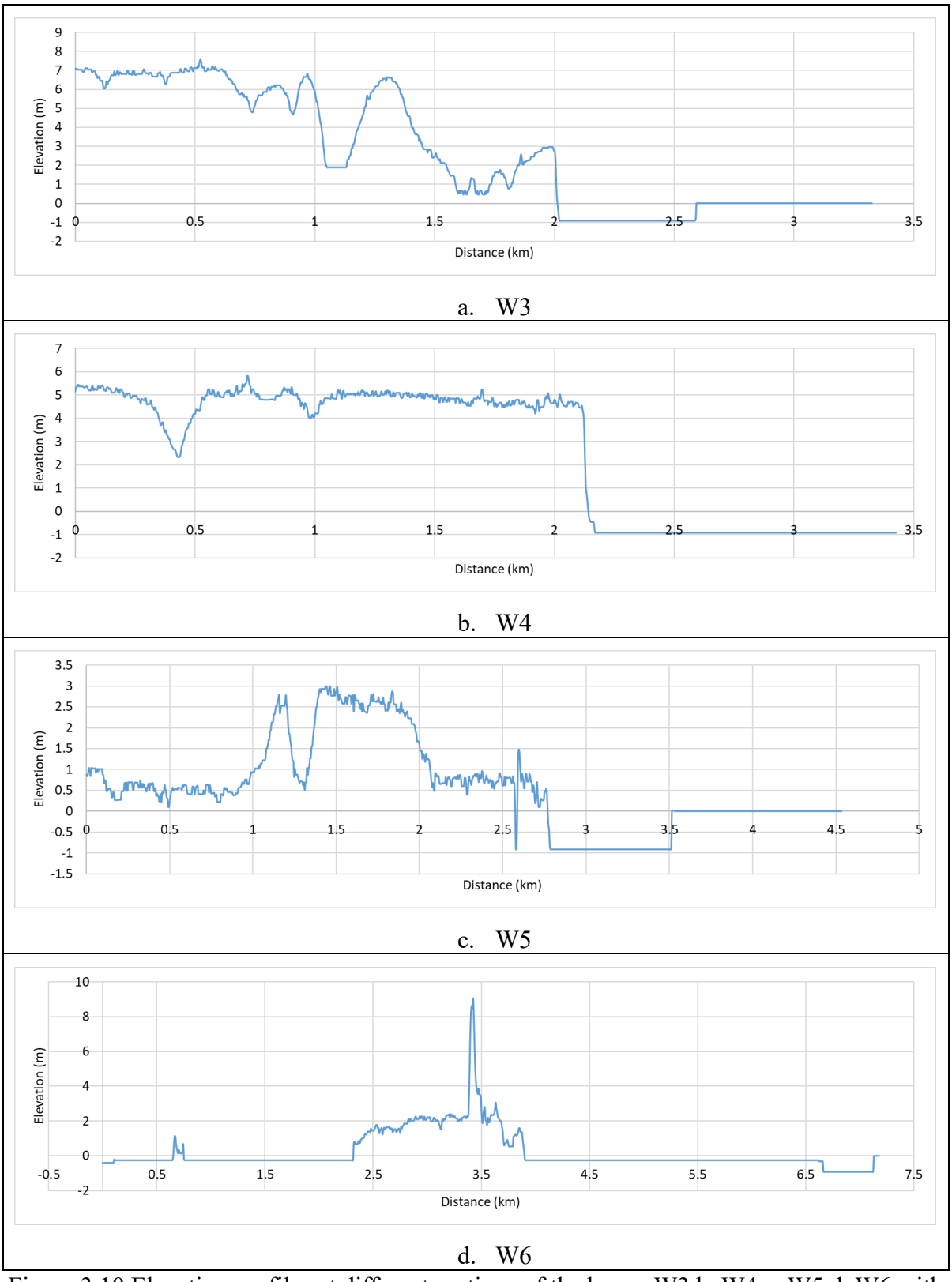

Figure 3.10 Elevation profiles at different sections of the bay a. W3 b. W4 c. W5 d. W6 with respective to Figure 3.7

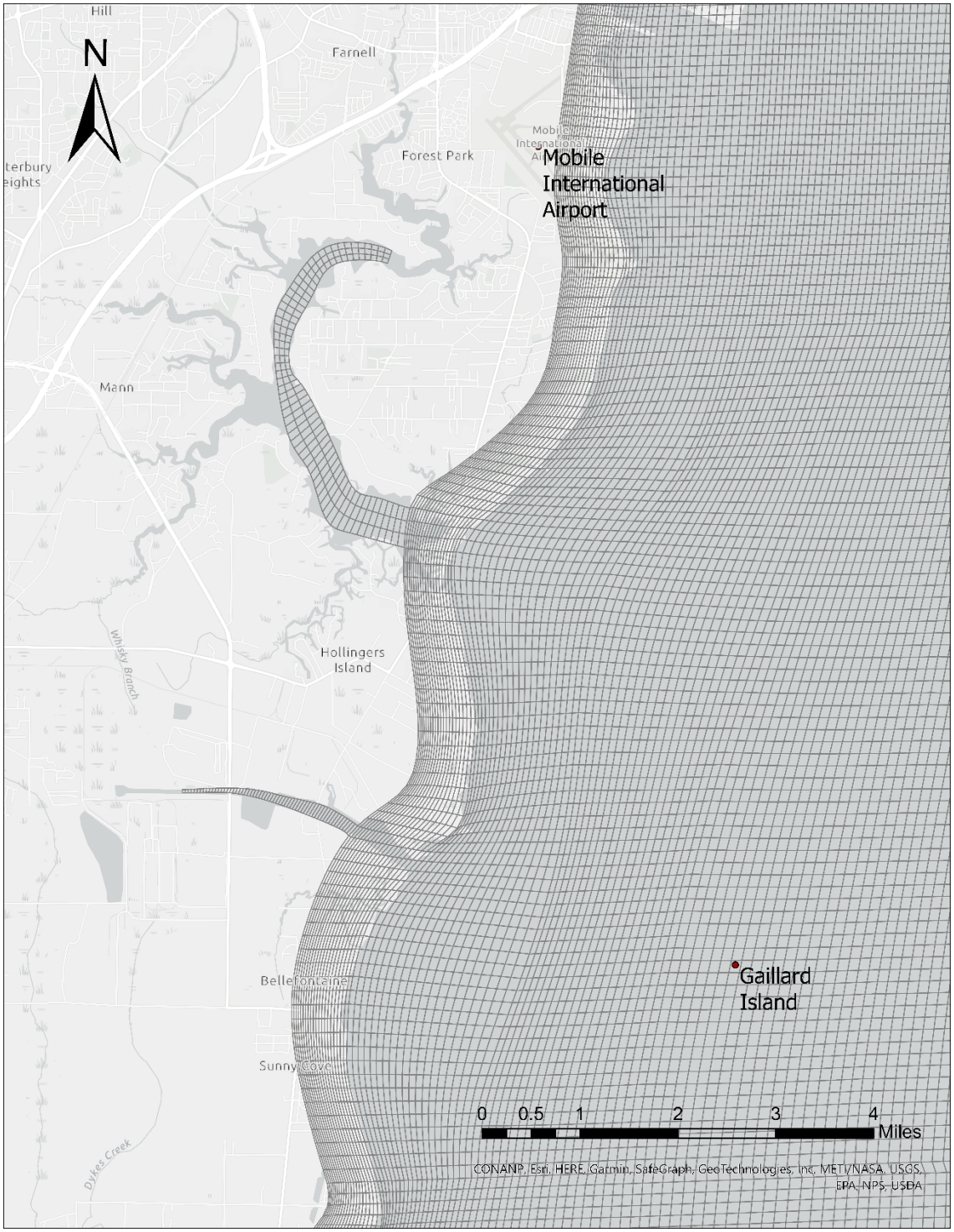

Figure 3.11 Coarser grid size on the water body and finer grid size as moved towards the coastal land (ArcGIS Pro)

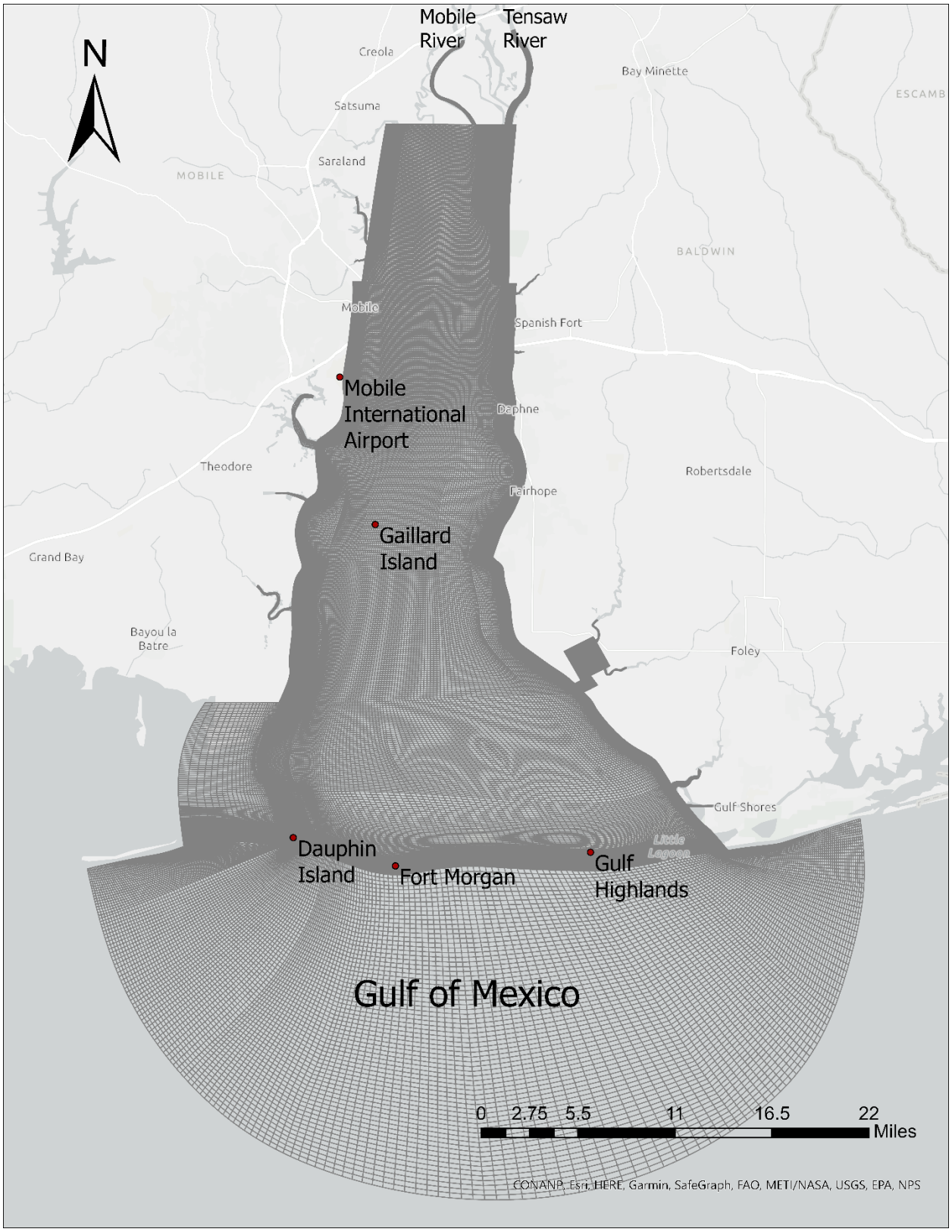

Figure 3.12 Curvilinear grid for Mobile Bay EFDC Model (ArcGIS Pro)

Steps involved in developing curvilinear grid for the "Mobile Bay EFDC Model" using CVLGrid are given below.

1) The first step is to create a geo-referenced backdrop image of the Mobile Bay. This backdrop geo file will be used in CVLGrid to create a grid with the help of underlying image of the study area. Basic steps for creating a geo-referenced image are given below.
   a) With the help of Google Earth Pro, locate the study area.
   b) Plot two points LR and UL (LR- lower right and UL- upper left) on google earth and note the northing and easting of those points in UTM (Universal Transverse Mercator).
   c) Save the high-resolution image of that area using Google Earth Pro.
   d) Open CVLGrid and under setup of Geo-Referenced Background tab, load the saved image and enter northing(Y) and easting(X) for two points i.e., LR and UL.
   e) After updating the northing and easting of those two points save it as georeferenced file.
   f) Now, we have successfully created a geo-referenced backdrop image to be used in CVLGrid for grid generation.
2) The geo-referenced backdrop file was then imported into CVLGrid.
3) As per the requirement of this study, to develop a curvilinear grid with finer grids at the coastal region, grid generation was carried out by dividing the bay into different sections vertically as well as horizontally as shown in Figure 3.13. Splines were used to divide the bay into different sections both vertical as well as horizontal. At the coastal boundary, splines were created in such a way that they follow the curvilinear nature of the boundary.
4) After that, grids were generated for each of the horizontal sections separately keeping the "j" value same for all the individual vertical sections, so that there will be same number of vertical cells for each grid sections.
5) For the grid section in Gulf of Mexico, the grid was created like an arc as shown in Figure 3.12 to provide a semi-circular open boundary.
6) All the individual grid sections were connected one by one to create a single grid for the whole Mobile Bay as shown in Figure 3.12.
7) For different inflow rivers and creeks, the grids were created and connected individually to the final grid created in step 5.
8) Finally, the curvilinear grid for the Mobile Bay was imported in EFDC+ explorer to create "Mobile Bay EFDC Model".

Figure 3.13 Splines for one of the grid section

The grid generated by CVLGrid process might have an issue with the cell rotation angle. The proper cell rotation angle and wind direction needs to be applied for the proper functioning of a model which is further discussed in Chapter 4.3.2. There is another process to create the grid using a tool called Grid+. Grid+ is an updated version of CVLGrid developed by the EEMS team. This updated version automatically corrects the cell rotation angle, so we have developed the grid for our model using Grid+. The process involved in developing grid in Grid+ is quicker and easier compared to CVLGrid as the same background map, which is available in EFDC+ explorer as well, is already available in this updated version and users are not required to create a new geo-referenced background map. All the other steps are similar to the steps involved in CVLGrid. The Mobile Bay EFDC Model has an area of around 3320.89 km^2 and it consists of 77585 total number

of curvilinear horizontal cells with cell sizes ranging from (10.39 m, 9.63 m) to (1359.94 m, 537.82 m).

3.5 BATHEMETRY

Bathymetry, also known as bottom elevation, is the measurement of depth of water in oceans, seas, lakes, rivers, or any other water bodies. Just like topography is related to the study of landforms above sea level, bathymetry is related to the study of landform below sea level. In other words, bathymetry provides us with information about the underwater terrain of the water bodies. The accuracy of the bathymetry data plays a very important role in the proper functioning of hydrodynamics in modeling studies.

3.5.1 DATA SOURCE

There are various sources of bathymetry data available on the internet. For this study, the data provided by National Oceanic and Atmospheric Administration (NOAA) was used because of its reliability and accuracy. NOAA provides a web-based mapping tool known as Bathymetric Data Viewer, which provides different formats for bathymetry data. The bathymetry data are available in both raster and vector formats for the Mobile Bay region. Since raster data cannot be used directly in the EFDC+, vector data was downloaded and assigned to the Mobile Bay EFDC Model. But the vector data is only available for the water body of the bay and the available resolution was lower than the requirement of the study. Due to the lower resolution of this vector data, it was not able to represent the bathymetry near the boundary of the coastal regions of the bay. Therefore, we used a higher resolution digital elevation model (DEM) which is available for both coastal lands and water bodies of the Mobile Bay. These DEMs were converted to EFDC+ input file for bathymetry with the help of ArcGIS Pro. DEM is available in different cell sizes which are represented in arcseconds. Cell size is the dimension of the area that is covered on the ground and represented by a cell or pixel in a raster file. The DEM with lower cell size covers smaller area on the earth's surface, so it will be able to represent the terrain with higher accuracy and precision as compared to the DEM with higher cell size. But the file size and the data points are higher for the lower cell size DEM. DEMs are required to be converted to points data which was done with the help of ArcGIS Pro and if we use higher resolution DEMs for whole study region, it will create large number of data points which cannot be handled by ArcGIS Pro. Therefore, we have used DEMs with two different cell sizes according to the need of this study.

The two different cell sizes of DEMS that were used in this study are 3 arcseconds (~90 m) and 1/3 arcseconds (~10m). The lower cell size DEM (high resolution) was used for coastal region, rivers, island, and shipping channel (which is the deepest area of the bay) because we have finer grid cells, and we need higher accuracy in these areas as the major focus of the study is along these parts of the bay. The larger cell size DEM (lower resolution) was used for water bodies and wetlands on the north of the bay. First of all, required DEM files were downloaded from NOAA using grid extract which allows users to download the data by drawing a rectangle over the map. After drawing a rectangle over the required region, the DEMs can be downloaded with required cell sizes. Depending on the DEM resolution and study area, required DEM file may or may not be downloaded at once for the whole study area. These downloaded DEM files were later processed using a GIS tool.

3.5.2 GIS METHOD ON DEM

The downloaded DEM files were in raster format which cannot be used directly in the EFDC+. Therefore, it was converted to a format which can be used in EFDC+ using a GIS tool. Geographic Information System (GIS) is a computer system which is used to visualize, analyze, compile, and interpret spatial data. This tool is a multidisciplinary tool and has many uses. For this study, a GIS tool was used to extract bathymetry data and convert those data into EFDC+ input file format. A well-known GIS software, ArcGIS Pro developed by ESRI, was used for preparing bathymetry data. The input bathymetry file for the EFDC+ is a notepad file and it consists of coordinates (UTM Easting and UTM Northing) and bottom elevation (in meters) of every data point. To create the bathymetry input file, the data points were extracted from the available DEM file, and then coordinates and depth values were copied to the notepad file. This notepad file was imported to the EFDC+ explorer to assign the bathymetry to the model.

Steps involved in developing bathymetry input file for the “Mobile Bay EFDC Model” using ArcGIS Pro are given below.

1) The downloaded DEM files: 3 arcseconds (~90 m) and 1/3 arcseconds (~10 m) were imported into ArcGIS Pro.
2) Both the DEM files were projected to the North American Datum 1983 (NAD 1983) Universal Transverse Mercator (UTM) zone 16N coordinate system which is the required coordinate system for the study area.

3) After that different polygons were created for coastal regions, rivers, islands, and shipping channel in ArcGIS Pro. These are the regions where 1/3 arcseconds DEM were to be used as the grid cells are finer in these regions.
4) The next step was to extract the portion of 1/3 arcseconds which covers the coastal regions, rivers, island, and shipping channel. This was done using the "Clip Raster" tool in the ArcGIS Pro. The 1/3 arcseconds DEM was clipped with the polygons created in step 2. Now, we have required 1/3 arcseconds DEM covering only the coastal region, rivers, island, and shipping channel of the Mobile Bay.
5) At this point we have clipped 1/3 arcseconds DEM and original 3 arcseconds DEM raster file. Next step was to convert those raster files to vector files (point data) which was done using the tool called "Raster to Point". This will create new individual point data files for those DEMs consisting of bottom elevation values. These values will be placed under the "grid code" field of the attribute table.
6) Next step was to calculate the coordinates for every individual points. To do this, two new fields X and Y were added to the attribute table for latitude and longitude respectively. Now, using the option known as "Calculate Geometry", from the attribute table, was used to calculate the coordinates for all the points. ArcGIS Pro automatically calculates and populates the fields X and Y with their respective latitude and longitude. This process was repeated for all the points data that was created.
7) Before merging all the points data, the attribute tables were adjusted so that all the files have same field names. Thus, the fields X, Y, and grid code were arranged accordingly, and all the other fields were deleted from the attribute tables.
8) After that all the point data files were merged using the tool "Merge", which created a single new point dataset consisting of all the points.
9) Now all the values from the attribute table of dataset created in step 8 were copied to a notepad file and saved.
10) Finally, we have created the required input file for bathymetry data which was then assigned to the "Mobile Bay EFDC Model". Figure 3.14 shows the EFDC+ bathymetry map of the Mobile Bay.

The Mobile Bay EFDC Model has 77585 curvilinear horizontal cells with 10 vertical water layers with minimum bottom elevation of -32.946 m and maximum bottom elevation of 50.761 m. The

vertical water layers are divided using SGZ: Uniform Layers with a minimum of 3 active layers as discussed in Chapter 3.2.5 with a total of 255058 number of 3D computational cells.

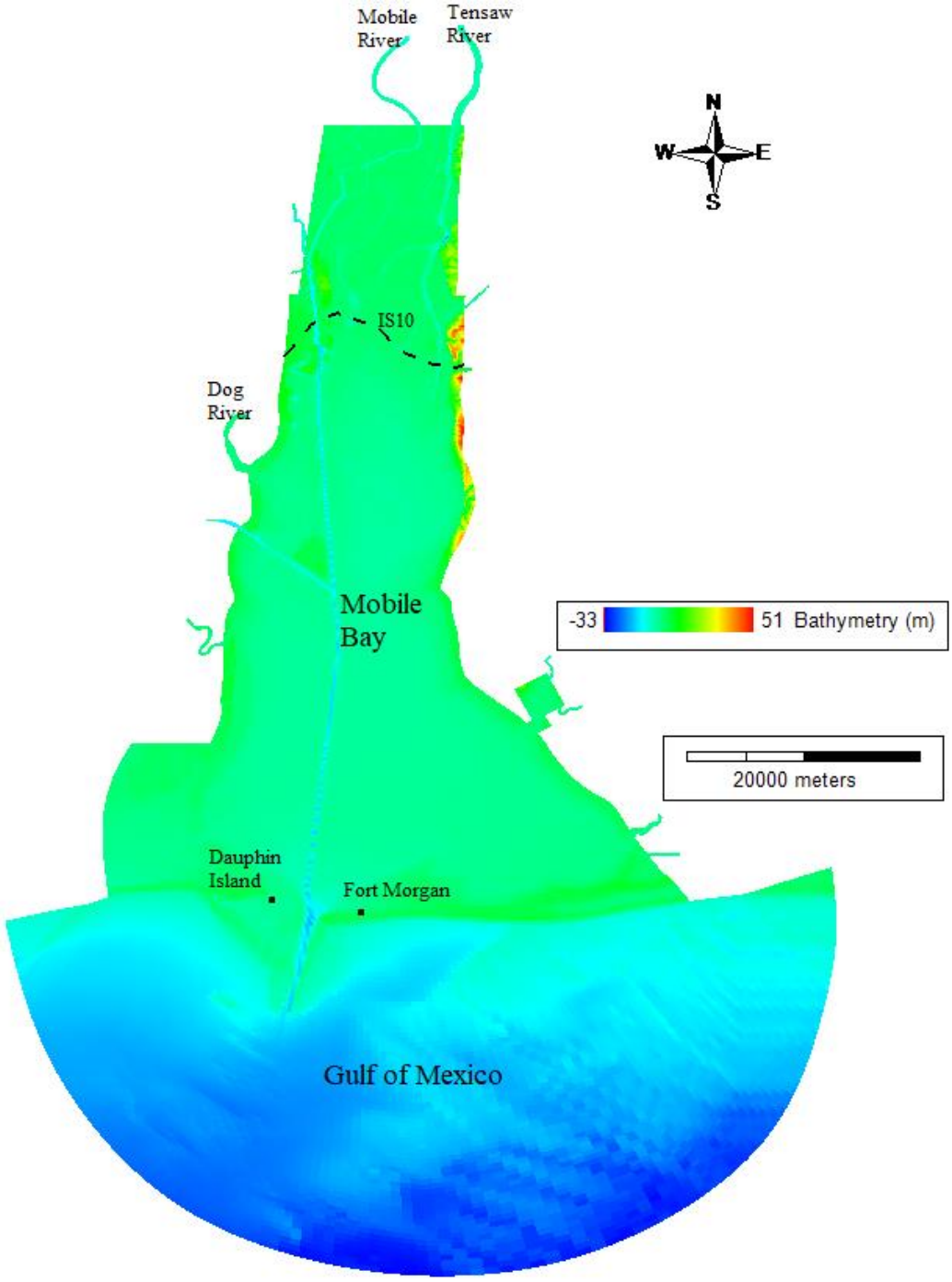

Figure 3.14 Bathymetry(m) map in Mobile Bay and Gulf of Mexico for Mobile Bay EFDC Model

3.6 INITIAL CONDITIONS

Initial Conditions (ICs) are required for the unsteady state simulations and it basically describes the state of the model at the very beginning of the simulation (Ji, 2008). For any unsteady simulations, the ICs should be properly assigned in such a way that they represent the real environment (as per the requirement of the study) of the waterbody at the start of the simulation period. IC are very important for proper representation of the real world scenario, and are required to solve hydrodynamics and water quality equations in EFDC+(Ji, 2008; Qin et al., 2022). IC are important for the modeling of large reservoirs and estuaries like Mobile Bay (having long retention time), the initial water surface elevation plays a critical role in the modeling study (Ji, 2008).

3.7 BOUNDARY CONDITIONS AND EXTERNAL FORCING DATA

Boundary conditions are the values of different parameters at the boundary of the water body to be studied such as flow boundary, open boundary. Boundary Conditions (BCs) and external forcings are the important driving forces which should be specified by the user, as they cannot be acquired from the mathematical equations, for the proper model simulations depending upon the nature of the study (Ji, 2008). In any modeling studies, it is necessary to identify the area of interest and include required ICs, BCs, and other forcings according to the necessity of the study (Ji, 2008; Qin et al., 2022). The boundary conditions include parameters such as flows, water levels, groundwater flows, etc. and the external forcing data includes parameters such as wind, atmospheric data, harmonic tides, etc. BCs are divided into two parts: horizontal BCs and vertical BCs. Horizontal BCs include solid BCs and open BCs. Solid BCs are no-slip conditions (flow is not permitted along and through the boundary) and free slip conditions (flow is permitted along but not perpendicular to the boundary) (Ji, 2008). Vertical BCs are the boundary conditions at the surface and bottom of the model. For this study, two flow boundaries for inflow and two open boundaries for water level are provided. Vertical BC equations in EFDC+ models are given as (DSI LLC., 2023):

$$q^2 = B_1^{\frac{2}{3}}\sqrt{t_{sx}^2 + t_{sy}^2} \quad l = 0, at\ z = 1 \tag{3.26}$$

$$q^2 = B_1^{\frac{2}{3}}\sqrt{t_{bx}^2 + t_{by}^2} \quad l = 0, at\ z = 0 \tag{3.27}$$

where,

B_1 is the turbulence closure constant (=10.1),

t_{bx}, t_{by} are the bottom friction drag in *x* and *y* directions,

t_{sx}, t_{sy} are the wind surface drag in *x* and *y* directions,

q^2 is the turbulent intensity (m^2/s^2).

3.7.1 FRESHWATER INFLOW

Reservoirs and estuaries have various sources of inflows such as rivers, watershed runoff, groundwater inflow, etc. It plays a vital role in hydrodynamics as well as water quality simulations. An inflow displaces the standing or slowly-moving water after entering the waterbody, and if there is no density difference between inflow and waterbody, mixing of these two water occurs rapidly whereas density differences results in turbulent mixing (Ji, 2008). Depending on the nature of the study, required inflows should be added to the model.

There are several inflows to the Mobile Bay, among which two major freshwater inflows are from Mobile River and Tensaw River. Both rivers are located on the northern part of the bay as shown in Figure 3.14. USGS gaging stations which are used to download the flow data for Mobile and Tensaw rivers are given in Table 3.1. Mobile River and Tensaw River flow data were downloaded for two different time periods: August 26 to September 26, 2004, and August 20 to September 20, 2020. The flow time series are shown in Figure 3.15 and Figure 3.16 which are later used for model calibration for two different storm events.

Table 3.1 USGS discharge stations with their coordinates

Station ID	**Station Name**	**Latitude**	**Longitude**
2470629	Mobile River at river mile 31.0 at Bucks	31°00'56"	88°01'15"
2471019	Tensaw River Nr Mount Vernon	31°04'01"	87°57'31"

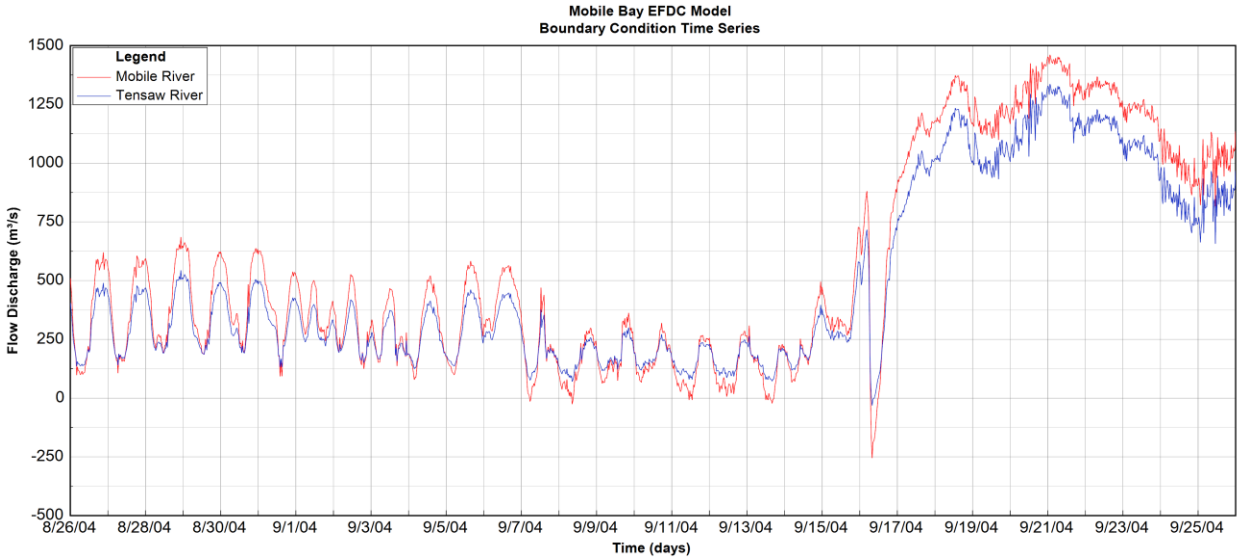

Figure 3.15 Flow time series for Mobile and Tensaw River from 26-Aug to 26-Sept 2004 for Mobile Bay EFDC Model (Hurricane Ivan 2004)

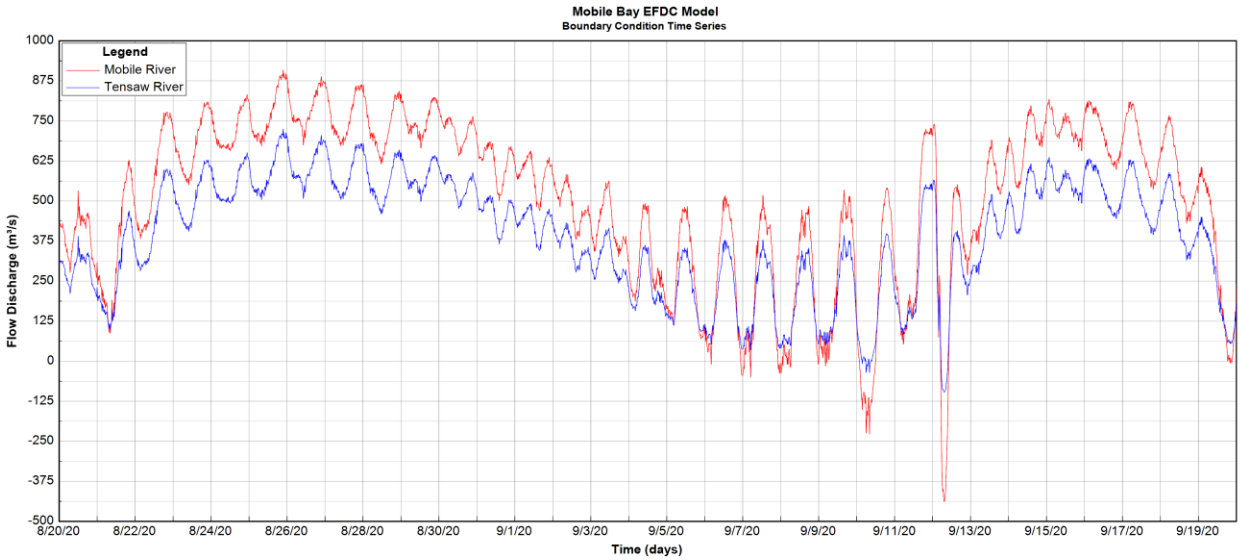

Figure 3.16 Flow time series for Mobile and Tensaw River from 20-Aug to 20-Sept 2020 for Mobile Bay EFDC Model (Hurricane Sally 2020)

3.7.2 WIND

Wind is a major forcing in large lakes, coastal water, and large estuaries which exerts a drag on the water surface resulting in waves and storm surges depending on the strength of the wind (Ji, 2008). The strong winds during the severe storm events can generate large wind shear stresses on the

water level causing large water level fluctuations resulting in disastrous impact on the low-lying coastal regions (Ji, 2008). The stress on the surface of water due to wind forcing is (DSI LLC., 2023):

$$\frac{1}{\rho_w}\begin{bmatrix}\tau_{sx}\\ \tau_{sy}\end{bmatrix} = C_D \frac{\rho_a}{\rho_w} W_s \begin{bmatrix}W_{sx}\\ W_{sy}\end{bmatrix} \tag{3.28}$$

$$W_s = \sqrt{W_{sx}^2 + W_{sy}^2} \tag{3.29}$$

where,

$W_s, W_{sx,} W_{sy}$ are the wind velocity (m/s) and its component in *x* and *y* directions,

τ_{sx}, τ_{sy} are the wind surface drag in *x* and *y* directions,

C_D is the wind drag coefficient,

ρ_a, ρ_w are the density of air and water.

EFDC+ offers four different options for calculating wind drag coefficients among which the default option has been used for this study which is calculated using the following equation (DSI LLC., 2023):

$$C_D = \begin{cases} 3.83111 \times 10^{-5} W_s^{-3} - 0.000308715 W_s^{-2} \\ +0.00116012 W_s^{-1} + 0.000899602, & W_s < 5 \text{ m/s} \\ -5.37642 \times 10^{-6} W_s^3 + 0.000112556 W_s^2 \\ -0.000721203 W_s + 0.00259657, & 5 \text{ m/s} \le W_s < 7 \text{ m/s} \\ -3.99677 \times 10^{-7} W_s^2 + 7.32937 \times 10^{-5} W_s \\ +0.000726716, & W_s \ge 7 \text{ m/s} \end{cases} \tag{3.30}$$

Wind is one of the major forces for this study as this is the major force exerting drag on the water surface resulting in waves and storm surge. The wind data consists of time series of windspeed (m/s) and wind direction. Wind direction is defined as the direction of the wind coming from. For example, a north wind is the wind generated from the north and blows towards the south. Most of the meteorological stations measure the wind direction in the same way and report the wind direction in compass direction or in degrees (from 0 to 360 degrees). The National Oceanic and Atmospheric Administration (NOAA) also measures the wind direction in a similar fashion.

According to NOAA, “The true direction from which the wind is blowing at a given location (i.e., wind blowing from the north to the south is a north wind). It is normally measured in tens of degrees from 10 degrees clockwise through 360 degrees. North is 360 degrees. A wind direction of 0 degrees is only used when wind is calm.”

By default, EFDC+ uses an opposite wind direction which means the wind blowing from north towards the south is a south wind instead of a north wind. Therefore, it is needed to properly adjust the wind direction in the EFDC+ using proper adjustment. If a wind direction from NOAA is more than 180 degrees, it needs to be subtracted by 180 degrees and if it is less than 180 degrees it needs to be added by 180 degrees. We can simply use the formula given below in a spreadsheet to transform the data to EFDC+ default sign convention.

$$=\text{IF}(\text{WDIR} > 180, \text{WDIR} - 180, \text{WDIR} + 180) \tag{3.31}$$

The following Figure 3.17 shows the wind direction before and after correction. The left side of the picture shows the wind direction angle of the wind blowing from which is the NOAA wind direction and right side of the picture shows the angle of the wind direction blowing towards which is the EFDC+ default.

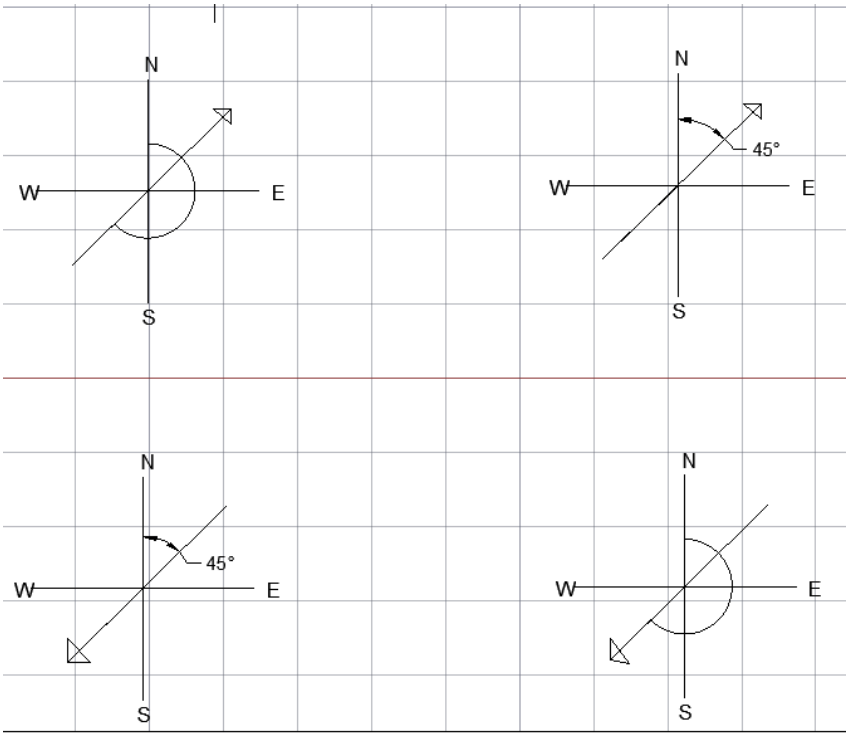

Figure 3.17 Direction of the wind blowing from (Left) and wind blowing towards (Right)

Before applying this sign convention, we need to make sure cell rotation angle of the grid cells are properly adjusted. The cell rotation angle for most of the grid cells should be in the range of -10° to +10° which can be identified in the 2DH view within the EFDC+ as shown below in Figure 3.18.

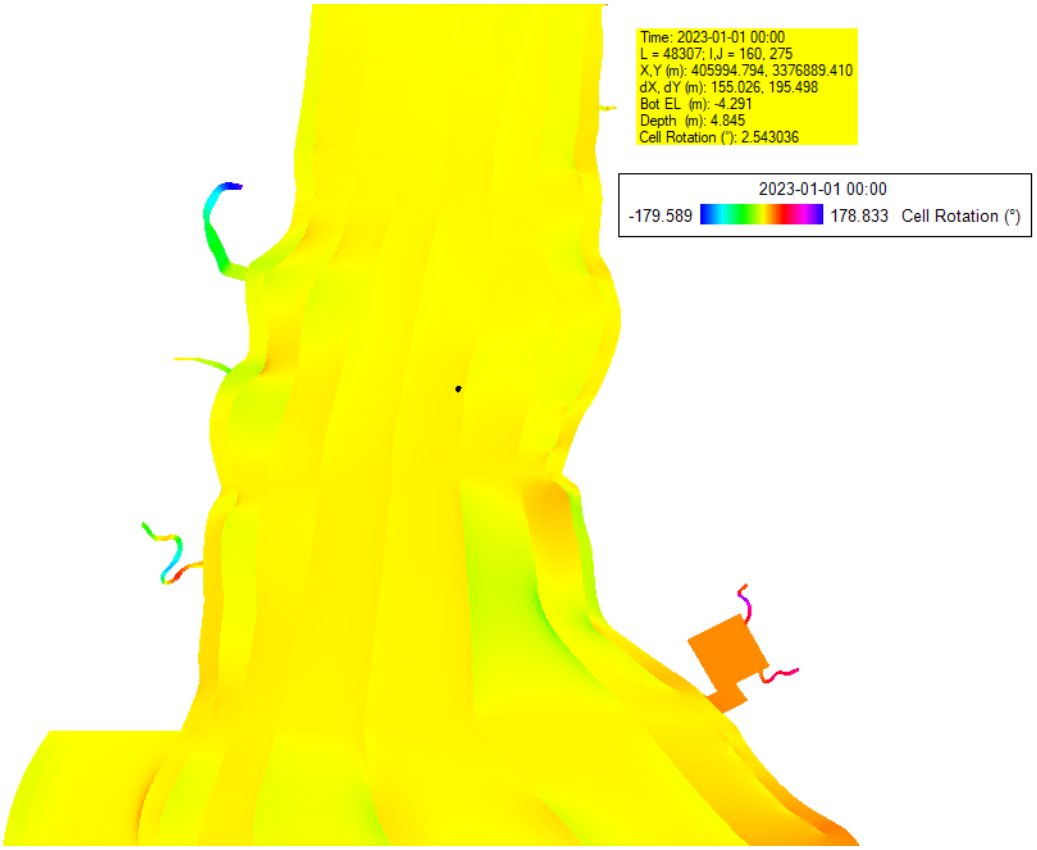

Figure 3.18 Cell rotation angle (Yellow region shows the angle within -10° to +10°) for Mobile Bay EFDC Model

There is another method to apply this sign convention in the EFDC+ itself while assigning the wind data under the External Forcing Data. There is a wind direction option under the parameters tab (Figure 3.19) of the wind data window where user can specify the numbers 0 or 1 or 2.

- 0 is for speed in (m/s) and direction (deg) towards (EE default)
- 1 is for speed in (m/s) and direction (deg) from
- 2 is for east velocity, north velocity (m/s)

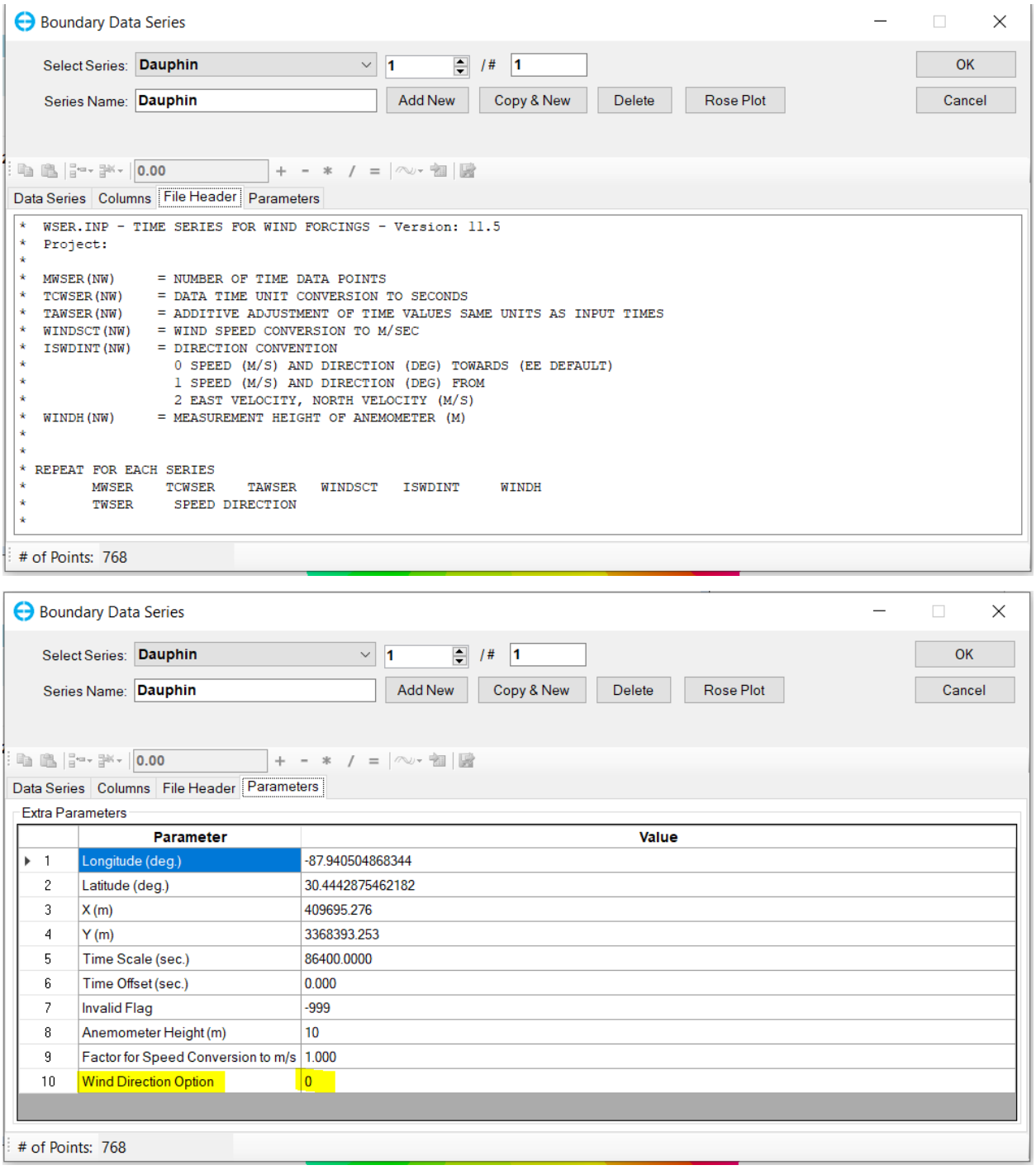

Figure 3.19 EFDC+ wind data windows for Mobile Bay EFDC Model

Dauphin Island station from NOAA was used to download the wind data for this study. The wind data were downloaded for two different time periods: August 26 to September 26, 2004, and August 20 to September 20. The wind data time series for wind speed and wind directions are shown in Figure 3.20 and Figure 3.21.

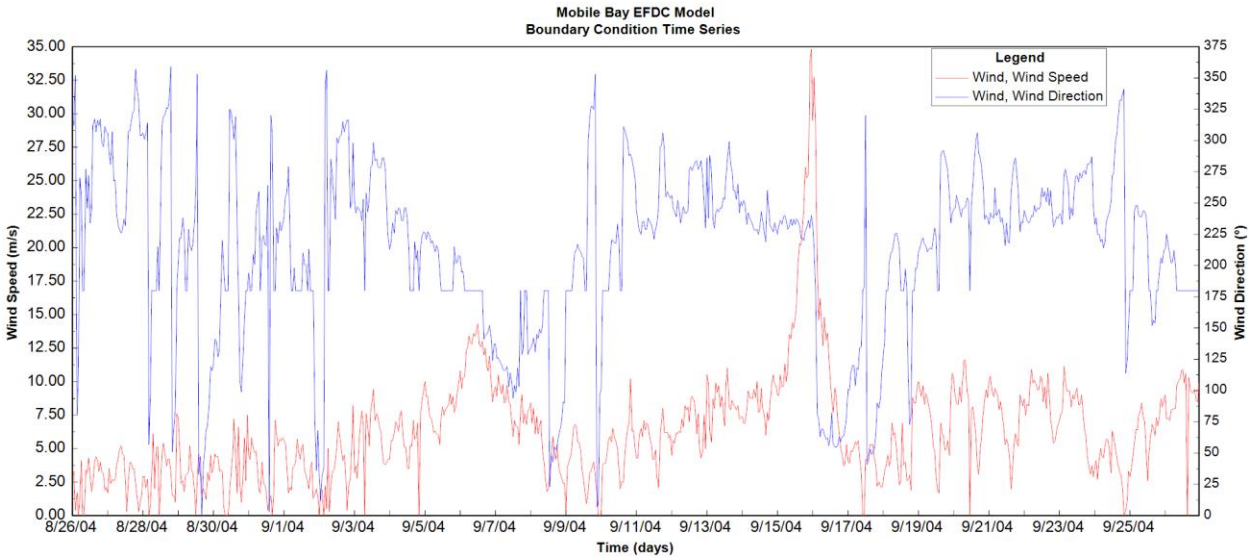

Figure 3.20 Wind data time series for Mobile Bay EFDC Model from 26-Aug to 26-Sept 2004 (Hurricane Ivan 2004)

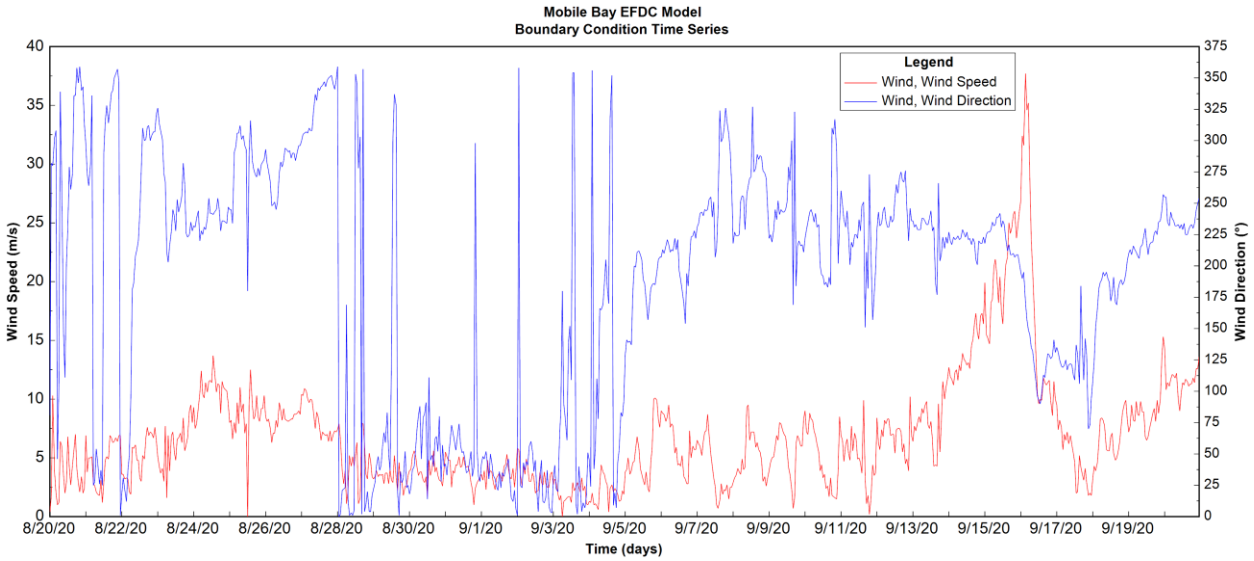

Figure 3.21 Wind data time series for Mobile Bay EFDC Model from 20-Aug to 20-Sept 2020 (Hurricane Sally 2020)

3.7.3 TROPICAL CYCLONES

The strong winds and rapid changes in atmospheric pressure during a tropical cyclone has a strong influence on the hydrodynamics and waves in the water body. Such type of storms can be added

in the EFDC+ Tropical Cyclone Module. The module allows the user to import and edit the cyclone data from different sources such as NOAA (National Oceanic and Atmospheric Administration of the United States), JTWC (Joint Typhoon Warning Center of the U.S Navy), and RSMC (Regional Specialized Meteorological Centre). Among the four different cyclone modeling approaches provided in EFDC+, the default approach developed by Holland (Holland, 1980) has been used for this study for Mobile Bay simulation model.

The tropical cyclones data was obtained from NOAA National Hurricane Center. The database provides hurricane track information from the year 1851. This dataset is available in comma-delimited text format and has information of latitude, longitude, maximum winds, radius of maximum winds, central pressure, direction, and forward moving speed for every 6 hours interval of the hurricane. The required data for Hurricane Ivan and Hurricane Sally was obtained from the dataset and the time zone was adjusted to central time (Universal time is 5 hours ahead of central time). The default EFDC+ tropical cyclone module by Holland (Holland, 1980) was used for simulating cyclones in this study.

3.7.4 OPEN BOUNDARY

The open boundary conditions in EFDC+ can be specified as a water level forcing as a time series data and/or harmonic forcings. Users can provide information related to the harmonic tides using the 234 predefined harmonic constituents available in the EFDC+. The time series of the harmonic tides is represented using the following sine and cosine combinations (DSI LLC., 2023):

$$\zeta(t) = \zeta_0(t) + a_0 + \sum_{k=1}^{N} [a_k \cos(\omega_k t) + b_k \sin(\omega_k t)] \quad (3.32)$$

where,

$\omega_k = \frac{2\pi}{T_k}$ is the angular speed of constituent k (radians/s),

T_k is the period constituent k (s),

t is the time in sec,

$\zeta(t)$ is the residual signal other than the periodic components (m),

a_0 is the mean value of the periodic components (m),

N is the number of the harmonic constituents,

a_k, b_k are the harmonic constant of the constituent k (m).

The southern part of the bay is open to Gulf of Mexico where flow exchange takes place. Open boundary conditions are assigned to the south most and southwest part of the model as shown in Figure 3.22. Time series data for water surface elevation obtained from NOAA Dauphin Island station was used as open boundary conditions.

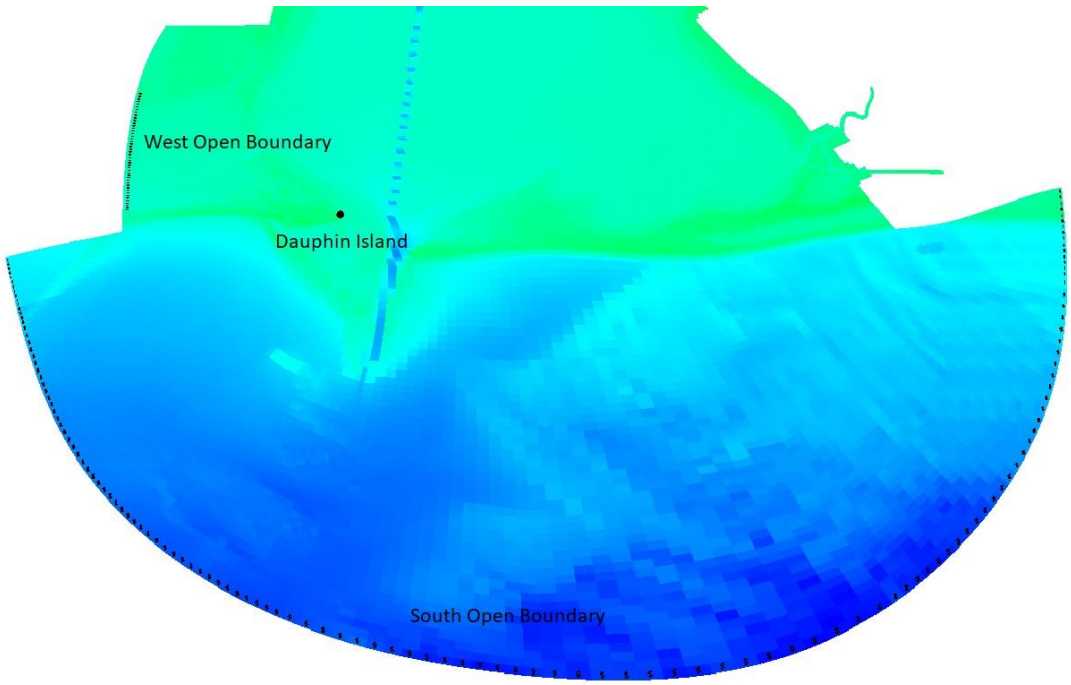

Figure 3.22 Open boundary location for Mobile Bay EFDC Model

From the Figure 3.22, we can see that the distance between the Dauphin Island station and the open boundary on the south is large ranging from 23 km to 50 km. Because of this, there was a small time shift between modeled results and observed water levels. Along with the time shift, there was also water level shift, and this shift was higher during the time when hurricane passes through the Dauphin Island Station. This case was similar during both the hurricane events: Hurricane Ivan and Hurricane Sally. The shift was calculated and the original water level data from the Dauphin Island station was adjusted for the shift. Since the open boundary on the west is not that far from Dauphin Island, and this open boundary is protected by the barrier island, the adjustment was only applied to the open boundary on the south. The original and adjusted water

level for two different time periods: August 26 to September 26, 2004, and August 20 to September 20, are shown in Figure 3.23 and Figure 3.24.

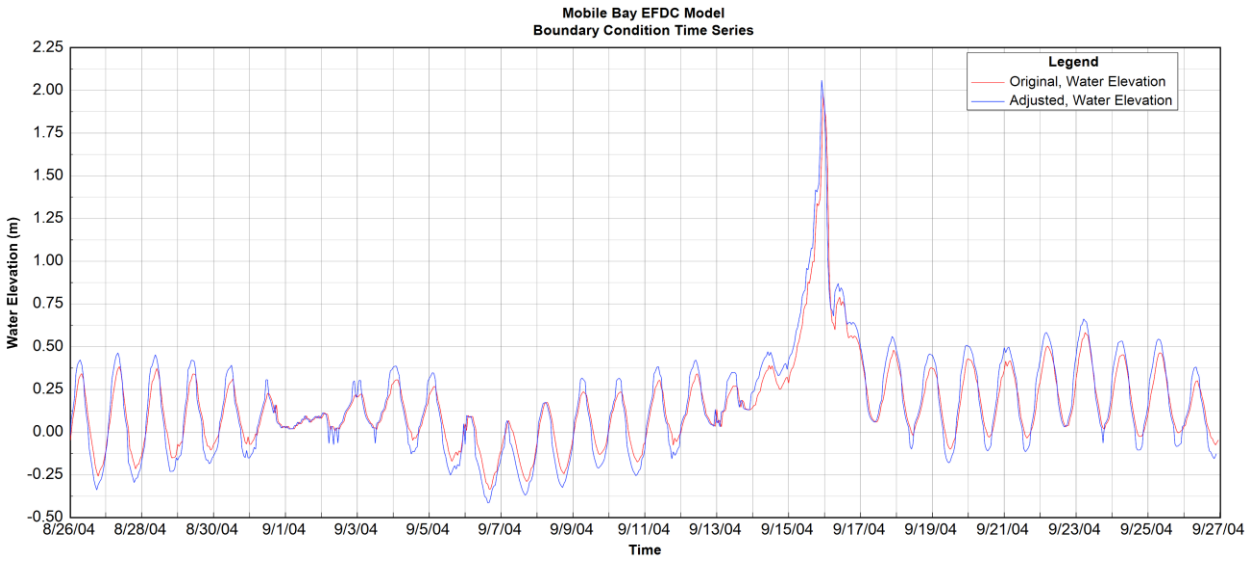

Figure 3.23 Original and adjusted water level time series for Mobile Bay EFDC Model from 26-Aug to 26-Sept 2004 (Hurricane Ivan 2004)

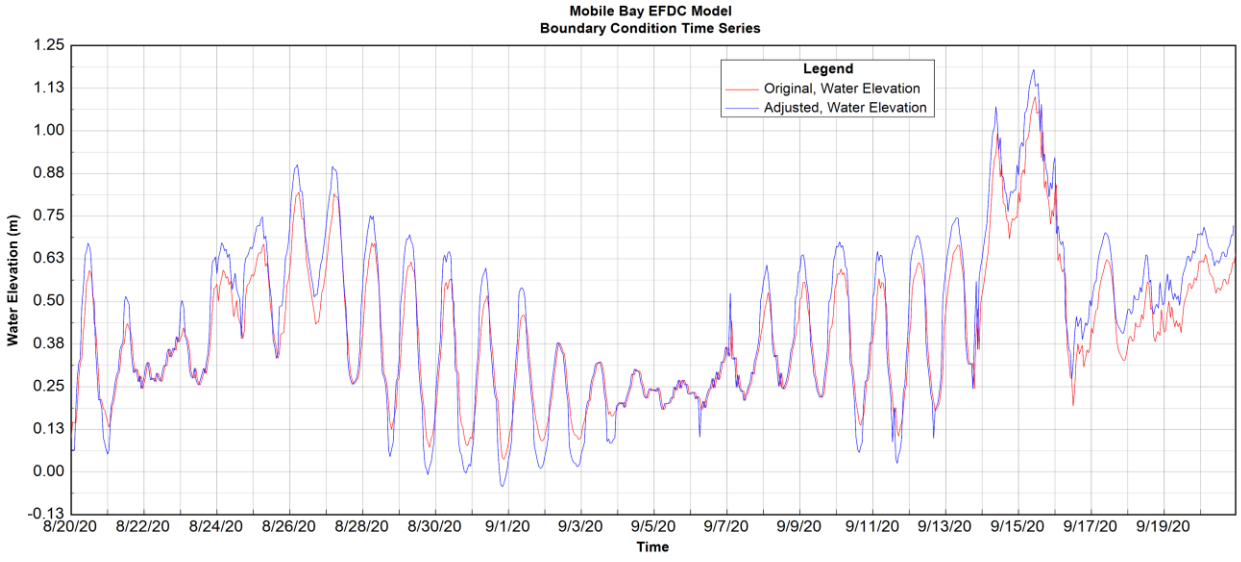

Figure 3.24 Original and adjusted water level time series for Mobile Bay EFDC Model from 20-Aug to 20-Sept 2020 (Hurricane Sally 2004)

3.8 MODEL CALIBRATION AND VERIFICATION

Calibration is one of the important processes in the generation of a good working model. It is the process of assigning the proper model parameters in such a way that the model functions as accurately as it would in a real natural scenario. A properly calibrated model will produce much more reliable and accurate results. The EFDC Mobile Bay model was calibrated for two different time periods for two hurricane events i.e., Hurricane Ivan (2004) and Hurricane Sally (2020). Monitoring stations at different locations withing the bay is shown in Figure 3.25 and the coordinates of those stations are given Table 3.2 and Table 3.3 .

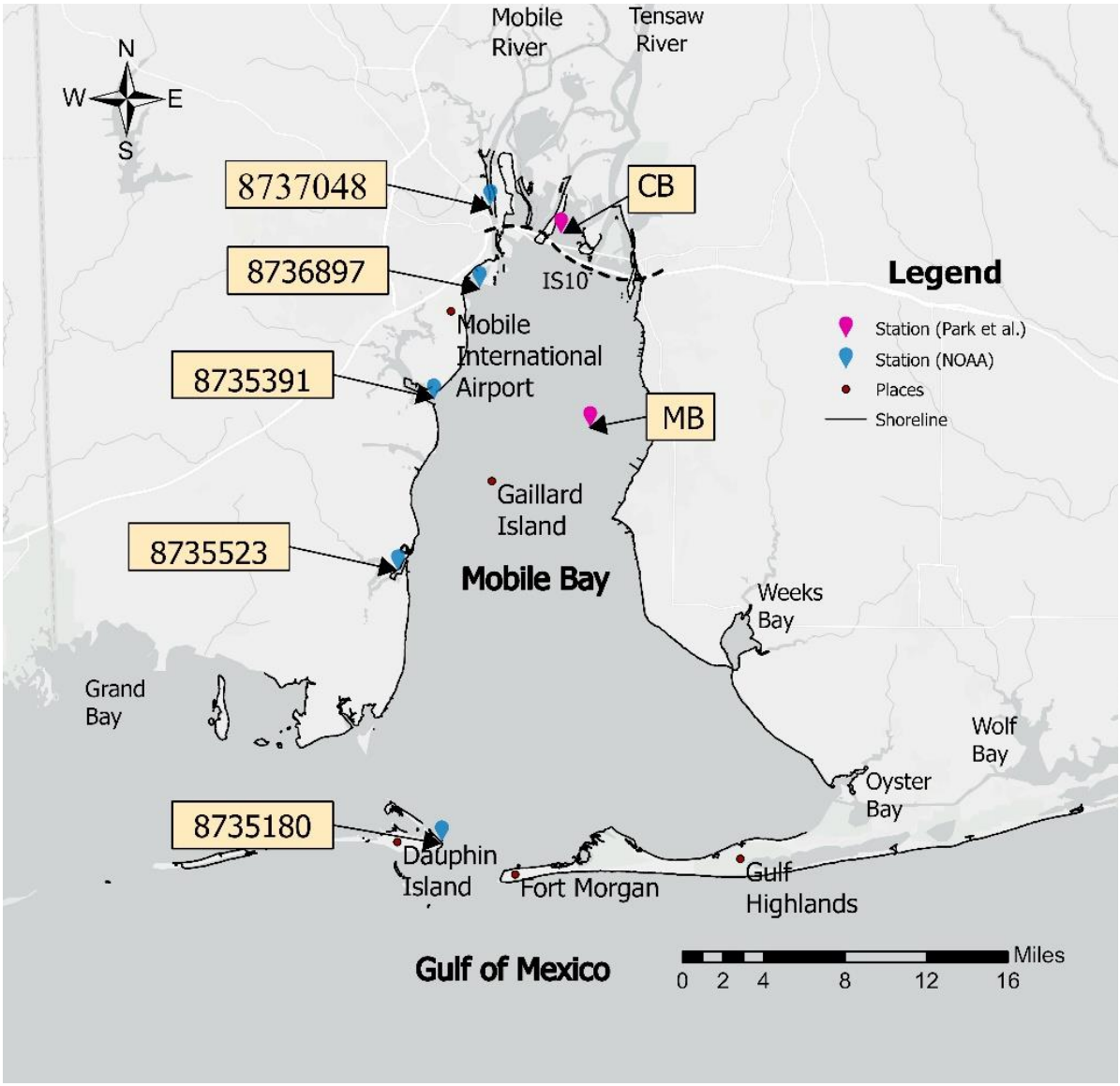

Figure 3.25 Mobile Bay with different places and monitoring stations at different locations

Table 3.2 NOAA Tides and Currents stations

Station ID	Station Name	Latitude	Longitude
8735180	Dauphin Island	30° 15.0 N	88° 4.5 W
8735523	East Fowl River Bridge	30° 26.6 N	88° 6.8 W
8735391	Dog River Bridge	30° 33.9 N	88° 5.3 W
8736897	Coast Guard Sector Mobile	30° 39.0 N	88° 3.5 W
8737048	Mobile State Docks	30° 42.3 N	88° 2.4 W

Table 3.3 Monitoring Stations (Park et al., 2007)

Station ID	Station Name	Latitude	Longitude
MB	Northeastern Mobile Bay	30°32.825"	87°57.354'
CB	Chocolatta Bay	30°41.114'	87°58.879'

3.8.1 WATER LEVEL CALIBRATION

Water level calibration is a very essential step for the scope of this study, as we are looking at the changes in water level during storm events. Thus, two hurricane events are used for calibration to increase model accuracy. The model was calibrated for water surface elevation using the observed data from the Dauphin Island monitoring station and the simulated water surface elevation results were verified using available data at different monitoring stations at various location throughout the Mobile Bay. The calibration results for water surface elevation for two events are discussed below.

A. Hurricane Ivan

The EFDC model was calibrated for Hurricane Ivan period from August 26, 2004 (Julian day 238) to September 26, 2004 (Julian day 269) for water surface elevation. It was calibrated with observed data at three different locations around the bay. Among the five NOAA monitoring stations around Mobile Bay (Table 3.2) only Dauphin Island station has the data for WSEL for this time. There was a study conducted, in 2007, to study the effects of hurricane Ivan in the Mobile Bay (Park et

al., 2007). In this study, time series data collected from four mooring stations, in the inner part of the bay, were used to observe the water surface level changes during the passage of Hurricane Ivan in 2004. Data obtained from two of the stations used in the paper (Park et al., 2007) is used for calibration. The coordinates of all the stations used for calibration are shown in Table 3.2 and Table 3.3 and locations are shown in Figure 3.25. Simulated and observed water elevation plots and the correlation plots are shown in Figure 3.26 to Figure 3.29.

As we can see from the Figure 3.26, Figure 3.28, and Figure 3.29, the observed data points for Northeastern MB and Chocolotta Bay are only available for seven days (13 September to 20 September, 2004) with relatively fewer number of data points as compared to the Dauphin Island station, where observed water surface elevation data points are available for whole month of calibration period. From the Figure 3.26 and Figure 3.27, we can see that there is a good agreement between the modeled results and the observed data at Dauphin Island station with correlation coefficient (R), coefficient of determination (R^2), and root-mean-square error (RMSE) of 0.98, 0.96, and 0.05 respectively. Even though the data was unavailable for whole calibration period at Northeastern MB and Chocolotta CB, we can see some similarity in water level pattern between modeled results and the available observed data (Figure 3.28 and Figure 3.29) with some shifts which was higher as we move north. The correlation coefficient (R), coefficient of determination (R^2), and root-mean-square error (RMSE) for Northeastern Mobile Bay station are 0.62, 0.38, and 0.34 respectively. The correlation coefficient (R), coefficient of determination (R^2), and root-mean-square error (RMSE) for Chocolotta Bay CB station are 0.28, 0.08, and 0.51 respectively. The lower values of R, R^2, and RMSE for Northeastern MB and Chocolotta CB are due to lack of observed data points. The statistics for all three stations are shown in Table 3.4.

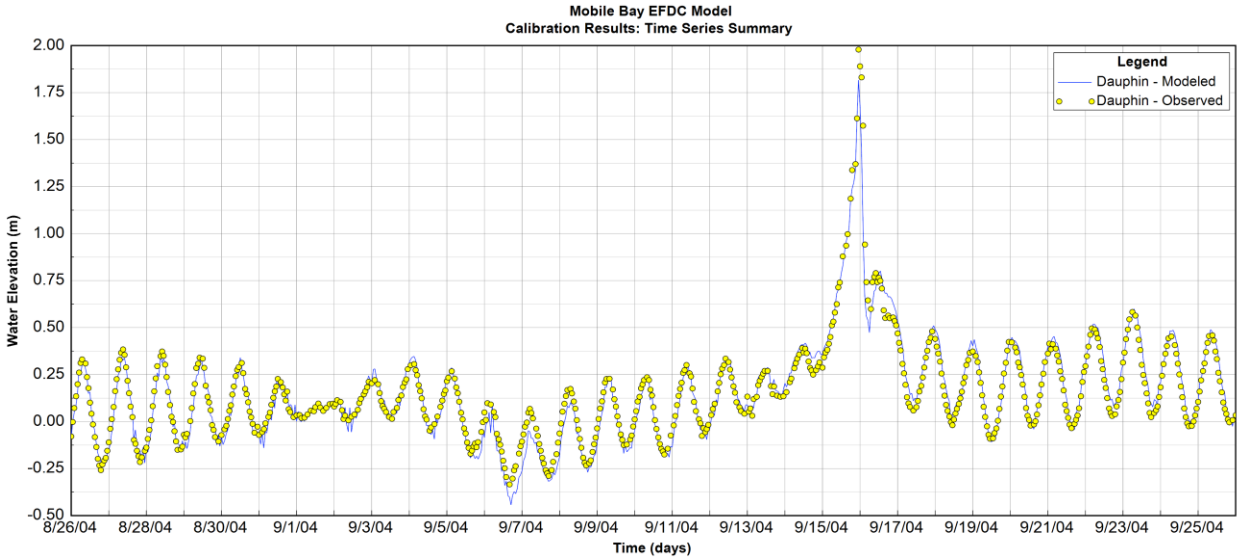

Figure 3.26 Modeled Results Vs Observed Data for water elevation at Dauphin Island station (Hurricane Ivan 2004)

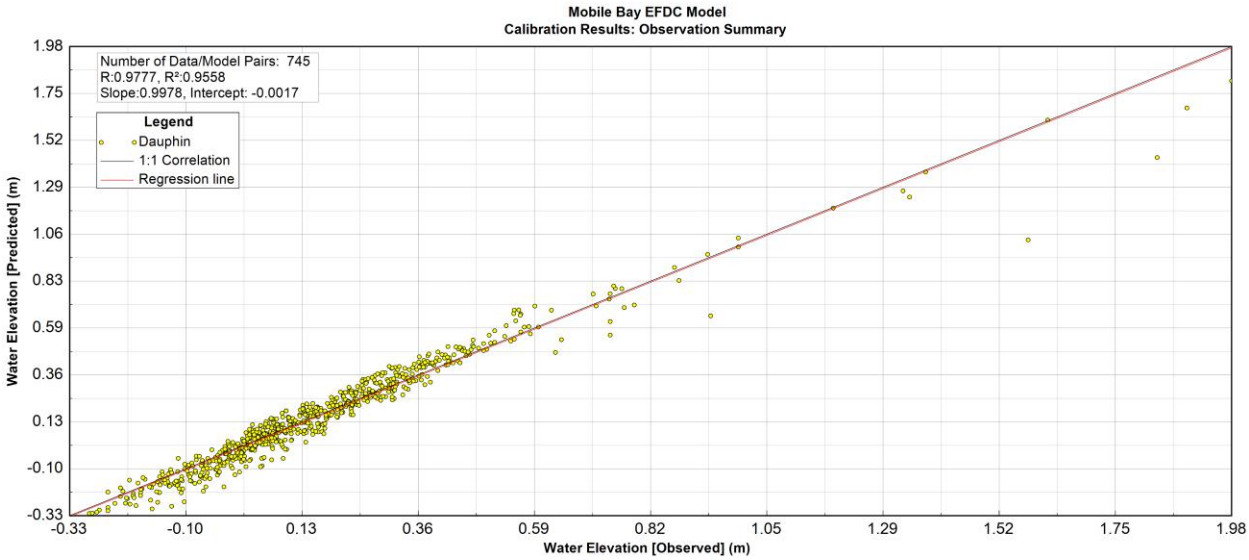

Figure 3.27 Correlation and regression line for modeled results vs observed data for water elevation at Dauphin Island station (Hurricane Ivan 2004)

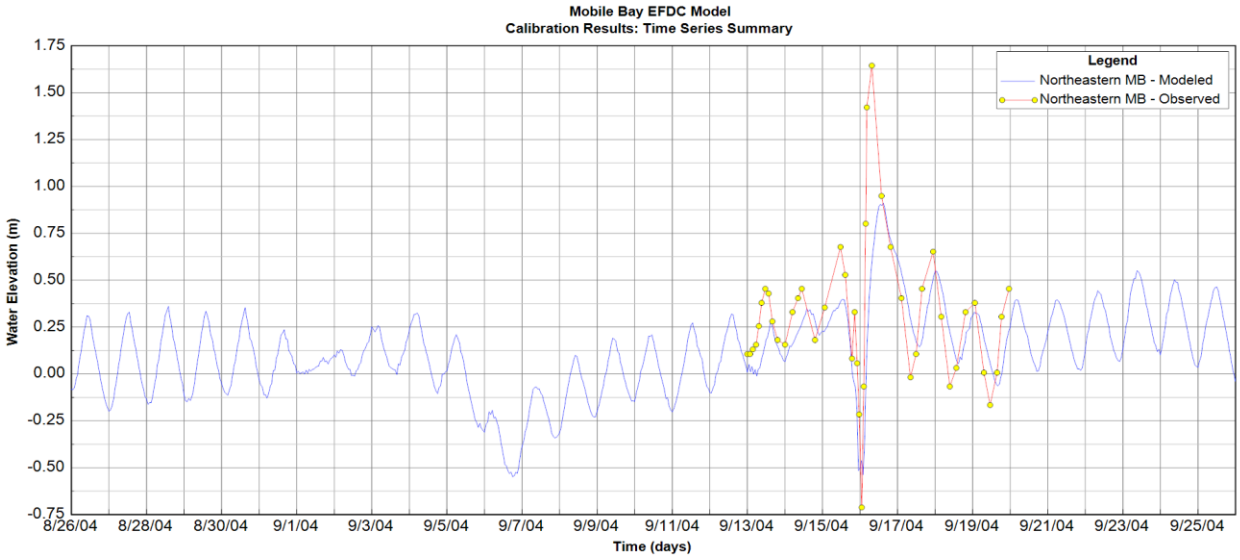

Figure 3.28 Modeled Results Vs Observed Data for water elevation at Northeastern MB station (Hurricane Ivan 2004)

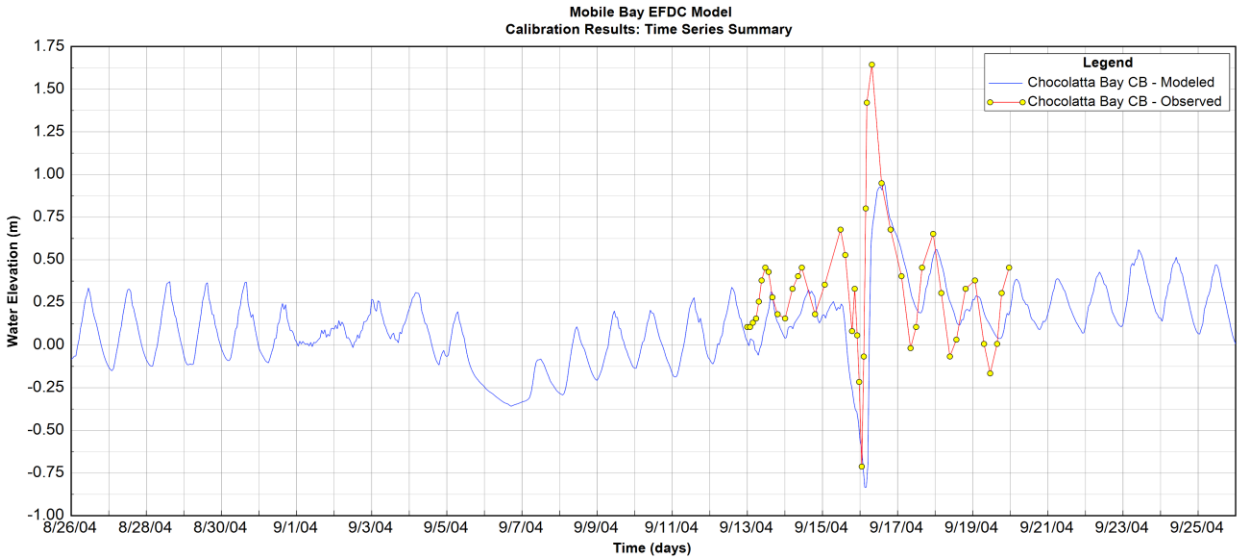

Figure 3.29 Modeled Results Vs Observed Data for water elevation at Chocolotta Bay CB station (Hurricane Ivan 2004)

Table 3.4 Statistics for model calibration for Hurricane Ivan at three different stations

Station ID	Station Name	Correlation coefficient, R	Coefficient of determination, R^2	RMS Error
8735180	Dauphin Island	0.98	0.96	0.05
MB	Northeastern Mobile Bay	0.62	0.38	0.34
CB	Chocolatta Bay	0.28	0.08	0.51

B. Hurricane Sally

The EFDC model was also calibrated for Hurricane Sally period from August 20, 2020 (Julian day 232) to September 20, 2020 (Julian day 263) for water surface elevation. It was calibrated with observed data at five different locations around the bay. As this is a recent event, all the five NOAA monitoring stations in Mobile Bay have WSEL time series data. The coordinates of these stations are mentioned in Table 3.2 and the location are shown in Figure 3.25. Simulated and observed water elevation plots and correlation plots are shown in Figure 3.30 to Figure 3.36 below at all five stations.

From the Figure 3.30 and Figure 3.31, we can see that there is a good agreement between the modeled results and the observed data at Dauphin Island station with correlation coefficient (R), coefficient of determination (R^2), and root-mean-square error (RMSE) of 0.96, 0.92, and 0.05 respectively. There is a good agreement between modeled results and observed data at other four stations as well with small shifts as we move towards the north which can be seen in Figure 3.32 to Figure 3.35. The coefficient of determination (R^2) between modeled results and observed data at East Fowl River Bridge, Dog River Bridge, Coast Guard Sector Mobile, and Mobile State Docks are 0.92, 0.79, 0.80, 0.78, and 0.61 respectively. The statistics for all five stations are shown in Table 3.5. There is some shift as we move towards the north for both the hurricane events which might have been caused due to the increasing distance from the southern open boundary.

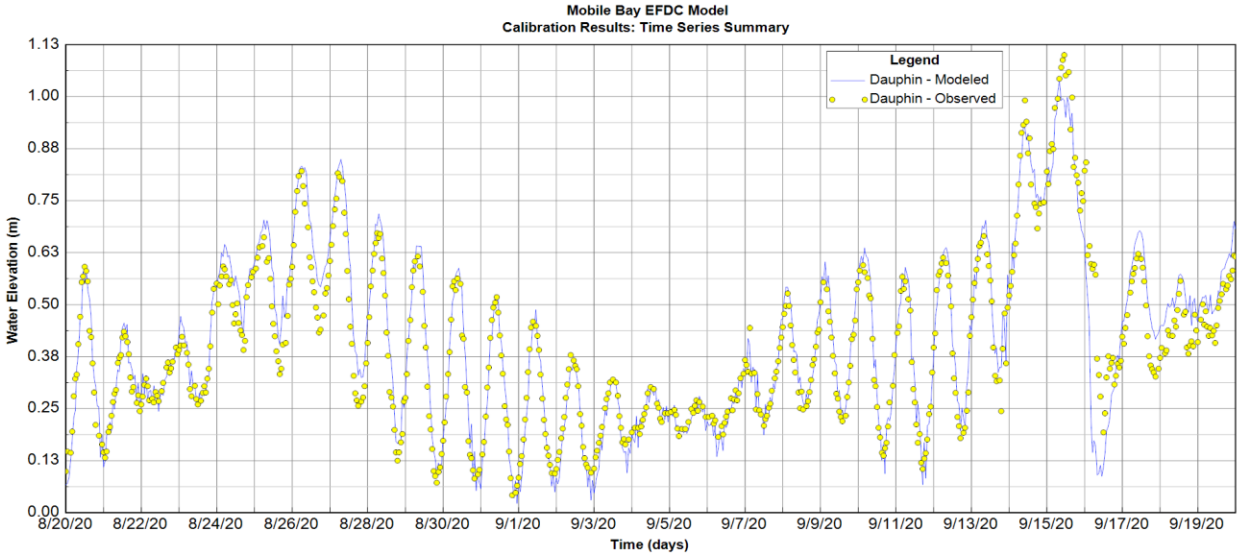

Figure 3.30 Modeled Results Vs Observed Data for water elevation at Dauphin Island station (Hurricane Sally 2020)

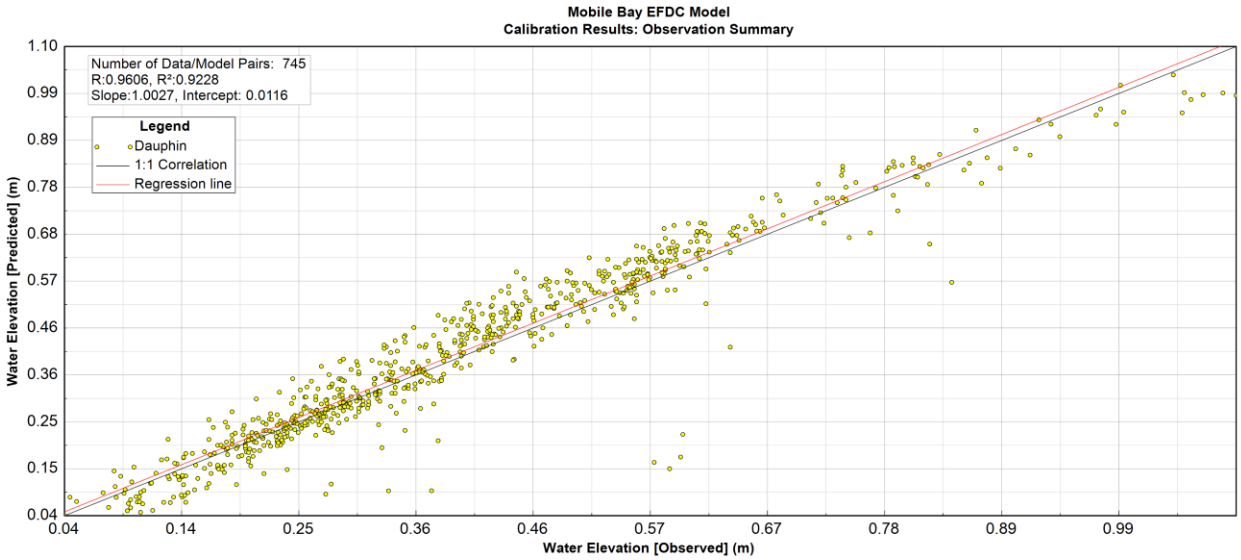

Figure 3.31 Correlation and regression line for modeled results vs observed data for water elevation at Dauphin Island station (Hurricane Sally 2020)

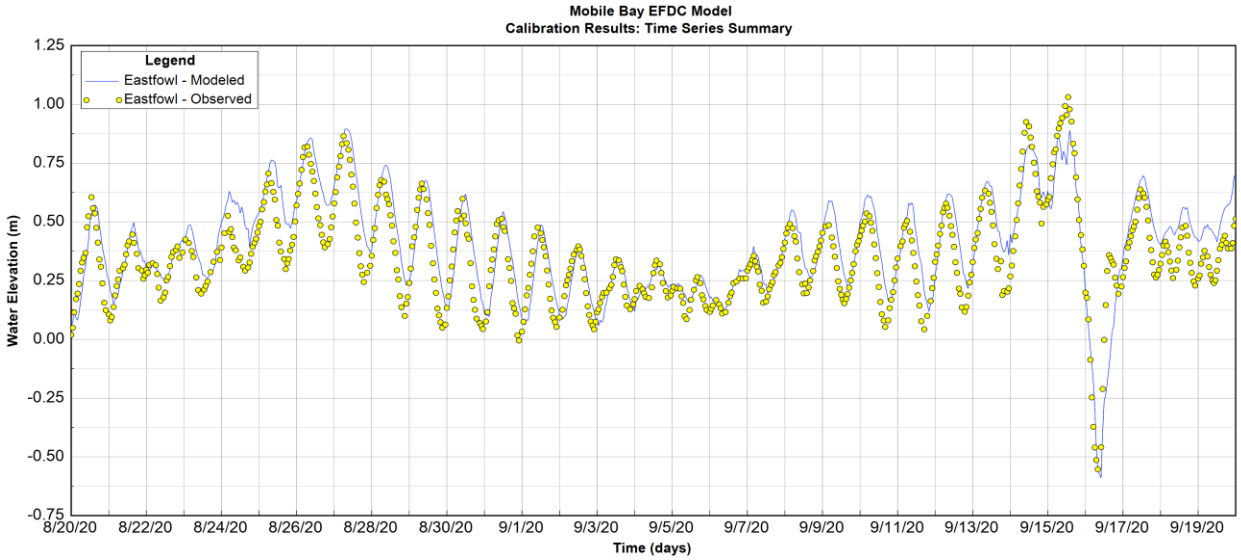

Figure 3.32 Modeled Results Vs Observed Data for water elevation at East Fowl River Bridge (Hurricane Sally 2020)

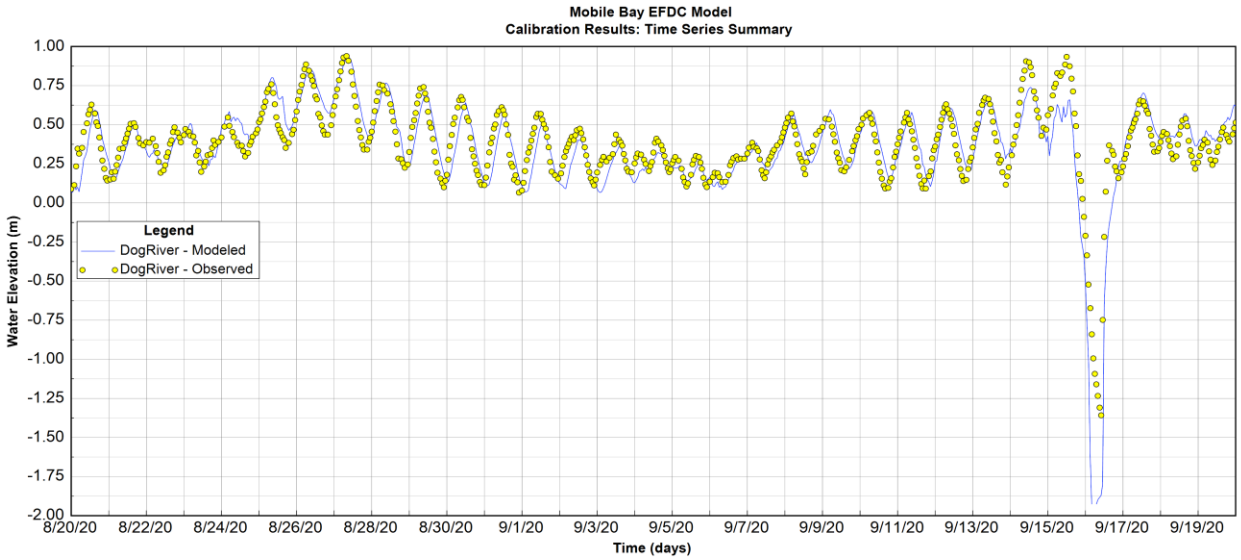

Figure 3.33 Modeled Results Vs Observed Data for water elevation at Dog River Bridge (Hurricane Sally 2020)

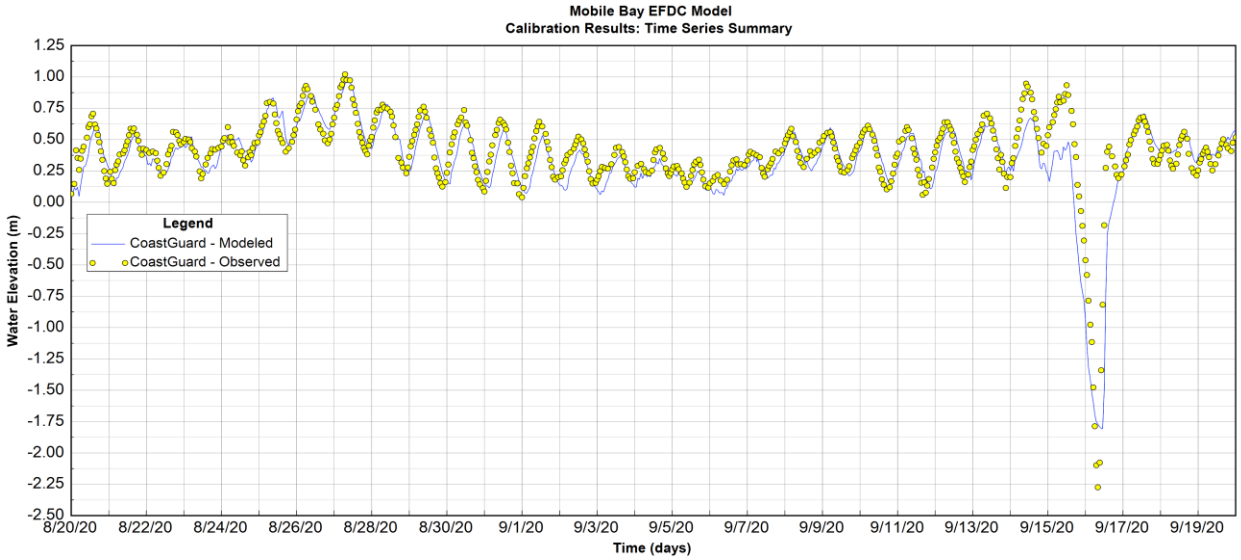

Figure 3.34 Modeled Results Vs Observed Data for water elevation at Coast Guard Sector Mobile (Hurricane Sally 2020)

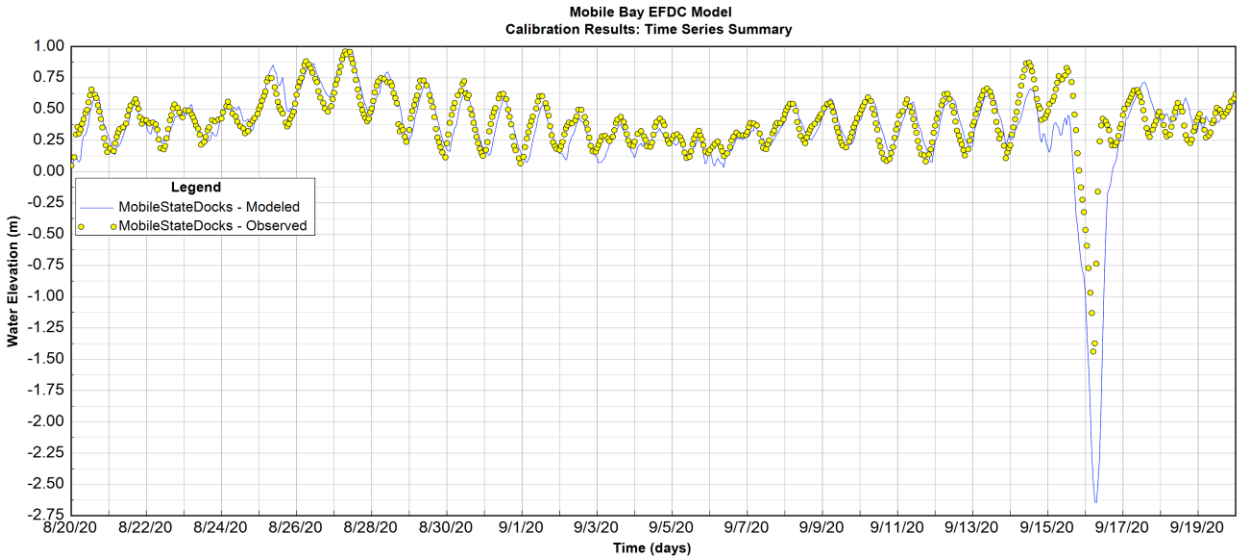

Figure 3.35 Modeled Results Vs Observed Data for water elevation at Mobile State Docks station (Hurricane Sally 2020)

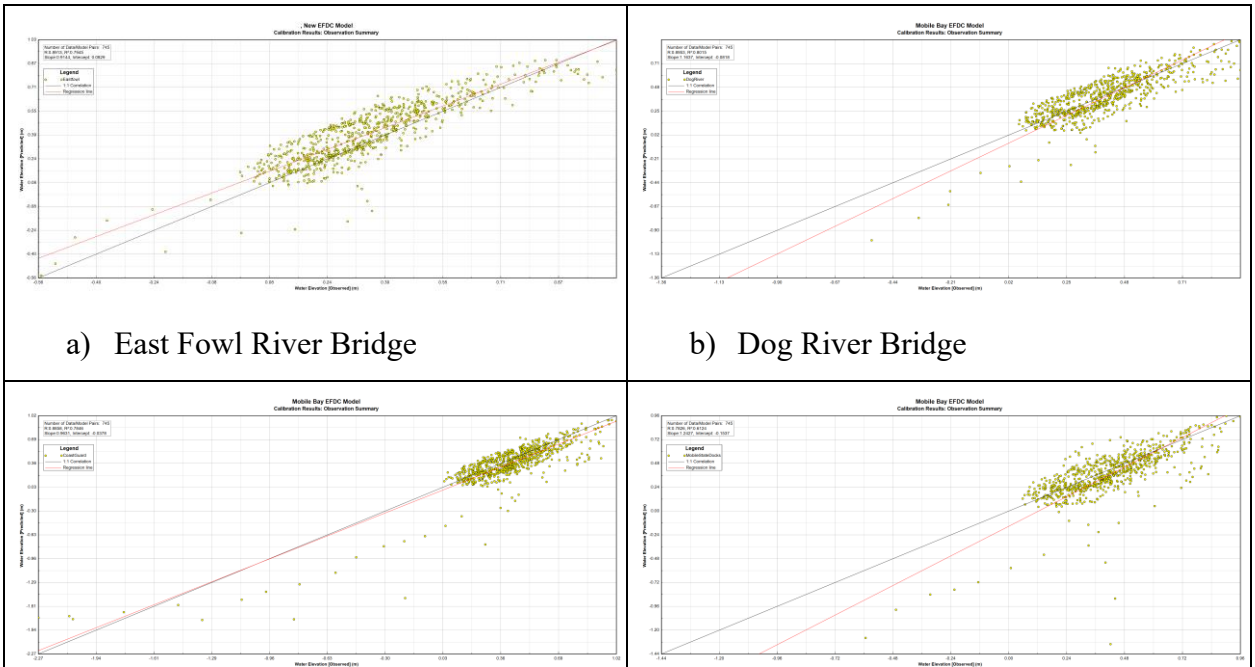

a) East Fowl River Bridge

b) Dog River Bridge

c) Coast Guard Sector Mobile

d) Mobile State Docks

Figure 3.36 Correlation and regression line for modeled results vs observed data for water elevation (Hurricane Sally 2020) at various stations: a) East Fowl River Bridge, b) Mobile State Docks, c) Coast Guard Sector Mobile, and d) Dog River Bridge

Table 3.5 Statistics for model calibration for Hurricane Sally at five different stations

Station ID	**Station Name**	**Correlation coefficient, R**	**Coefficient of determination, R^2**	**RMS Error**
8735180	Dauphin Island	0.96	0.92	0.05
8735523	East Fowl River Bridge	0.89	0.79	0.11
8735391	Dog River Bridge	0.9	0.8	0.15
8736897	Coast Guard Sector Mobile	0.89	0.78	0.16
8737048	Mobile State Docks	0.78	0.61	0.24

CHAPTER 4. MODELING SCENARIOS AND RESULTS

4.1 INTRODUCTION

The impacts of hurricanes are based on the different hurricane parameters such as hurricane track, maximum wind speed, radius of maximum wind speed, forward speed, and central pressure. These are the hurricane parameters that are required for modeling a hurricane in EFDC+. For this study, we have worked on extracting these parameters based on two different methods: First one is based on the information gathered from Hazus application, and second one is based on the hypothetical parameters based on Saffir-Simpson Hurricane categories. The main purpose for making different scenario runs is to identify the impact of different hurricanes parameters and how would the model react after the implementation of different NNBFs. This will basically provide information on the impacts of different hurricane scenarios on the coast of Mobile Bay before and after the implementation of NNBFs.

The model duration for the all the scenario runs were kept as 10 days. For both modeling scenarios, the initial conditions such as bathymetry and water surface elevation (WSEL), and boundary conditions such as inflows and water level are kept identical whereas hurricane parameters and wind data were calculated based on modeling scenarios. The different boundaries that are used for the scenario runs are discussed below.

a. Bathymetry and WSEL

The same bathymetry and initial water surface elevation was used for all the scenario runs as that was used in model calibrations. For some visualization of the impacts of hurricanes after the implementation of NNBFs, bathymetry of some region of the Mobile Bay were altered which are discussed further in the report.

b. Flow Boundary

The flow boundaries are kept identical for all the scenario runs. Based on the data from NHC season, it can be identified that the Atlantic hurricane season runs from June 1 to November 30 as shown in Figure 2.1, which shows the peak of the Atlantic Hurricane season to fall around mid-September. The time-period of the two hurricanes, Hurricane Ivan (2004) and Hurricane Sally (2020) that were used for calibration of this model, was around mid-September as well. Since 2020

being the latest year, we have adopted the flow data from September 10, 2020, to September 20, 2020, for all the scenario runs. The time series for the flow data for Tensaw River and Mobile River are shown in Figure 4.1.

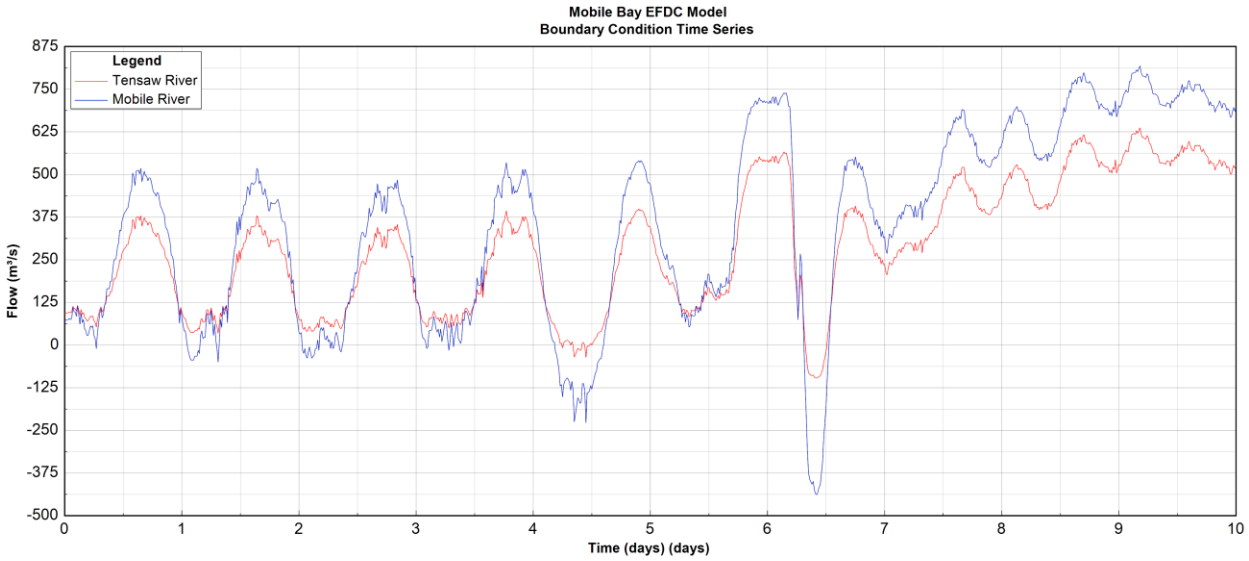

Figure 4.1 Flow boundary time series for Mobile and Tensaw rivers

c. Water Level

The water level boundary conditions for all the scenario runs were developed using harmonic constituents. There are eight major harmonic constituents that are commonly used as a tidal forcing for storm surge simulations are K1, O1, P1, Q1, M2, S2, N2, and K2 (Moore & Torres, 2020). Among these eight major constituents K1, O1, P1, and Q1 are four diurnal constituents, and M2, S2, N2, and K2 are four semi-diurnal constituents (Moore & Torres, 2020). The dominant harmonic constituents among these eight major constituents in the Mobile Bay region are K1 and O1, which are also called Lunisolar diurnal constituents as the generating force behind these constituents are Moon and Sun (Devkota et al., 2013). For this study, the harmonic constituent's data were gathered using the Dauphin Island station from NOAA. Table 4.1 shows the speed, amplitude, phase, and generating force for all eight harmonic constituents and Figure 4.2 shows the plot for harmonic times series used for this study.

Table 4.1 Major harmonic constituents for Mobile Bay

ID	Name	Speed (deg/hr.)	Amplitude (m)	Phase, Sec	Generating Force
24	**Q1**	13.398661	0.03	95760	Moon
28	**O1**	13.943036	0.138	150840	Moon
40	**P1**	14.958931	0.043	179640	Sun
43	**K1**	15.041069	0.141	182160	Moon, Sun
80	**N2**	28.43973	0	0	Moon
92	**M2**	28.984104	0.015	477000	Moon
108	**S2**	30	0.007	422280	Sun
111	**K2**	30.082137	0.005	802080	Moon, Sun

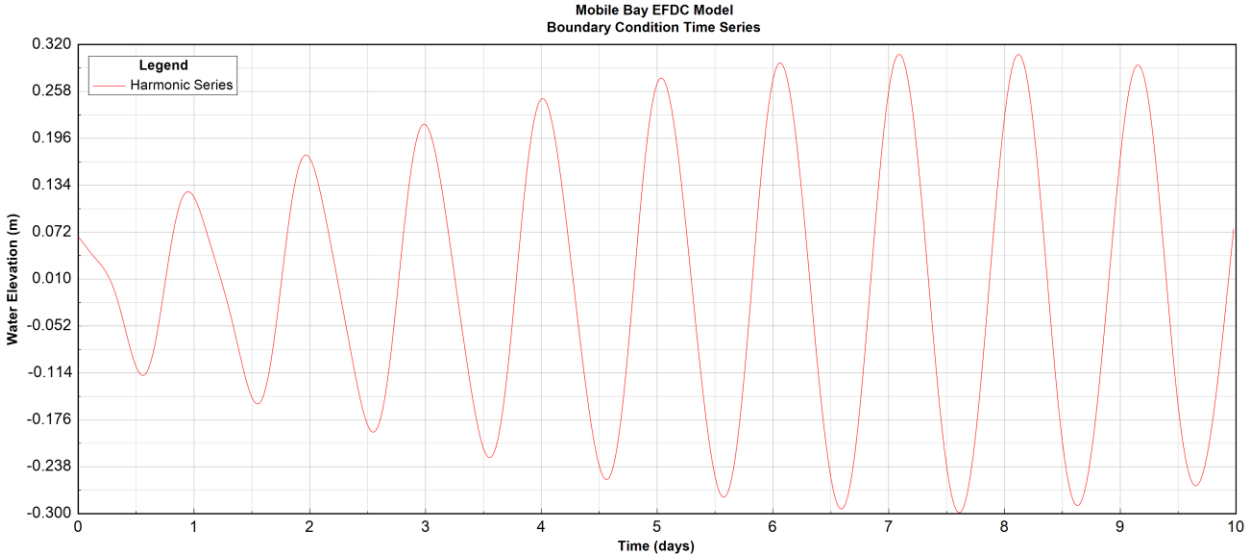

Figure 4.2 Harmonic time series plot

d. Wind

The wind data for different modeling scenarios were calculated based on the wind data from Hurricane Sally. Three types of methods were analyzed to figure out the best adjustment method to be used for different Hurricane scenarios. The wind data for Hurricane Sally was used from the NOAA Dauphin Island station.

Steps involved:

1. First, 10 days Hurricane Sally wind data was plotted to study the increment in wind during the hurricane period in Mobile Bay.

2. This data was analyzed to find out the windspeed at start, peak, and end of the Hurricane Sally period.
3. For this analysis, a category 5 hurricane maximum sustained wind speed was used to compare linear adjustment, constant adjustment, and factor adjustment for the start, peak, and end of hurricane period which were identified in step 2.
4. For linear adjustment, the wind speed values were linearly interpolated to the maximum wind speed for a category 5 hurricane.
5. For constant adjustment, constant value was first calculated by subtracting the Hurricane Sally maximum wind from a category 5 hurricane maximum wind. This constant value was then added to the Hurricane Sally wind data to get the wind data for a category 5 hurricane.
6. For factor adjustment, a factor was calculated by dividing the maximum Hurricane Sally wind from maximum category 5 hurricane wind. This factor was then multiplied with Hurricane Sally wind data to get the wind data for a category 5 hurricane.
7. The comparison plot of these methods is shown in Figure 4.3.
8. The factor method provided more realistic wind data as compared to the other two methods, so the factor method was selected for the wind data calculation for all the scenario runs.

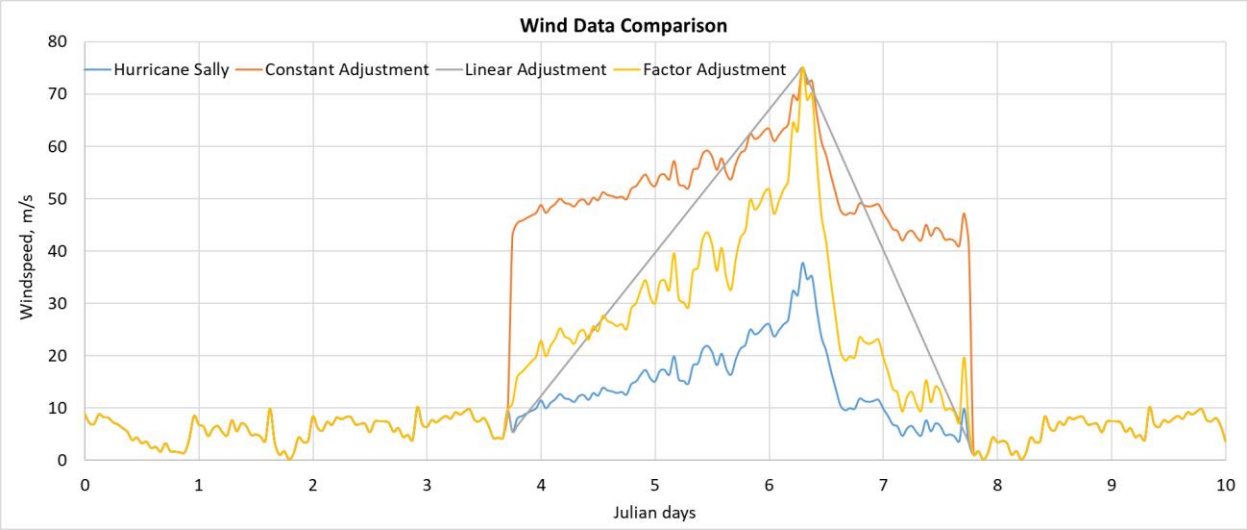

Figure 4.3 Comparison plot for different methods on wind data

The calibrated model was then used for carrying out all the different testing as discussed earlier. The input data was then used to set up the individual EFDC+ model for each test. For the modeling

scenario 1, seven individual EFDC+ models were prepared for each storm event provided by Hazus. And for the modeling scenario 2, five individual EFDC+ models (fifteen models in total) were prepared for each hurricane direction. These were the primary model simulations for both modeling scenarios which were used to study the impacts of hurricane in terms of maximum inundation of coastal regions for different tests.

After the completion of the primary simulation runs, all the coastal cells having positive bottom elevation were selected in EFDC+ (23,225 cells). These cells are along the shorelines and typical dry cells since they are above the mean sea level. These coastal shoreline cells with positive bottom elevation are shown in Figure 4.4. On the east side of Mobile Bay, there are some steep slopes with the elevation increase to 51 m. We can see that eastern coast of the bay sits at relatively higher elevations (maximum elevation of 51 m on the northern part) with steep slopes as compared to the western coast of the bay (with maximum elevation of around 9 m). This makes the western coast of the bay vulnerable to hurricane flooding as compared to the eastern coast on the northern part of the bay. On the southern part of the bay, both eastern and western coast have similar ground elevation.

The simulated time series data for the water depths, in meters (m), for all the coastal shoreline cells were then exported as a text file. This text file contains the hourly water depths data for the simulation period of 10 days for each of the coastal cells. This text file was then imported into an excel spreadsheet to calculate the maximum depths, minimum depths, average depths, standard deviation depths, time of inundation (days), and initial time of inundation (days) from the hourly water depth data for each of the coastal cell. Finally, these data were imported into the ArcGIS Pro to create different types of maps as per the requirements. Using the inundation maps for different hurricane scenarios, the most impacted region was identified which was common to most of the hurricane scenarios to test three different types of NNBFs: (1) vegetations with three different plant densities (#/m^2), (2) artificial reefs modeled as partially blocking fixed masks, (3) artificial sand dunes modeled by increasing the bottom elevation, and also (4) artificial sand dunes with vegetation.

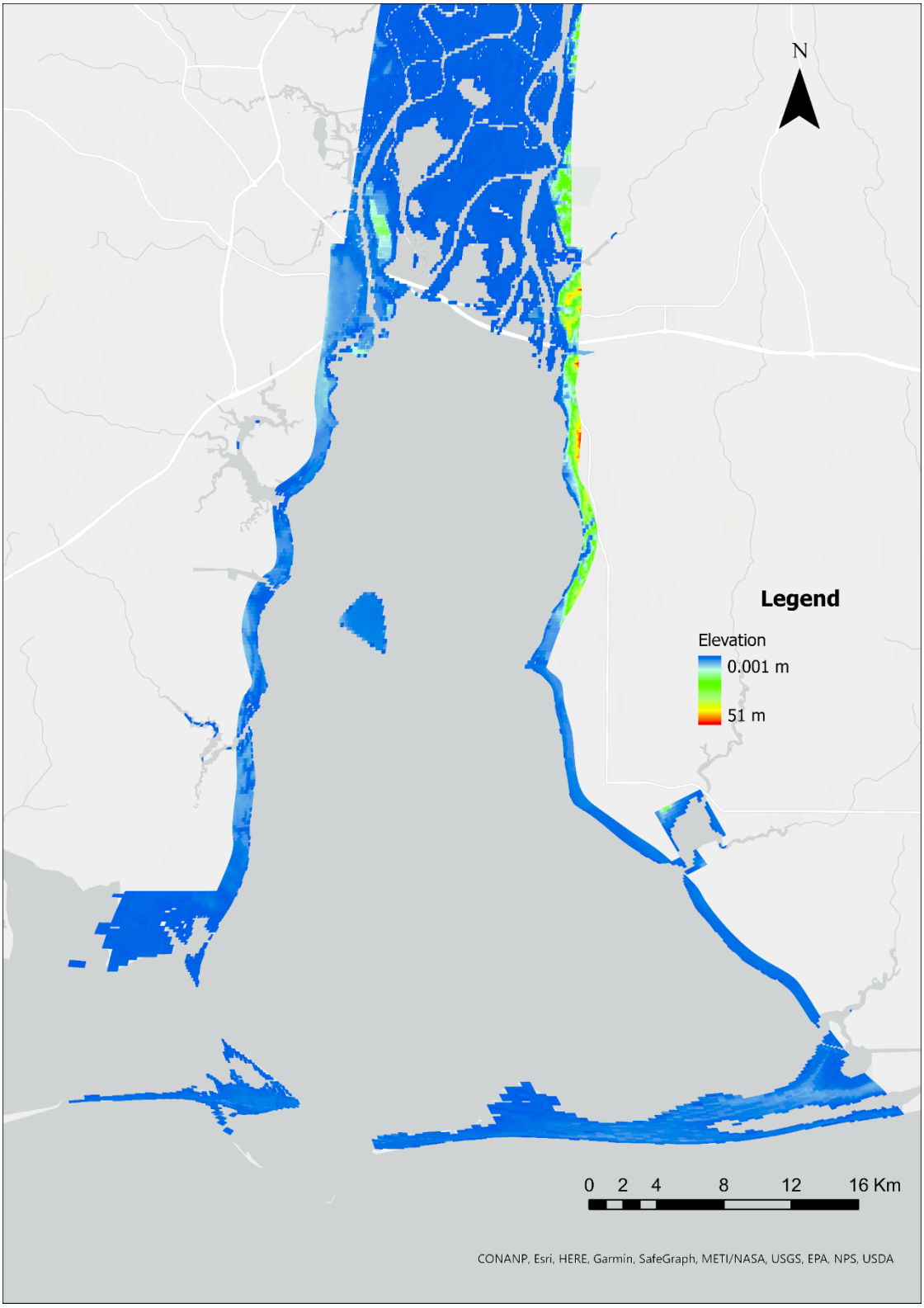

Figure 4.4 Elevation (in meters) of the coastal shoreline cells within the study area (ArcGIS Pro)

4.2 SCENARIO 1: USING HAZUS STORM TRACKS

Hazus is a GIS-based application from Federal Emergency Management Agency (FEMA) which basically focuses on the loss estimation from four different natural calamities, i.e., floods, hurricanes, earthquakes, and tsunamis (*Hazus 6.0 Inventory Technical Manual*, 2022). This application provides the users with a wide range of background and technical knowledge, to study the geographic areas of different scales with diverse demographic characteristics in response to the four natural hazards. The major focus of this application is to provide the decision-makers with information which can be used to anticipate the emergency response to a disaster, developing recovery and reconstruction plan after a disaster, and mitigating the probable impact of natural hazards (*Hazus 6.0 Inventory Technical Manual*, 2022).

Hazus 6.0 was used for one of the modeling scenarios for this study. The probabilistic hurricane scenario approach in Hazus provides the hurricane tracks and maximum wind gust for different storm events. This scenario considers the combined impacts of thousands of hurricanes based on the historical information and provides the probable hurricane track information from the stochastic (random probability distribution) assessment that produces the greatest economic damages for the specific study area (*Hazus 6.0 Inventory Technical Manual*, 2022). Since Hazus is a GIS based application, so a GIS software needs to be installed before installing the Hazus. For Hazus 6.0, the compatible GIS software is ArcGIS 10.8.2. After properly installing ArcGIS 10.8.2 and Hazus 6.0, a region was created with Hurricane hazard for the study area. The steps involved in this process are given below.

Steps involved in generating Hazus hurricane model are given below.

1. Hazus 6.0 was launched and on the “Hazus Startup” window, “Create New Region” was selected.
2. On the “Create New Region” window, name of the study region and description (optional) was entered.
3. After that “Hazard” was selected, which is “Hurricane” for this study. The Hurricane scenarios for Hazus can be accessed later in the application.

4. On the next window, Hazus provides the user with an option to select the scale of their study area. For this study, county level was selected as Mobile Bay lies in two counties, i.e., Mobile County and Baldwin County.
5. Then the state was selected following the counties, i.e., State – Alabama (AL) and County – Mobile and Baldwin.
6. This automatically creates the study region with all data required for the Hurricane hazard analysis. This newly created region was then selected in the "Open Region" window which opens the ArcGIS with Hazus with the Mobile Bay region.
7. "Hurricane Scenarios" wizard was activated using the Hazard tab followed by scenario option.
8. After that "Probabilistic" scenario was activated.
9. To run the probabilistic hurricane scenario, "Run analysis" option was selected from the "Analysis" tab. This will start running the probabilistic hurricane scenarios based on the Hazus historical hurricane database of the study region.
10. The probabilistic hurricane tracks for storm events with different return period can be accessed using the "Storm Track" option under the "Results" tab. All the storm tracks data provided by the Hazus are shown in Figure 4.5 below for the return periods from 10 years to 1000 years. The track of 10-year hurricane does not go through Mobile Bay but Pensacola in Florida. EFDC+ model grid is also shown in Figure 4.5.
11. Similarly, the peak gust data for different return period storm events can be accessed from the "Layers" under the "Table of Contents". The summary of the wind gust data is shown in Table 4.2.
12. This data was then exported to be used in EFDC+ for "Hazus Storm Tracks" scenarios for different return year storm events.

Table 4.2 Wind gust for different return year storm events from Hazus application

	Wind Gust, mph						
Storm Events	**1000-year**	**500-year**	**200-year**	**100-year**	**50-year**	**20-year**	**10-year**
Minimum:	134.60	127.30	115.10	104.50	91.00	68.30	0.00
Maximum:	160.20	149.30	133.80	121.00	106.50	83.20	62.40
Mean:	148.93	139.83	126.14	114.04	99.61	75.21	54.07
	Wind Gust, m/s						
Storm Events	**1000-year**	**500-year**	**200-year**	**100-year**	**50-year**	**20-year**	**10-year**
Minimum:	60.17	56.91	51.45	46.72	40.68	30.53	0.00
Maximum:	71.62	66.74	59.81	54.09	47.61	37.19	27.90
Mean:	66.58	62.51	56.39	50.98	44.53	33.62	24.17

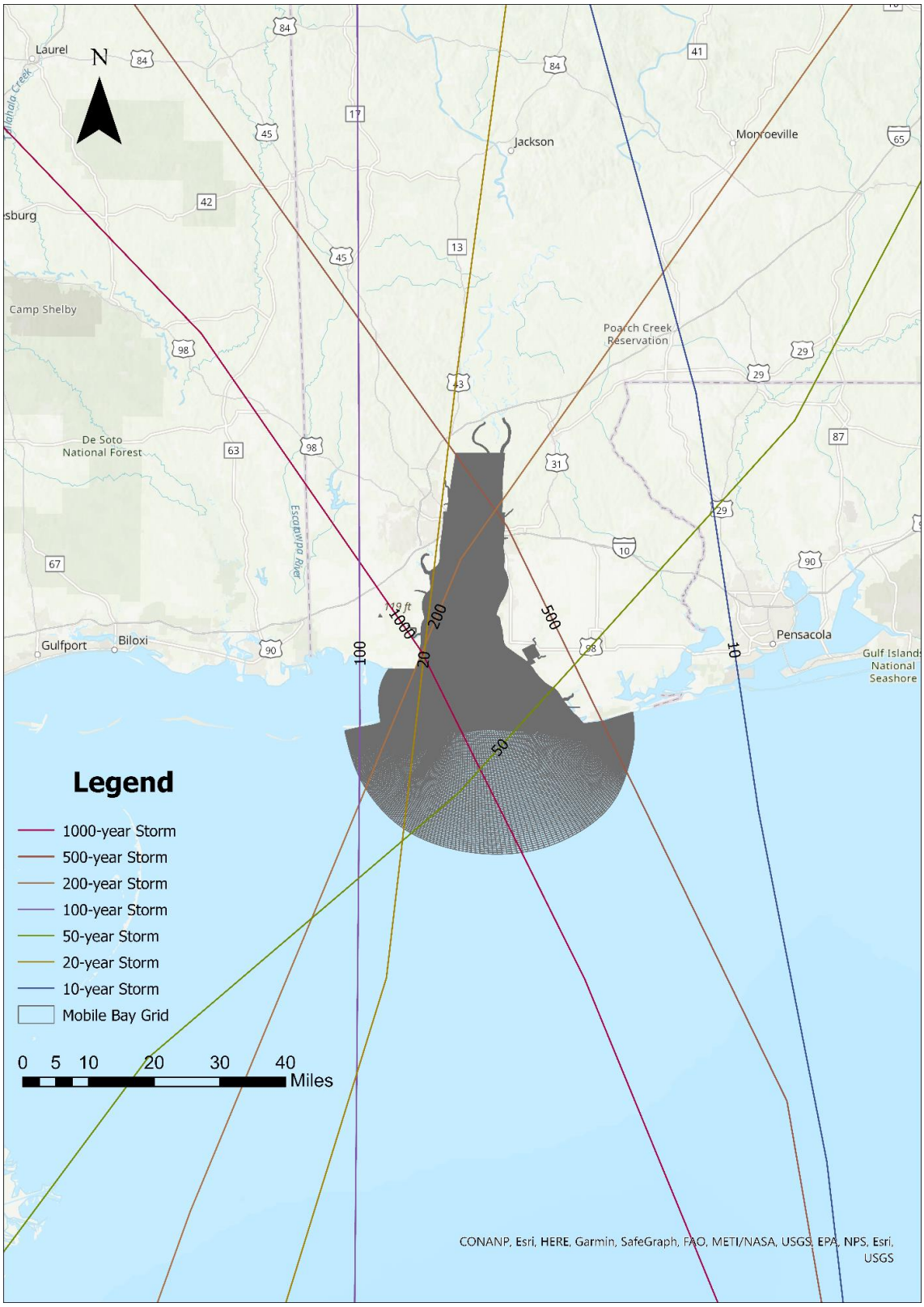

Figure 4.5 Hazus storm tracks in Mobile area (ArcGIS Pro)

Hazus probabilistic hurricane approach provides storm tracks and wind gust data for seven different return period storm events which are 10-year, 20-year, 50-year, 100-year, 200-year, 500-year, and 1000-year. Based on this information, Mobile Bay EFDC models were configured and run for every return period storm event to identify the areas around the bay that are most impacted by that storm (hurricane) event.

a. Wind Data:

To study the maximum possible impacts from storm events, the wind data for different storm events in this scenario was calculated based on the maximum wind gust for that storm event. The maximum wind gust was used as the maximum sustained windspeed for that particular storm event and the factor method for creating wind time-series data was applied to get wind time series for that storm event. The wind direction was kept identical as the direction of storm track for individual storm events. The time series of windspeed for all storm events are shown in Figure 4.6.

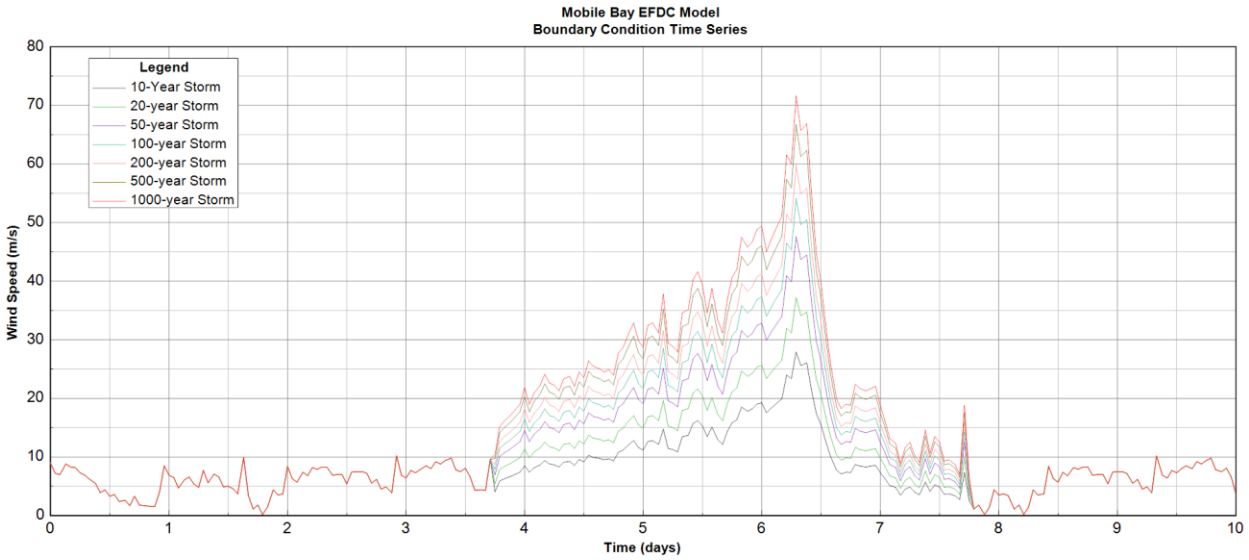

Figure 4.6 Windspeed time series for all seven storm events

b. Hurricane Parameters:

Again, the maximum wind gust was used as the Hurricane maximum sustained windspeed for this scenario. Based on the Saffir-Simpson Hurricane Scale and NHC, every storm event was classified into different storm categories. The central pressure was also calculated based on the Saffir-Simpson Hurricane Scale (Simpson & Saffir, 2007). The forward moving speed of a hurricane is

kept around 5 m/s, which is the average forward speed (15 to 20 mph) of a hurricane according to NOAA on a lower side. Since slow moving hurricanes are more dangerous as it creates higher storm surge as compared to a faster hurricane, we have used 5 m/s for this study to study the maximum possible impacts from storm events. The radius of maximum wind was calculated using the default option in EFDC+ (Takagi et al., 2012), which is popular among Japanese coastal engineers as it is based on the hurricanes central pressure (Takagi & Wu, 2015). The total runs and hurricane parameters for different storm events for this scenario are shown in Table 4.3.

Table 4.3 Total runs and hurricane parameters for different Hazus storm events

Storm Events	1000-year	500-year	200-year	100-year	50-year	20-year	10-year
Max Windspeed, m/s	71.62	66.74	59.81	54.09	47.61	37.19	27.90
Category	Cat 5	Cat 4	Cat 4	Cat 3	Cat 2	Cat 1	Tropical storm
Central Pressure, hPa	900	932	932	954.5	972	1000	1020
Forward Speed, m/s	5	5	5	5	5	5	5
Number of Runs	1	1	1	1	1	1	1

4.2.1 RESULTS

The input data, for all the seven different storm events provided by Hazus, was prepared as discussed earlier in this Chapter to set up the EFDC+ models. The simulations were then carried out individually for all the seven storm events. After the completion of the simulation runs, the water depths for all the coastal grid cells were exported as a text file. This text file contains the hourly time series water depth data for all the coastal grid cells, which was then organized to find out the average inundation, maximum inundation, and minimum inundation. This data was used to create maps for the maximum inundation for each of the storm events with the help of ArcGIS Pro as discussed earlier. The maximum inundations (in meters) and hurricane tracks for 10-year, 20-year, 50-year, 100-year, 200-year, 500-year, and 1000-year storm events are shown in Figure 4.7 to Figure 4.13, respectively, and the statistics of inundation for all the coastal cells for all seven storm events are shown in Table 4.4 to Table 4.10.

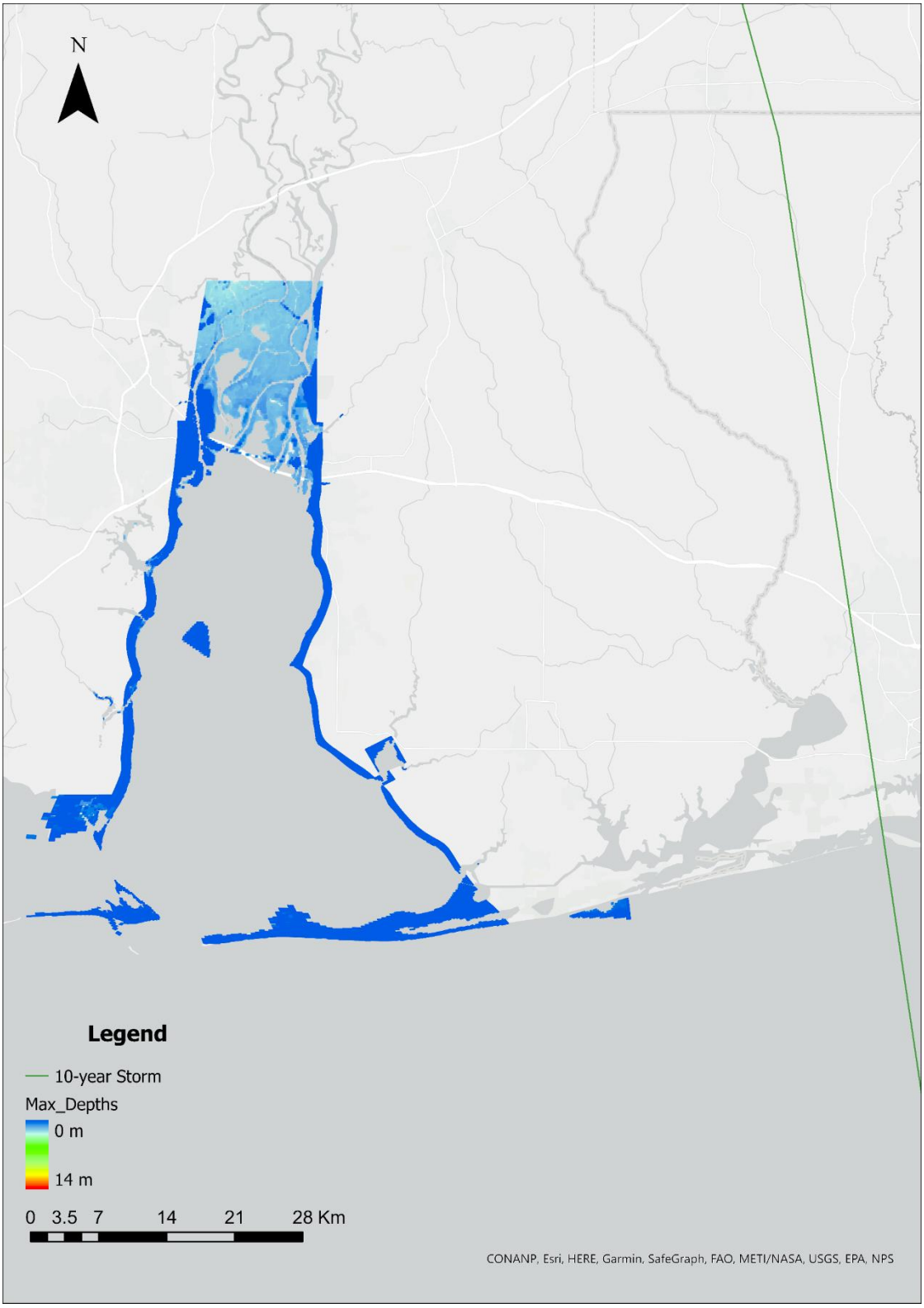

Figure 4.7 Maximum inundation and hurricane track for 10-year return period storm event (ArcGIS Pro)

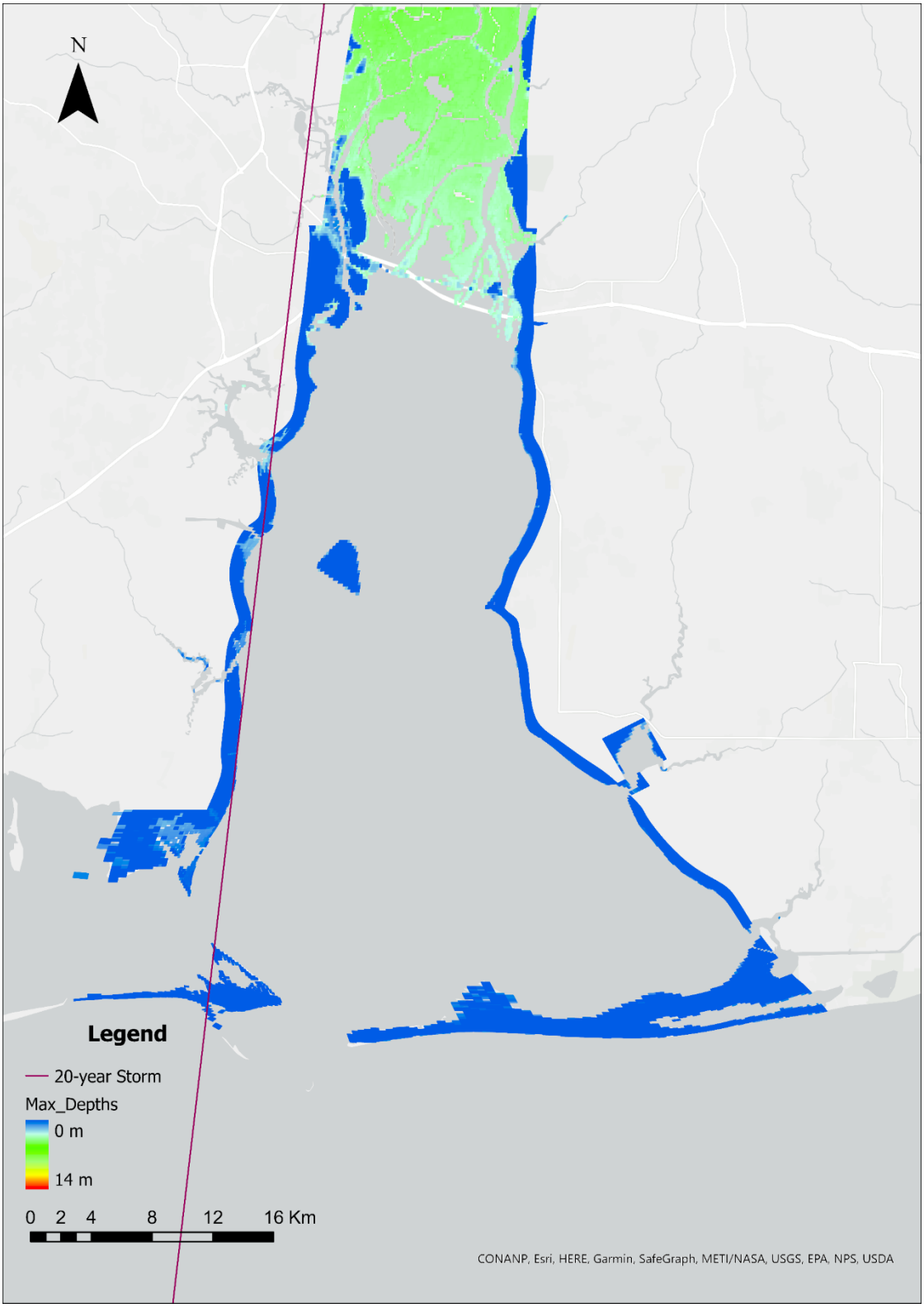

Figure 4.8 Maximum inundation and hurricane track for 20-year return period storm event (ArcGIS Pro)

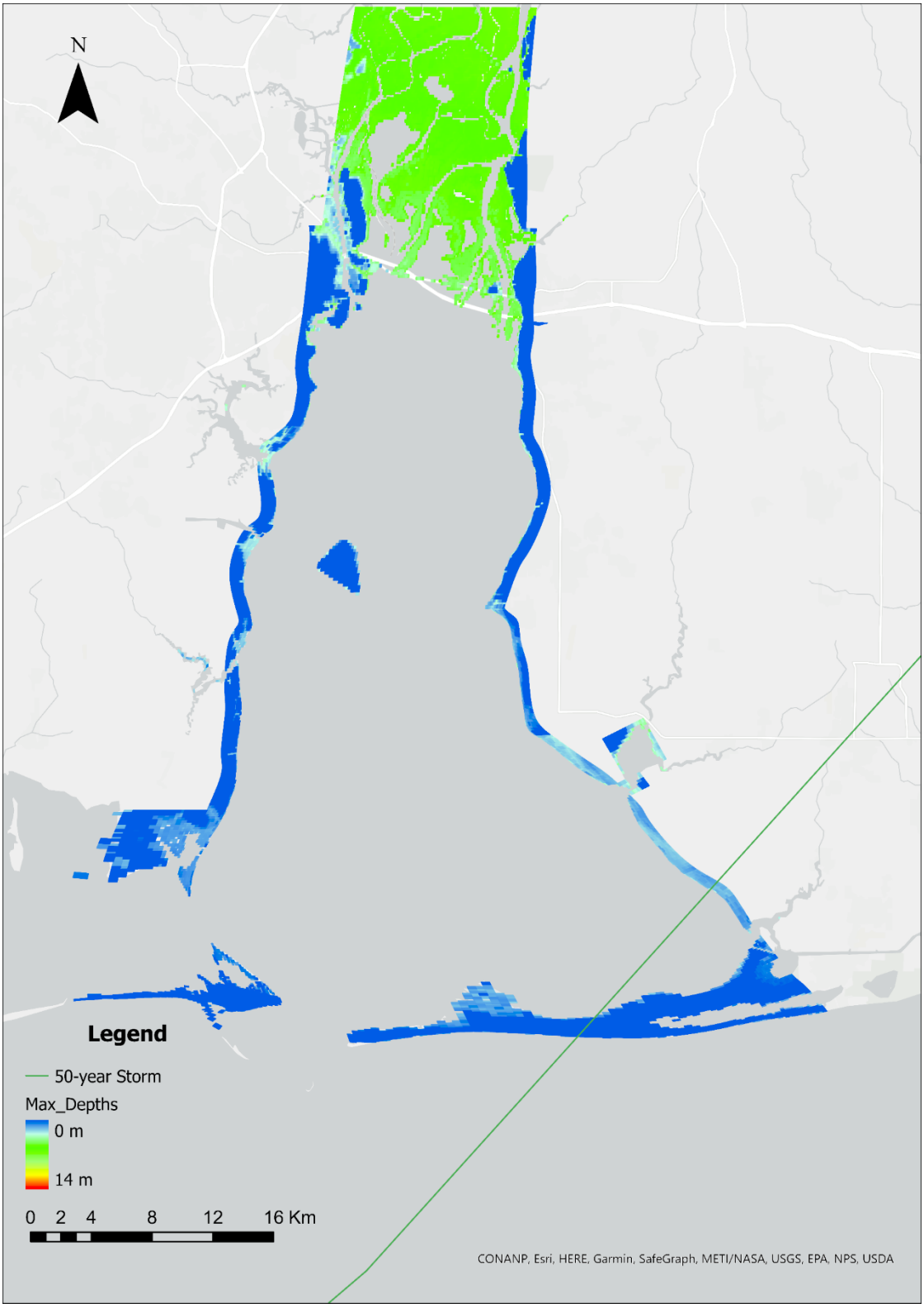

Figure 4.9 Maximum inundation and hurricane track for 50-year return period storm event (ArcGIS Pro)

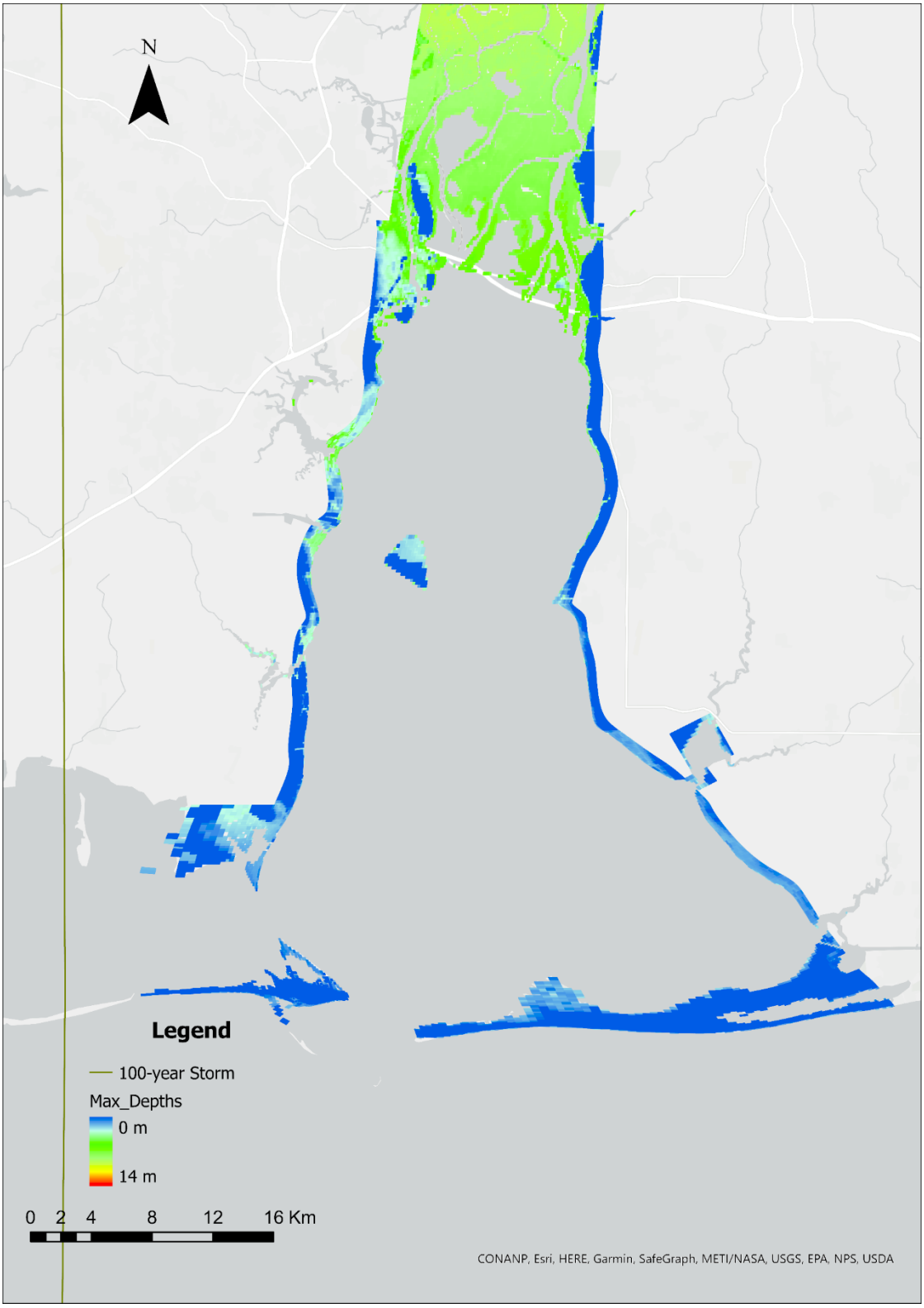

Figure 4.10 Maximum inundation and hurricane track for 100-year return period storm event (ArcGIS Pro)

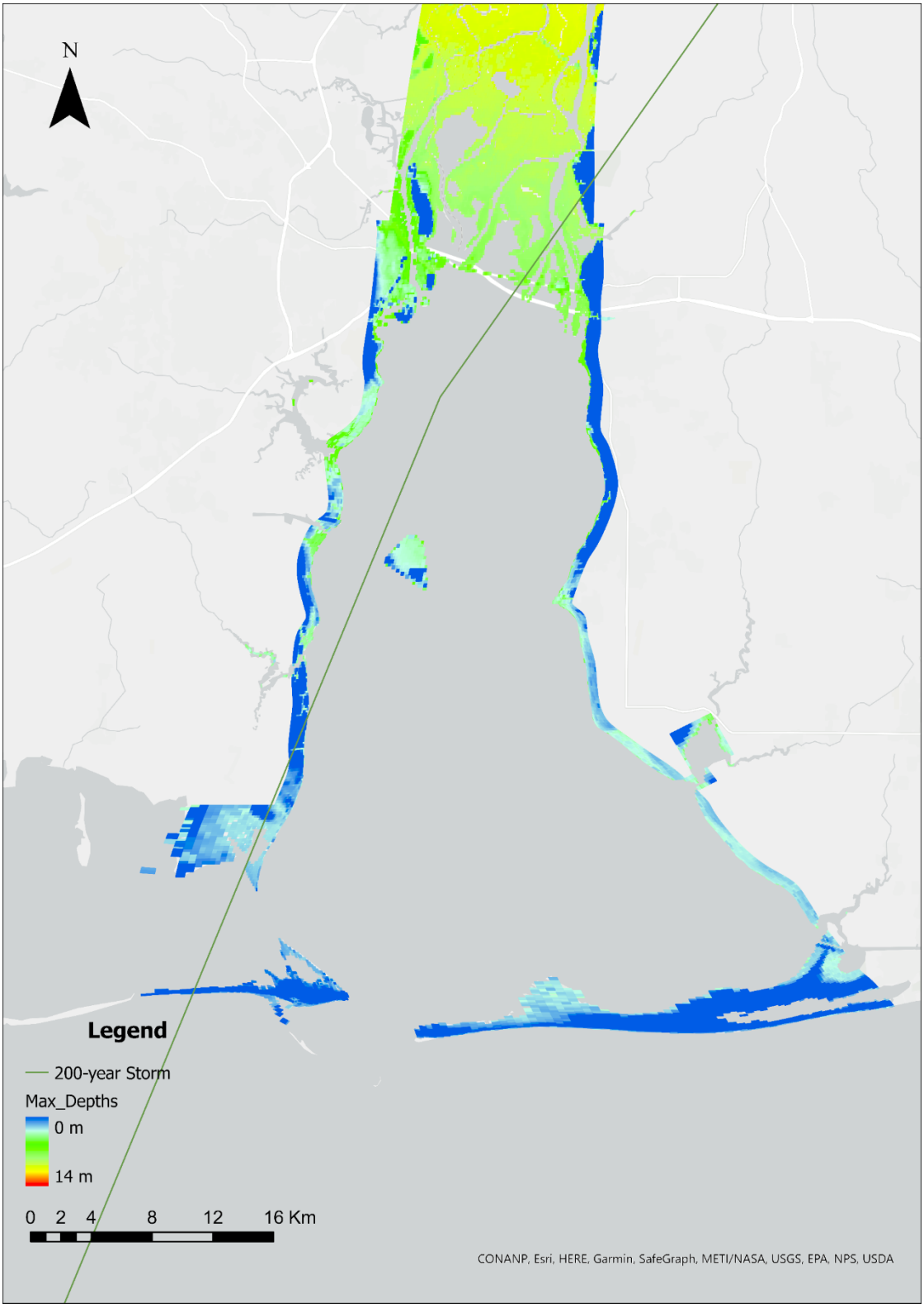

Figure 4.11 Maximum inundation and hurricane track for 200-year return period storm event (ArcGIS Pro)

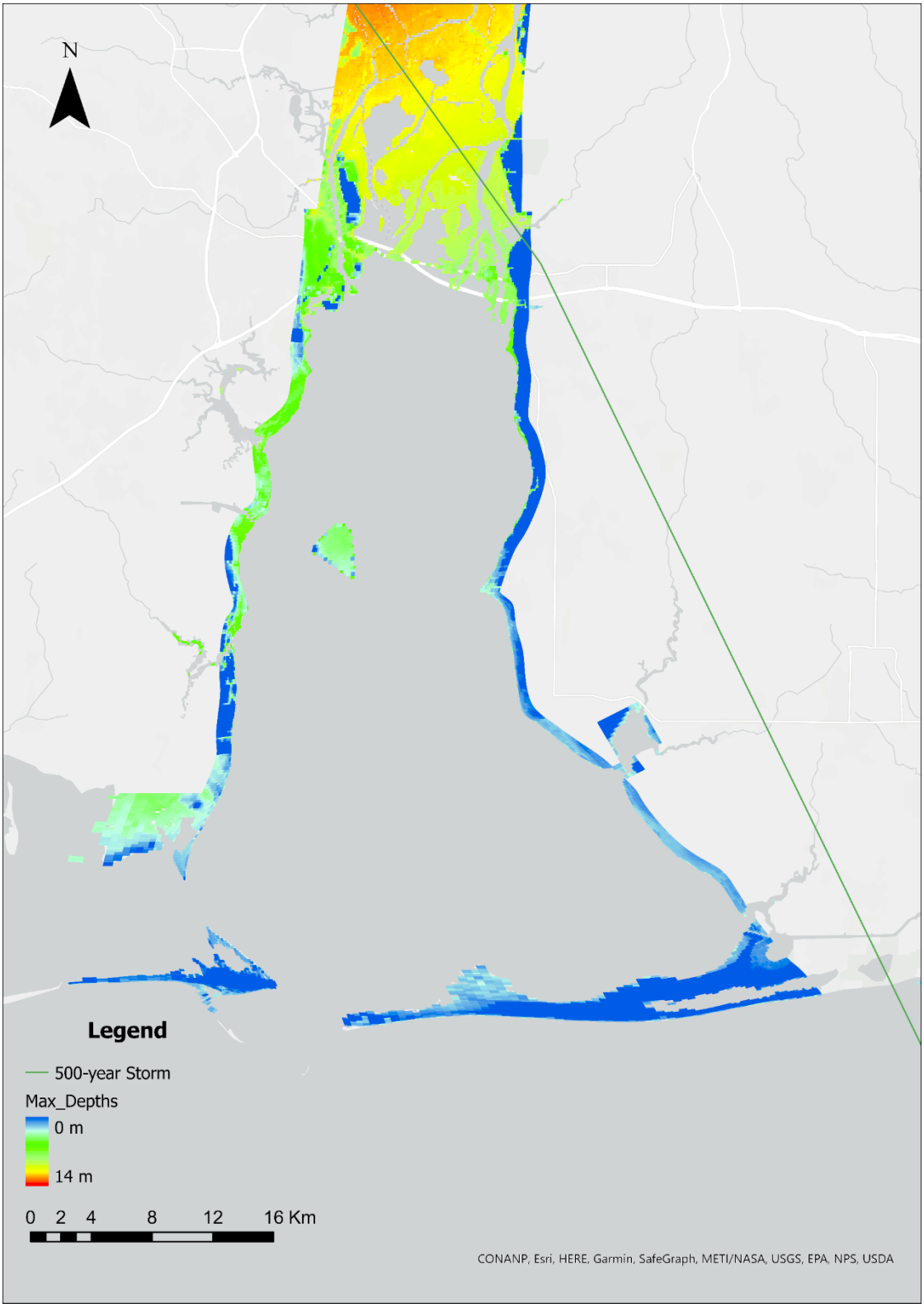

Figure 4.12 Maximum inundation and hurricane track for 500-year return period storm event (ArcGIS Pro)

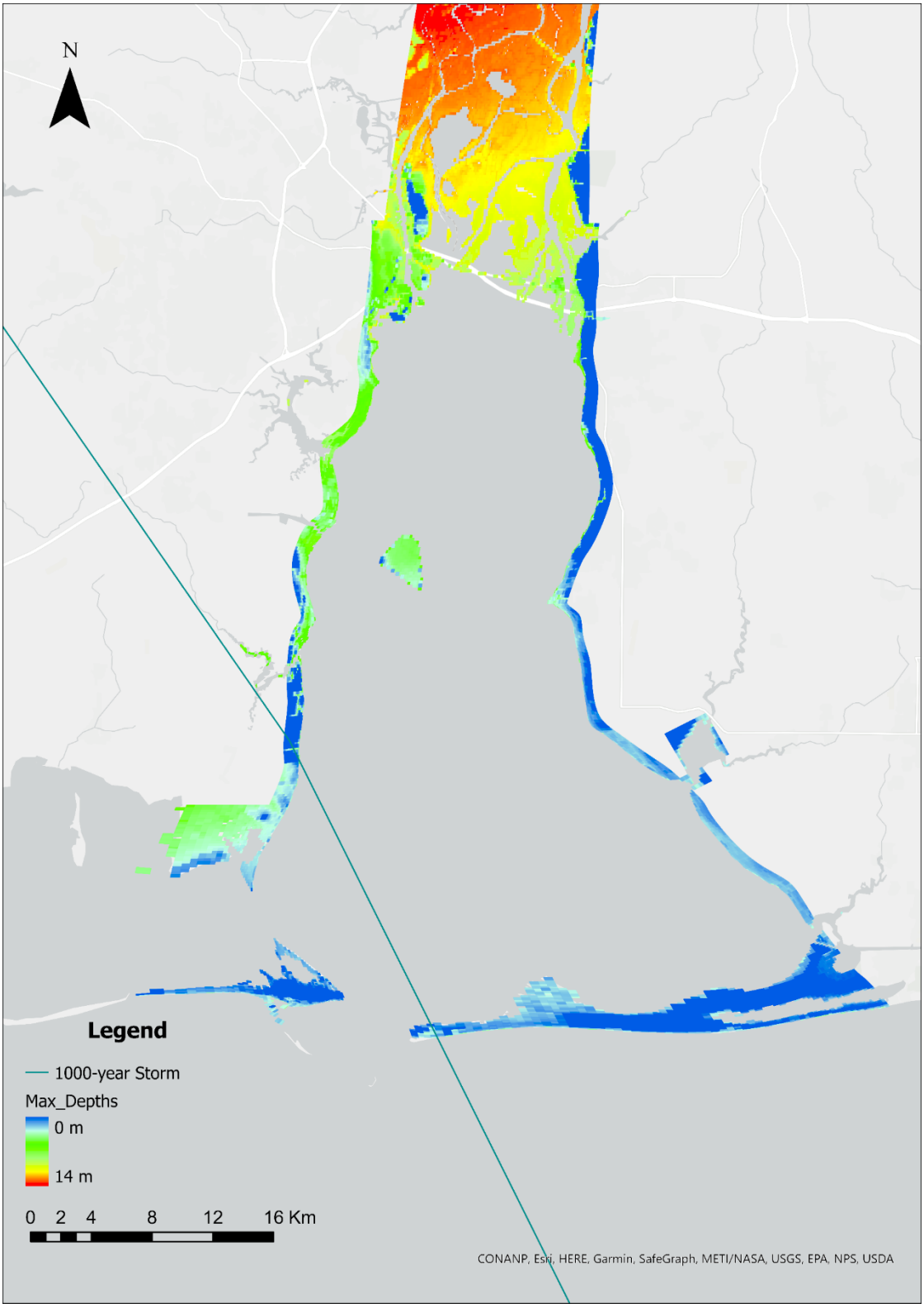

Figure 4.13 Maximum inundation and hurricane track for 1000-year return period storm event (ArcGIS Pro)

Table 4.4 Statistics of inundation for all the coastal cells for 10-year storm events.

Stats for all cells	Average depth, m	Max depth, m	Min depth, m	Std. Dev depth, m
Average depth	0.16	0.57	0.04	0.12
Maximum depth	0.93	2.62	0.62	0.57
Std. Dev	0.23	0.83	0.07	0.18

Table 4.5 Statistics of inundation for all the coastal cells for 20-year storm events.

Stats for all cells	Average depth, m	Max depth, m	Min depth, m	Std. Dev depth, m
Average depth	0.31	1.35	0.05	0.30
Maximum depth	2.53	5.05	2.47	1.21
Std. Dev	0.43	1.81	0.10	0.40

Table 4.6 Statistics of inundation for all the coastal cells for 50-year storm events.

Stats for all cells	Average depth, m	Max depth, m	Min depth, m	Std. Dev depth, m
Average depth	0.55	2.16	0.07	0.50
Maximum depth	3.25	7.25	3.11	1.67
Std. Dev	0.60	2.46	0.13	0.56

Table 4.7 Statistics of inundation for all the coastal cells for 100-year storm events.

Stats for all cells	Average depth, m	Max depth, m	Min depth, m	Std. Dev depth, m
Average depth	0.81	3.26	0.10	0.76
Maximum depth	4.11	9.71	4.01	2.23
Std. Dev	0.81	3.50	0.17	0.79

Table 4.8 Statistics of inundation for all the coastal cells for 200-year storm events.

Stats for all cells	Average depth, m	Max depth, m	Min depth, m	Std. Dev depth, m
Average depth	1.08	4.09	0.13	0.98
Maximum depth	4.25	11.34	4.00	2.61
Std. Dev	0.89	3.85	0.21	0.88

Table 4.9 Statistics of inundation for all the coastal cells for 500-year storm events.

Stats for all cells	Average depth, m	Max depth, m	Min depth, m	Std. Dev depth, m
Average depth	1.28	4.88	0.13	1.18
Maximum depth	4.26	12.78	3.58	2.97
Std. Dev depth	1.07	4.54	0.20	1.05

Table 4.10 Statistics of inundation for all the coastal cells for 1000-year storm events.

Stats for all cells	Average depth, m	Max depth, m	Min depth, m	Std. Dev depth, m
Average depth	1.37	5.26	0.13	1.27
Maximum depth	4.30	13.71	2.99	3.20
Std. Dev depth	1.13	4.83	0.20	1.12

4.2.2 DISCUSSION

For the 10-year storm event, there is not much inundation in the coastal region of Mobile and Baldwin Counties which can be visualized from the inundation map. The average (maximum) of the average depths is only 0.16 m (0.93 m) and average (maximum) of the maximum depths is only 0.57m (2.62 m). The coastal highways: Dauphin Island Parkway 193 in Mobile County and Scenic Highway 98 and Fort Morgan Road in Baldwin County are not flooded. The highest depths occurred can be seen on the north wetland (near the City of Mobile) whereas other coastal areas are not much impacted.

For the 20-year storm event, there can be seen some inundation on some low-lying areas of the Mobile County whereas there is not much impact on the Baldwin County as compared to the 10-year storm. The affected areas lie along the path of the storm which can be seen in the inundation map. The average (maximum) of the average depths is 0.31 m (2.53 m) and average (maximum) of the maximum depths is 1.35 m (5.05 m). The coastal highways are not affected by this storm event as well. Again, the north wetland area is much impacted than other coastal areas.

For the 50-year storm event, the storm track passes through the bottom wetland region of Baldwin County. There can be seen higher inundation in the same low-lying areas of the Mobile County as compared to the 20-year storm. However, the bottom wetland regions lying along the storm path

are much more impacted than other coastal areas. The average (maximum) of the average depths is 0.55 m (3.25 m) and average (maximum) of the maximum depths is 2.16 m (7.25 m). Some flooding in Dauphin Island Parkway 193 near the Dauphin Island Bridge, and some part of Scenic Highway 98 can be seen. Again, the north wetland area has the highest water depths.

For the 100-year storm event, the storm track passes through the Mobile County. There can be seen higher inundation in the coastal regions of the Mobile County as compared to the coastal regions of Baldwin County. As the intensity of the 100-year storm is higher (Category 3) than that of 50-year storm (Category 2), the coastal region of the Baldwin County is also affected but the inundation is lower as compared to the 50-year storm as the track is farther from this region. The average (maximum) of the average depths is 0.81 m (4.11 m) and average (maximum) of the maximum depths is 3.26 m (9.71 m). Higher flooding depths can be seen near the Dauphin Island Bridge. The north wetland area has the highest water depths for this storm event as well.

For the 200-year storm event, the storm track passes through Mobile County towards Baldwin County as storms travel more inland. There can be seen higher inundation in the low-lying coastal regions of both Mobile County and Baldwin counties with higher inundation than all the previous storm events. The average (maximum) of the average depths is 1.08 m (4.25 m) and average (maximum) of the maximum depths is 4.09 m (11.34 m). More areas near the Dauphin Island Bridge along the highway is flooded with higher depths of around 2.33 m. Scenic Highway 98 is much impacted with flooding depths around 3.71 m and some regions of Fort Morgan Road is also flooded.

For the 500-year storm event, the storm track passes through Baldwin County towards Mobile County as storms travel more inland. Even though the 200-year and 500-year storm events are Category 4, the maximum windspeed for a 500-year storm is much higher. This is why flooding is even higher this storm event than 200-year storm event. Some areas around the mobile regional airport were also flooded by this storm. The average (maximum) of the average depths is 1.28 m (4.26 m) and average (maximum) of the maximum depths is 4.88 m (12.78 m).

The 1000-year storm event is an extremely rare event as this is the Category 5 storm which is the maximum intensity a storm can achieve according to the Saffir-Simpson Hurricane wind scale. The hurricane track passes through Dauphin Island towards Mobile County away from Baldwin County. The coastal regions are heavily flooded by this event in both the counties. This storm has

completely flooded the mobile regional airport as well. The flooding depth in the top wet land regions could be seen reaching almost 14 m. The average (maximum) of the average depths is 1.37 m (4.30 m) and average (maximum) of the maximum depths is 5.26 m (13.71 m). For both 500 and 1000-year storm events, the coastal highways are heavily flooded with depths reaching from 3.12 m to 6.15 m.

There was seen an increasing flooding depth with the increasing intensity of the storm events. The low-lying coast in the Mobile County was the most impacted region whereas the northern coastal area with relatively higher elevation, in the Baldwin County, was the least impacted region in terms of flooding for all the storm events. From the results, it can be inferred that the low-lying regions and low-lying coastal highways are at greater risk for all the major storms (Category 3 and higher) whereas for the minor storms the low-lying regions which fall along the storm tracks are at greater risk. Also, we have modeled the storms in such a way that they reach their peak intensity when it's near the center of the bay, which is why the low-lying coastal region near the Mobile Regional Airport was mostly impacted by all the major storms. This is the same reason the maximum flooding was seen on the top wetland region, which is also the region with the least bottom elevation, for all the storm events.

4.3 SCENARIO 2: USING HYPOTHETICAL TRACKS

For this second scenario, we have tried to create a worst-case scenario situation where the hurricane passes through the center of the Mobile Bay. We have assumed three hypothetical hurricane tracks directions to study the impact of hurricane directions on the coast of Mobile Bay in term of inundation. Three hurricane directions that are used for this study are: first hurricane moving north, second hurricane moving north-east, and third hurricane movie north-west as shown in Figure 4.14.

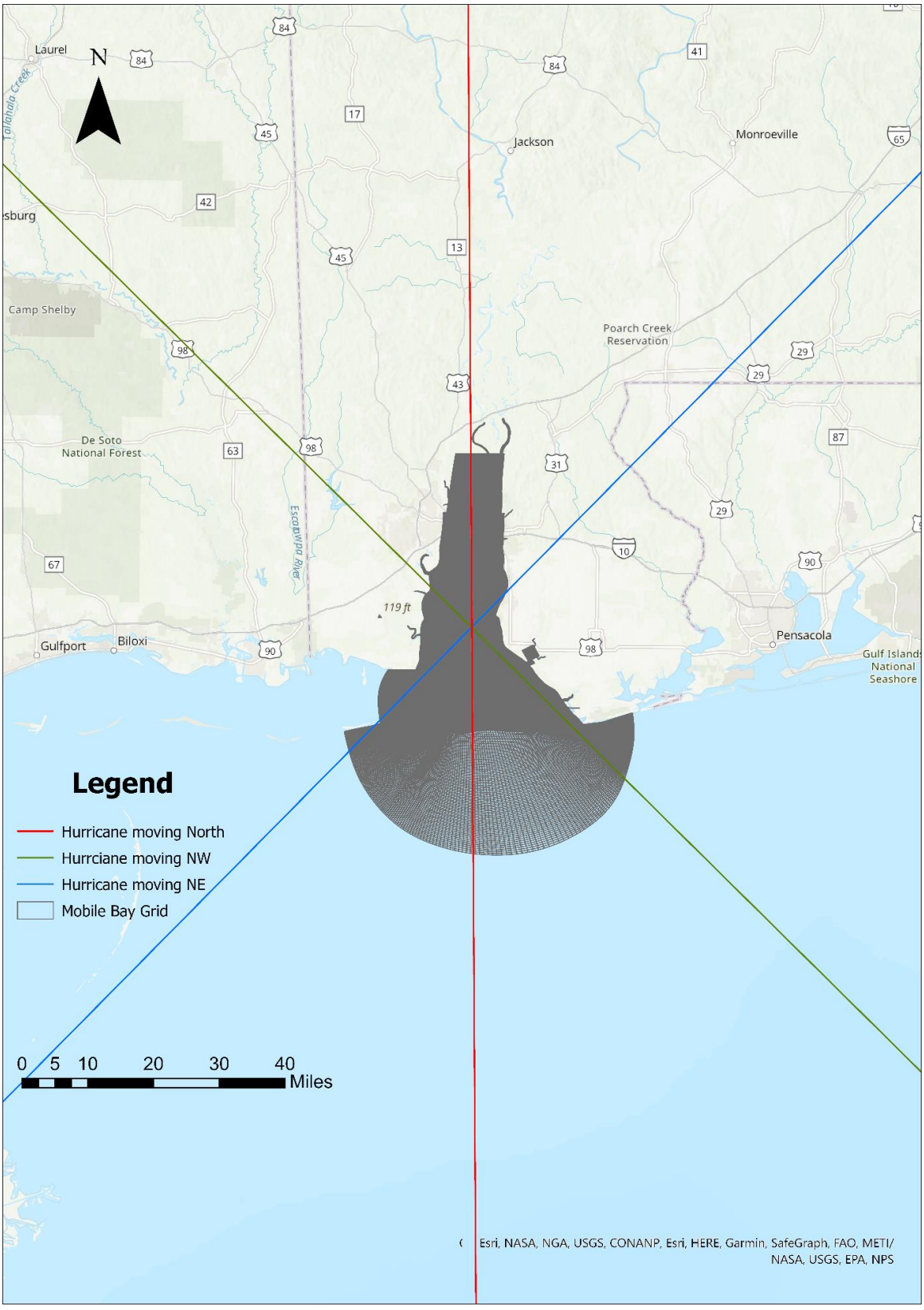

Figure 4.14 Hypothetical hurricane tracks (ArcGIS Pro)

a. Wind Data:

Wind data for this scenario was also calculated using a similar approach that was used in scenario 1. For this scenario, maximum wind data for individual runs were calculated using the Saffir-Simpson Hurricane scale depending on the category of the hurricane that was used for that run. The maximum windspeed is kept as 37.51 m/s, 45.99 m/s, 53.99 m/s, 64.01 m/s, and 74.99 m/s for Category 1, 2, 3, 4, and 5 respectively. The wind direction was kept identical to the direction of the hurricane track. The time series of windspeed for all the hurricane categories are shown in Figure 4.15.

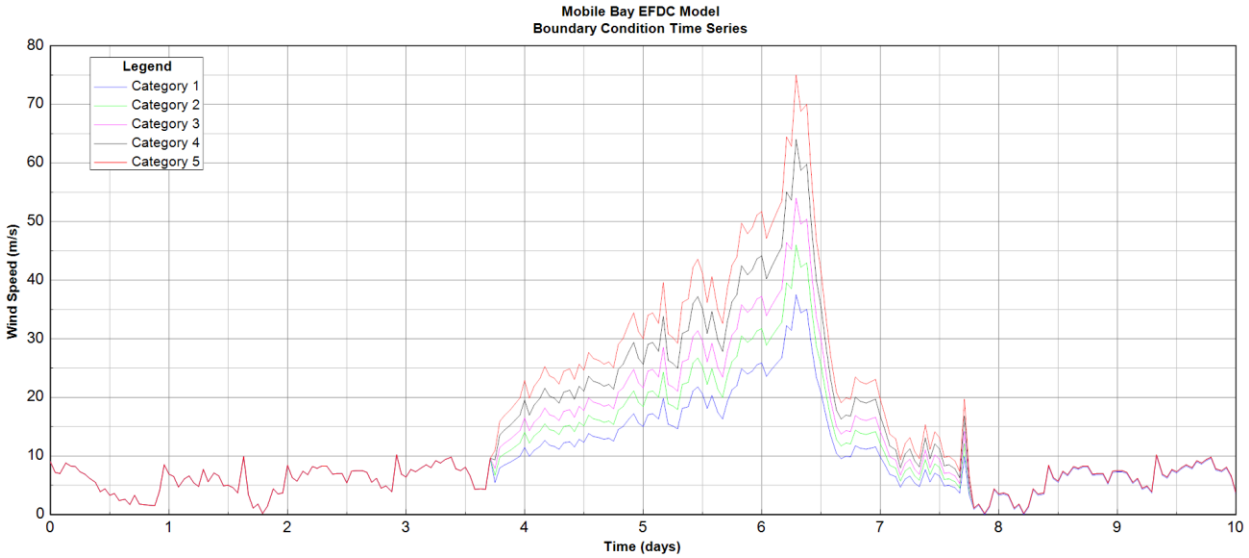

Figure 4.15 Windspeed time series for all 5 hurricane categories

b. Hurricane Parameters:

The central pressure for this scenario was also calculated based on the Saffir-Simpson Hurricane Scale (Simpson & Saffir, 2007) and 5 m/s was used as the forward moving speed for this scenario as well. Again, the radius of maximum wind was also calculated using the EFDC+ default option. The central pressure is kept as 1000 hPa, 972 hPa, 954.5 hPa, 932 hPa, and 900 hPa for Category 1, 2, 3, 4, and 5 respectively. All the five hurricane categories were simulated for all three hurricane directions. The total number of runs for this scenario are shown in Table 4.11.

Table 4.11 Total runs for hypothetical hurricane scenario

SN	Direction	Forward Speed m/s	Category	Tracks	Runs
1	North	5	1 to 5	1	5
2	NE	5	1 to 5	1	5
3	NW	5	1 to 5	1	5
Total Runs					15

4.3.1 RESULTS

The input data for all fifteen hypothetical hurricanes with categories 1-5 was prepared as discussed earlier in this chapter to set up the EFDC+ models. The simulations were then carried out individually for all fifteen hypothetical hurricanes. After the completion of the simulation runs, the map for the maximum inundation for each of the storm events was prepared in ArcGIS Pro as discussed earlier. The maximum inundations (in meters) and hurricane tracks for all hypothetical hurricanes are shown in Figure 4.16 to Figure 4.30 and the statistics for all the coastal cells for all hypothetical hurricanes are given in Table 4.12 to Table 4.26.

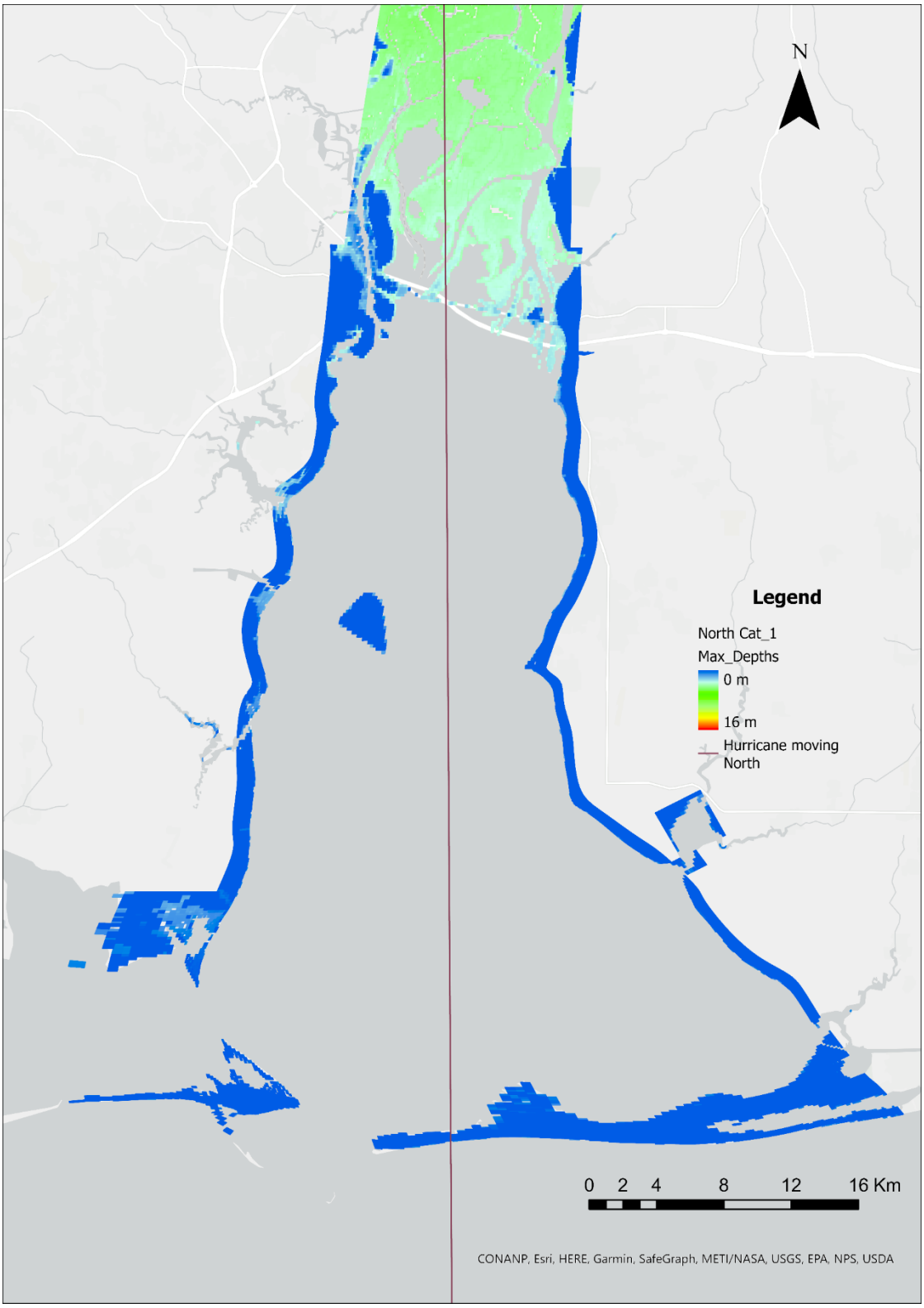

Figure 4.16 Maximum inundation by hurricane category 1 moving North (ArcGIS Pro)

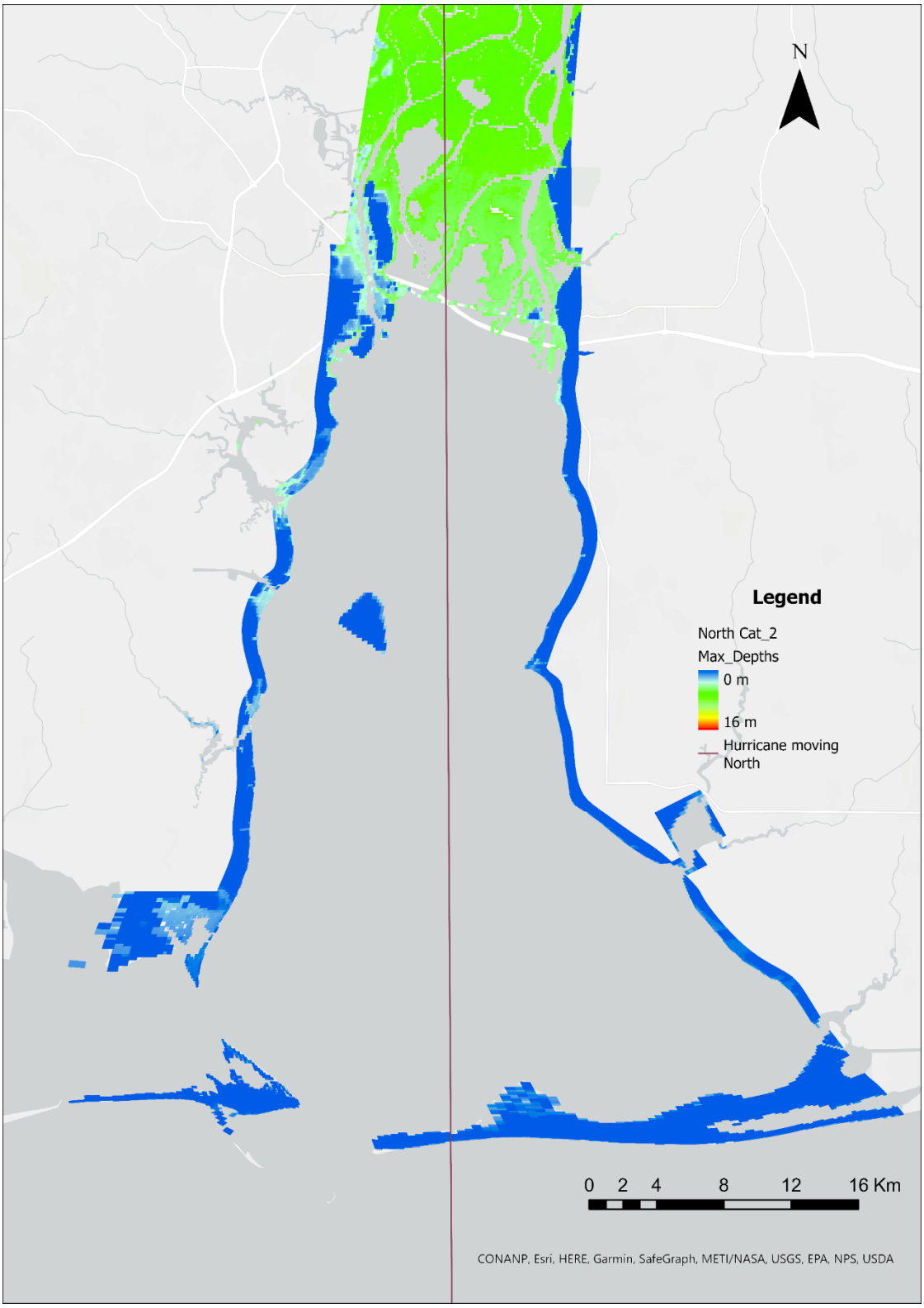

Figure 4.17 Maximum inundation by hurricane category 2 moving North (ArcGIS Pro)

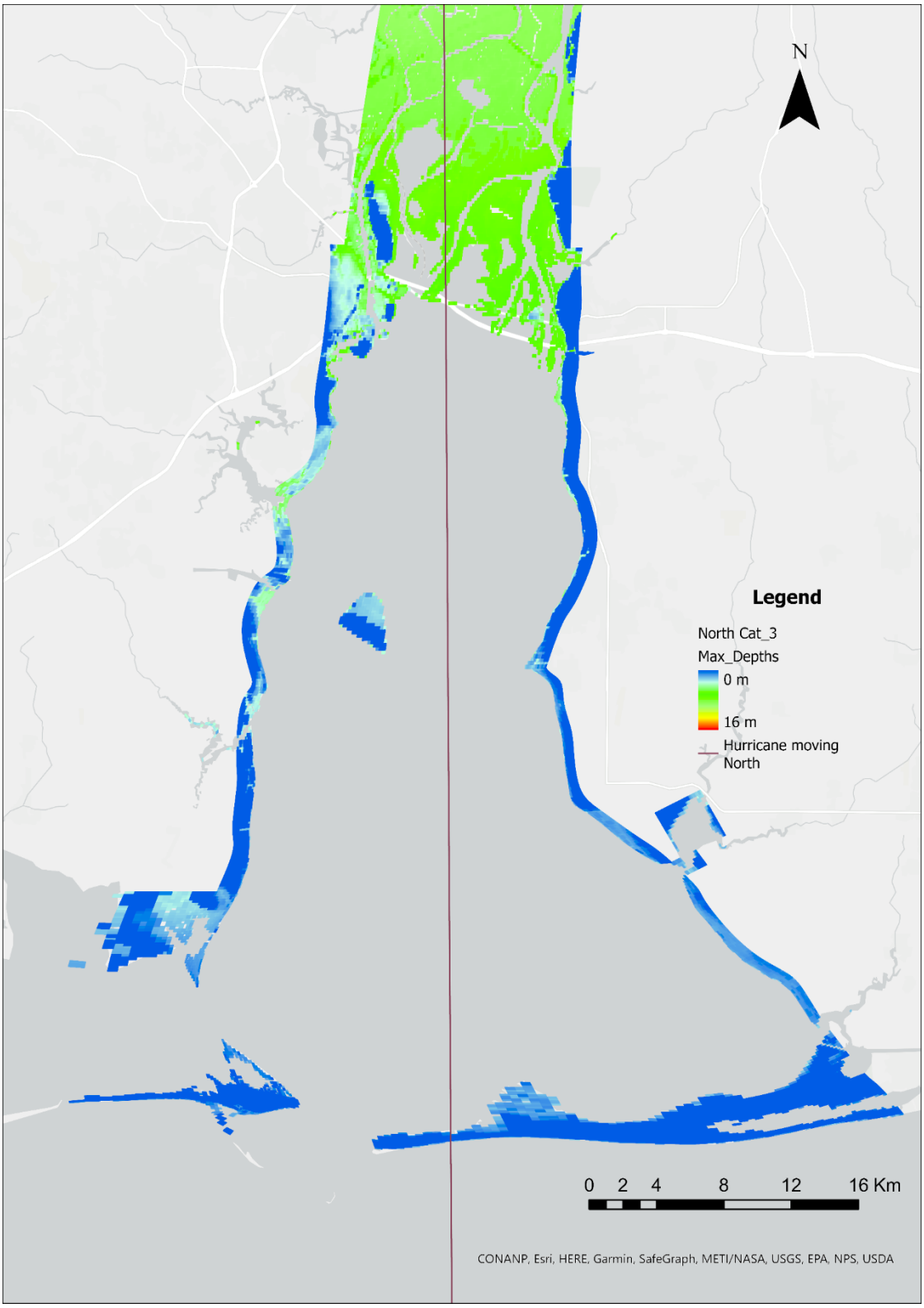

Figure 4.18 Maximum inundation by hurricane category 3 moving North (ArcGIS Pro)

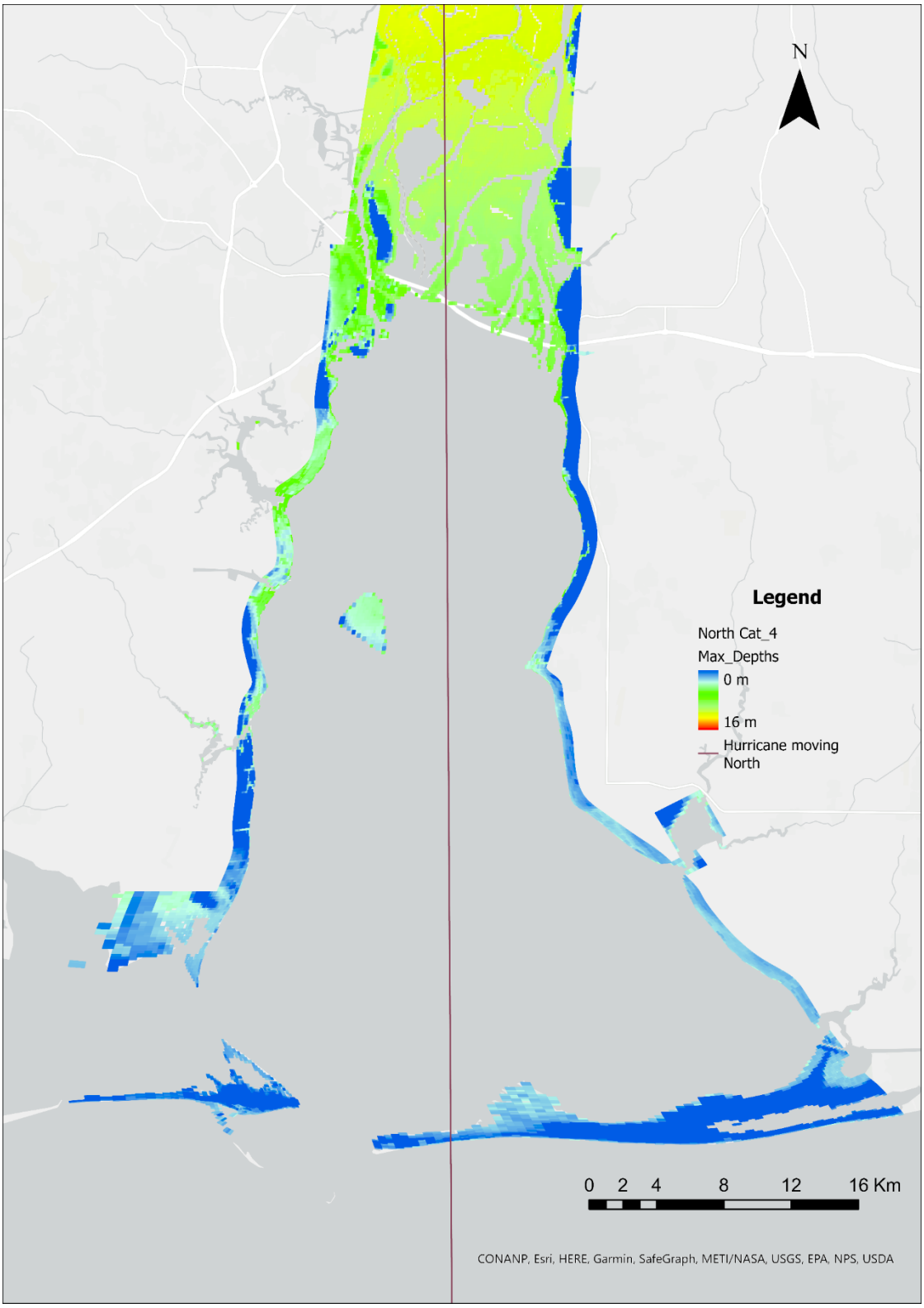

Figure 4.19 Maximum inundation by hurricane category 4 moving North (ArcGIS Pro)

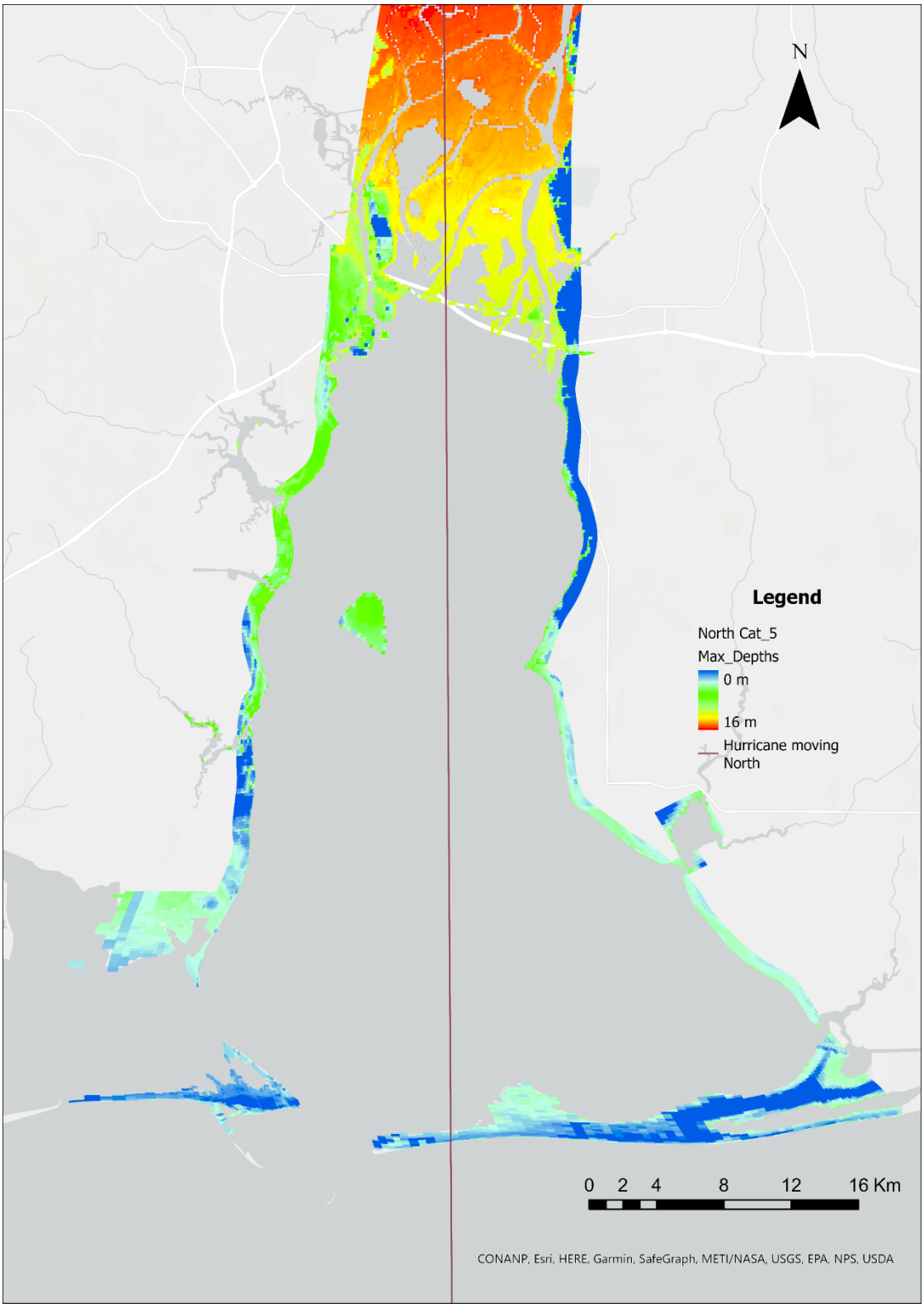

Figure 4.20 Maximum inundation by hurricane category 5 moving North (ArcGIS Pro)

Table 4.12 Inundation statistics for all the coastal cells for Category 1 Hurricane moving North.

Stats for all cells	Average depth, m	Max depth, m	Min depth, m	Std. Dev depth, m
Average depth	0.32	1.39	0.05	0.30
Maximum depth	2.55	5.19	2.47	1.21
Std. Dev.	0.44	1.86	0.10	0.41

Table 4.13 Inundation statistics for all the coastal cells for Category 2 Hurricane moving North.

Stats for all cells	Average depth, m	Max depth, m	Min depth, m	Std. Dev depth, m
Average depth	0.52	2.22	0.07	0.50
Maximum depth	3.28	7.51	3.10	1.71
Std. Dev.	0.63	2.74	0.13	0.61

Table 4.14 Inundation statistics for all the coastal cells for Category 3 Hurricane moving North.

Stats for all cells	Average depth, m	Max depth, m	Min depth, m	Std. Dev depth, m
Average depth	0.80	3.23	0.10	0.76
Maximum depth	4.11	9.68	4.01	2.22
Std. Dev. depth	0.80	3.49	0.17	0.79

Table 4.15 Inundation statistics for all the coastal cells for Category 4 Hurricane moving North.

Stats for all cells	Average depth, m	Max depth, m	Min depth, m	Std. Dev depth, m
Average depth	1.23	4.75	0.13	1.13
Maximum depth	4.20	12.59	3.58	2.86
Std. Dev. depth	1.00	4.42	0.22	1.00

Table 4.16 Inundation statistics for all the coastal cells for Category 5 Hurricane moving North.

Stats for all cells	Average depth, m	Max depth, m	Min depth, m	Std. Dev depth, m
Average depth	1.77	6.72	0.16	1.62
Maximum depth	8.47	15.90	6.67	3.63
Std. Dev.	1.19	5.32	0.25	1.20

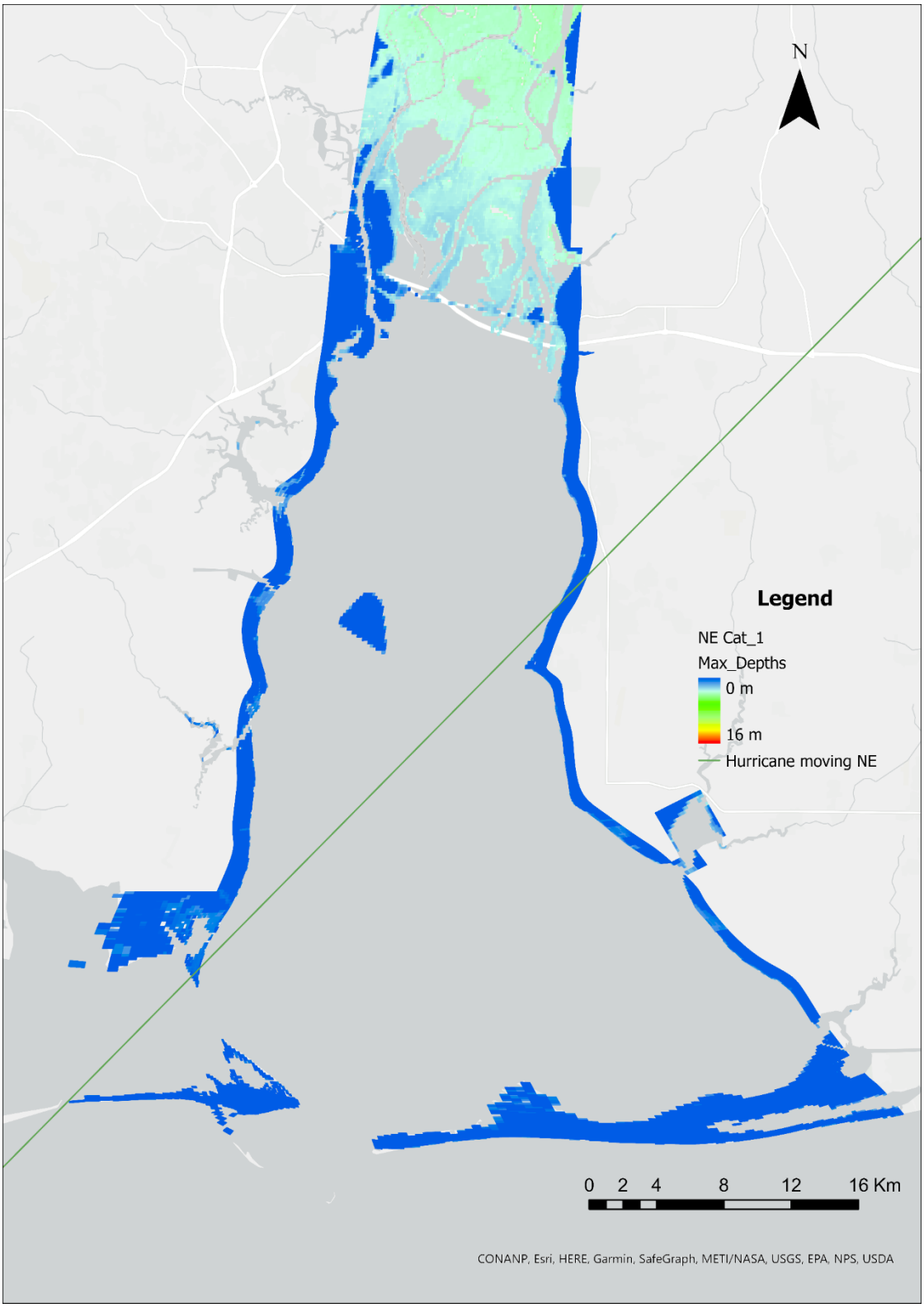

Figure 4.21 Maximum inundation by hurricane category 1 moving Northeast (ArcGIS Pro)

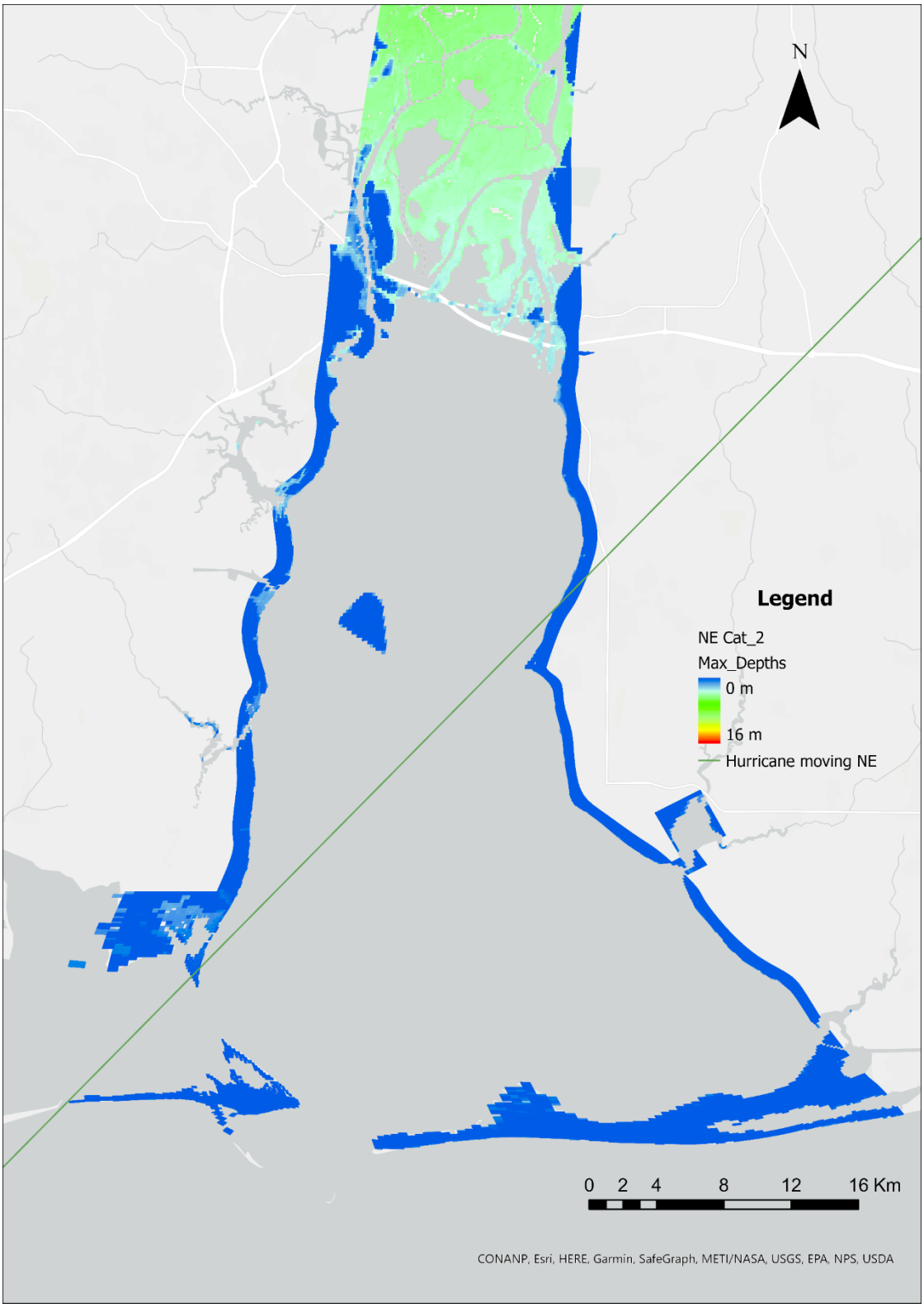

Figure 4.22 Maximum inundation by hurricane category 2 moving Northeast (ArcGIS Pro)

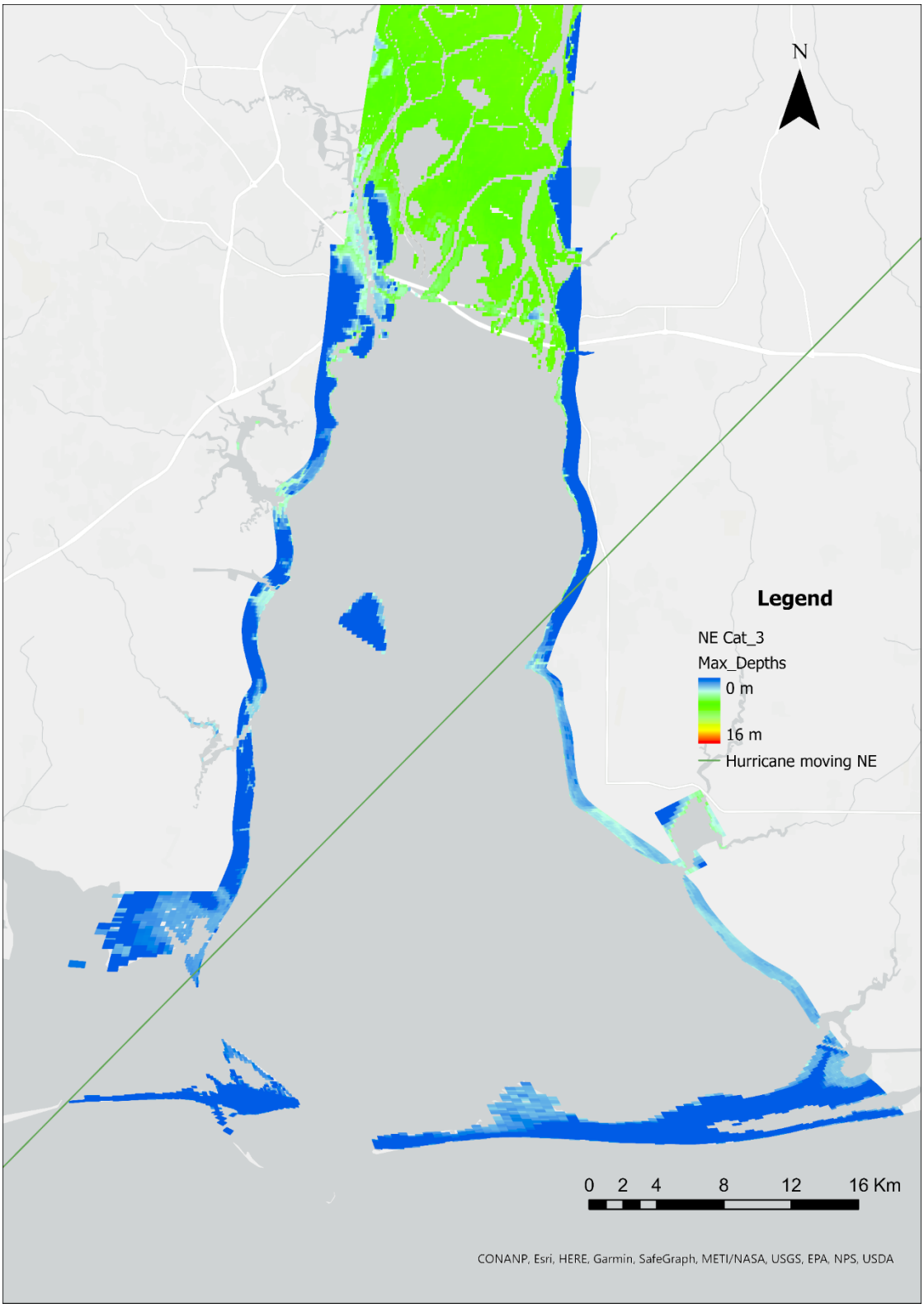

Figure 4.23 Maximum inundation by hurricane category 3 moving Northeast (ArcGIS Pro)

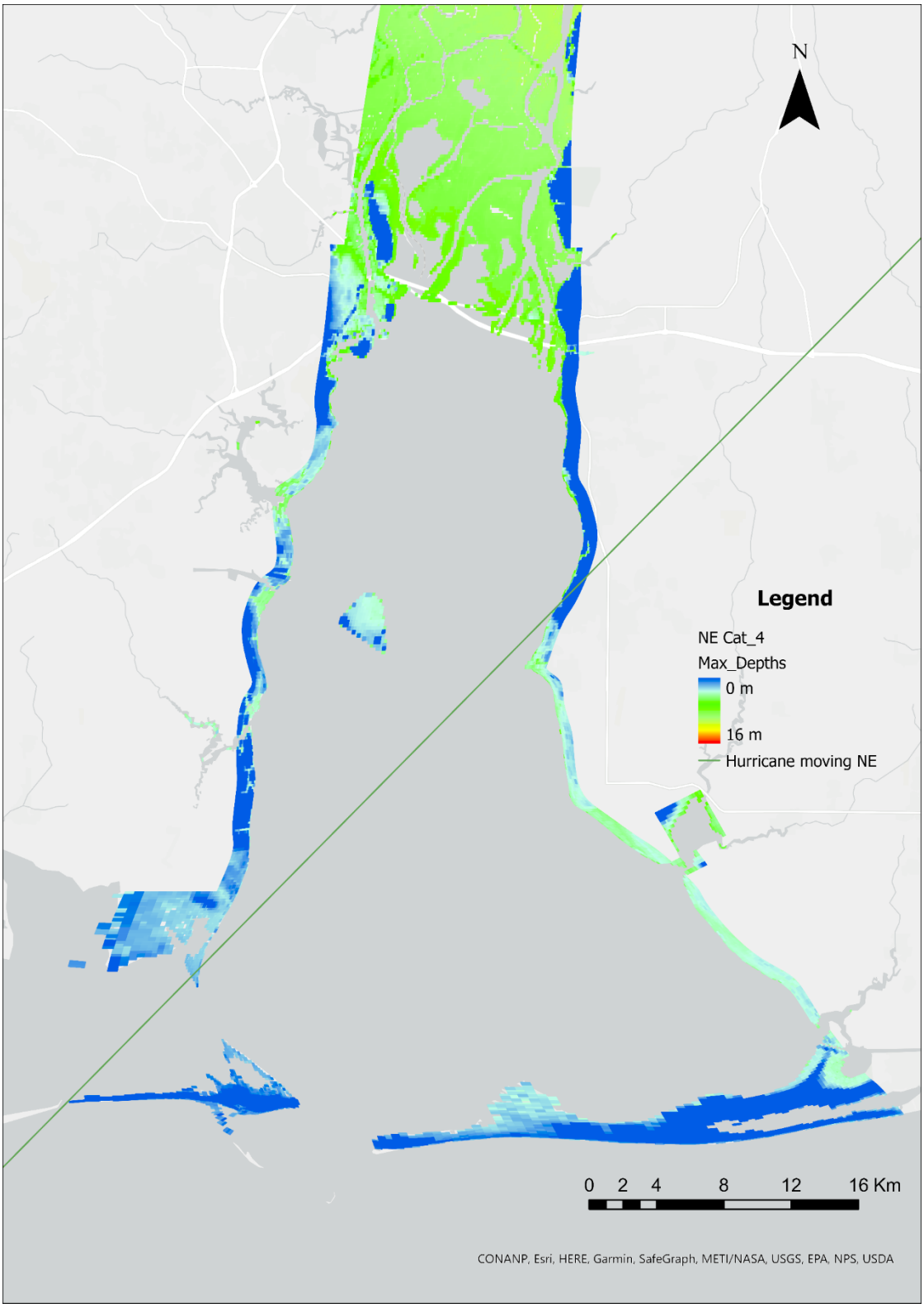

Figure 4.24 Maximum inundation by hurricane category 4 moving Northeast (ArcGIS Pro)

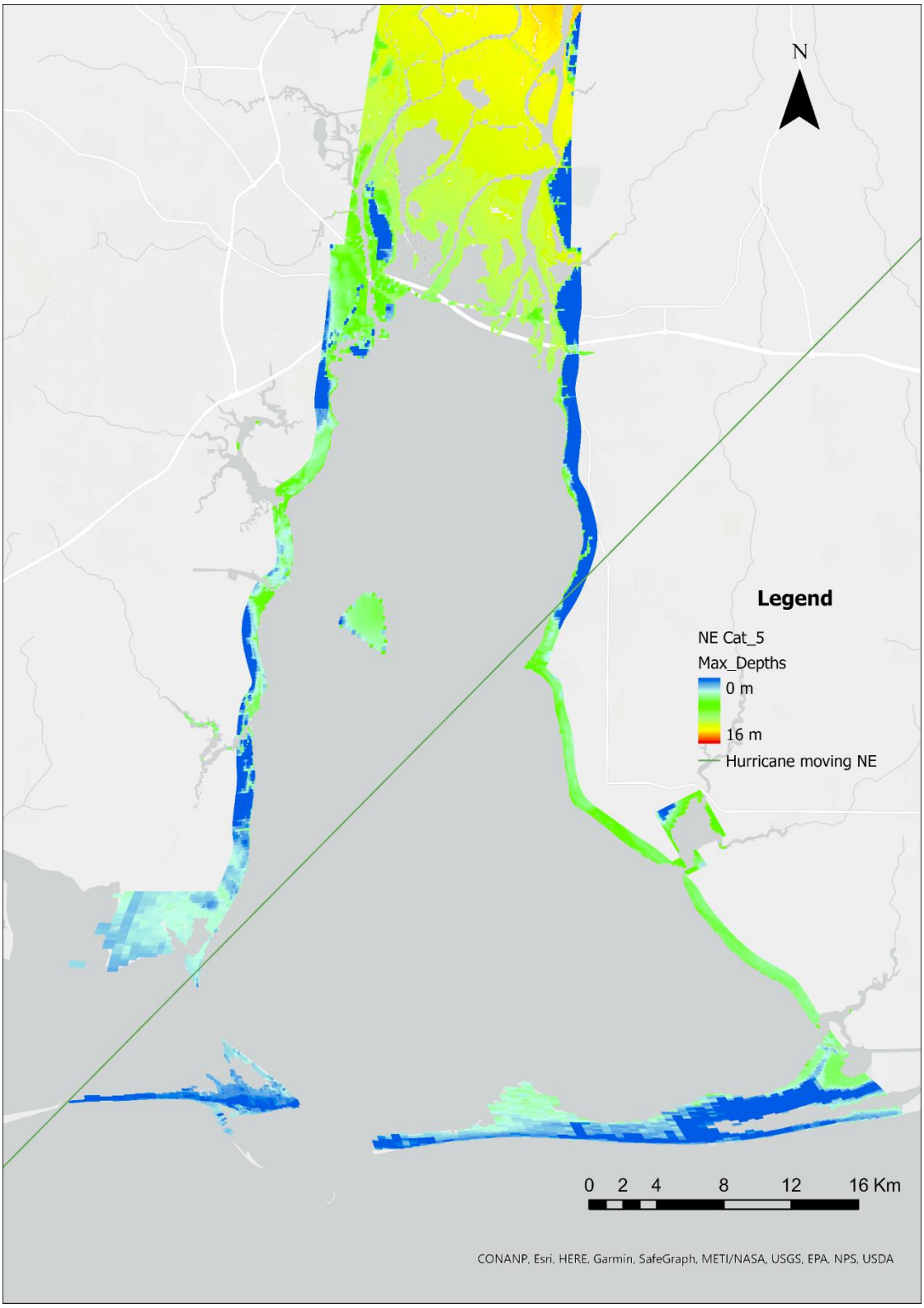

Figure 4.25 Maximum inundation by hurricane category 5 moving Northeast (ArcGIS Pro)

Table 4.17 Inundation statistics for all the coastal cells for Category 1 Hurricane moving NE.

Stats for all cells	Average depth, m	Max depth, m	Min depth, m	Std. Dev depth, m
Average depth	0.27	1.11	0.05	0.25
Maximum depth	1.46	4.56	1.32	1.04
Std. Dev.	0.37	1.49	0.09	0.33

Table 4.18 Inundation statistics for all the coastal cells for Category 2 Hurricane moving NE.

Stats for all cells	Average depth, m	Max depth, m	Min depth, m	Std. Dev depth, m
Average depth	0.32	1.38	0.05	0.30
Maximum depth	2.55	5.19	2.47	1.21
Std. Dev.	0.44	1.86	0.10	0.41

Table 4.19 Inundation statistics for all the coastal cells for Category 3 Hurricane moving NE.

Stats for all cells	Average depth, m	Max depth, m	Min depth, m	Std. Dev depth, m
Average depth	0.72	2.77	0.10	0.65
Maximum depth	4.11	8.62	3.36	1.99
Std. Dev.	0.70	2.88	0.19	0.66

Table 4.20 Inundation statistics for all the coastal cells for Category 4 Hurricane moving NE.

Stats for all cells	Average depth, m	Max depth, m	Min depth, m	Std. Dev depth, m
Average depth	1.11	4.10	0.12	0.99
Maximum depth	4.29	11.19	3.10	2.57
Std. Dev.	0.87	3.65	0.20	0.84

Table 4.21 Inundation statistics for all the coastal cells for Category 5 Hurricane moving NE.

Stats for all cells	Average depth, m	Max depth, m	Min depth, m	Std. Dev depth, m
Average depth	1.59	5.79	0.15	1.42
Maximum depth	8.40	14.16	6.69	3.28
Std. Dev.	1.06	4.46	0.23	1.03

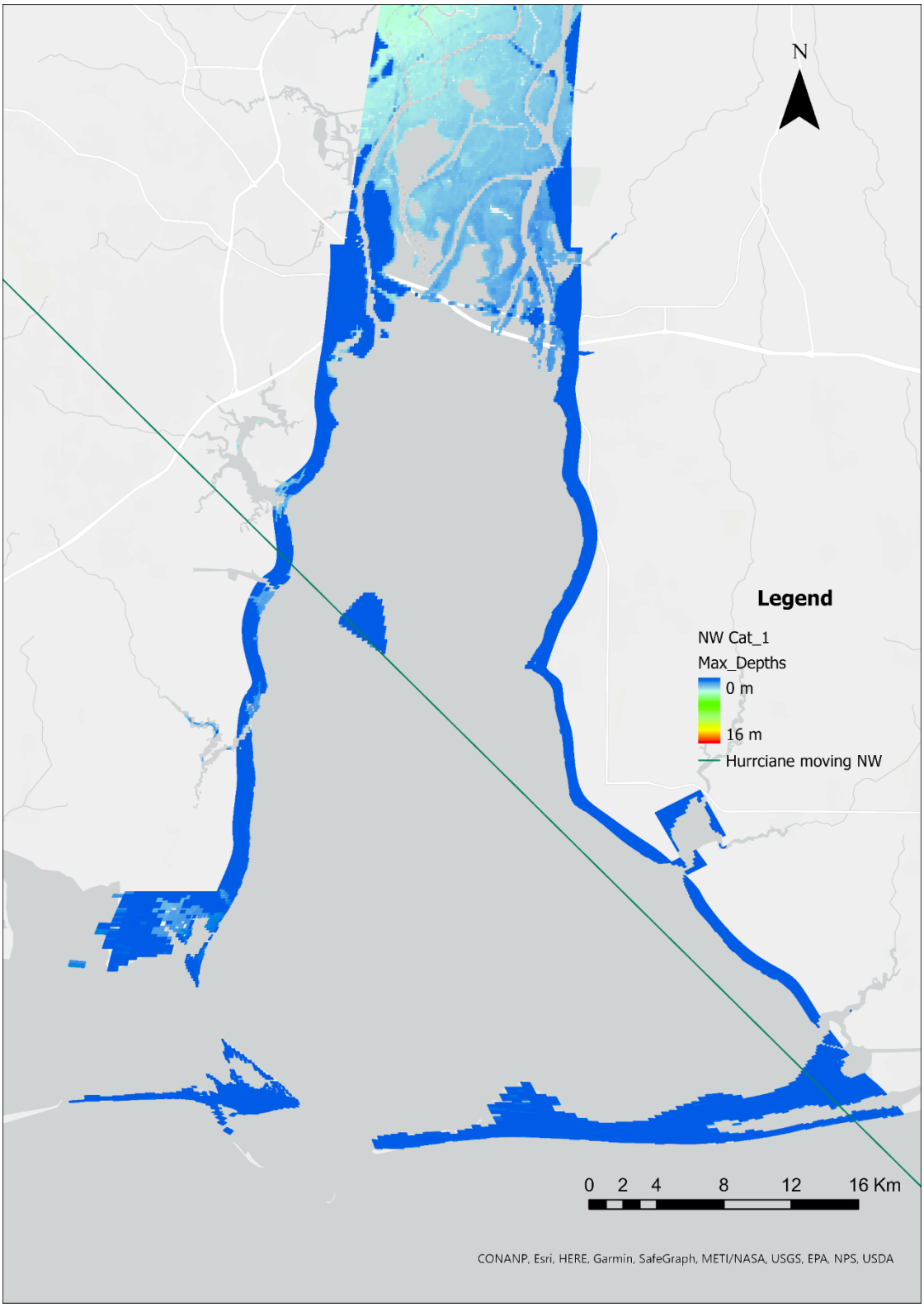

Figure 4.26 Maximum inundation by hurricane category 1 moving Northwest (ArcGIS Pro)

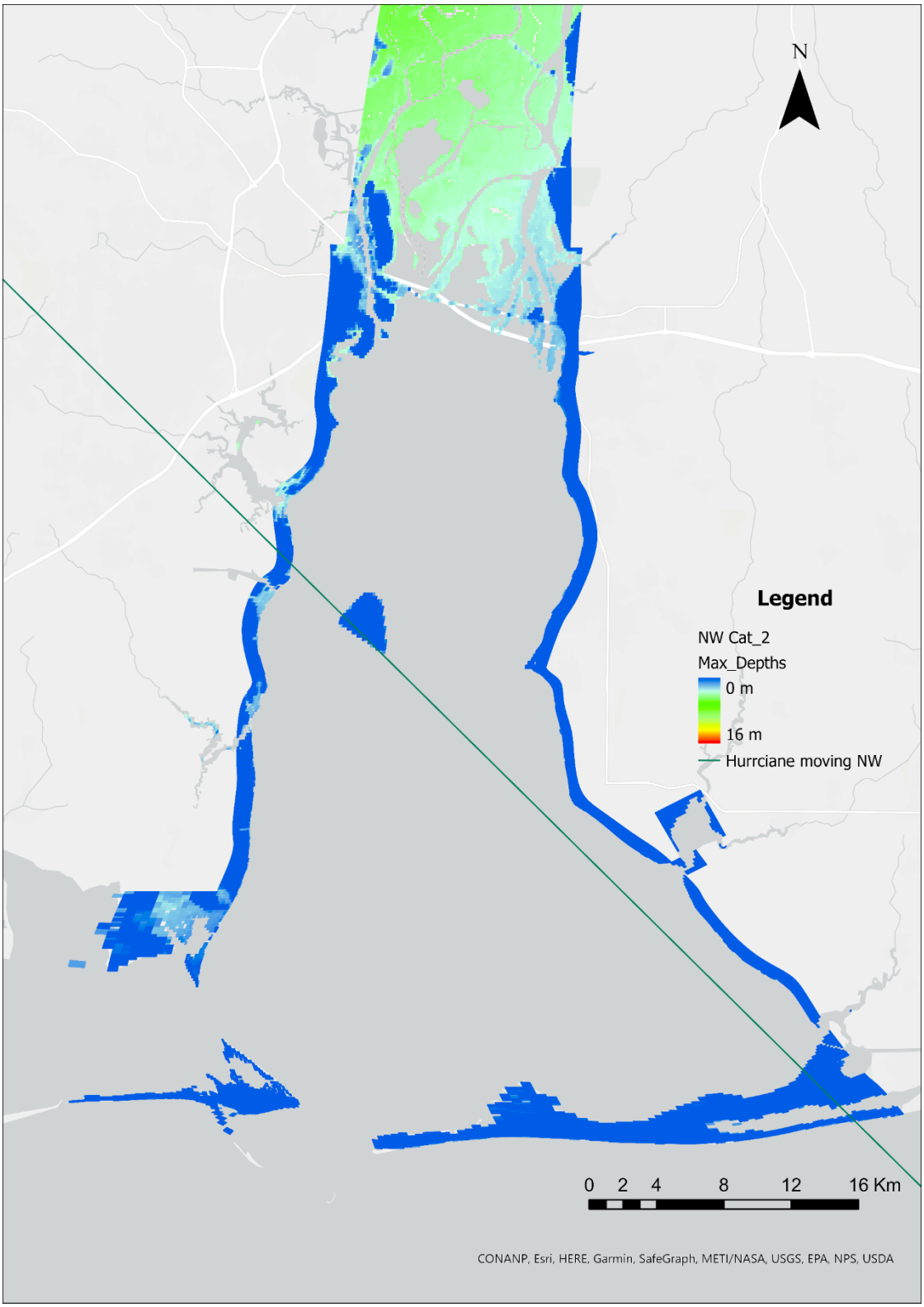

Figure 4.27 Maximum inundation by hurricane category 2 moving Northwest (ArcGIS Pro)

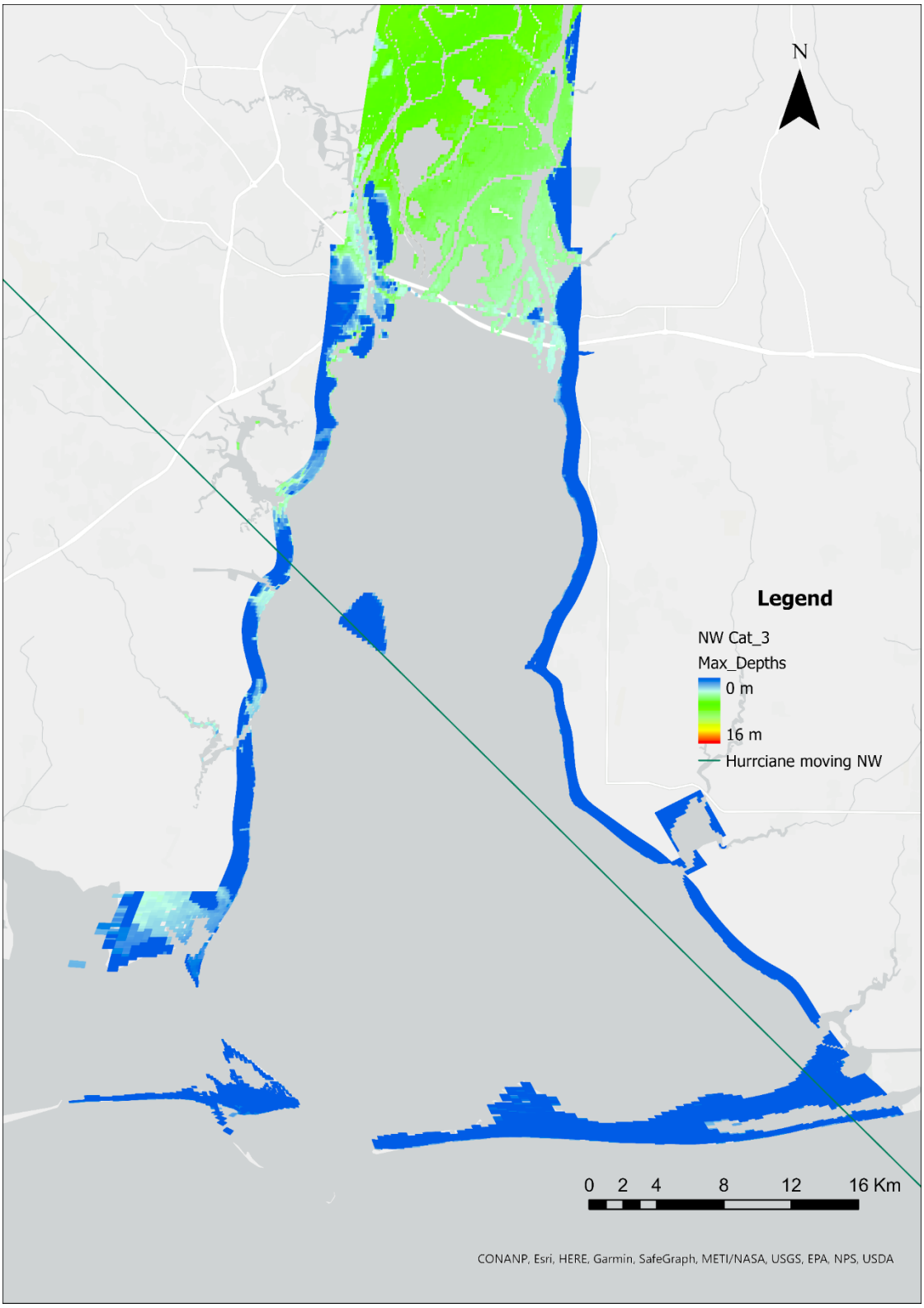

Figure 4.28 Maximum inundation by hurricane category 3 moving Northwest (ArcGIS Pro)

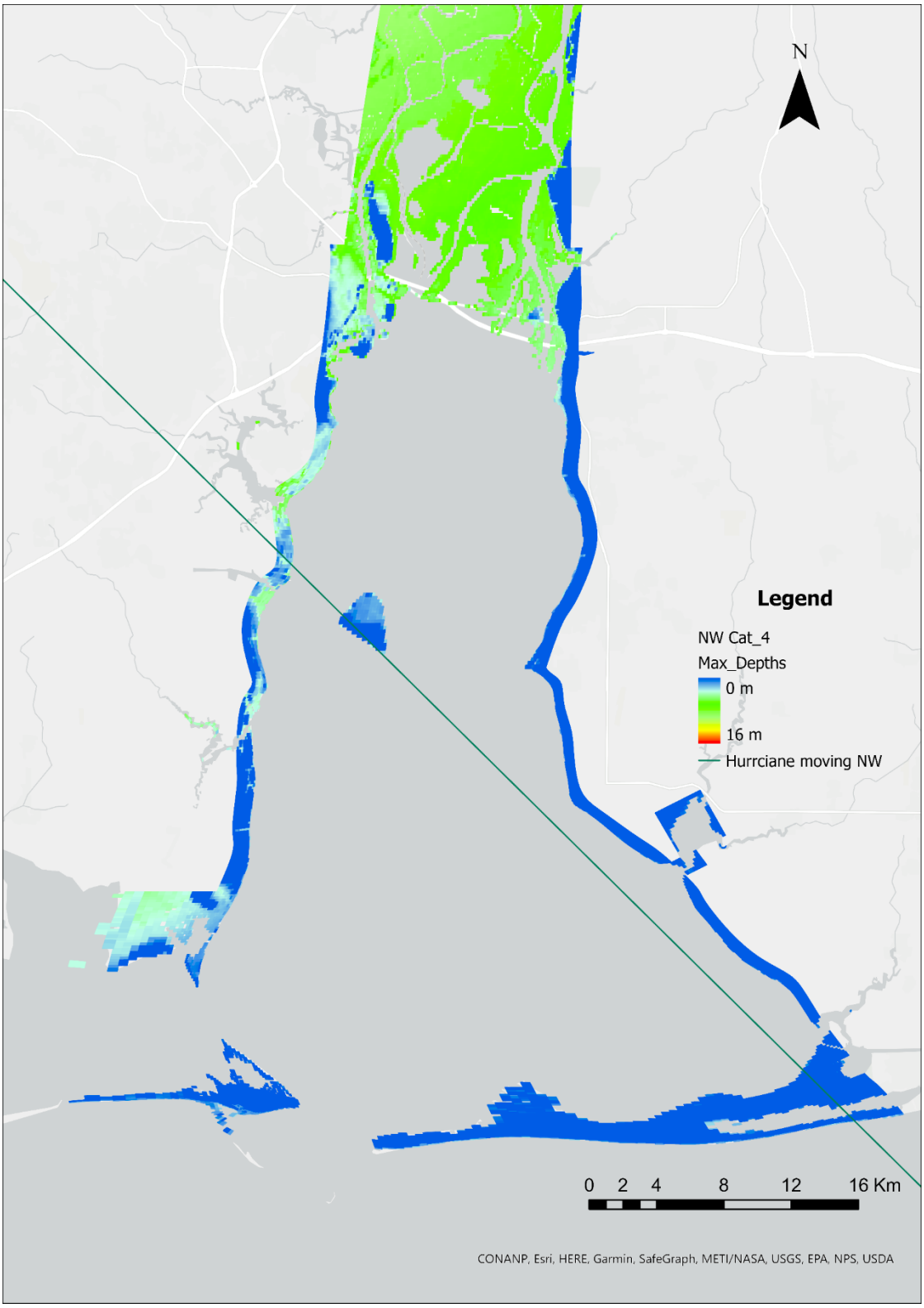

Figure 4.29 Maximum inundation by hurricane category 4 moving Northwest (ArcGIS Pro)

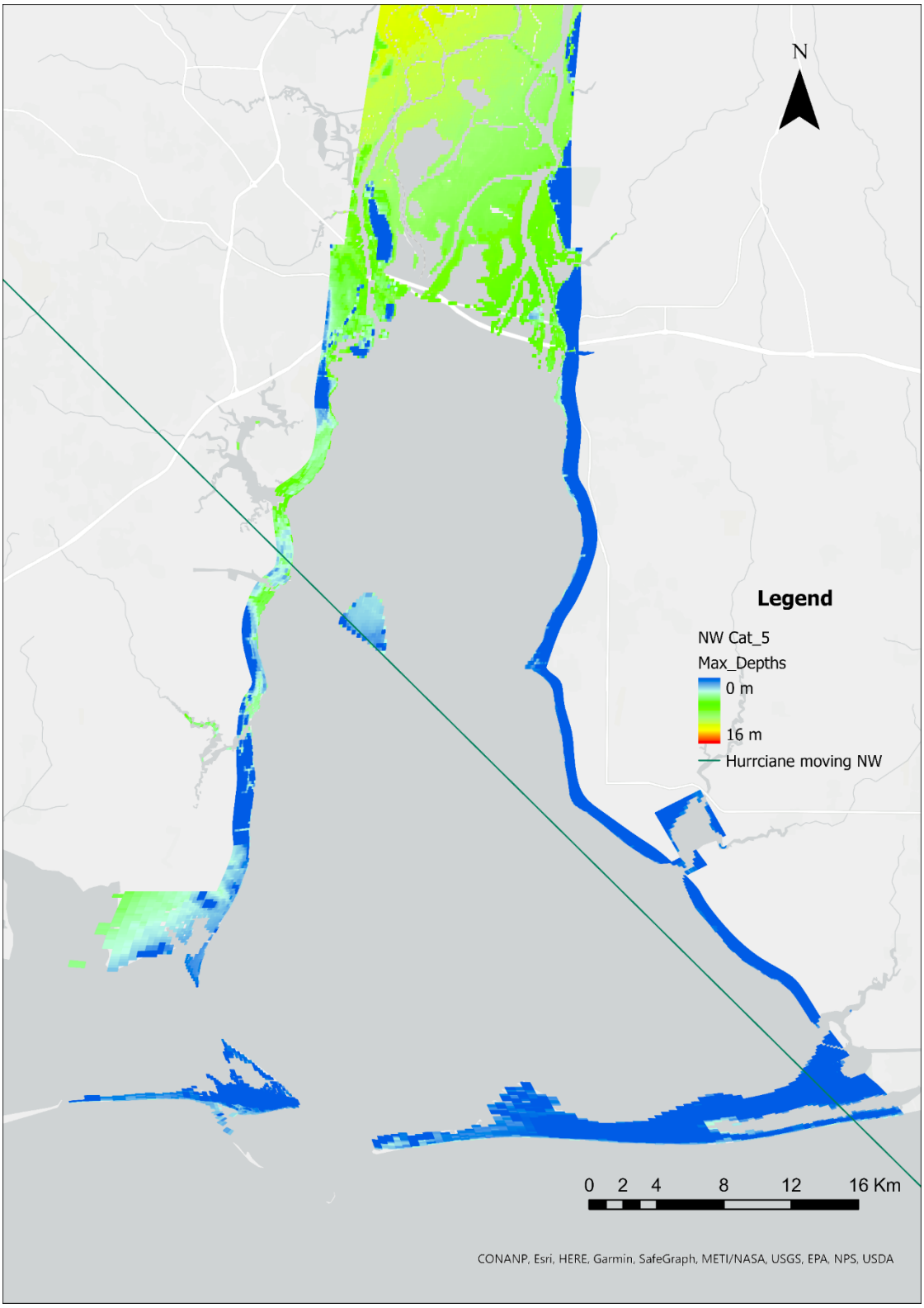

Figure 4.30 Maximum inundation by hurricane category 5 moving Northwest (ArcGIS Pro)

Table 4.22 Inundation statistics for all the coastal cells for Category 1 Hurricane moving NW.

Stats for all cells	Average depth, m	Max depth, m	Min depth, m	Std. Dev. depth, m
Average depth	0.19	0.77	0.04	0.17
Maximum depth	1.27	3.71	0.78	0.86
Std. Dev.	0.28	1.09	0.07	0.24

Table 4.23 Inundation statistics for all the coastal cells for Category 2 Hurricane moving NW.

Stats for all cells	Average depth, m	Max depth, m	Min depth, m	Std. Dev. depth, m
Average depth	0.33	1.41	0.05	0.31
Maximum depth	2.61	5.69	2.47	1.31
Std. Dev.	0.44	1.87	0.11	0.41

Table 4.24 Inundation statistics for all the coastal cells for Category 3 Hurricane moving NW.

Stats for all cells	Average depth, m	Max depth, m	Min depth, m	Std. Dev. depth, m
Average depth	0.49	2.08	0.07	0.47
Maximum depth	3.18	7.57	3.11	1.77
Std. Dev.	0.60	2.56	0.14	0.57

Table 4.25 Inundation statistics for all the coastal cells for Category 4 Hurricane moving NW.

Stats for all cells	Average depth, m	Max depth, m	Min depth, m	Std. Dev. depth, m
Average depth	0.73	2.97	0.09	0.70
Maximum depth	3.27	9.74	2.73	2.26
Std. Dev.	0.79	3.32	0.16	0.76

Table 4.26 Inundation statistics for all the coastal cells for Category 5 Hurricane moving NW.

Stats for all cells	Average depth, m	Max depth, m	Min depth, m	Std. Dev. depth, m
Average depth	1.01	4.01	0.10	0.96
Maximum depth	4.01	12.11	3.96	2.80
Std. Dev.	0.99	4.17	0.19	0.97

4.3.2 DISCUSSION

For the hurricane moving North, some low-lying coastal region of the Mobile County was slightly flooded whereas Baldwin County was not much impacted by the Category 1 hurricane which can be visualized from the inundation map. With Category 2 hurricane, more areas on the top half coastal region of the Mobile County were flooded with higher depths and there was some flooding on the bottom half of the Baldwin County as well. With Category 3 and above, many more areas were impacted on both Mobile and Baldwin Counties along with all three coastal highways. Almost all the coastal region of the Mobile County was heavily flooded by the Category 5 hurricane whereas the top half of the Baldwin County was affected only along the boundary. The average (maximum) of the average depths is 0.32 m (2.55 m), 0.52 m (3.28 m), 0.8 m (4.11 m), 1.23m (4.20 m), and 1.77 m (8.47 m) for Category 1, 2, 3, 4, and 5 respectively. The average (maximum) of the maximum depths is 1.39 m (5.19 m), 2.22 m (7.51 m), 3.23 m (9.68 m), 4.75 m (12.59 m), and 6.72 m (15.90 m) for Category 1, 2, 3, 4, and 5 respectively. The maximum flooding could be seen on the top wetland regions for all five hurricane categories.

For the hurricane moving Northeast, same area of the Mobile County was slightly flooded (with lower depths) including some wetland areas on the bottom part of the Baldwin County by the category 1 hurricane as compared to the north moving hurricane. With Category 2 hurricane, more areas in the top half coastal region of the Mobile County were flooded. With Category 3 and above, many more areas were impacted on both the both counties but the impact on the mobile coastal regions were lesser whereas that on the Baldwin coastal regions on the bottom part was higher as compared to the hurricane moving North. Almost all the coastal region of the Mobile County was heavily flooded by the Category 5 hurricane whereas the top half of the Baldwin County was affected only along the boundary. The results are similar to that of the hurricane moving north but the inundation depths were higher along the coastal region of Mobile County in the former whereas in the latter the inundation depths were higher along the coastal region of Baldwin County. The average (maximum) of the average depths is 0.27 m (1.46 m), 0.32 m (2.55 m), 0.72 m (4.11 m), 1.11 m (4.29 m), and 1.59 m (8.40 m) for Category 1, 2, 3, 4, and 5 respectively. The average (maximum) of the maximum depths is 1.11 m (4.56 m), 1.38 m (5.19 m), 2.77 m (8.62 m), 4.10 m (11.19 m), and 5.79 m (14.16 m) for Category 1, 2, 3, 4, and 5 respectively. The maximum flooding could be seen on the top wetland regions for all five hurricane categories with depths lower than hurricane moving north.

For the hurricane moving Northwest, same area of the Mobile County was slightly flooded (with similar depths) by the category 1 hurricane as compared to the north moving hurricane. With Category 2 hurricanes, the results are similar to those of hurricane moving NE as more areas in the top half coastal region of the Mobile County were flooded. With Category 3 and above, many more areas were impacted on Mobile County which can be seen on the inundation maps, but the impacted regions and inundation depths are lower than Hurricane moving N but higher than hurricane moving NE. The coastal regions in Baldwin County were least impacted even on the wetland regions in the bottom half of the bay compared to the other two hurricane directions for all five categories. The average (maximum) of the average depths is 0.19 m (1.27 m), 0.33 m (2.61 m), 0.49 m (3.18 m), 0.73 m (3.27 m), and 1.01 m (4.01 m) for Category 1, 2, 3, 4, and 5 respectively. The average (maximum) of the maximum depths is 0.77 m (3.71 m), 1.41 m (5.69 m), 2.08 m (7.57 m), 2.97 m (9.74 m), and 4.01 m (12.11 m) for Category 1, 2, 3, 4, and 5 respectively. The maximum flooding could be seen on the top wetland regions for all five hurricane categories with depths lower than hurricane moving Northeast and North.

If we compared all the data for hurricane category among all three directions, it can be inferred that the average (maximum) of the average depths and average (maximum) of the maximum depths is highest for the Hurricane moving N followed by Hurricane moving NE followed by Hurricane moving NW. This can be visualized from the inundation maps as well. The coastal regions of the Mobile County were impacted highly by the hurricane moving North whereas the coastal regions of the Baldwin County were impacted highly by the hurricane moving Northeast. The coastal highways: Dauphin Island Parkway 193 in Mobile County and Scenic Highway 98 and Fort Morgan Road in Baldwin County are heavily affected by category 4 and 5 with highest impact by hurricane moving north and northeast followed by northwest. On the top wetland, the inundation is highest for hurricane N and results are similar for both NE and NW hurricane.

If we compare the Hazus results with Hypothetical track results, we can see similar kind of effect for similar intensity and direction of the hurricane. The 10-year storm events have the hurricane track farthest from the bay and it falls in the category of tropical storm which is why it has the lowest level of inundation in terms of the average and the maximum depths compared to all other scenarios. The 20-year storm falls under the category 1 hurricane and the track is similar to that of Category 1 hurricane moving North. Comparing the inundation depths data between 20-year storm

and Category 1 hurricane moving North, it can be seen that there is a close match between each other compared to hurricane moving NE and NW. The 50-year storm inundation data matches with the Category 2 hurricane moving North. The 100-year storm inundation data closely matches with the Category 3 hurricane moving North as both storms fall under same category and have similar direction as well. 200-year storm inundation data closely matches with the Category 4 hurricane moving Northeast as both storms fall under same category, and both have similar hurricane tracks which can be seen in the inundation maps. Similarly, the 500-year and 1000-year storms inundation data matches with Category 4 hurricane moving North and Category 5 hurricane moving Northwest. There is a similar nature of inundation among the hurricanes with same category which follows the similar direction. The area near the Mobile International Airport was the most impacted region which was common for most of the scenario runs.

4.4 NNBFS TEST

The most vulnerable coastal region was identified based on the results from the scenario runs. The most common area that was most impacted under many runs was the area near the Mobile Regional Airport which is shown in Figure 4.31.Therefore, this region was selected to test different NNBFs for this study. The different NNBFs that are tested are vegetations with three different plant densities (#/m2), Artificial Reefs modeled as partially blocking fixed masks, Artificial Sand Dunes modeled by increasing the bottom elevation, and also artificial sand dunes with vegetation.

For testing NNBFs, we have used one event from both scenarios which falls in the category of major hurricanes. From scenario 1, 100-year storm event (which is a Category 3 hurricane) was selected and from scenario 2, category 4 hurricane moving north was selected. For this testing, we have not tested a Category 5 hurricane as this is an extremely rare event, and even more rare for them to make landfall as there have only been 4 in US history according to NHC NOAA.

a) NNBFs Test Region

The NNBFs test region is shown in Figure 4.31 within red polygon. There are 437 active cells with a total area of around 4 km^2. The cell size ranges from (26.2 m, 139 m) to (94.9 m, 229 m) with an average size of (51 m, 180 m). The different parameters that were used for comparing before and after the implementation of NNBFs are water depths, velocity, flow, and bed shear.

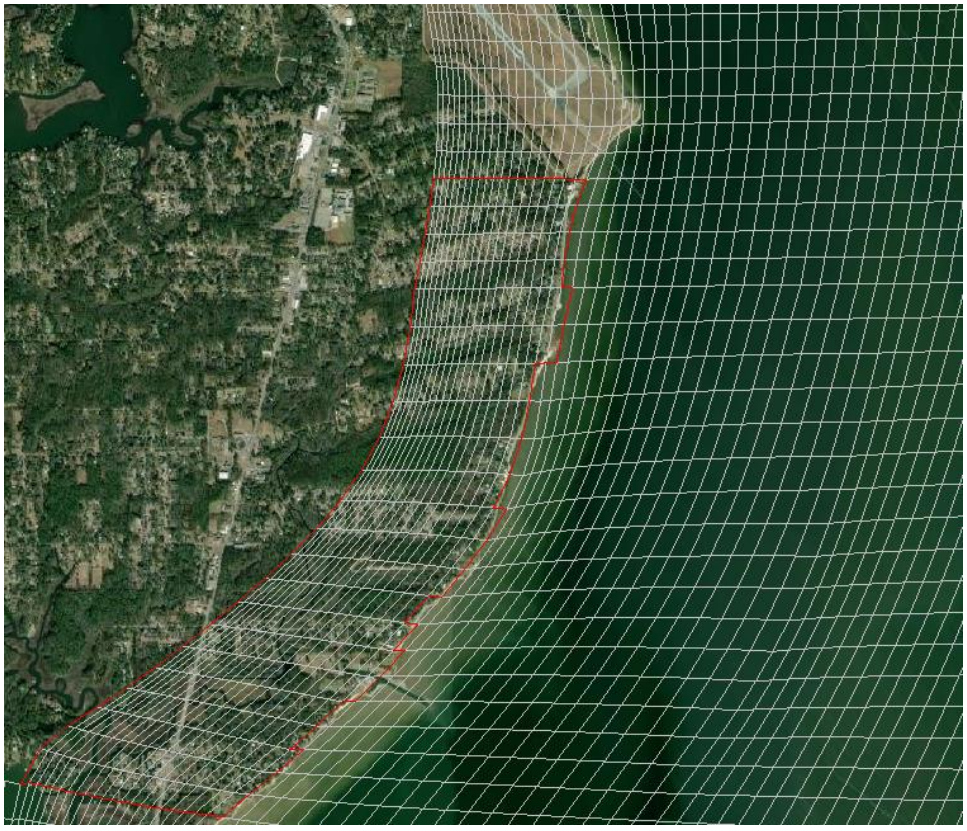

Figure 4.31 NNBFs Test Region (inside red polygon) near Mobile Regional Airport

b) Vegetation

The vegetation installation region is shown in Figure 4.32 with green cells. There are 158 active cells with a total area of around 2.2 km^2. The cell size ranges from (52.4 m, 139 m) to (123 m, 228 m) with an average size of (82.5 m, 175 m). For the vegetation tests, three different plant densities were used: 340 #/m^2 (Normal vegetation density), 3400 #/m^2 (High vegetation density), and 9645 #/m^2 (Very high vegetation density). Other vegetation parameters that are used in this study are highlighted in Table 2.3.

Figure 4.32 Vegetation installation region (green cells)

c) Artificial Reefs

The artificial reefs installation cells are shown in Figure 4.33 with red dashed lines. The artificial reefs are modeled as partially blocking masks applied on western boundary of the selected cells. The height of the mask is around 1 meter. There are 23 cells used for the implementation of the partially blocking masks.

Figure 4.33 Artificial reefs modeled as partially blocking masks (Red dashed lines)

d) Artificial Sand Dunes

The Artificial Sand Dunes installation region is shown in Figure 4.34 within red polygon. There are 47 active cells with a total area of around 0.62 km^2. The cell size ranges from (57.7 m, 139 m) to (124 m, 228 m) with an average size of (75.9 m, 176 m). The artificial sand dunes are modeled by increasing the existing bottom elevation of the selected region (shown in Figure 4.34) by 4

meters as discussed in Chapter 2.3.3. For the implementation of the combination of NNBFs, artificial sand dunes with vegetation were used with two plant densities (Normal Vegetation Density and Very High Vegetation Density).

Figure 4.34 Artificial Sand Dunes installation region (inside red polygon)

4.4.1 RESULTS

The time series data for all four parameters (water depths, velocity, flow, and bed shear) for all the cells within NNBFs test region were exported as a text file. This text file was then imported into an excel spreadsheet to calculate the maximum, minimum, average, and standard deviation of all those four parameters. Finally, these data were imported into the ArcGIS Pro to create different types of maps as per the requirements. The results for different parameters were compared visually as well as with statistics which are discussed further below.

4.4.1.1 NNBFs test for 100-year storm event

A. Water Depths (m)

The maximum water depth (in meters) was used for comparing the maximum inundation for the 100-year storm event provided by Hazus. All the maps showing maximum water depths for the NNBFs test region for different NNBFs are shown in Figure 4.35 and Figure 4.36.

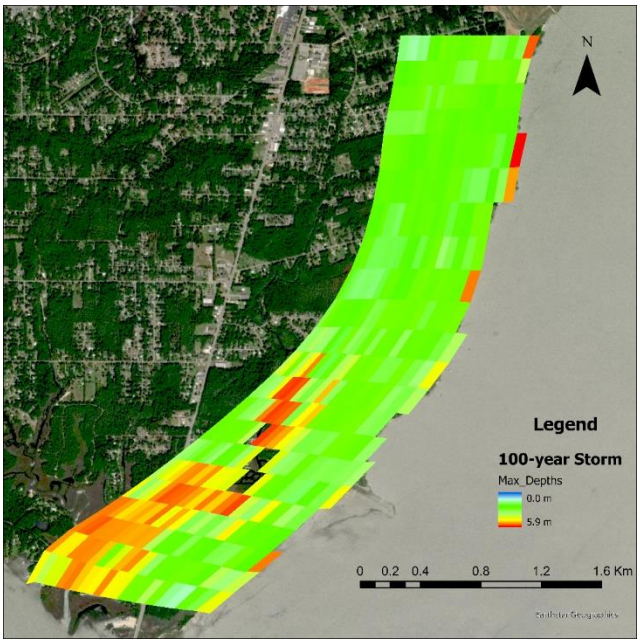

a) Present Condition

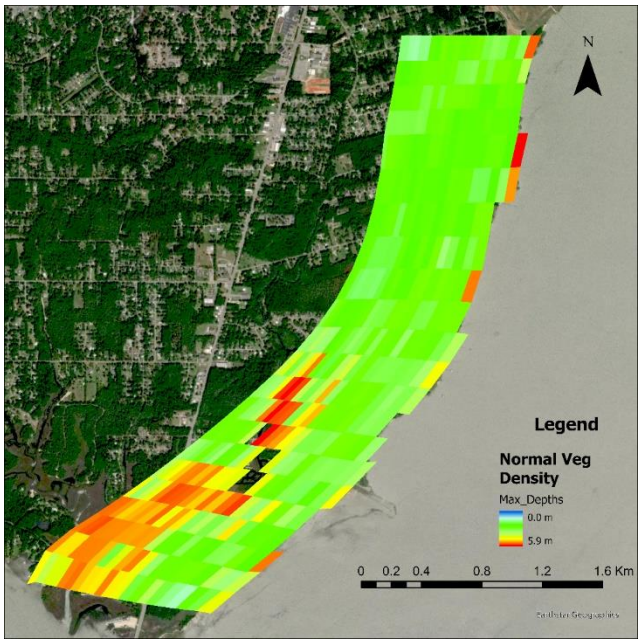

b) Normal Vegetation Density

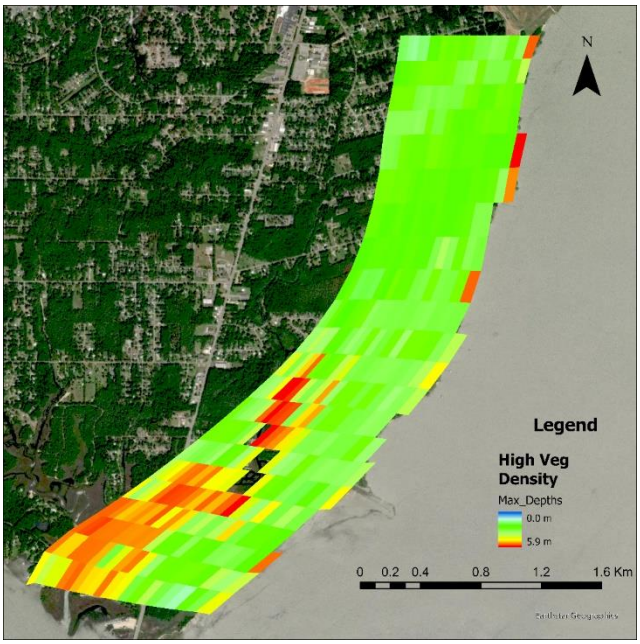

c) High Vegetation Density

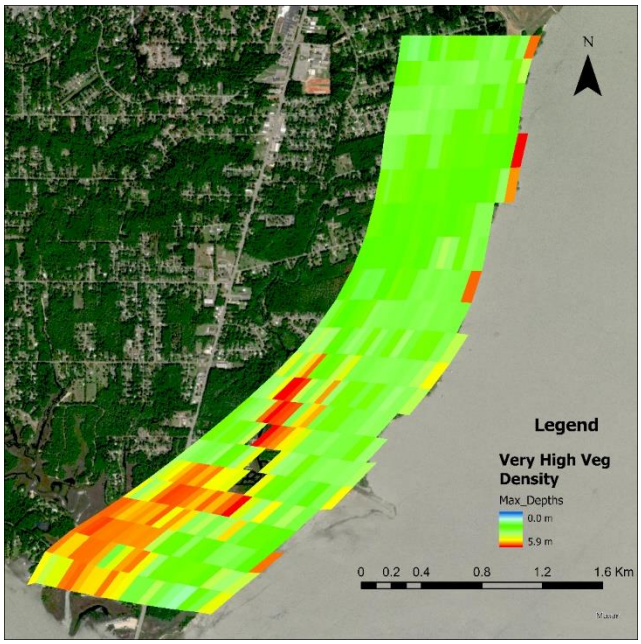

d) Very High Vegetation Density

Figure 4.35 Maximum inundation (in meters) for 100-year storm event with a) Present condition b) Normal Vegetation Density c) High Vegetation Density, and d) Very High Vegetation Density (ArcGIS Pro)

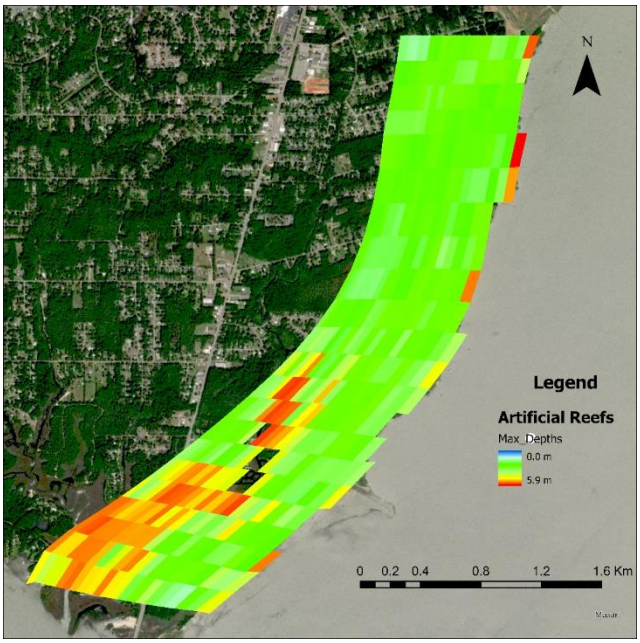

a) Artificial Reefs

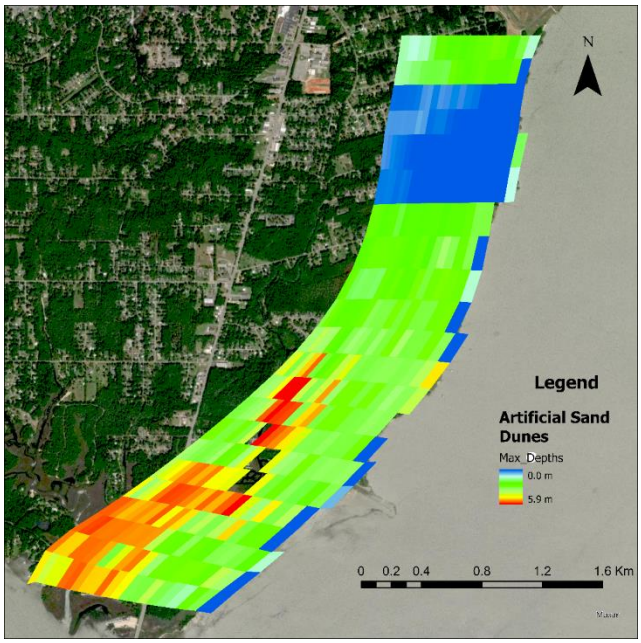

b) Artificial Sand Dunes

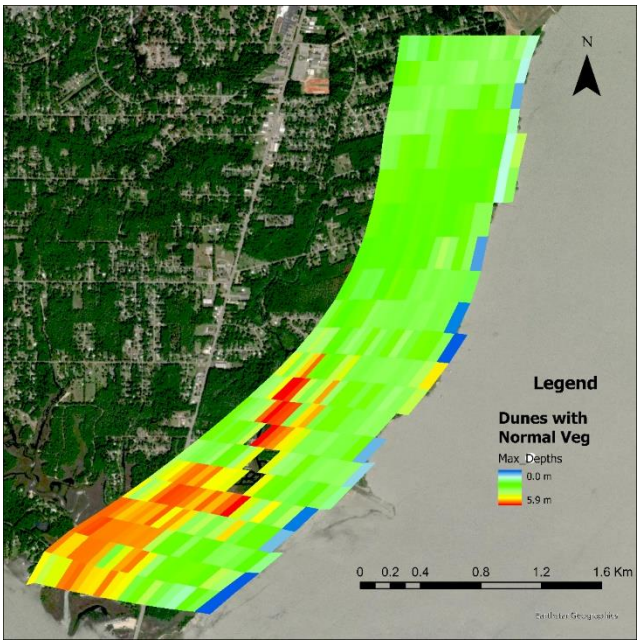

c) Dunes with Normal Vegetation Density

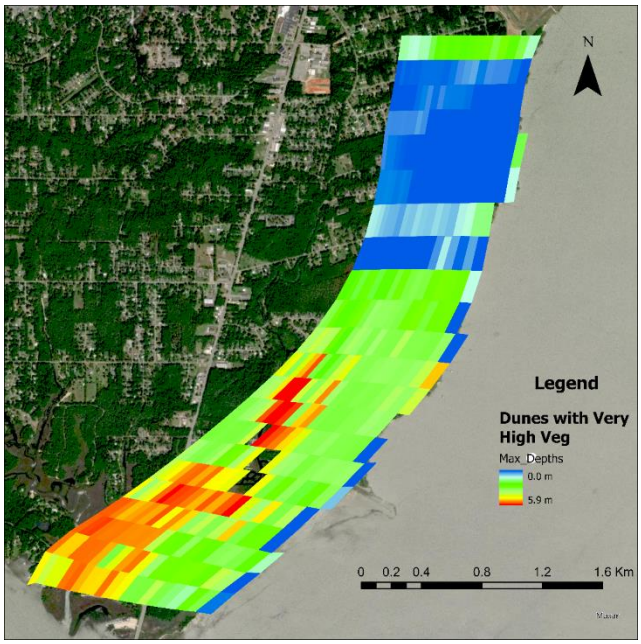

d) Dunes with Very High Vegetation Density

Figure 4.36 Maximum inundation (in meters) for 100-year storm event with a) Artificial Reefs b) Artificial Sand Dunes c) Dunes with Normal Vegetation Density, and d) Dunes with Very High Vegetation Density (ArcGIS Pro)

Difference in water depths for 100-year storm event i.e., Present condition without NNBFs – With NNBFs are shown in the Table 4.27 to Table 4.33 below.

Table 4.27 Difference in water depths with normal vegetation density (#340/ m^2).

Stats for all cells	Average depth, m	Max depth, m	Min depth, m	Standard Dev, m
Average depth	0.11	-0.05	0.04	0.02
Standard Dev	0.29	0.01	0.09	0.07
Max depth	1.18	0.03	0.45	0.29

Table 4.28 Difference in water depths with high vegetation density (#3400/m^2).

Stats for all cells	Average depth, m	Max depth, m	Min depth, m	Standard Dev, m
Average depth	0.05	-0.14	0.03	-0.03
Standard Dev	0.31	0.07	0.09	0.09
Max depth	0.93	0.07	0.45	0.23

Table 4.29 Difference in water depths with very high vegetation density (#9645/m^2).

Stats for all cells	Average depth, m	Max depth, m	Min depth, m	Standard Dev, m
Average depth	-0.09	-0.20	0.01	-0.07
Standard Dev	0.26	0.11	0.09	0.10
Max depth	0.98	0.11	0.43	0.20

Table 4.30 Difference in water depths with artificial reefs.

Stats for all cells	Average depth, m	Max depth, m	Min depth, m	Standard Dev, m
Average depth	0.00	-0.01	0.00	0.00
Standard Dev	0.04	0.02	0.02	0.01
Max depth	0.76	0.03	0.21	0.06

Table 4.31 Difference in water depths with artificial sand dunes.

Stats for all cells	Average depth, m	Max depth, m	Min depth, m	Standard Dev, m
Average depth	0.24	0.51	0.01	0.15
Standard Dev	0.48	1.15	0.16	0.30
Max depth	1.69	4.47	0.84	1.17

Table 4.32 Difference in water depths with dunes with normal vegetation density.

Stats for all cells	Average Depths, m	Max Depths, m	Min Depths, m	Standard Dev, m
Average depth	0.11	-0.08	-0.03	0.05
Standard Dev	0.41	0.65	0.16	0.20
Max depth	1.69	4.47	0.42	1.16

Table 4.33 Difference in water depths with dunes with very high vegetation density.

Stats for all cells	Average depth, m	Max depth, m	Min depth, m	Standard Dev, m
Average depth	0.31	0.71	0.02	0.20
Standard Dev	0.53	1.29	0.17	0.34
Max depth	1.61	4.26	0.50	1.17

B. Velocity (m/s)

The maximum velocity (m/s) was used for comparison for the 100-year storm event provided by Hazus. All the maps showing maximum velocity for the NNBFs test region for different NNBFs are shown in Figure 4.37 and Figure 4.38.

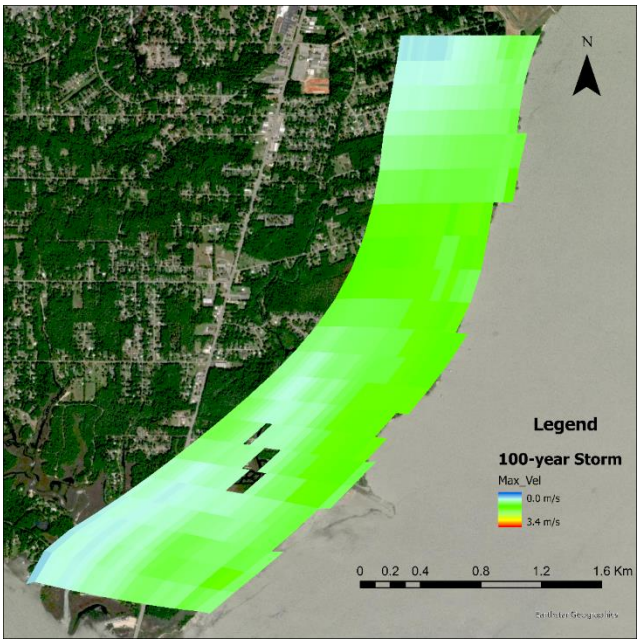

a) Present Condition

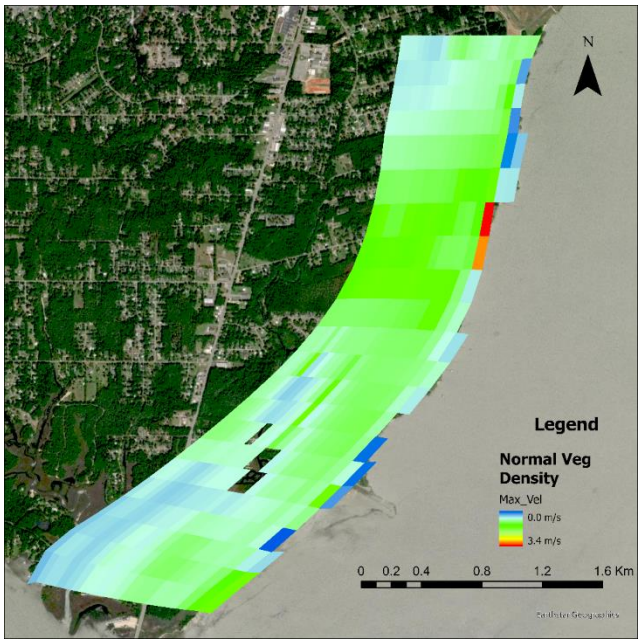

b) Normal Vegetation Density

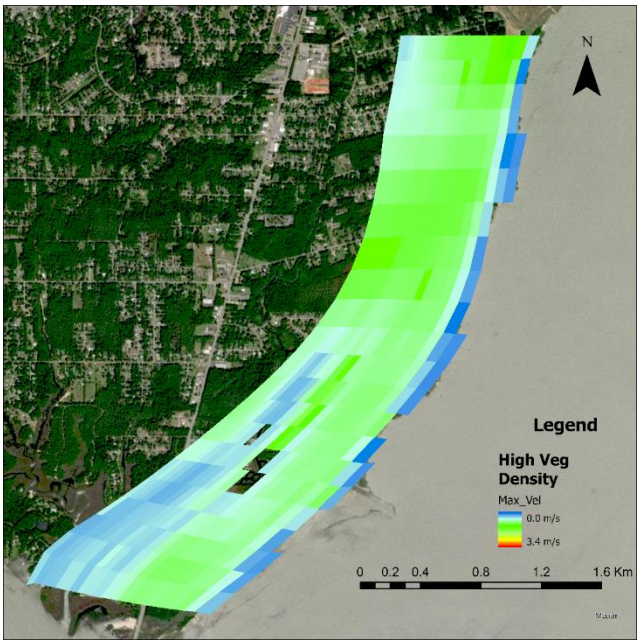

c) High Vegetation Density

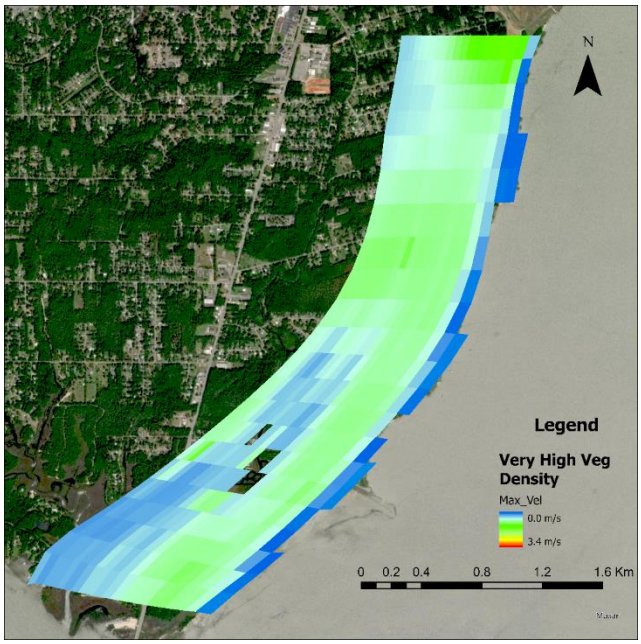

d) Very High Vegetation Density

Figure 4.37 Maximum velocity (in m/s) for 100-year storm event with a) Present condition b) Normal Vegetation Density c) High Vegetation Density, and d) Very High Vegetation Density (ArcGIS Pro)

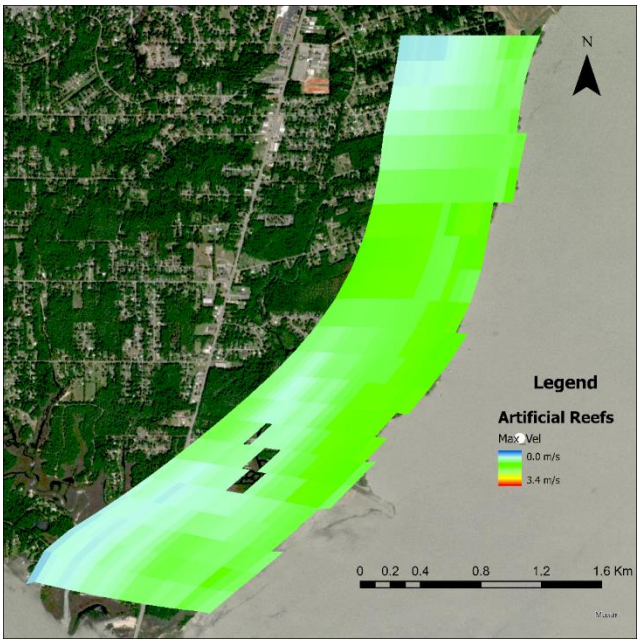

a) Artificial Reefs

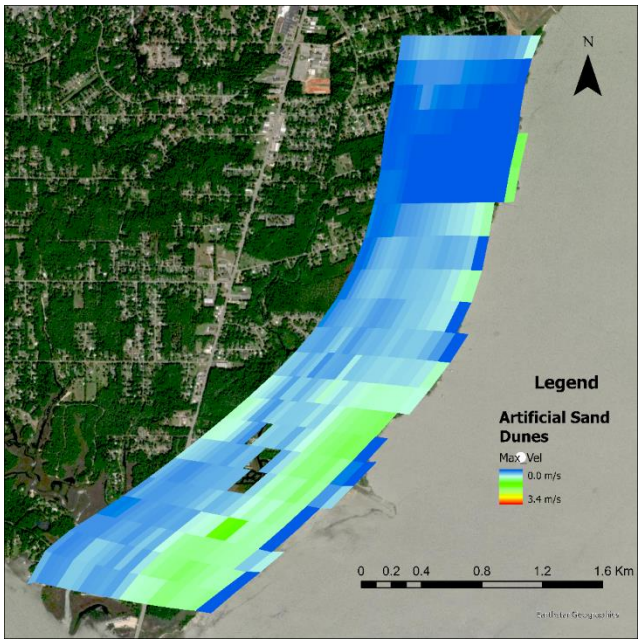

b) Artificial Sand Dunes

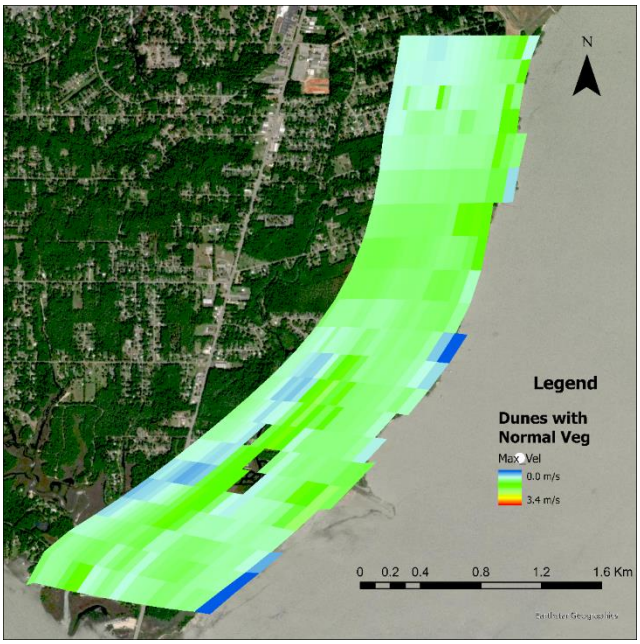

c) Dunes with Normal Vegetation Density

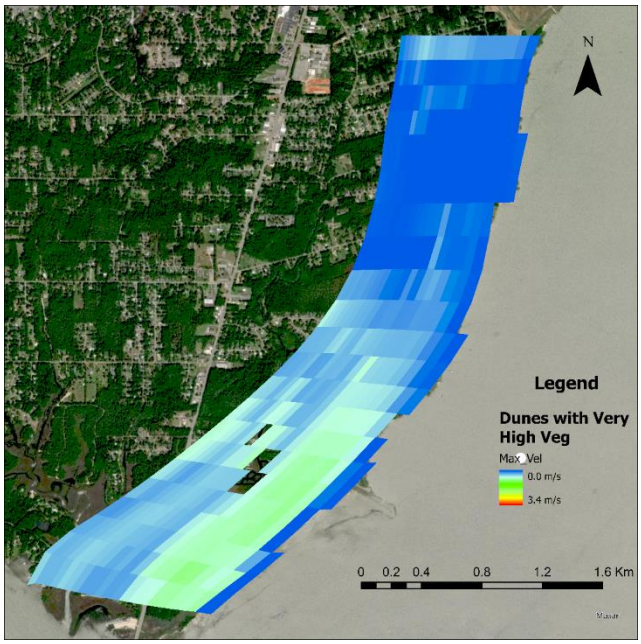

d) Dunes with Very High Vegetation Density

Figure 4.38 Maximum velocity (in m/s) for 100-year storm event with a) Artificial Reefs b) Artificial Sand Dunes c) Dunes with Normal Vegetation Density, and d) Dunes with Very High Vegetation Density (ArcGIS Pro)

Difference in velocity (m/s) for 100-year storm event i.e., Present condition without NNBFs – With NNBFs are shown in the Table 4.34 to Table 4.40 below.

Table 4.34 Difference in velocity (m/s) with normal vegetation density (#340/ m^2).

Stats for all cells	Average velocity (m/s)	Max velocity (m/s)	Min velocity (m/s)	Standard Dev velocity (m/s)
Average velocity	0.04	-0.03	0.03	-0.01
Standard Dev	0.13	0.22	0.06	0.06
Max velocity	0.58	0.99	0.36	0.28

Table 4.35 Difference in velocity (m/s) with high vegetation density (#3400/m^2).

Stats for all cells	Average velocity (m/s)	Max velocity (m/s)	Min velocity (m/s)	Standard Dev velocity (m/s)
Average velocity	0.08	0.18	0.02	0.04
Standard Dev	0.15	0.26	0.06	0.08
Max velocity	0.65	1.10	0.34	0.33

Table 4.36 Difference in velocity (m/s) with very high vegetation density (#9645/m^2).

Stats for all cells	Average velocity (m/s)	Max velocity (m/s)	Min velocity (m/s)	Standard Dev velocity (m/s)
Average velocity	0.10	0.31	0.02	0.07
Standard Dev	0.16	0.27	0.05	0.08
Max velocity	0.70	1.23	0.29	0.35

Table 4.37 Difference in velocity (m/s) with artificial reefs.

Stats for all cells	Average velocity (m/s)	Max velocity (m/s)	Min velocity (m/s)	Standard Dev velocity (m/s)
Average velocity	0.00	0.01	0.00	0.00
Standard Dev	0.02	0.02	0.03	0.01
Max velocity	0.14	0.07	0.38	0.06

Table 4.38 Difference in velocity (m/s) with artificial sand dunes.

Stats for all cells	Average velocity (m/s)	Max velocity (m/s)	Min velocity (m/s)	Standard Dev velocity (m/s)
Average velocity	0.21	0.62	0.03	0.16
Standard Dev	0.24	0.32	0.08	0.11
Max velocity	0.78	1.32	0.36	0.43

Table 4.39 Difference in velocity (m/s) with dunes with normal vegetation density.

Stats for all cells	Average velocity (m/s)	Max velocity (m/s)	Min velocity (m/s)	Standard Dev velocity (m/s)
Average velocity	0.05	0.08	0.01	0.02
Standard Dev	0.20	0.27	0.15	0.11
Max velocity	0.62	1.32	0.33	0.37

Table 4.40 Difference in velocity (m/s) with dunes with very high vegetation density.

Stats for all cells	Average velocity (m/s)	Max velocity (m/s)	Min velocity (m/s)	Standard Dev velocity (m/s)
Average velocity	0.23	0.67	0.04	0.17
Standard Dev	0.25	0.36	0.08	0.12
Max velocity	0.87	1.48	0.38	0.46

C. Flow (m^3/s)

The maximum flow (m^3/s) was used for comparison for the 100-year storm event provided by Hazus. All the maps showing maximum flow for the NNBFs test region for different NNBFs are shown in Figure 4.39 and Figure 4.40.

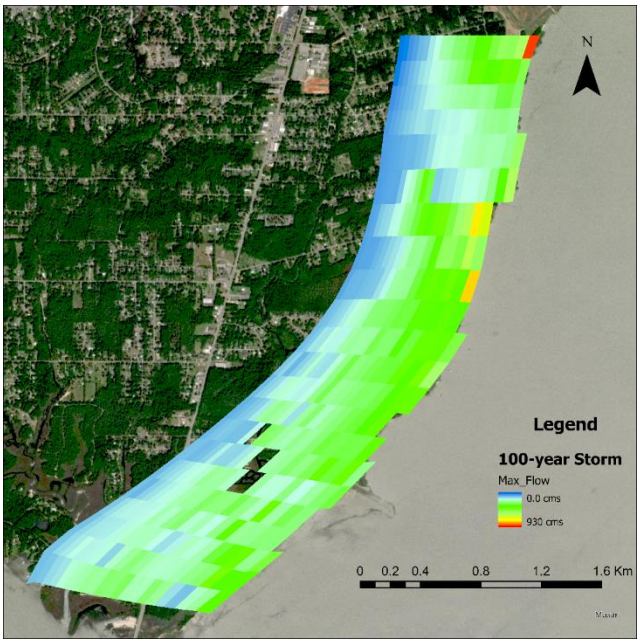

a) Present Condition

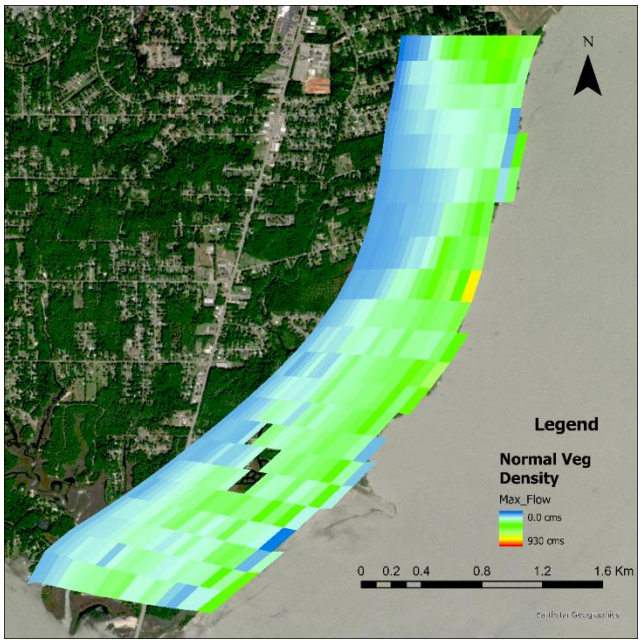

b) Normal Vegetation Density

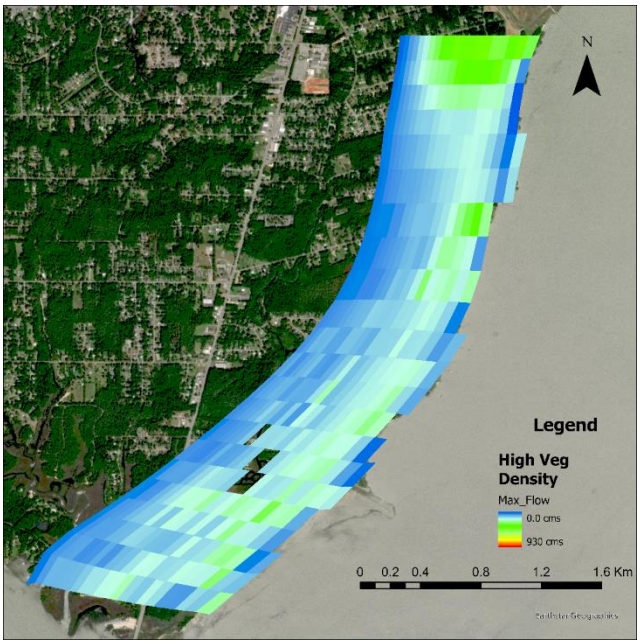

c) High Vegetation Density

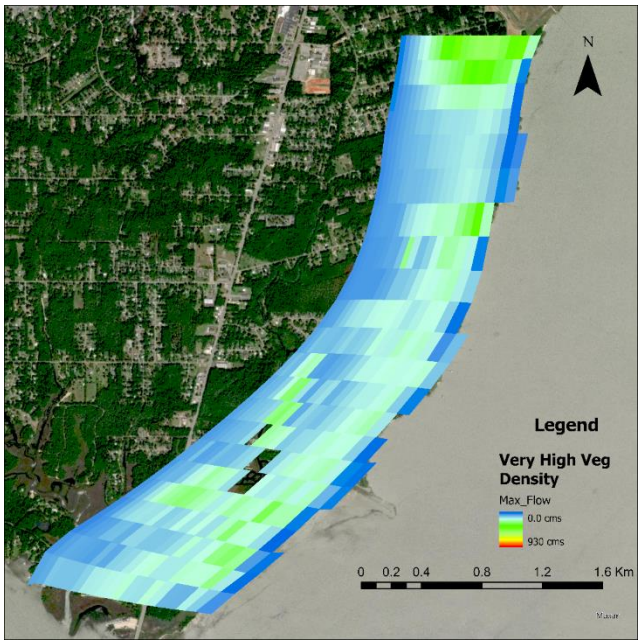

d) Very High Vegetation Density

Figure 4.39 Maximum flow (in m^3/s) for 100-year storm event with a) Present condition b) Normal Vegetation Density c) High Vegetation Density, and d) Very High Vegetation Density (ArcGIS Pro)

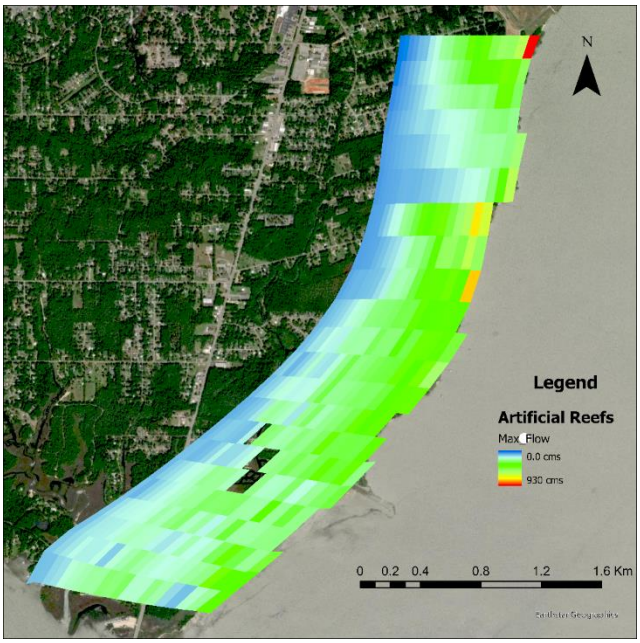

A. Artificial Reefs

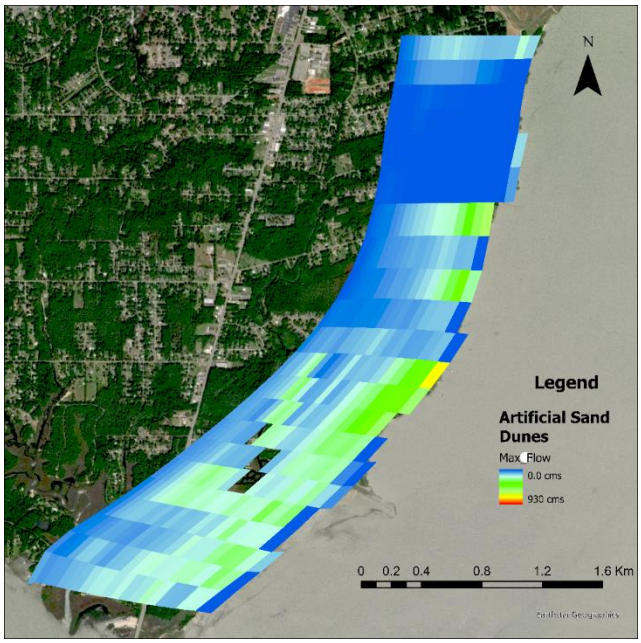

B. Artificial Sand Dunes

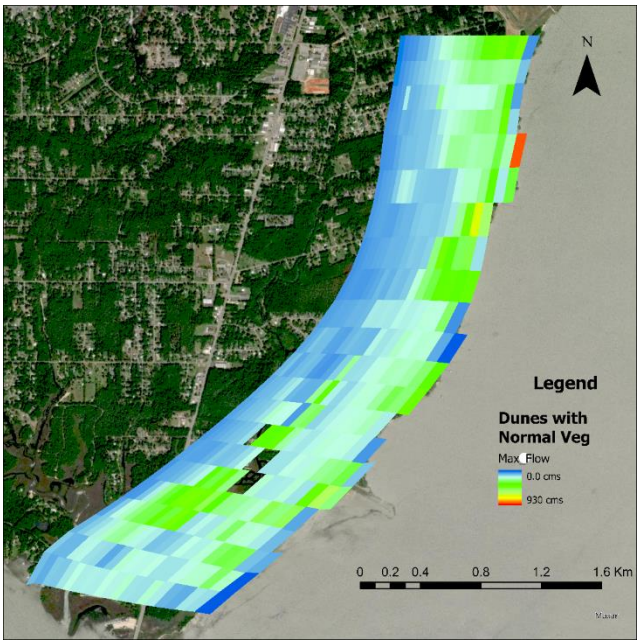

C. Dunes with Normal Vegetation Density

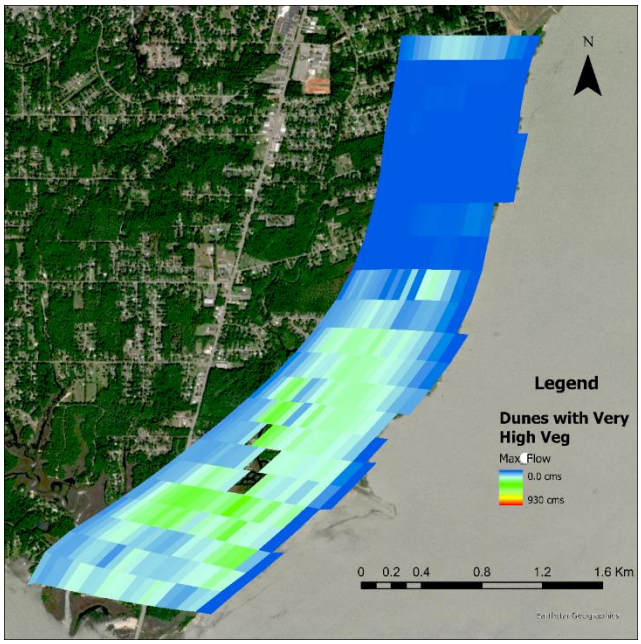

D. Dunes with Very High Vegetation Density

Figure 4.40 Maximum flow (in m^3/s) for 100-year storm event with a) Artificial Reefs b) Artificial Sand Dunes c) Dunes with Normal Vegetation Density, and d) Dunes with Very High Vegetation Density (ArcGIS Pro)

Difference in flow (m^3/s) for 100-year storm event i.e., Present condition without NNBFs – With NNBFs are shown in the Table 4.41 to Table 4.47 below.

Table 4.41 Difference in flow (m^3/s) with Normal Vegetation Density (#340/ m^2).

Stats for all cells	Average flow (m^3/s)	Max flow (m^3/s)	Min flow (m^3/s)	Standard Dev flow (m^3/s)
Average flow	12.34	28.65	0.58	9.83
Standard Dev	26.30	66.80	2.54	20.21
Max flow	115.69	385.09	25.64	105.39

Table 4.42 Difference in flow (m^3/s) with high vegetation density (#3400/m^2).

Stats for all cells	Average flow (m^3/s)	Max flow (m^3/s)	Min flow (m^3/s)	Standard Dev flow (m^3/s)
Average flow	18.78	66.01	0.46	19.25
Standard Dev	34.14	95.66	2.65	28.92
Max flow	145.76	556.90	25.66	131.80

Table 4.43 Difference in flow (m^3/s) with very high vegetation density (#9645/m^2).

Stats for all cells	Average flow (m^3/s)	Max flow (m^3/s)	Min flow (m^3/s)	Standard Dev flow (m^3/s)
Average flow	17.32	79.99	0.35	20.69
Standard Dev	31.56	107.54	2.72	29.97
Max flow	147.19	660.73	24.45	139.28

Table 4.44 Difference in flow (m^3/s) with artificial reefs.

Stats for all cells	Average flow (m^3/s)	Max flow (m^3/s)	Min flow (m^3/s)	Standard Dev flow (m^3/s)
Average flow	0.43	1.07	-0.02	0.34
Standard Dev	4.47	22.01	0.49	6.44
Max flow	42.93	303.72	6.88	92.20

Table 4.45 Difference in flow (m^3/s) with artificial sand dunes.

Stats for all cells	Average flow (m^3/s)	Max flow (m^3/s)	Min flow (m^3/s)	Standard Dev flow (m^3/s)
Average flow	29.71	123.08	0.46	31.86
Standard Dev	38.07	112.92	3.46	29.61
Max flow	162.24	746.26	16.57	148.20

Table 4.46 Difference in flow (m^3/s) with dunes with normal veg density.

Stats for all cells	Average flow (m^3/s)	Max flow (m^3/s)	Min flow (m^3/s)	Standard Dev flow (m^3/s)
Average flow	13.73	53.62	-0.35	16.70
Standard Dev	34.51	101.75	7.74	31.52
Max flow	137.15	823.27	24.69	148.20

Table 4.47 Difference in flow (m^3/s) with dunes with very high veg density.

Stats for all cells	Average flow (m^3/s)	Max flow (m^3/s)	Min flow (m^3/s)	Standard Dev flow (m^3/s)
Average flow	32.24	130.41	0.89	33.75
Standard Dev	42.65	146.14	2.84	38.42
Max flow	191.34	882.45	23.77	162.88

D. Bed shear (N/m^2)

The average bed shear (N/m^2) was used for the comparison for the 100-year storm event provided by Hazus. All the maps showing average bed shear for the NNBFs test region for different NNBFs are shown in Figure 4.41 and Figure 4.42.

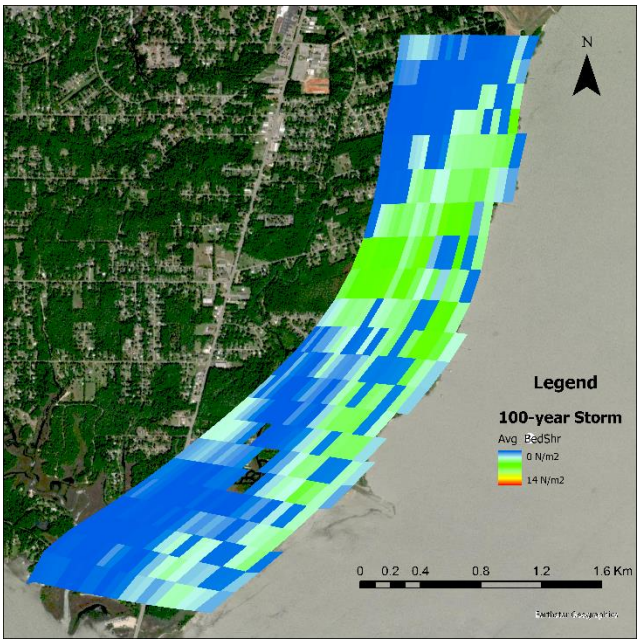

a) Present Condition

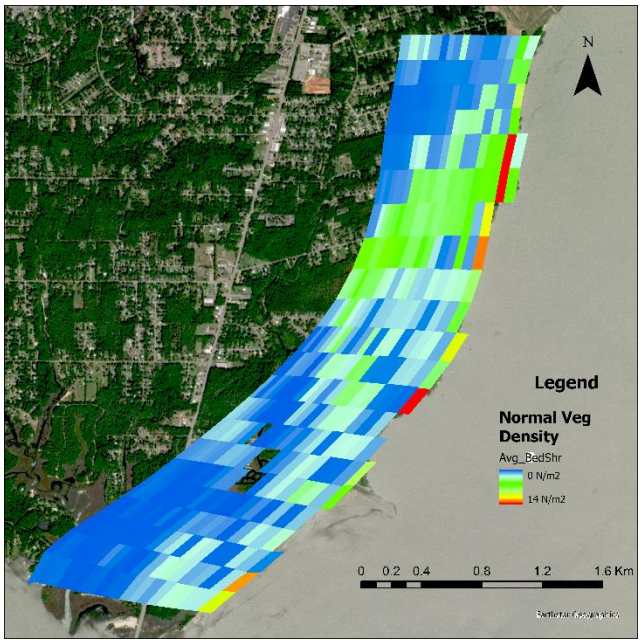

b) Normal Vegetation Density

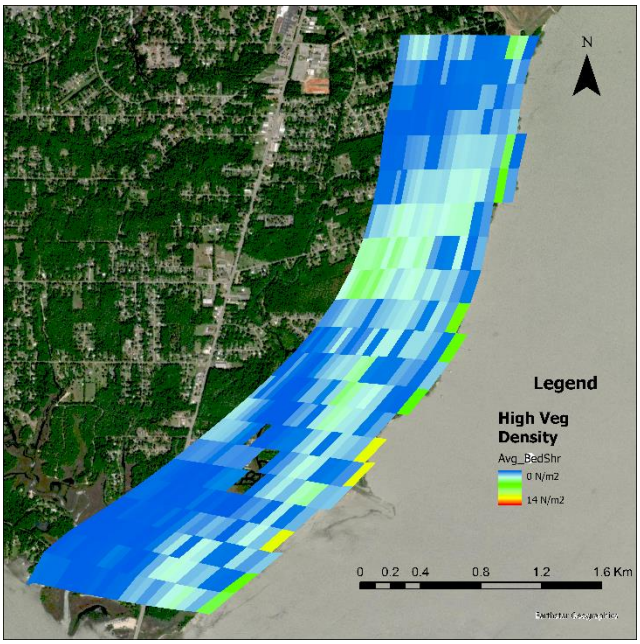

c) High Vegetation Density

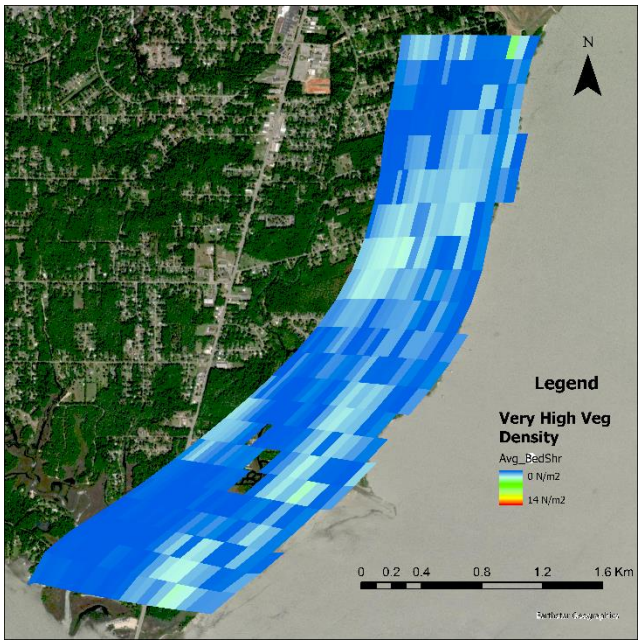

d) Very High Vegetation Density

Figure 4.41 Average bed shear (in N/m^2) for 100-year storm event with a) Present condition b) Normal Vegetation Density c) High Vegetation Density, and d) Very High Vegetation Density (ArcGIS Pro)

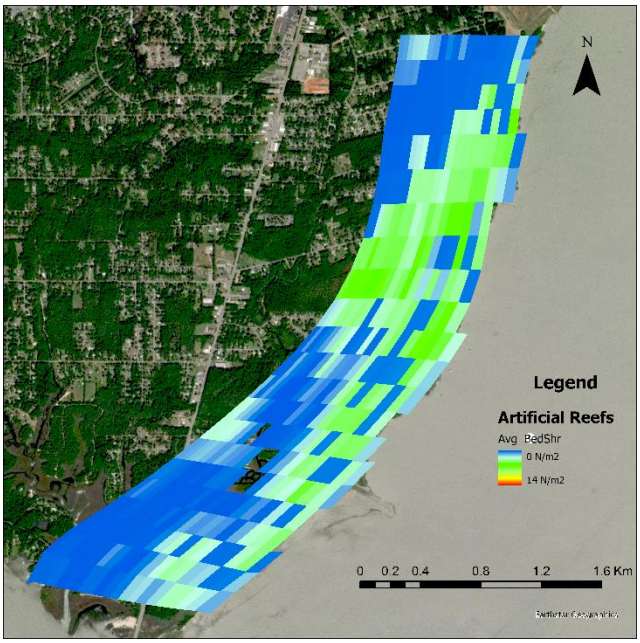

a) Artificial Reefs

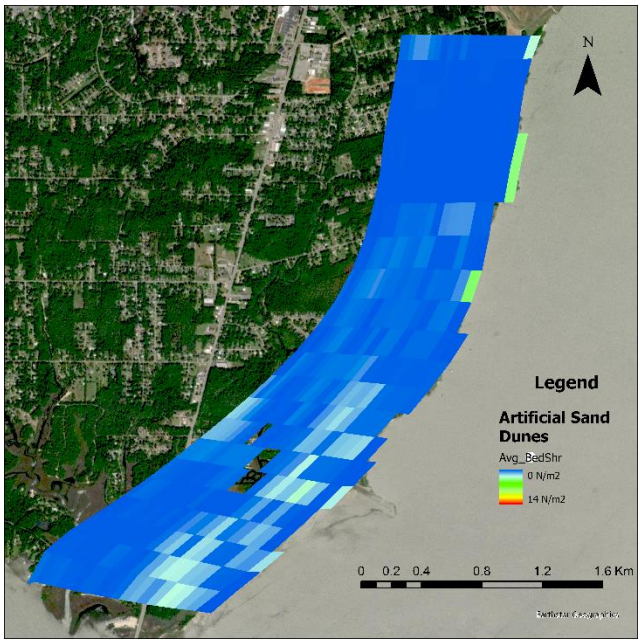

b) Artificial Sand Dunes

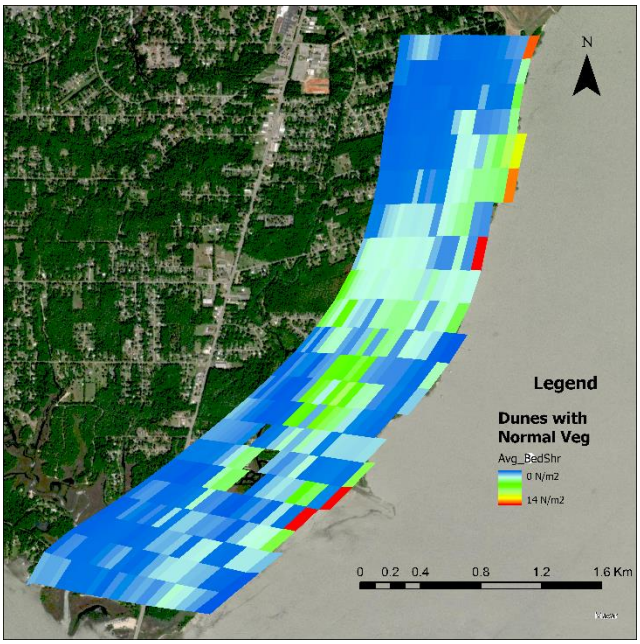

c) Dunes with Normal Vegetation Density

.

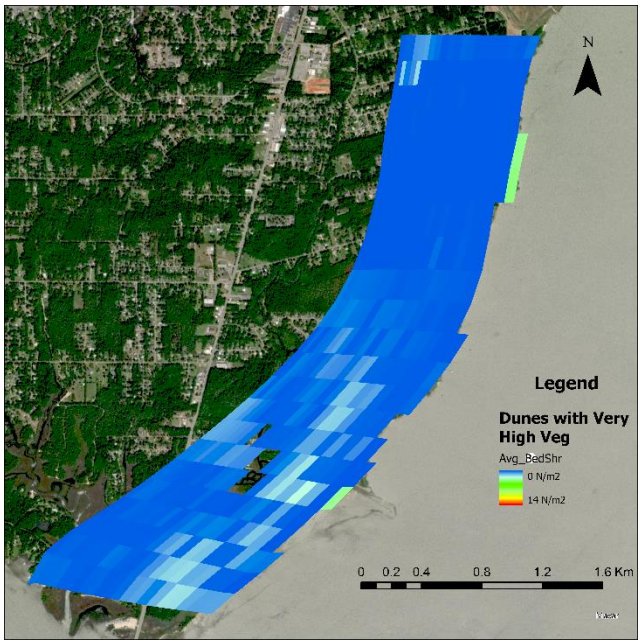

d) Dunes with Very High Vegetation Density

Figure 4.42 Average bed shear (in N/m^2) for 100-year storm event with a) Artificial Reefs b) Artificial Sand Dunes c) Dunes with Normal Vegetation Density, and d) Dunes with Very High Vegetation Density (ArcGIS Pro)

Difference in bed shear (N/m^2) for 100-year storm event i.e., Present condition without NNBFs – With NNBFs are shown in the Table 4.48 to Table 4.54 below.

Table 4.48 Difference in bed shear (N/m^2) with normal vegetation density (#340/ m^2).

Stats for all cells	Average bed shear (N/m^2)	Max bed shear (N/m^2)	Min bed shear (N/m^2)	Std. dev. bed shear (N/m^2)
Average bed shear	-0.29	-4.55	0.12	-0.80
Std. dev.	1.72	18.23	0.31	3.13
Max bed shear	3.62	11.80	1.62	3.55

Table 4.49 Difference in bed shear (N/m^2) with high vegetation density (#3400/m^2).

Stats for all cells	Average bed shear (N/m^2)	Max bed shear (N/m^2)	Min bed shear (N/m^2)	Std. dev. bed shear (N/m^2)
Average bed shear	0.42	0.10	0.12	0.18
Std. dev.	1.31	7.51	0.31	1.72
Max bed shear	4.54	14.47	1.65	4.07

Table 4.50 Difference in bed shear (N/m^2) with very high vegetation density (#9645/m^2).

Stats for all cells	Average bed shear (N/m^2)	Max bed shear (N/m^2)	Min bed shear (N/m^2)	Std. dev. bed shear (N/m^2)
Average bed shear	0.93	2.95	0.09	0.82
Std. dev.	1.27	3.68	0.26	1.03
Max bed shear	5.35	15.34	1.61	4.47

Table 4.51 Difference in bed shear (N/m^2) with artificial reefs.

Stats for all cells	Average bed shear (N/m^2)	Max bed shear (N/m^2)	Min bed shear (N/m^2)	Std. dev. bed shear (N/m^2)
Average bed shear	0.03	0.13	0.00	0.03
Std. dev.	0.21	0.73	0.15	0.22
Max bed shear	1.48	6.48	1.86	1.74

Table 4.52 Difference in bed shear (N/m^2) with artificial sand dunes.

Stats for all cells	Average bed shear (N/m^2)	Max bed shear (N/m^2)	Min bed shear (N/m^2)	Std. dev. bed shear (N/m^2)
Average bed shear	1.42	4.99	0.13	1.35
Std. dev.	1.76	4.56	0.39	1.35
Max bed shear	5.96	15.68	1.68	4.83

Table 4.53 Difference in bed shear (N/m^2) with dunes with normal veg density.

Stats for all cells	Average bed shear (N/m^2)	Max bed shear (N/m^2)	Min bed shear (N/m^2)	Std. dev. bed shear (N/m^2)
Average bed shear	-0.02	-1.78	0.01	-0.21
Std. dev.	2.43	12.52	1.54	2.89
Max bed shear	4.70	11.75	1.85	4.12

Table 4.54 Difference in bed shear (N/m^2) with dunes with very high veg density.

Stats for all cells	Average bed shear (N/m^2)	Max bed shear (N/m^2)	Min bed shear (N/m^2)	Std. dev. bed shear (N/m^2)
Average bed shear	1.47	5.23	0.14	1.40
Std. dev.	1.81	4.04	0.43	1.33
Max bed shear	6.63	18.73	1.88	5.29

4.4.1.2 NNBFs test for Category 4 hurricane moving North.

A. Water Depths (m)

The maximum water depth (in meters) was used for comparing the maximum inundation for the Category 4 hurricane moving North. All the maps showing maximum water depths for the NNBFs test region for different NNBFs are shown in Figure 4.43 and Figure 4.44.

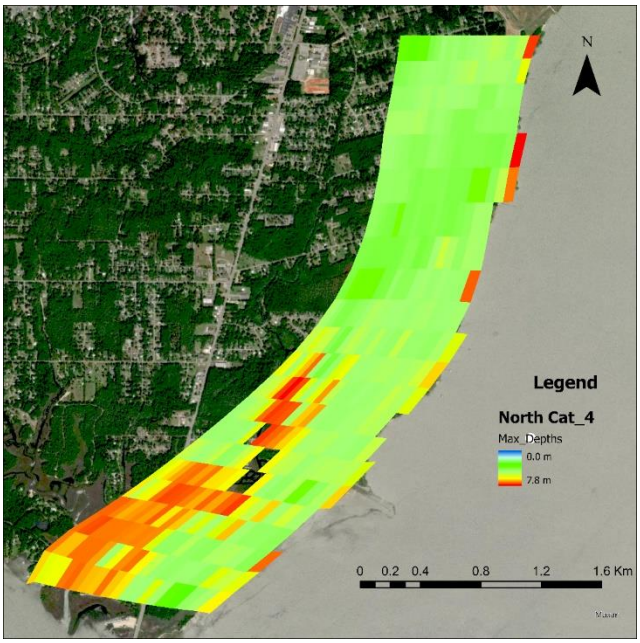

a) Present Condition

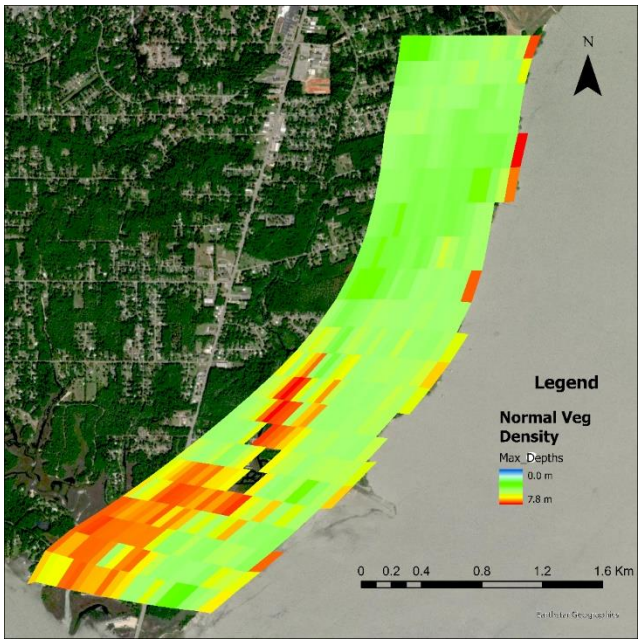

b) Normal Vegetation Density

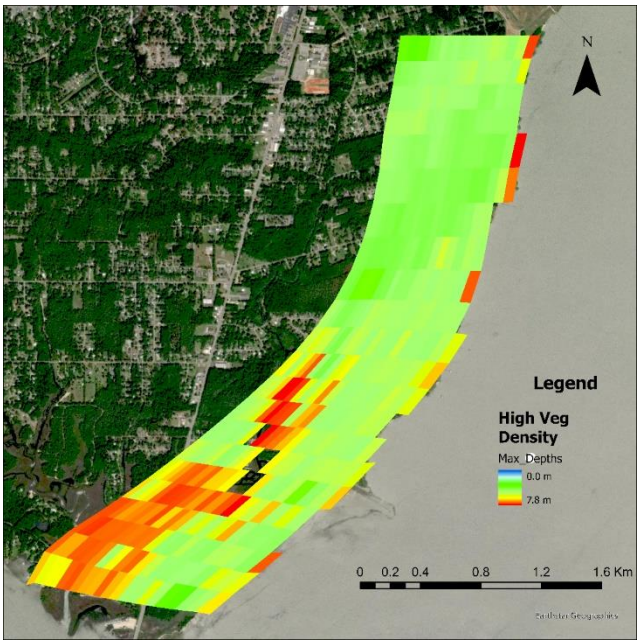

c) High Vegetation Density

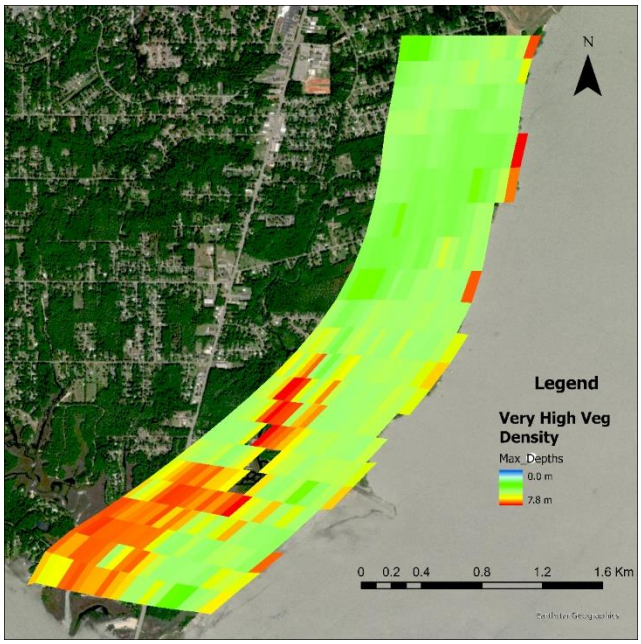

d) Very High Vegetation Density

Figure 4.43 Maximum inundation (in meters) for Category 4 hurricane moving North with a) Present condition b) Normal Vegetation Density c) High Vegetation Density, and d) Very High Vegetation Density (ArcGIS Pro)

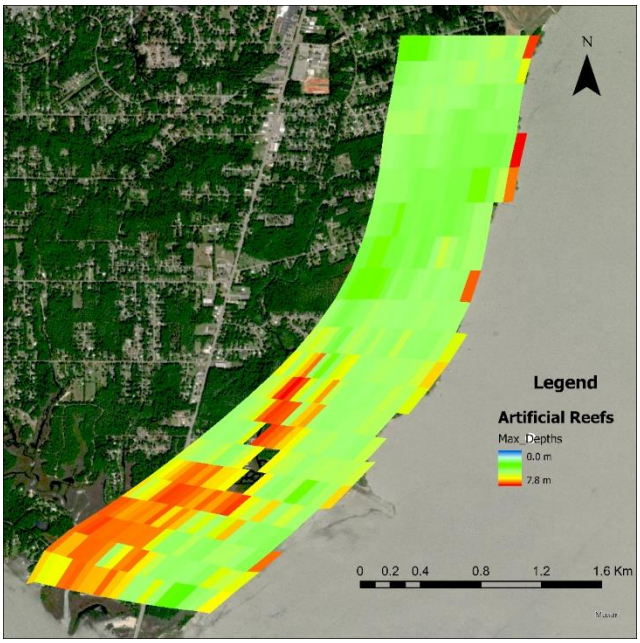

a) Artificial Reefs

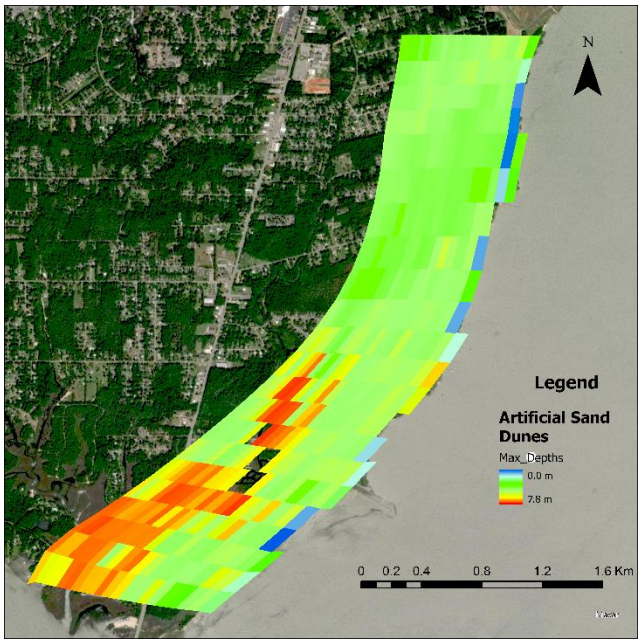

b) Artificial Sand Dunes

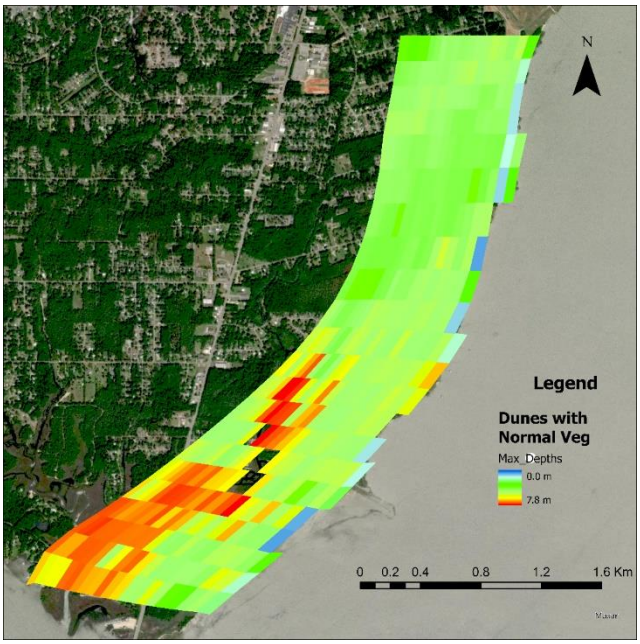

c) Dunes with Normal Vegetation Density

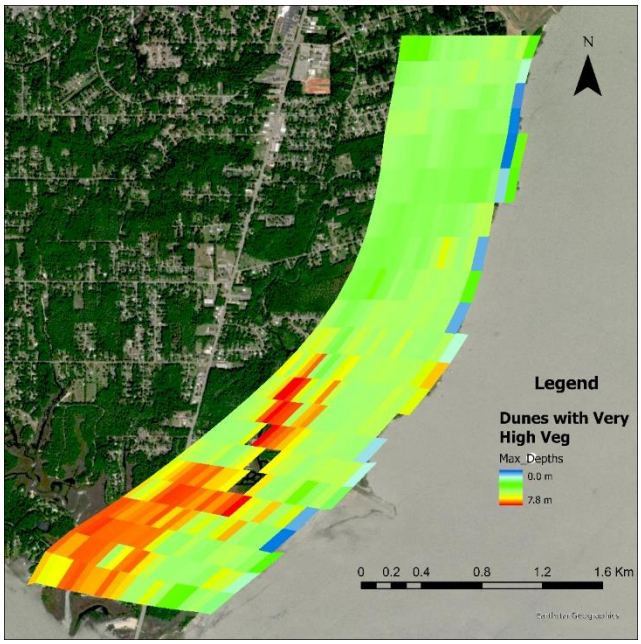

d) Dunes with Very High Vegetation Density

Figure 4.44 Maximum inundation (in meters) for Category 4 hurricane moving North with a) Artificial Reefs b) Artificial Sand Dunes c) Dunes with Normal Vegetation Density, and d) Dunes with Very High Vegetation Density (ArcGIS Pro)

Difference in water depths for Category 4 hurricane moving North i.e., Present condition without NNBFs –With NNBFs are shown in the Table 4.55 to Table 4.61 below.

Table 4.55 Difference in water depths with normal vegetation density (#340/ m^2).

Stats for all cells	Average depth, m	Max depth, m	Min depth, m	Standard Dev, m
Average depth	0.18	-0.01	0.03	0.07
Standard Dev	0.34	0.03	0.08	0.09
Max depth	1.58	0.09	0.61	0.45

Table 4.56 Difference in water depths with high vegetation density (#3400/m^2).

Stats for all cells	Average depth, m	Max depth, m	Min depth, m	Standard Dev, m
Average depth	0.14	-0.05	0.03	0.02
Standard Dev	0.30	0.03	0.09	0.06
Max depth	1.58	0.11	0.60	0.42

Table 4.57 Difference in water depths with very high vegetation density (#9645/m^2).

Stats for all cells	Average depth, m	Max depth, m	Min depth, m	Standard Dev, m
Average depth	-0.04	-0.07	0.01	-0.01
Standard Dev	0.15	0.04	0.07	0.05
Max depth	0.52	0.14	0.45	0.18

Table 4.58 Difference in water depths with artificial reefs.

Stats for all cells	Average depth, m	Max depth, m	Min depth, m	Standard Dev, m
Average depth	0.00	0.00	0.00	0.00
Standard Dev	0.07	0.03	0.02	0.01
Max depth	1.14	0.08	0.09	0.13

Table 4.59 Difference in water depths with artificial sand dunes.

Stats for all cells	Average depth, m	Max depth, m	Min depth, m	Standard Dev, m
Average depth	0.10	0.19	-0.04	0.04
Standard Dev	0.46	0.84	0.16	0.28
Max depth	1.92	4.32	0.46	1.32

Table 4.60 Difference in water depths with dunes with normal vegetation density.

Stats for all cells	Average depth, m	Max depth, m	Min depth, m	Standard Dev, m
Average depth	0.18	0.10	-0.03	0.14
Standard Dev	0.46	0.81	0.14	0.23
Max depth	1.54	4.14	0.46	1.23

Table 4.61 Difference in water depths with dunes with very high vegetation density.

Stats for all cells	Average depth, m	Max depth, m	Min depth, m	Standard Dev, m
Average depth	0.08	0.09	-0.04	0.02
Standard Dev	0.47	0.86	0.15	0.30
Max depth	1.92	4.22	0.45	1.34

B. Velocity (m/s)

The maximum velocity (m/s) was used for comparison Category 4 hurricane moving North for all the NNBFs. All the maps showing maximum velocity for the NNBFs test region for different NNBFs are shown in Figure 4.45 and Figure 4.46.

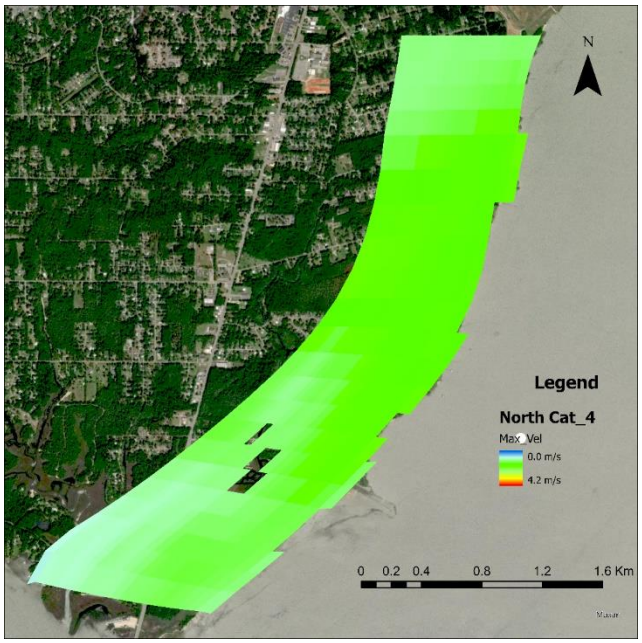

a) Present Condition

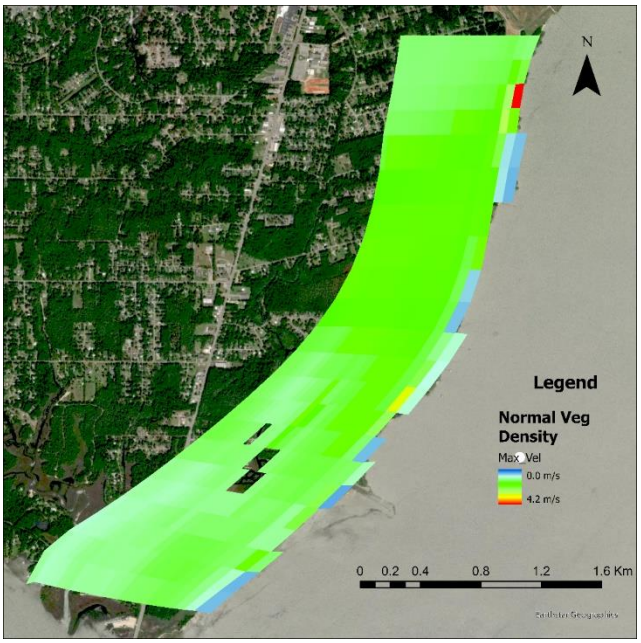

b) Normal Vegetation Density

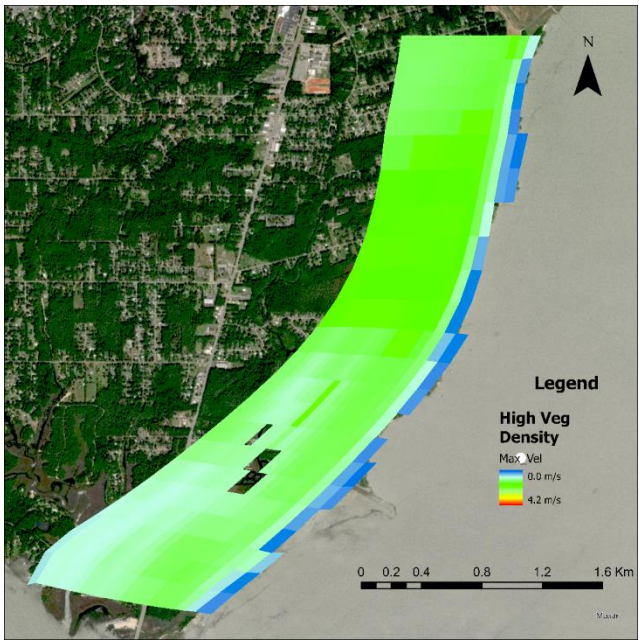

c) High Vegetation Density

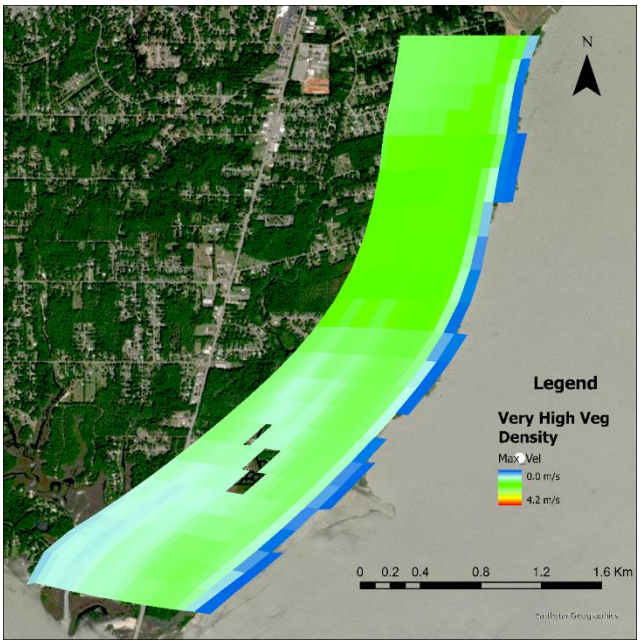

d) Very High Vegetation Density

Figure 4.45 Maximum velocity (in m/s) for Category 4 hurricane moving North with a) Present condition b) Normal Vegetation Density c) High Vegetation Density, and d) Very High Vegetation Density (ArcGIS Pro)

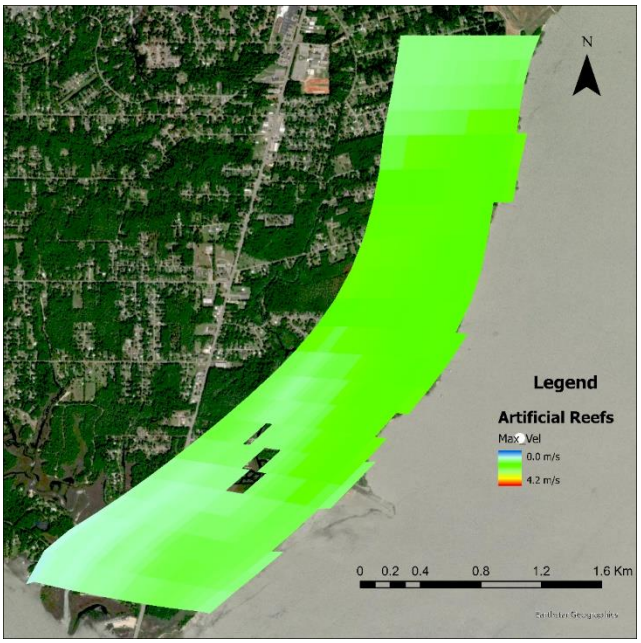

a) Artificial Reefs

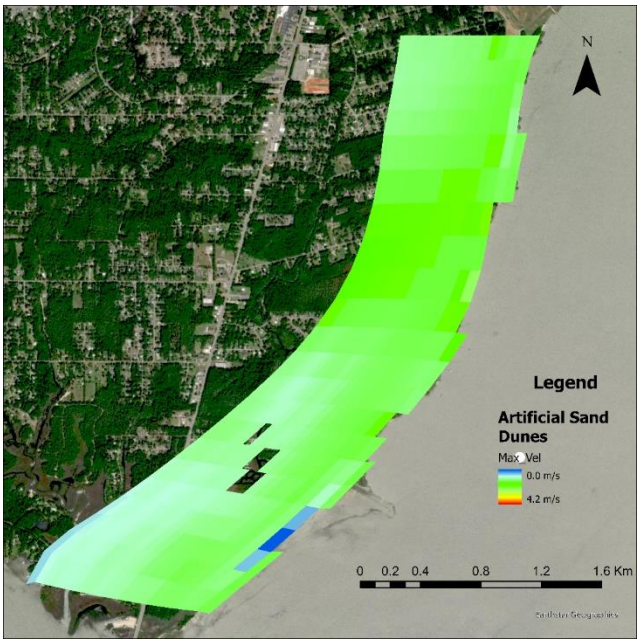

b) Artificial Sand Dunes

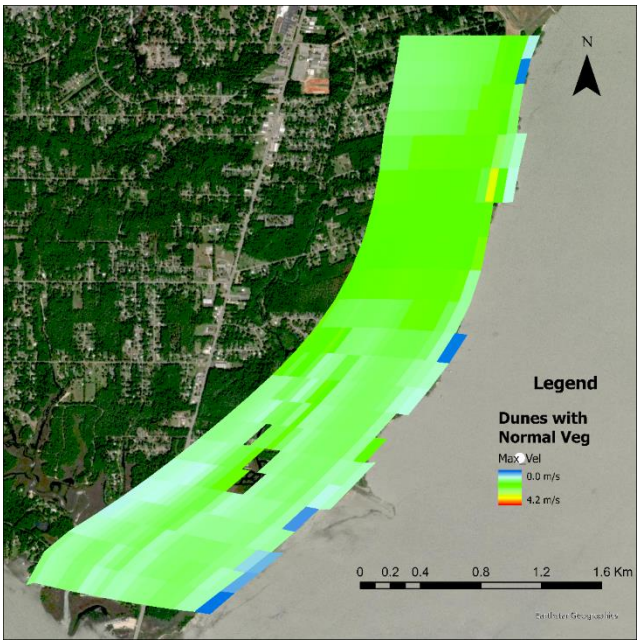

c) Dunes with Normal Vegetation Density

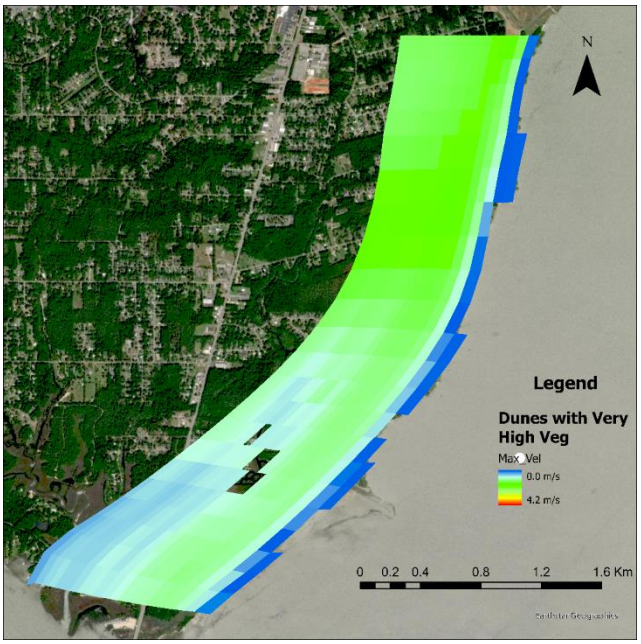

d) Dunes with Very High Vegetation Density

Figure 4.46 Maximum velocity (in m/s) for Category 4 hurricane moving North with a) Artificial Reefs b) Artificial Sand Dunes c) Dunes with Normal Vegetation Density, and d) Dunes with Very High Vegetation Density (ArcGIS Pro)

Difference in velocity (m/s) for Category 4 hurricane moving North i.e., Present condition without NNBFs – With NNBFs are shown in the Table 4.62 to Table 4.68 below.

Table 4.62 Difference in velocity (m/s) with normal vegetation density (#340/ m^2).

Stats for all cells	Average velocity (m/s)	Max velocity (m/s)	Min velocity (m/s)	Standard Dev velocity (m/s)
Average velocity	0.04	0.00	0.02	0.01
Standard Dev	0.14	0.26	0.04	0.06
Max velocity	0.65	1.16	0.18	0.29

Table 4.63 Difference in velocity (m/s) with high vegetation density (#3400/m^2).

Stats for all cells	Average velocity (m/s)	Max velocity (m/s)	Min velocity (m/s)	Standard Dev velocity (m/s)
Average velocity	0.10	0.17	0.02	0.06
Standard Dev	0.15	0.29	0.05	0.07
Max velocity	0.70	1.50	0.21	0.38

Table 4.64 Difference in velocity (m/s) with very high vegetation density (#9645/m^2).

Stats for all cells	Average velocity (m/s)	Max velocity (m/s)	Min velocity (m/s)	Standard Dev velocity (m/s)
Average velocity	0.09	0.20	0.01	0.05
Standard Dev	0.14	0.33	0.04	0.08
Max velocity	0.76	1.60	0.20	0.41

Table 4.65 Difference in velocity (m/s) with artificial reefs.

Stats for all cells	Average velocity (m/s)	Max velocity (m/s)	Min velocity (m/s)	Standard Dev velocity (m/s)
Average velocity	0.00	0.00	0.00	0.00
Standard Dev	0.02	0.01	0.01	0.01
Max velocity	0.41	0.02	0.09	0.03

Table 4.66 Difference in velocity (m/s) with artificial sand dunes.

Stats for all cells	Average velocity (m/s)	Max velocity (m/s)	Min velocity (m/s)	Standard Dev velocity (m/s)
Average velocity	0.15	0.16	0.00	0.08
Standard Dev	0.21	0.14	0.11	0.07
Max velocity	0.76	1.39	0.23	0.37

Table 4.67 Difference in velocity (m/s) with dunes with normal vegetation density.

Stats for all cells	Average velocity (m/s)	Max velocity (m/s)	Min velocity (m/s)	Standard Dev velocity (m/s)
Average velocity	0.06	0.10	0.02	0.03
Standard Dev	0.19	0.25	0.05	0.10
Max velocity	0.68	1.52	0.23	0.34

Table 4.68 Difference in velocity (m/s) with dunes with very high vegetation density.

Stats for all cells	Average velocity (m/s)	Max velocity (m/s)	Min velocity (m/s)	Standard Dev velocity (m/s)
Average velocity	0.22	0.36	0.02	0.13
Standard Dev	0.19	0.35	0.05	0.09
Max velocity	0.76	1.68	0.23	0.43

C. Flow (m^3/s)

The maximum flow (m^3/s) was used for comparison for Category 4 hurricane moving North. All the maps showing maximum flow for the NNBFs test region for different NNBFs are shown in Figure 4.47 and Figure 4.48.

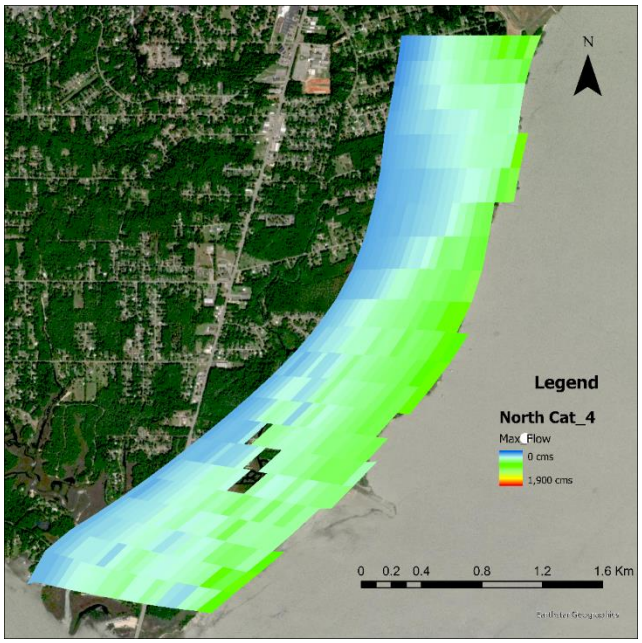

a) Present Condition

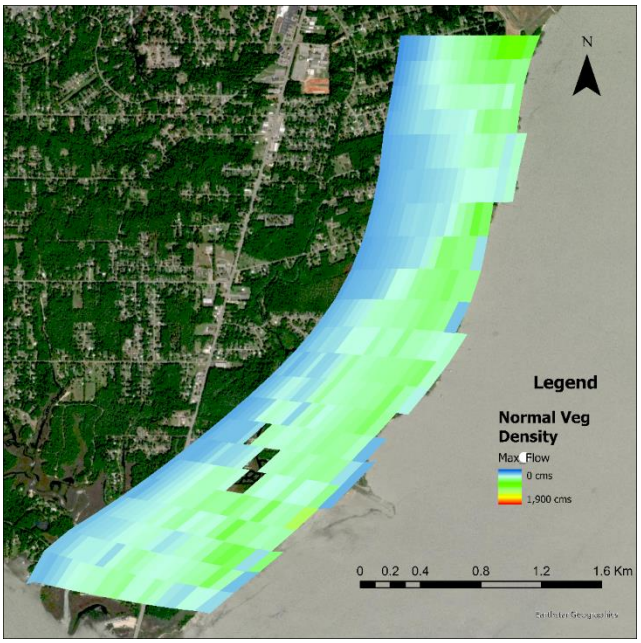

b) Normal Vegetation Density

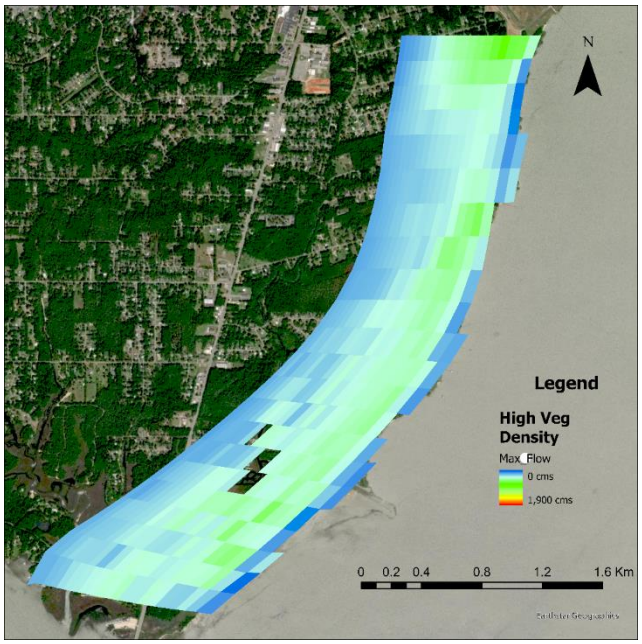

c) High Vegetation Density

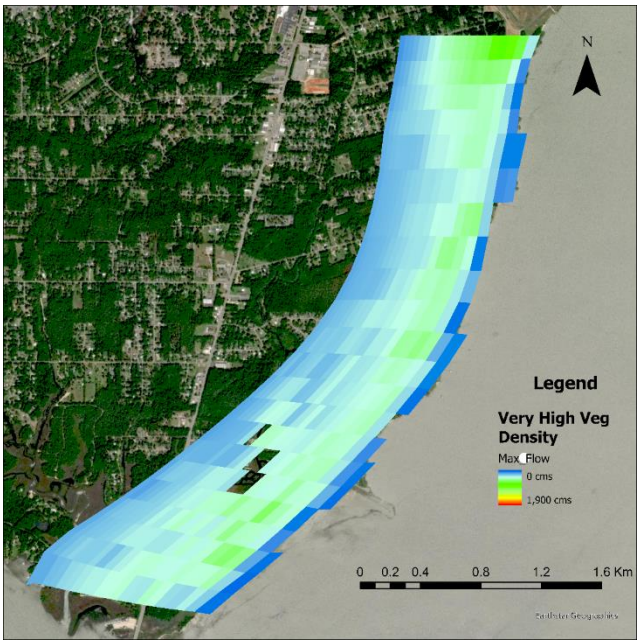

d) Very High Vegetation Density

Figure 4.47 Maximum flow (m^3/s) for Category 4 hurricane moving North with a) Present condition b) Normal Vegetation Density c) High Vegetation Density, and d) Very High Vegetation Density (ArcGIS Pro)

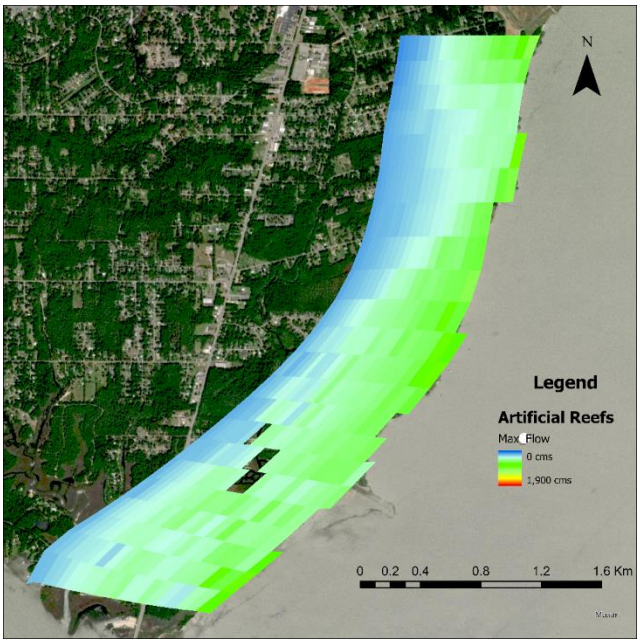

a) Artificial Reefs

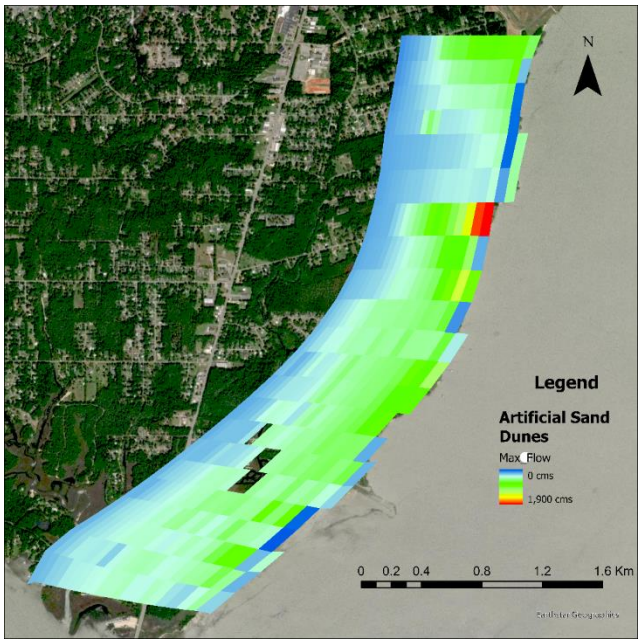

b) Artificial Sand Dunes

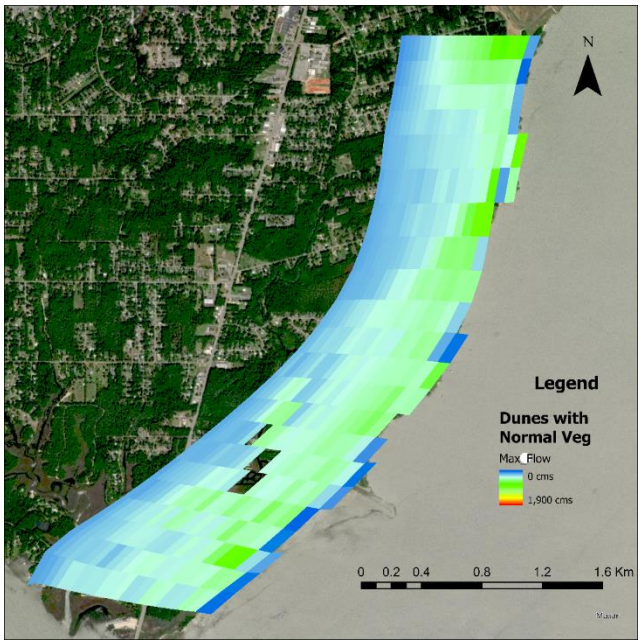

c) Dunes with Normal Vegetation Density

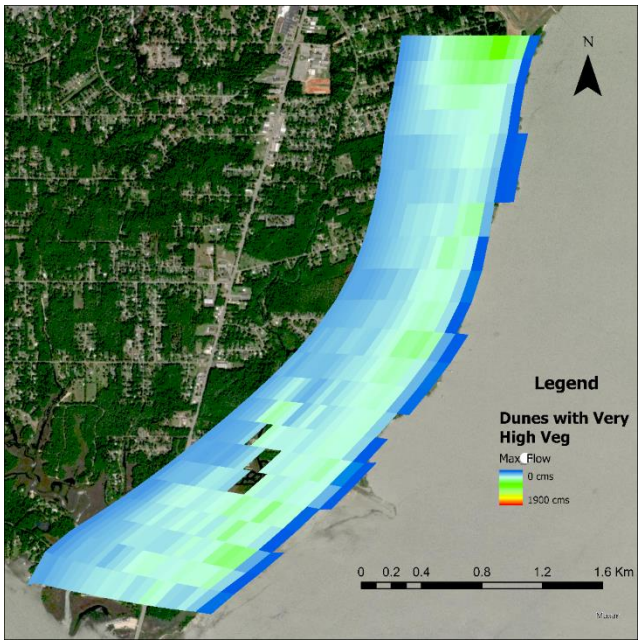

d) Dunes with Very High Vegetation Density

Figure 4.48 Maximum flow (m^3/s) for Category 4 hurricane moving North with a) Artificial Reefs b) Artificial Sand Dunes c) Dunes with Normal Vegetation Density, and d) Dunes with Very High Vegetation Density (ArcGIS Pro)

Difference in maximum flow (m^3/s) for Category 4 hurricane moving North i.e., Present condition without NNBFs – With NNBFs are shown in the Table 4.69 to Table 4.75 below.

Table 4.69 Difference in maximum flow (m^3/s) with normal vegetation density (#340/ m^2).

Stats for all cells	Average flow (m^3/s)	Max flow (m^3/s)	Min flow (m^3/s)	Standard Dev flow (m^3/s)
Average flow	15.95	25.66	0.22	13.31
Standard Dev	31.08	92.09	1.30	23.57
Max flow	125.60	567.12	9.93	129.39

Table 4.70 Difference in maximum flow (m^3/s) with high vegetation density (#3400/m^2).

Stats for all cells	Average flow (m^3/s)	Max flow (m^3/s)	Min flow (m^3/s)	Standard Dev flow (m^3/s)
Average flow	29.16	68.61	0.26	24.12
Standard Dev	37.35	124.93	1.26	31.74
Max flow	160.80	784.99	7.12	169.70

Table 4.71 Difference in maximum flow (m^3/s) with very high vegetation density (#9645/m^2).

Stats for all cells	Average flow (m^3/s)	Max flow (m^3/s)	Min flow (m^3/s)	Standard Dev flow (m^3/s)
Average flow	21.90	77.82	0.12	21.65
Standard Dev	35.53	147.57	1.39	36.41
Max flow	164.86	842.42	7.49	196.38

Table 4.72 Difference in maximum flow (m^3/s) with artificial reefs.

Stats for all cells	Average flow (m^3/s)	Max flow (m^3/s)	Min flow (m^3/s)	Standard Dev flow (m^3/s)
Average flow	-0.06	-8.85	0.00	-0.70
Standard Dev	3.49	21.52	0.32	2.43
Max flow	39.63	35.02	4.20	15.20

Table 4.73 Difference in maximum flow (m^3/s) with artificial sand dunes.

Stats for all cells	Average flow (m^3/s)	Max flow (m^3/s)	Min flow (m^3/s)	Standard Dev flow (m^3/s)
Average flow	21.36	-6.29	-0.50	8.18
Standard Dev	39.20	157.40	4.78	36.81
Max flow	174.98	560.76	8.18	154.29

Table 4.74 Difference in maximum flow (m^3/s) with dunes with normal veg density.

Stats for all cells	Average flow (m^3/s)	Max flow (m^3/s)	Min flow (m^3/s)	Standard Dev flow (m^3/s)
Average flow	17.99	48.12	0.17	20.35
Standard Dev	41.84	119.62	1.59	34.26
Max flow	182.99	872.15	9.42	192.79

Table 4.75 Difference in maximum flow (m^3/s) with dunes with very high veg density.

Stats for all cells	Average flow (m^3/s)	Max flow (m^3/s)	Min flow (m^3/s)	Standard Dev flow (m^3/s)
Average flow	37.37	98.47	0.24	34.52
Standard Dev	44.52	164.17	1.32	41.39
Max flow	193.11	1013.28	8.12	221.38

D. Bed shear (N/m^2)

The average bed shear (N/m^2) was used for the comparison for Category 4 hurricane moving North. All the maps showing average bed shear for the NNBFs test region for different NNBFs are shown in Figure 4.49 and Figure 4.50.

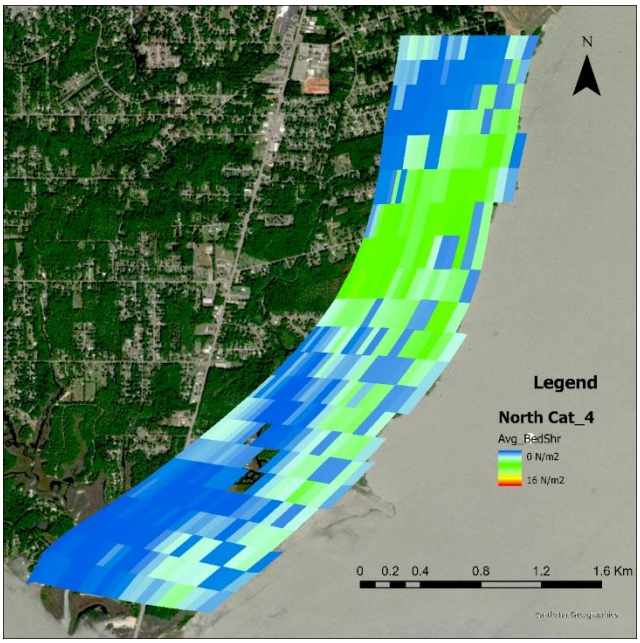

a) Present Condition

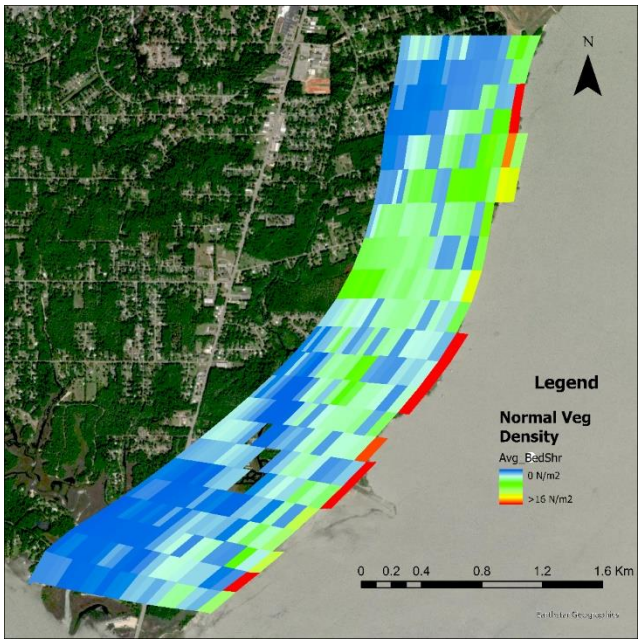

b) Normal Vegetation Density

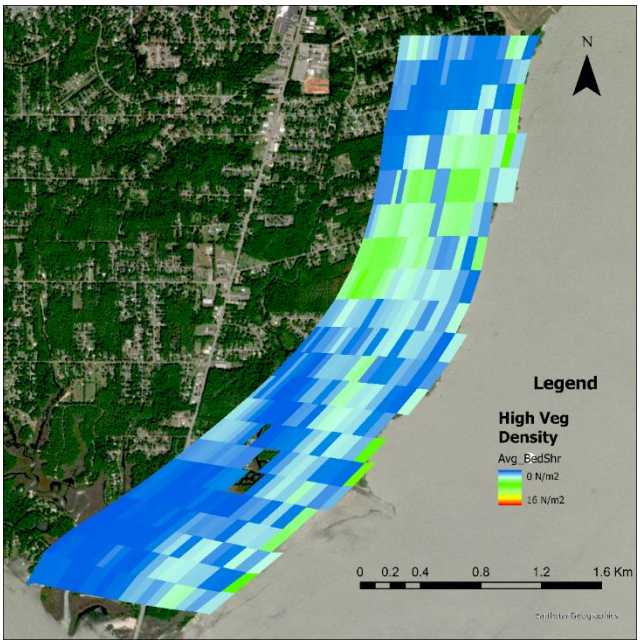

c) High Vegetation Density

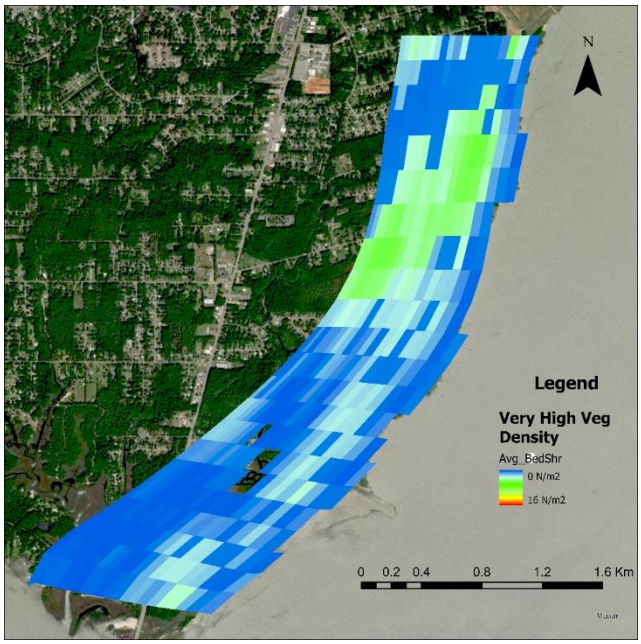

d) Very High Vegetation Density

Figure 4.49 Average bed shear (in N/m^2) for Category 4 hurricane moving North with a) Present condition b) Normal Vegetation Density c) High Vegetation Density, and d) Very High Vegetation Density (ArcGIS Pro)

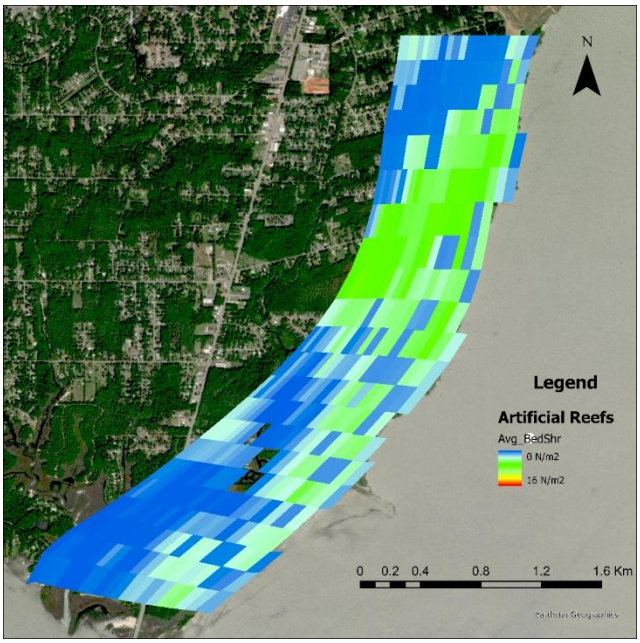

e) Artificial Reefs

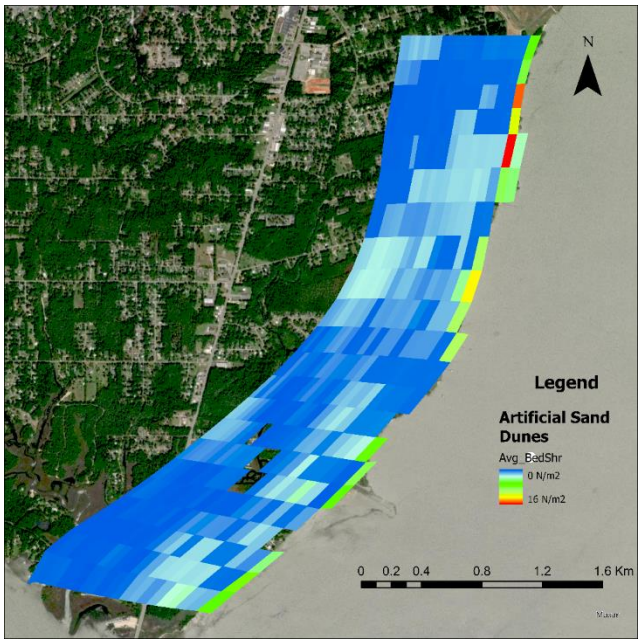

f) Artificial Sand Dunes

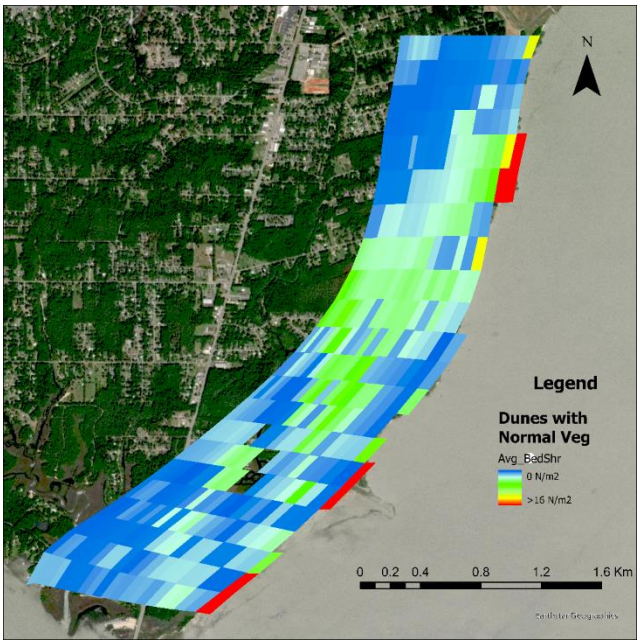

g) Dunes with Normal Vegetation Density

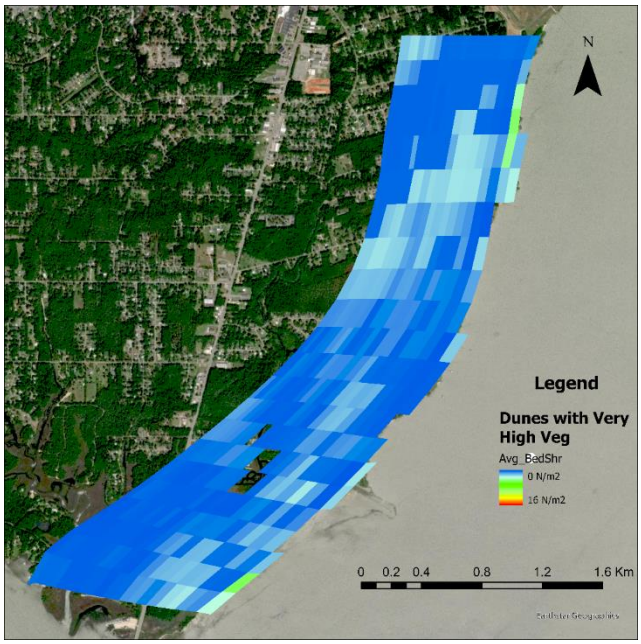

h) Dunes with Very High Vegetation Density

Figure 4.50 Average bed shear (in N/m^2) for Category 4 hurricane moving North with a) Artificial Reefs b) Artificial Sand Dunes c) Dunes with Normal Vegetation Density, and d) Dunes with Very High Vegetation Density (ArcGIS Pro)

Difference in bed shear (N/m^2) for Category 4 hurricane moving North i.e., Present condition without NNBFs – With NNBFs are shown in the Table 4.76 to Table 4.82 below.

Table 4.76 Difference in bed shear (N/m^2) with normal vegetation density (#340/ m^2).

Stats for all cells	Average bed shear (N/m^2)	Max bed shear (N/m^2)	Min bed shear (N/m^2)	Std. dev. bed shear (N/m^2)
Average bed shear	-0.86	-20.81	0.06	-3.26
Std. dev.	5.82	187.28	0.14	29.22
Max bed shear	4.37	8.54	0.71	2.31

Table 4.77 Difference in bed shear (N/m^2) with high vegetation density (#3400/m^2).

Stats for all cells	Average bed shear (N/m^2)	Max bed shear (N/m^2)	Min bed shear (N/m^2)	Std. dev. bed shear (N/m^2)
Average bed shear	0.57	-0.01	0.08	0.22
Std. dev.	1.13	8.99	0.16	1.91
Max bed shear	4.73	14.19	0.79	3.66

Table 4.78 Difference in bed shear (N/m^2) with very high vegetation density (#9645/m^2).

Stats for all cells	Average bed shear (N/m^2)	Max bed shear (N/m^2)	Min bed shear (N/m^2)	Std. dev. bed shear (N/m^2)
Average bed shear	0.81	2.08	0.07	0.54
Std. dev.	1.00	2.97	0.14	0.71
Max bed shear	4.84	14.50	0.81	3.76

Table 4.79 Difference in bed shear (N/m^2) with artificial reefs.

Stats for all cells	Average bed shear (N/m^2)	Max bed shear (N/m^2)	Min bed shear (N/m^2)	Std. dev. bed shear (N/m^2)
Average bed shear	0.02	0.04	0.00	0.01
Std. dev.	0.18	1.15	0.04	0.15
Max bed shear	2.52	9.34	0.29	1.00

Table 4.80 Difference in bed shear (N/m^2) with artificial sand dunes.

Stats for all cells	Average bed shear (N/m^2)	Max bed shear (N/m^2)	Min bed shear (N/m^2)	Std. dev. bed shear (N/m^2)
Average bed shear	1.12	2.33	-0.06	0.81
Std. dev.	2.17	4.03	0.90	1.20
Max bed shear	5.30	10.88	0.90	3.72

Table 4.81 Difference in bed shear (N/m^2) with dunes with normal veg density.

Stats for all cells	Average bed shear (N/m^2)	Max bed shear (N/m^2)	Min bed shear (N/m^2)	Std. dev. bed shear (N/m^2)
Average bed shear	-0.40	-5.63	0.04	-1.12
Std. dev.	5.44	43.02	0.47	9.71
Max bed shear	4.84	10.07	0.90	2.80

Table 4.82 Difference in bed shear (N/m^2) with dunes with very high veg density.

Stats for all cells	Average bed shear (N/m^2)	Max bed shear (N/m^2)	Min bed shear (N/m^2)	Std. dev. bed shear (N/m^2)
Average bed shear	1.59	4.34	0.03	1.26
Std. dev.	1.62	3.35	0.37	0.93
Max bed shear	5.69	15.18	0.90	3.98

4.4.2 DISCUSSION

4.4.2.1 NNBFs test for 100-year storm event

A. Water Depths (m)

From the maximum water depth maps, there is no visual difference in water depths before and after the installation of all three vegetation densities and artificial reefs but there can be seen reduction in water depths after the installation of artificial sand dunes and dunes with vegetation with some regions on the top completely free from floodings. The difference in water depths (m) between the present condition without NNBFs and with NNBFs was calculated. The positive difference shows the decrease in water depths after the installation of NNBFs. The difference of average (maximum) of the average depths of all the cells is 0.11 m (1.18 m), 0.05 m (0.93 m), -

0.09 m (0.98 m), 0 m (0.76 m), 0.24 m (1.69 m), 0.11 m (1.69 m), and 0.31 m (1.61 m) for normal vegetation density, high vegetation density, very high vegetation density, artificial reefs, artificial sand dunes, dunes with normal vegetation density, and dunes with very high vegetation density respectively. The difference of average (maximum) of the maximum depths of all the cells is -0.05 m (0.03 m), -0.14 m (0.07 m), -0.2 m (0.11 m), -0.01 m (0.03 m), 0.51 m (4.47 m), -0.08 m (4.47 m), and 0.71 m (4.26 m) for normal vegetation density, high vegetation density, very high vegetation density, artificial reefs, artificial sand dunes, dunes with normal vegetation density, and dunes with very high vegetation density respectively. The vegetation holds the water for longer duration, due to the vegetation drag, slightly increasing the average of the maximum water depths which is why some values are negative. These data also shows that the difference in water depths is higher for sand dunes and dunes with very high vegetation density for both average and maximum depths.

B. Velocity (m/s)

From the maximum velocity maps, we can see that there is decrease in velocity with increasing vegetation densities. There is no visual difference before and after the installation of artificial reefs which can be confirmed from the data as well. There can be seen even more reduction in velocities after the installation of artificial sand dunes and dunes with vegetation with some regions on top being completely unimpacted. The difference in velocity (m/s) between the present condition without NNBFs and with NNBFs was calculated. The positive difference shows the decrease in velocity after the installation of NNBFs. The difference of average (maximum) of the average velocity of all the cells is 0.04 m/s (0.58 m/s), 0.08 m/s (0.65 m/s), 0.10 m/s (0.70 m/s), 0 m/s (0.14 m/s), 0.21 m/s (0.78 m/s), 0.05 m/s (0.62 m/s), and 0.23 m/s (0.87 m/s) for normal vegetation density, high vegetation density, very high vegetation density, artificial reefs, artificial sand dunes, dunes with normal vegetation density, and dunes with very high vegetation density respectively. The difference of average (maximum) of the maximum velocity of all the cells is -0.03 m/s (0.99 m/s), 0.18 m/s (1.10 m/s), 0.31 m/s (0.27 m/s), 0.01m/s (0.07 m/s), 0.62 m/s (1.32 m/s), 0.08 m/s (1.32 m/s), and 0.67 m/s (1.48 m/s) for normal vegetation density, high vegetation density, very high vegetation density, artificial reefs, artificial sand dunes, dunes with normal vegetation density, and dunes with very high vegetation density respectively. From the maps and data, it can be

identified that the reduction in velocity is more for higher vegetation density with the greatest being the combination of sand dunes with higher vegetation density.

C. Flow (m^3/s)

From the maximum flow maps, we can see that there is decrease in flow with increasing vegetation densities. There is some difference before and after the installation of artificial reefs which can be confirmed from the data as well. There can be seen even more reduction in flow after the installation of artificial sand dunes and dunes with vegetation with some regions on top being completely unimpacted. The difference in flow (m^3/s) between the present condition without NNBFs and with NNBFs was calculated. The positive difference shows the decrease in flow after the installation of NNBFs. The difference of average (maximum) of the average flow of all the cells is 12.34 m^3/s (115.69 m^3/s), 18.78 m^3/s (145.76 m^3/s), 17.32 m^3/s (147.19 m^3/s), 0.43 m^3/s (42.93 m^3/s), 29.71 m^3/s (162.24 m^3/s), 13.73 m^3/s (137.15 m^3/s), and 32.24 m^3/s (191.34 m^3/s) for normal vegetation density, high vegetation density, very high vegetation density, artificial reefs, artificial sand dunes, dunes with normal vegetation density, and dunes with very high vegetation density respectively. The difference of average (maximum) of the maximum flow of all the cells is 28.65 m^3/s (385.09 m^3/s), 66.01 m^3/s (556.90 m^3/s), 79.99 m^3/s (660.73 m^3/s), 1.07 m^3/s (303.72 m^3/s), 123.08 m^3/s (746.26 m^3/s), 53.62 m^3/s (101.75 m^3/s), and 130.41m^3/s (882.45 m^3/s) for normal vegetation density, high vegetation density, very high vegetation density, artificial reefs, artificial sand dunes, dunes with normal vegetation density, and dunes with very high vegetation density respectively. From the maps and data, it can be identified that the reduction in flow is more for higher vegetation density with the greatest being the combination of sand dunes with higher vegetation density which is similar case with the velocity as well.

D. Bed Shear (N/m^2)

From the average bed shear maps, we can see that there is decrease in bed shear with increasing vegetation densities. There is no visual difference before and after the installation of artificial reefs which can be confirmed from the data as well. There can be seen even more reduction in bed shear after the installation of artificial sand dunes and dunes with vegetation with some regions on top being completely unimpacted. The difference in bed shear (N/m^2) between the present condition without NNBFs and with NNBFs was calculated. The positive difference shows the decrease in bed shear after the installation of NNBFs. The difference of average (maximum) of the average

bed shear of all the cells is -0.29 N/m^2 (3.62 N/m^2), 0.42 N/m^2 (4.54 N/m^2), 0.93 N/m^2 (5.35 N/m^2), 0.03 N/m^2 (1.48 N/m^2), 1.42 N/m^2 (5.96 N/m^2), -0.02 N/m^2 (4.70 N/m^2), and 1.47 N/m^2 (6.63 N/m^2) for normal vegetation density, high vegetation density, very high vegetation density, artificial reefs, artificial sand dunes, dunes with normal vegetation density, and dunes with very high vegetation density respectively. The difference of average (maximum) of the maximum bed shear of all the cells is -4.55 N/m^2 (11.80 N/m^2), 0.10 N/m^2 (14.47 N/m^2), 2.95 N/m^2 (15.34 N/m^2), 0.13N/m^2 (6.48 N/m^2), 4.99 N/m^2 (15.68 N/m^2), -1.78 N/m^2 (11.75 N/m^2), and 5.23 N/m^2 (18.73 N/m^2) for normal vegetation density, high vegetation density, very high vegetation density, artificial reefs, artificial sand dunes, dunes with normal vegetation density, and dunes with very high vegetation density respectively. From the maps and data, it can be identified that the reduction in bed shear is more for higher vegetation density with the greatest being the combination of sand dunes with higher vegetation density which is similar case with the velocity and flow as well.

4.4.2.2 NNBFs test for Category 4 hurricane moving North

A. Water Depths (m)

From the maximum water depth maps, there is no visual difference in water depths before and after the installation of all three vegetation densities and artificial reefs. Even after the installation of artificial sand dunes and dunes with vegetation, the reduction in water depth is visually small as compared to the NNBFs test for a 100-year storm event. The difference in water depths (m) between the present condition without NNBFs and with NNBFs was calculated. The positive difference shows the decrease in water depths after the installation of NNBFs. The difference of average (maximum) of the average depths of all the cells is 0.18 m (1.58 m), 0.14 m (1.58 m), -0.04 m (0.52 m), 0.00 m (1.14 m), 0.10 m (1.92 m), 0.18 m (1.54 m), and 0.08 m (1.92 m) for normal vegetation density, high vegetation density, very high vegetation density, artificial reefs, artificial sand dunes, dunes with normal vegetation density, and dunes with very high vegetation density respectively. The difference of average (maximum) of the maximum depths of all the cells is -0.01 m (0.09 m), -0.05 m (0.11 m), -0.07 m (0.14 m), 0.00 m (0.08 m), 0.19 m (4.32 m), 0.10 m (4.14 m), and 0.09 m (4.22 m) for normal vegetation density, high vegetation density, very high vegetation density, artificial reefs, artificial sand dunes, dunes with normal vegetation density, and dunes with very high vegetation density respectively. The vegetation holds the water for longer duration, due to the vegetation drag, slightly increasing the average of the maximum water depths

which is why some values are negative. These data also shows that the difference in water depths is higher for sand dunes and dunes with very high vegetation density for both average and maximum depths.

Due to the higher intensity of hurricane, we can see that the water depth is higher for this scenario than that for 100-year storm event. Because of the higher intensity of the storm, the water depths reduction is not visible on the maps, but we can see similar kind of reduction in water depths as compared to the NNBFs test for 100-year storm. Among the tested NNBFs from both the tested scenarios, we can see that combination of artificial sand dunes with vegetation with higher plant density is most effective in reducing the maximum flooding depths.

B. Velocity (m/s)

From the maximum velocity maps, we can see that there is decrease in velocity with increasing vegetation densities along the coastal boundary. There is no visual difference before and after the installation of artificial reefs which can be confirmed from the data as well. There can be seen even more reduction in velocities after the installation of artificial sand dunes and dunes with vegetation. The difference in velocity (m/s) between the present condition without NNBFs and with NNBFs was calculated. The positive difference shows the decrease in velocity after the installation of NNBFs. The difference of average (maximum) of the average velocity of all the cells is 0.04 m/s (0.65 m/s), 0.10 m/s (0.70 m/s), 0.09 m/s (0.76 m/s), 0.00 m/s (0.41 m/s), 0.15 m/s (0.76 m/s), 0.06 m/s (0.68 m/s), and 0.22 m/s (0.76 m/s) for normal vegetation density, high vegetation density, very high vegetation density, artificial reefs, artificial sand dunes, dunes with normal vegetation density, and dunes with very high vegetation density respectively. The difference of average (maximum) of the maximum depths of all the cells is 0.00 m/s (1.16 m/s), 0.17 m/s (1.50 m/s), 0.20 m/s (1.60 m/s), 0.00m/s (0.02 m/s), 0.16 m/s (1.39 m/s), 0.10 m/s (1.52 m/s), and 0.36 m/s (1.68 m/s) for normal vegetation density, high vegetation density, very high vegetation density, artificial reefs, artificial sand dunes, dunes with normal vegetation density, and dunes with very high vegetation density respectively. From the maps and data, it can be identified that the reduction in velocity is more for higher vegetation density with the greatest being the combination of sand dunes with higher vegetation density.

Due to the higher intensity of hurricane, we can see that the velocity is higher for this scenario than that for 100-year storm event. We can see a similar kind of reduction in velocity as compared to

the NNBFs test for 100-year storm. Among the tested NNBFs from both the tested scenarios, we can see that combination of artificial sand dunes with vegetation with higher plant density is most effective in reducing the velocities as well.

C. Flow (m^3/s)

From the maximum flow maps, we can see that there is decrease in flow with increasing vegetation densities with maximum reduction in the coastal boundary regions and there is no visible difference before and after the installation of artificial reefs. There can be seen even more reduction in flow after the installation of artificial sand dunes and dunes with vegetation. The difference in flow (m^3/s) between the present condition without NNBFs and with NNBFs was calculated. The positive difference shows the decrease in flow after the installation of NNBFs. The difference of average (maximum) of the average velocity of all the cells is 15.95 m^3/s (125.60 m^3/s), 29.16 m^3/s (160.80 m^3/s), 21.90 m^3/s (164.86 m^3/s), -0.06 m^3/s (39.63 m^3/s), 21.36 m^3/s (174.98 m^3/s), 17.99 m^3/s (182.99 m^3/s), and 37.37 m^3/s (193.11 m^3/s) for normal vegetation density, high vegetation density, very high vegetation density, artificial reefs, artificial sand dunes, dunes with normal vegetation density, and dunes with very high vegetation density respectively. The difference of average (maximum) of the maximum depths of all the cells is 25.66 m^3/s (567.12 m^3/s), 68.61 m^3/s (784.99 m^3/s), 77.82 m^3/s (842.42 m^3/s), -8.85 m^3/s (35.02 m^3/s), -6.29 m^3/s (560.76 m^3/s), 48.12 m^3/s (872.15 m^3/s), and 98.47 m^3/s (1013.28 m^3/s) for normal vegetation density, high vegetation density, very high vegetation density, artificial reefs, artificial sand dunes, dunes with normal vegetation density, and dunes with very high vegetation density respectively. From the maps and data, it can be identified that the reduction in flow is more for higher vegetation density with the greatest being the combination of sand dunes with higher vegetation density which is similar case with the velocity as well.

Due to the higher intensity of hurricane, we can see that the flow is higher for this scenario than that for 100-year storm event. We can see a similar kind of reduction in flow as compared to the NNBFs test for 100-year storm. Among the tested NNBFs from both the tested scenarios, we can see that combination of artificial sand dunes with vegetation with higher plant density is most effective in reducing the flow as well.

D. Bed Shear (N/m^2)

From the average bed shear maps, we can see that there is decrease in bed shear with increasing vegetation densities for most of the regions. There is no visual difference in bed shear before and after the installation of artificial reefs. There can be seen even more reduction in bed shear after the installation of artificial sand dunes and dunes with vegetation with some regions being completely unimpacted. There are some boundary cells which have higher bed shear which might be due to the higher category of the hurricane as compared to the 100-year storm event. The difference in bed shear (N/m^2) between the present condition without NNBFs and with NNBFs was calculated. The positive difference shows the decrease in bed shear after the installation of NNBFs. The difference of average (maximum) of the average velocity of all the cells is -0.86 N/m^2 (4.37 N/m^2), 0.57 N/m^2 (4.73 N/m^2), 0.81 N/m^2 (4.84 N/m^2), 0.02 N/m^2 (2.52 N/m^2), 1.12 N/m^2 (5.30 N/m^2), -0.40 N/m^2 (4.84 N/m^2), and 1.59 N/m^2 (5.69 N/m^2) for normal vegetation density, high vegetation density, very high vegetation density, artificial reefs, artificial sand dunes, dunes with normal vegetation density, and dunes with very high vegetation density respectively. The difference of average (maximum) of the maximum depths of all the cells is –20.81 N/m^2 (8.54 N/m^2), -0.01 N/m^2 (14.19 N/m^2), 2.08 N/m^2 (14.50 N/m^2), 0.04 N/m^2 (9.34 N/m^2), 2.33 N/m^2 (10.88 N/m^2), -5.63 N/m^2 (10.07 N/m^2), and 4.34 N/m^2 (15.18 N/m^2) for normal vegetation density, high vegetation density, very high vegetation density, artificial reefs, artificial sand dunes, dunes with normal vegetation density, and dunes with very high vegetation density respectively. From the maps and data, it can be identified that the reduction in bed shear is more for higher vegetation density with the greatest being the combination of sand dunes with higher vegetation density which is similar case with the velocity and flow as well.

Due to the higher intensity of hurricane, we can see that the bed shear is higher for this scenario than that for 100-year storm event. We can see a similar kind of reduction in bed shear as compared to the NNBFs test for 100-year storm. Among the tested NNBFs from both the tested scenarios, we can see that combination of artificial sand dunes with vegetation with higher plant density is most effective in reducing the bed shear as well.

4.5 SLOW MOVING VS FAST MOVING HURRICANES

4.5.1 RESULTS

For comparing the impacts due different forward speed of Hurricane, we have tested Hurricane category 3 moving North with two forward speeds of 5 m/s and 10 m/s. The maximum inundation

due to 5 m/s hurricane is shown in Figure 4.51 and due to 10 m/s hurricane is shown in Figure 4.52. The difference in maximum inundation between 5 m/s forward speed hurricane and 10 m/s forward speed hurricane is shown in Figure 4.53. The statistics of the difference between a 5 m/s hurricane and a 10 m/s hurricane are shown in Table 4.83.

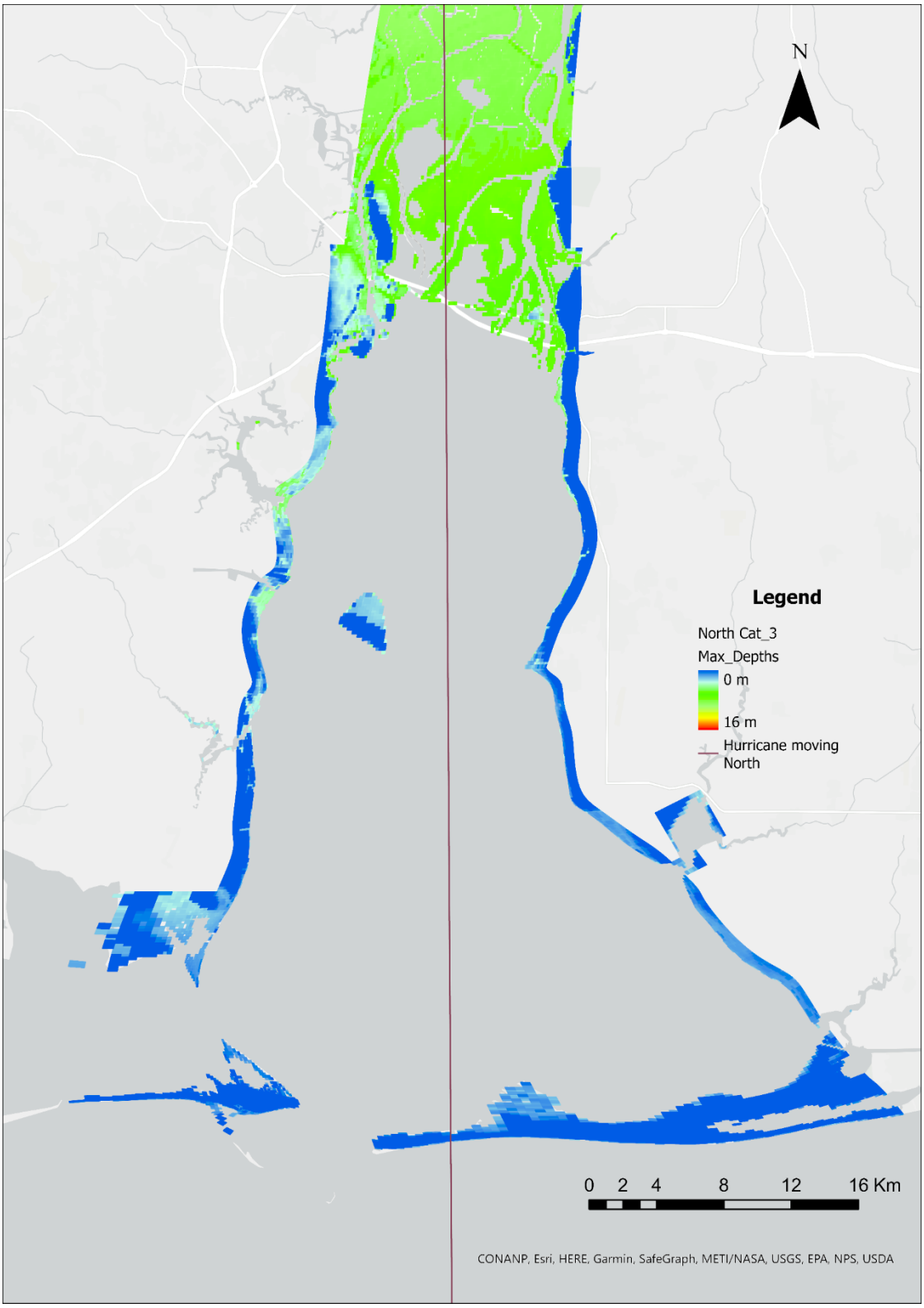

Figure 4.51 Maximum inundation by hurricane category 3 moving north with speed 5 m/s (ArcGIS Pro)

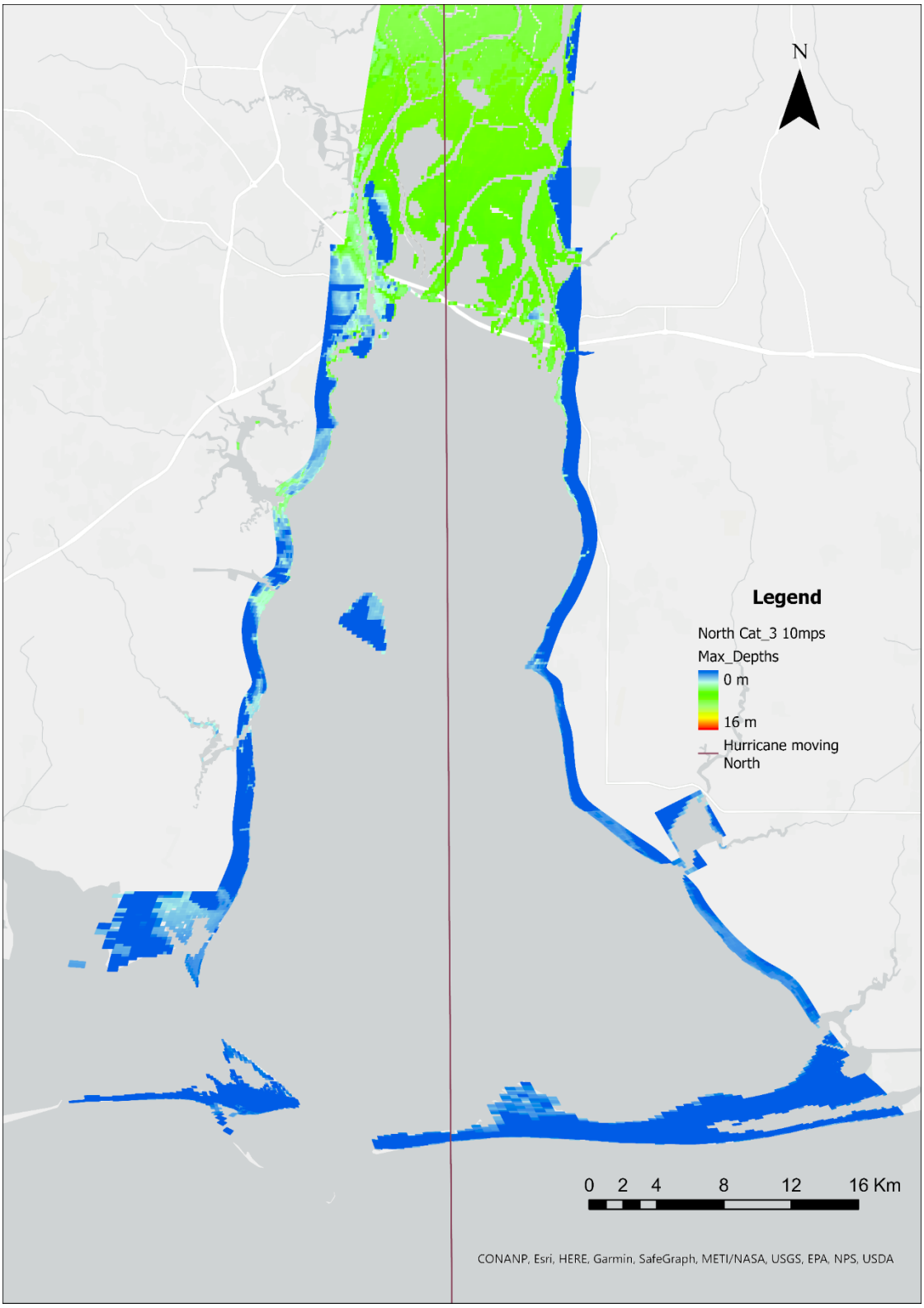

Figure 4.52 Maximum inundation by hurricane category 3 moving north with speed 10 m/s (ArcGIS Pro)

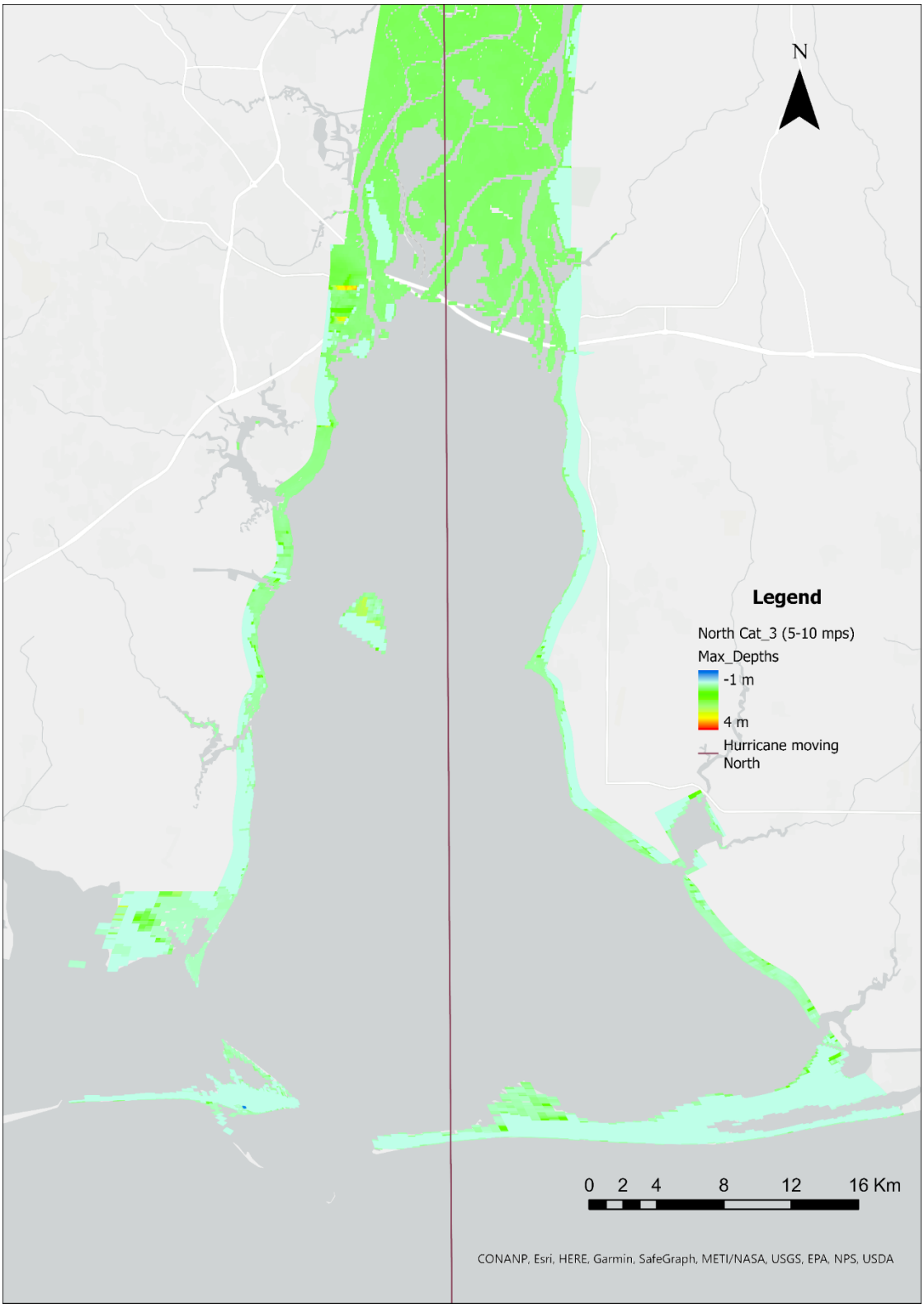

Figure 4.53 Difference inundation by hurricane category 3 moving north with speed 5 m/s and hurricane category 3 moving north with speed 10 m/s (ArcGIS Pro)

Table 4.83 Stats for difference in maximum depths (m) for 5 m/s hurricane and 10 m/s hurricane

Stats For all Cells	Average depth (m)	Max depth (m)	Min depth (m)	Std depth (m)
Average depth (m)	0.09	0.31	0.01	0.08
Maximum depth (m)	3.01	3.52	3.28	1.13
Std.Dev. (m)	0.15	0.32	0.10	0.09

4.5.2 DISCUSSION

From the result maps (Figure 4.51 and Figure 4.52) it can be visualized that the hurricane moving with 5 m/s is causing higher flooding depths on the coastal regions as compared to the hurricane moving with 10 m/s. This can be seen in the Figure 4.53, which shows the difference in maximum water depths between a slow-moving hurricane and a fast-moving hurricane. In the Figure 4.53, the light blue areas are the regions where there was no impact due to this difference in forward speed of hurricanes. However, the regions with light green, yellow and red are the areas with increasing flooding depths respectively for the slow-moving hurricane as compared to the fast-moving hurricane. Table 4.83 shows the stats for the difference in maximum inundation for slow moving hurricane and fast-moving hurricane for all the coastal cells. From this table, it can be seen that average of the difference in maximum inundation is 0.31 m (~1 ft) with maximum difference of 3.52 m (~11.5 ft). These results indicate that slow-moving hurricanes are much more dangerous compared to fast-moving hurricanes as discussed in Chapter 2.2.

4.6 MAXIMUM OF MAXIMUM (MOM) DEPTHS

MOM is the maximum water depth for an individual hurricane category from 1 to 5. The MOM for this study is similar to that of SLOSH model (Glahn et al., 2009) which is discussed in Chapter 2.4. MOM was calculated based on Scenario 2: Using Hypothetical tracks, the maximum water depths at each coastal cell for all three hurricane directions for a particular category was calculated. This data was then imported into ArcGIS Pro to develop a map for MOM for all five hurricane categories.

4.6.1 RESULTS

The MOM map developed for all five hurricane categories from hurricane scenario 2 is shown in Figure 4.54 to Figure 4.58.

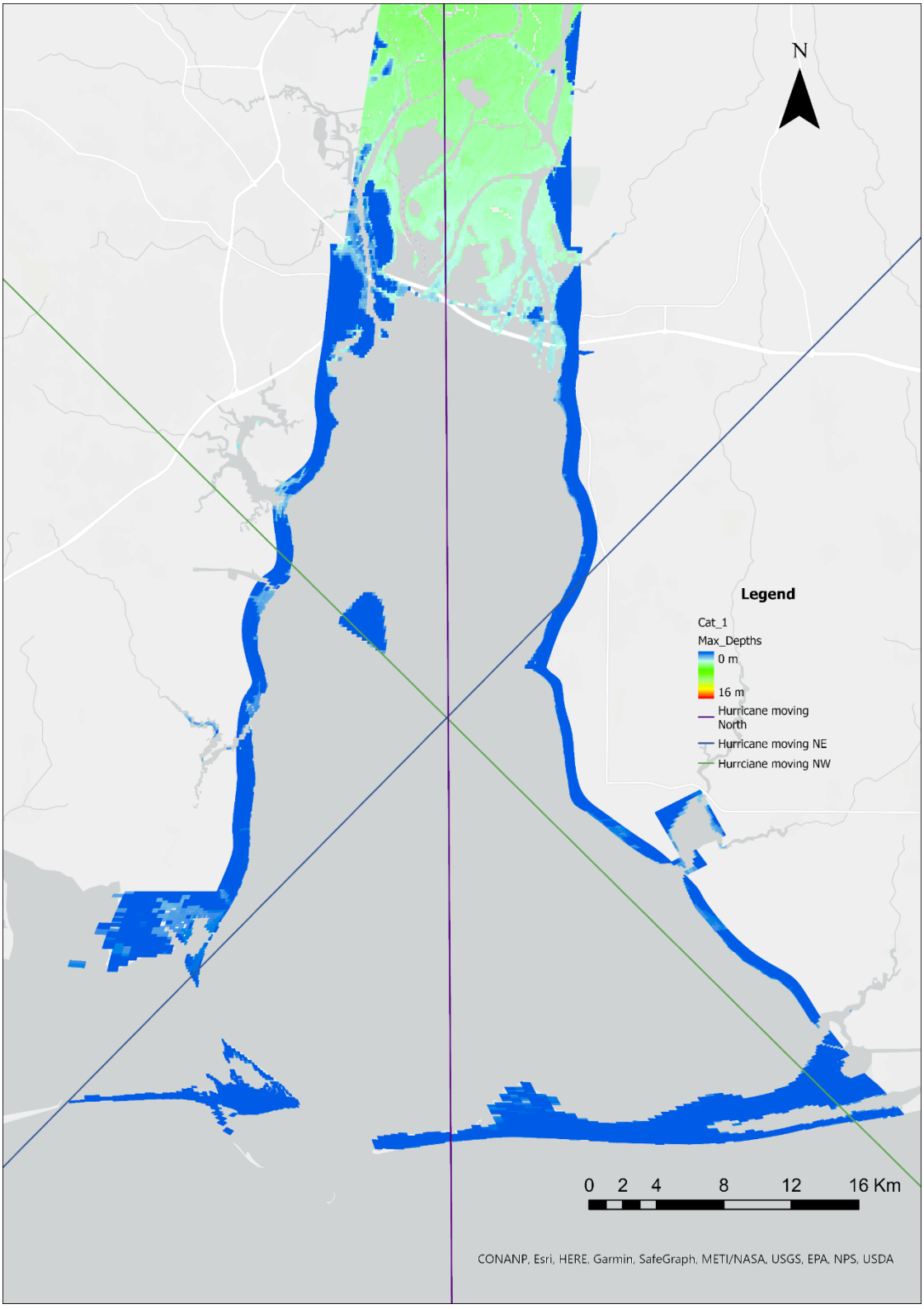

Figure 4.54 Maximum of maximum (MOM) depths for Hurricane Category 1 (ArcGIS Pro)

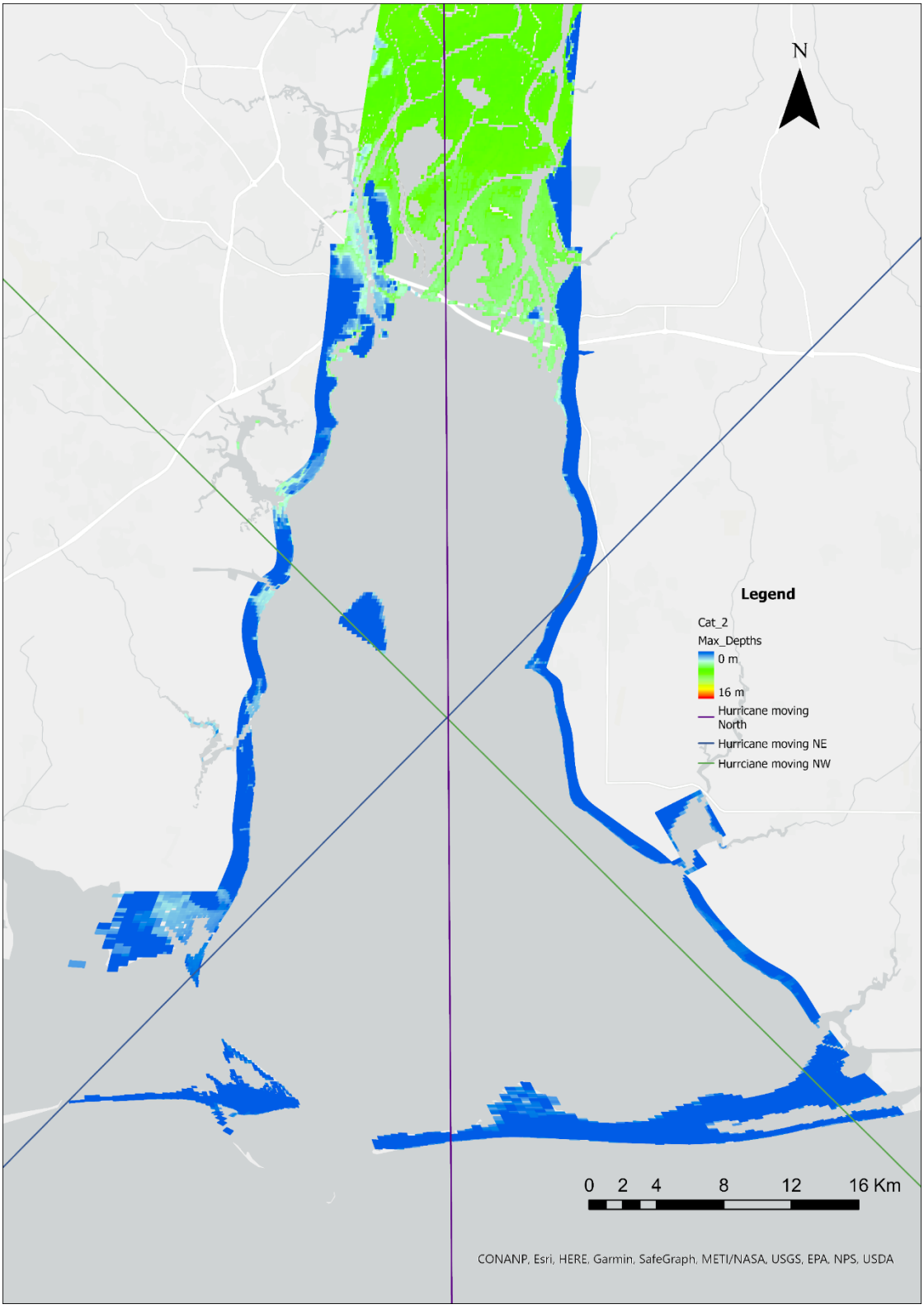

Figure 4.55 Maximum of maximum (MOM) depths for Hurricane Category 2 (ArcGIS Pro)

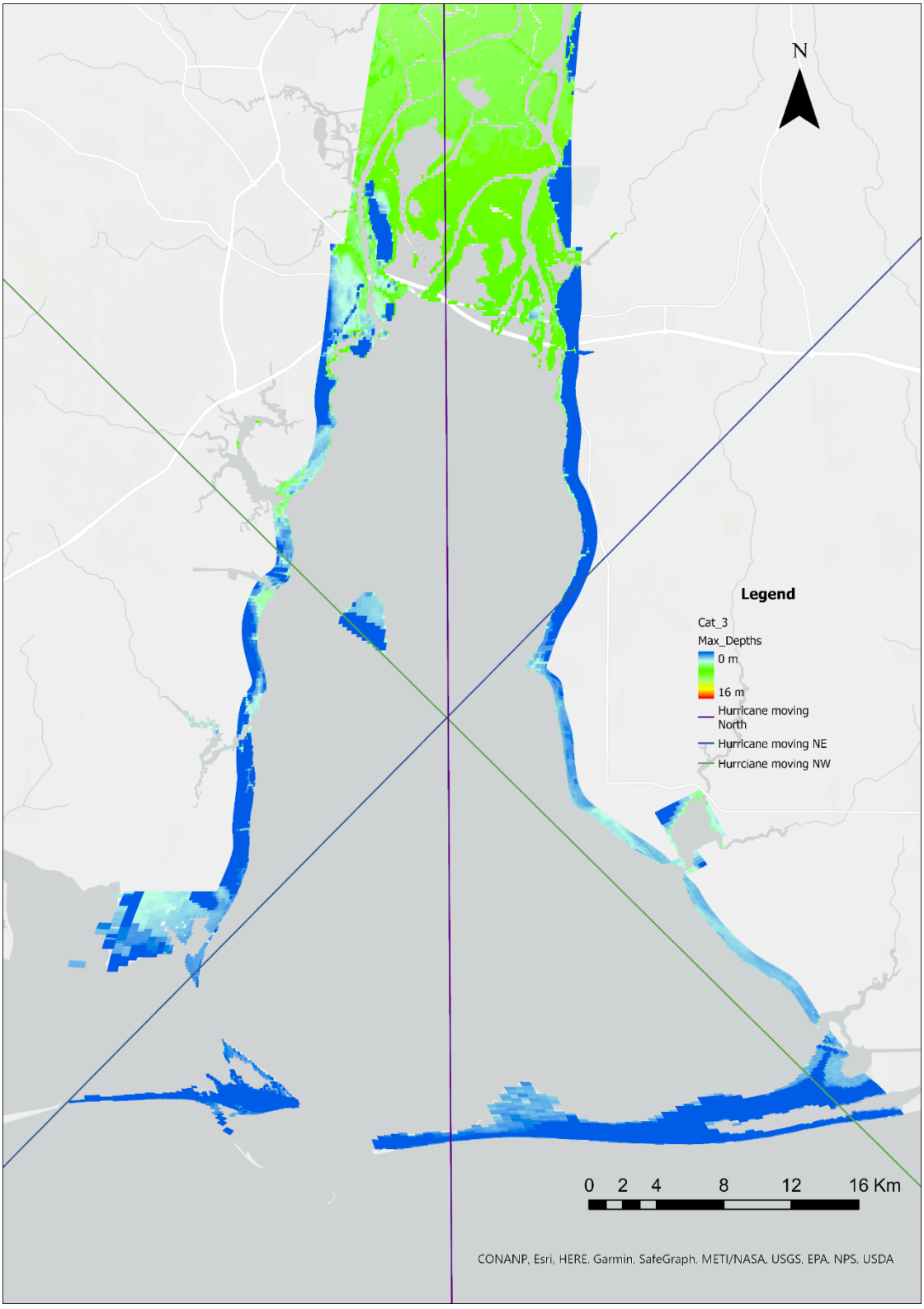

Figure 4.56 Maximum of maximum (MOM) depths for Hurricane Category 3 (ArcGIS Pro)

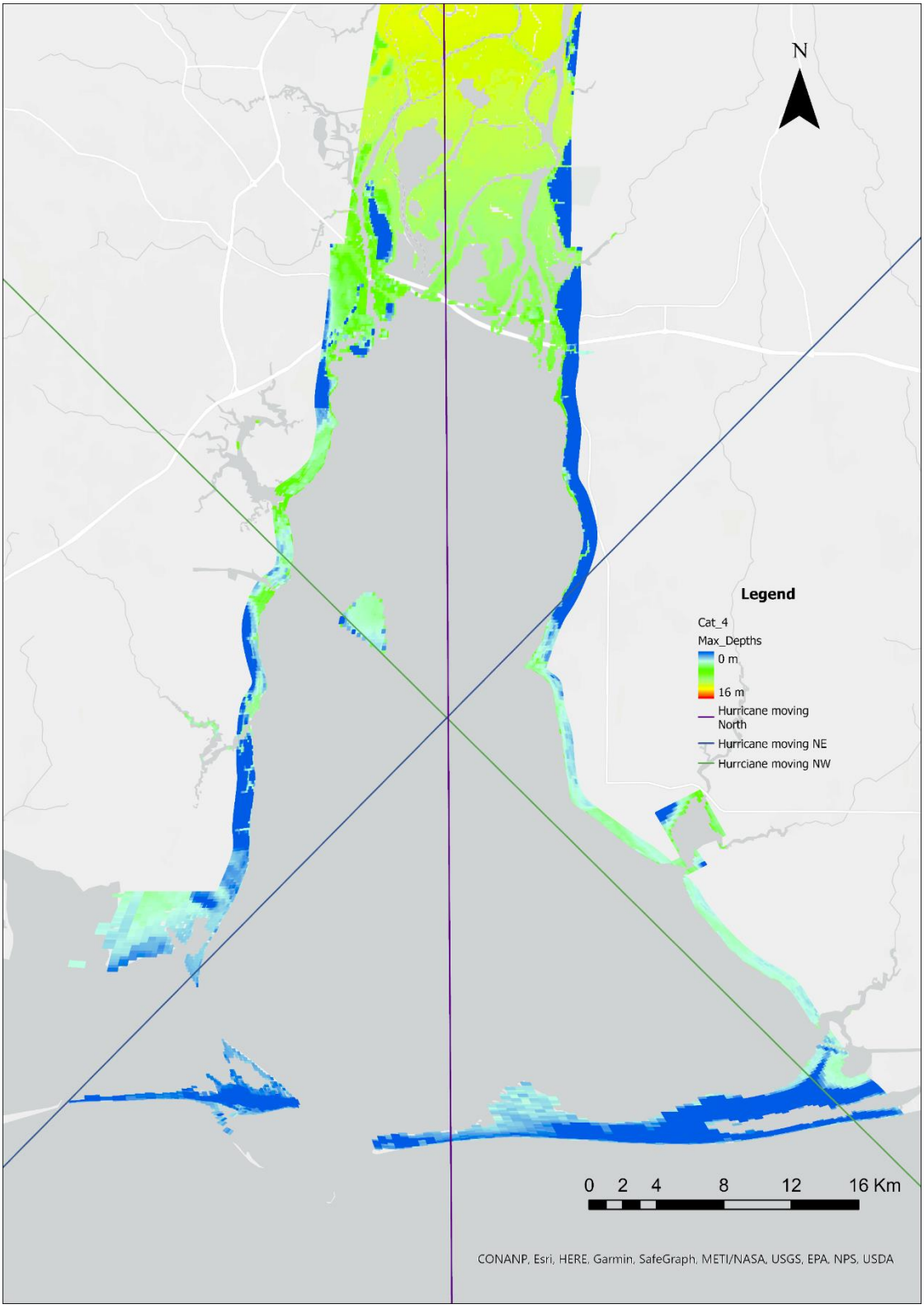

Figure 4.57 Maximum of maximum (MOM) depths for Hurricane Category 4 (ArcGIS Pro)

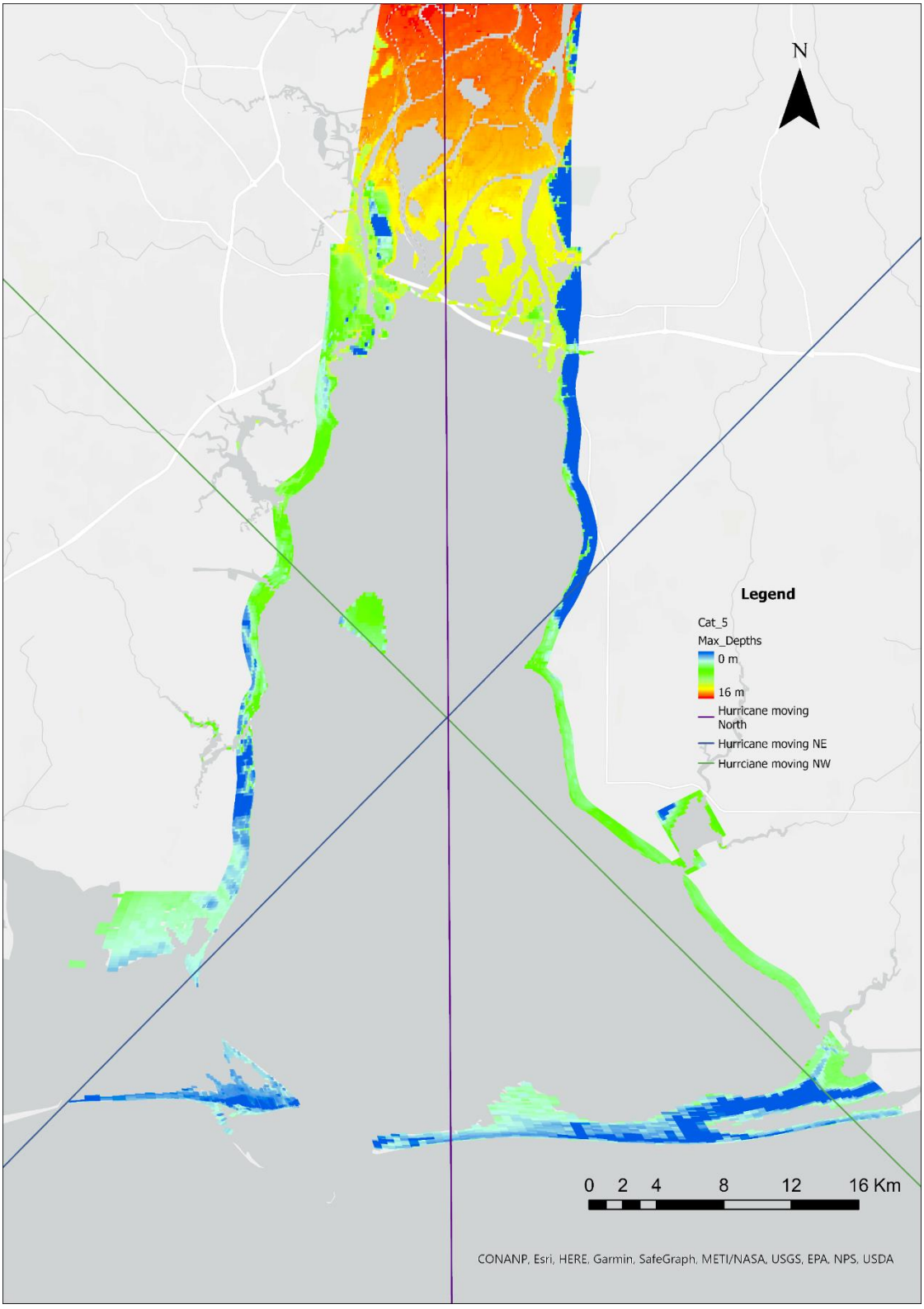

Figure 4.58 Maximum of maximum (MOM) depths for Hurricane Category 5 (ArcGIS Pro)

The SLOSH model data was downloaded from the National Surge Hazard Maps provided by National Hurricane Center (NHC). This website provides the MOM data (in TIF format) from the SLOSH model for all five hurricane categories for different coastal basins in the US. The TIF file for the Mobile Bay region was downloaded. This data was then imported to ArcGIS Pro to create a map for all five hurricane categories with respect to the EFDC Mobile Bay grid. First of all, the grid was converted to points and then "Extract Multi Values to Points" option was used to get value at all those points from SLOSH TIF data. Finally, this data was used to create maps for all five hurricane categories based on EFDC Mobile Bay grid for SLOSH data.

The maximum depths for all five hurricane categories from SLOSH model are shown in Figure 4.59 to Figure 4.63.

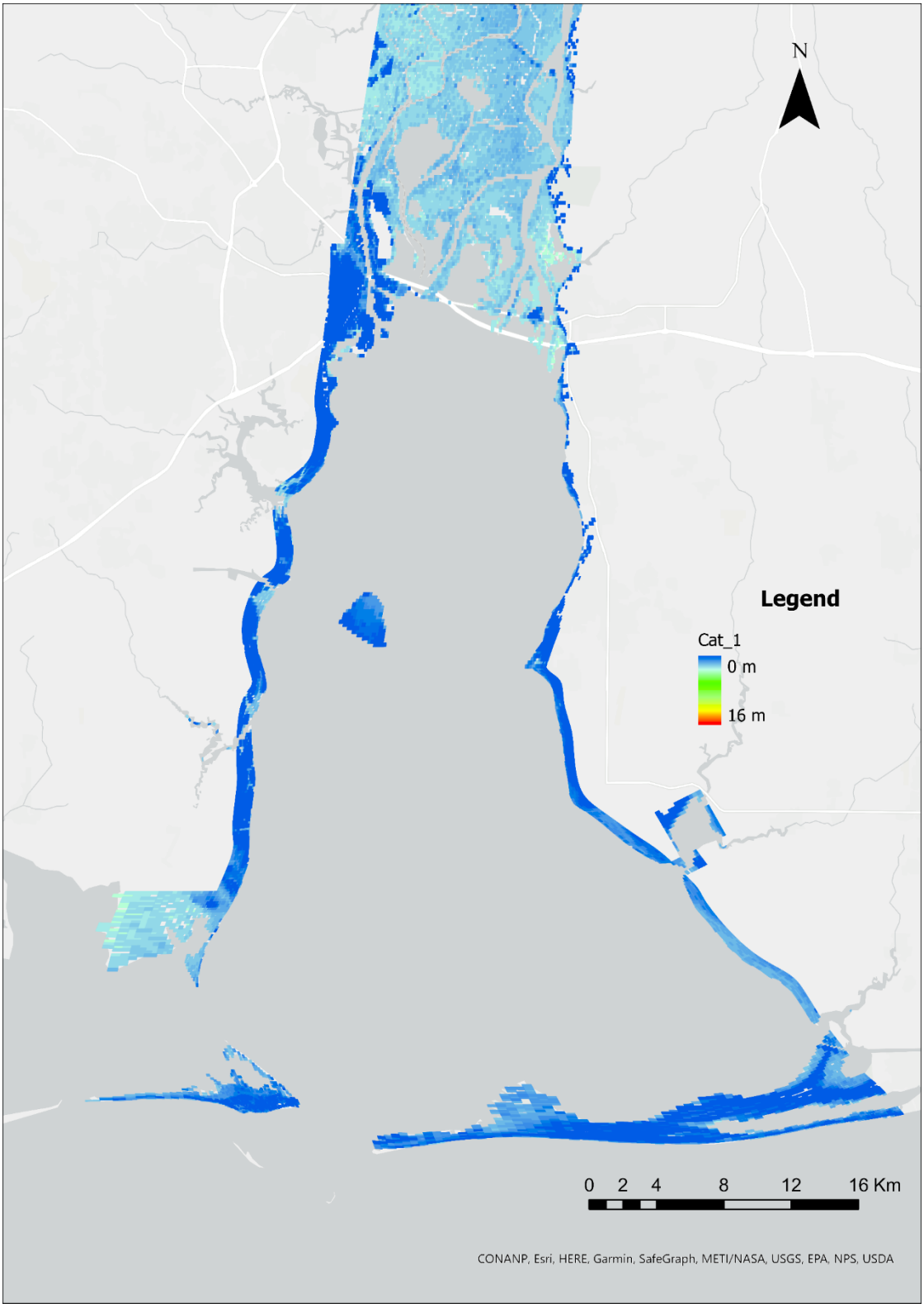

Figure 4.59 Maximum of maximum (MOM) depths for Hurricane Category 1 from SLOSH model (ArcGIS Pro)

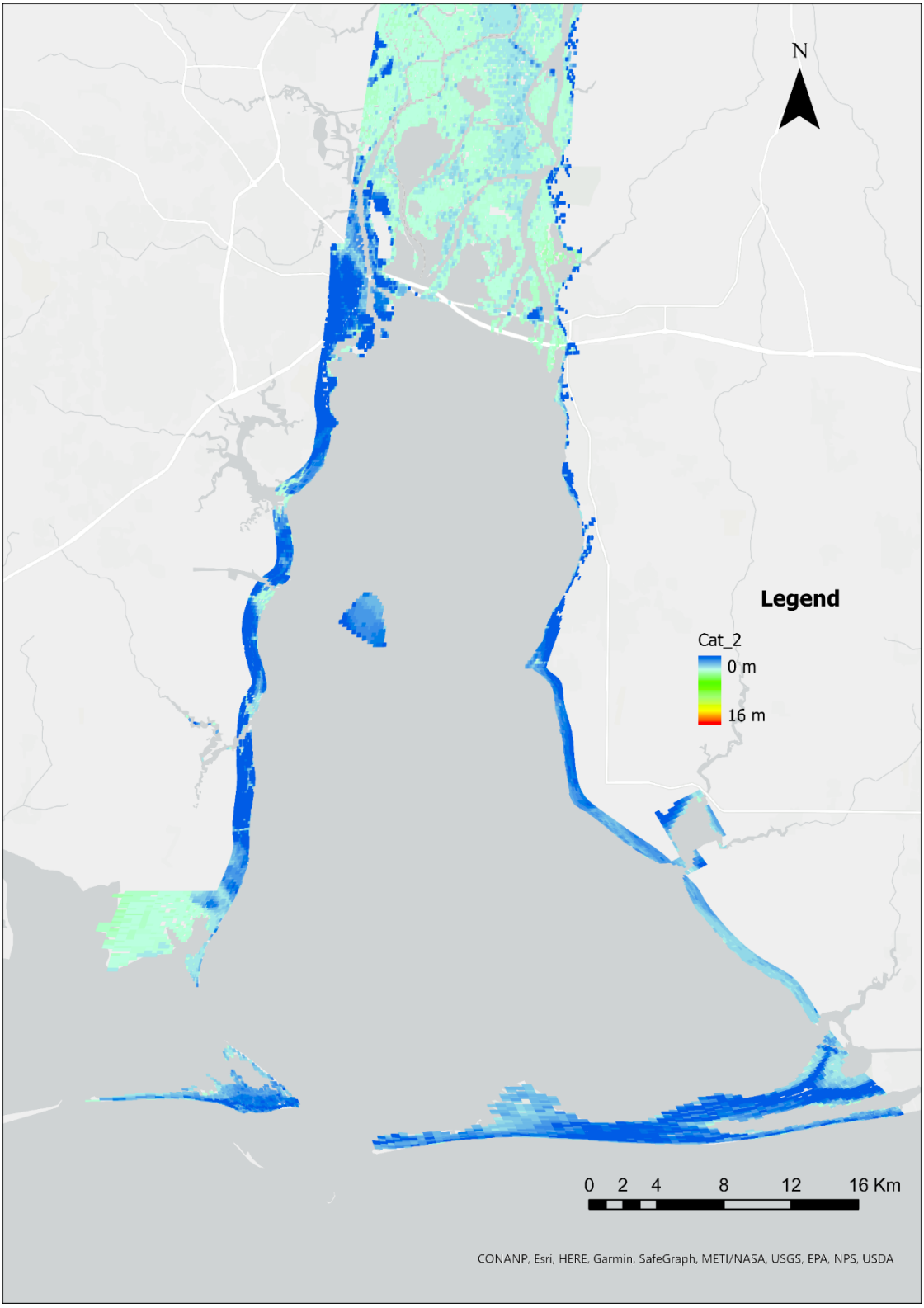

Figure 4.60 Maximum of maximum (MOM) depths for Hurricane Category 2 from SLOSH model (ArcGIS Pro)

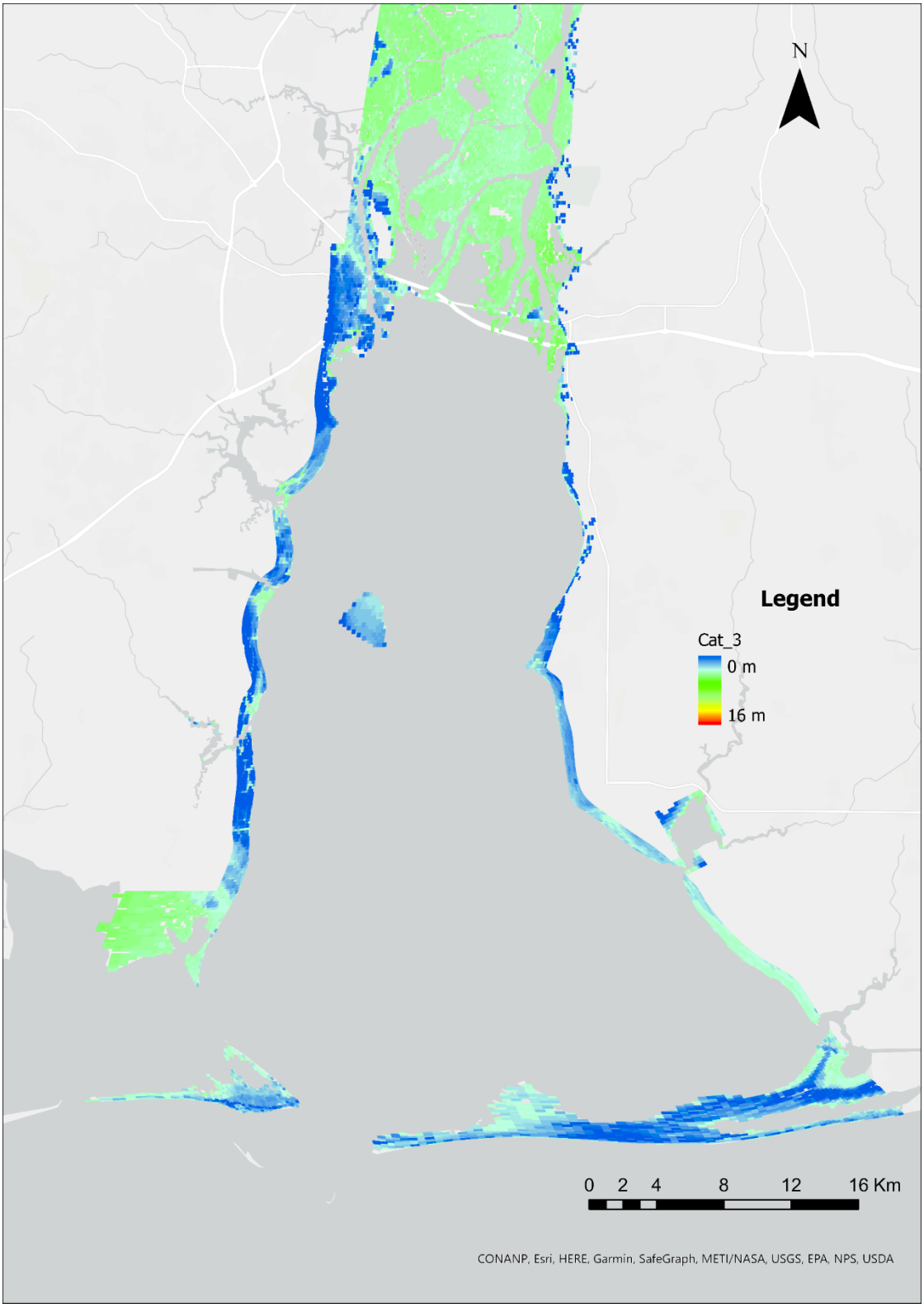

Figure 4.61 Maximum of maximum (MOM) depths for Hurricane Category 3 from SLOSH model (ArcGIS Pro)

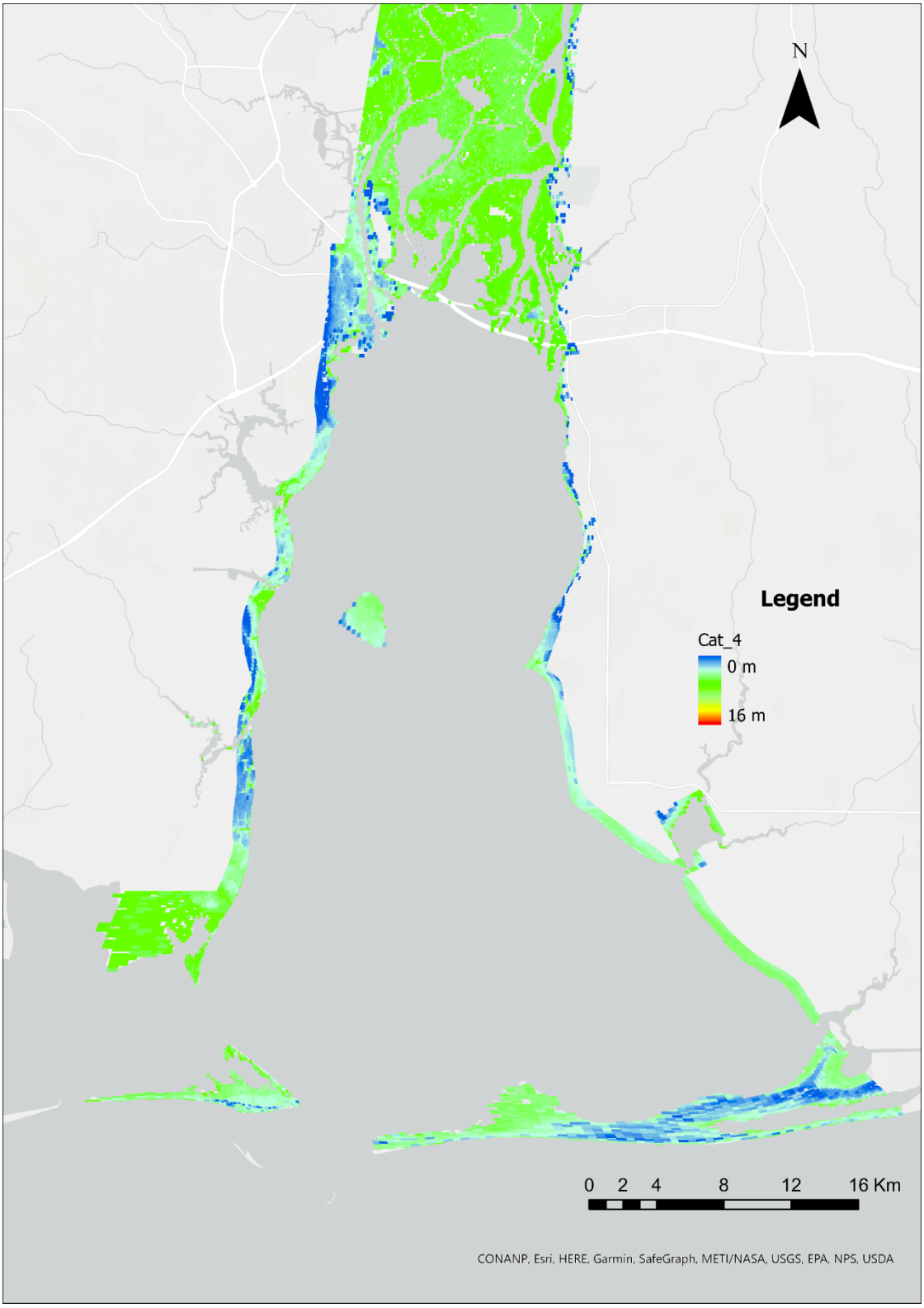

Figure 4.62 Maximum of maximum (MOM) depths for Hurricane Category 4 from SLOSH model (ArcGIS Pro)

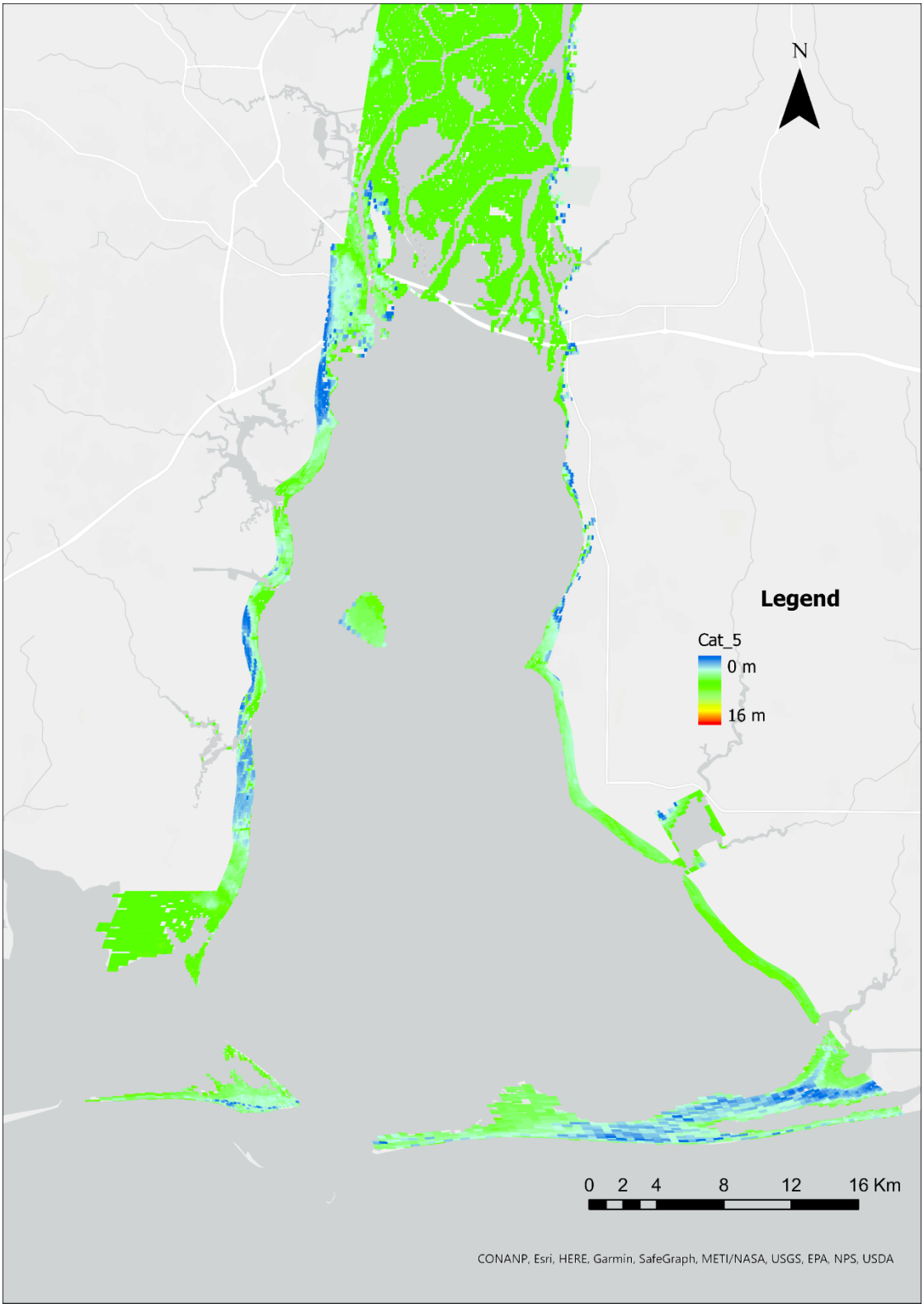

Figure 4.63 Maximum of maximum (MOM) depths for Hurricane Category 5 from SLOSH model (ArcGIS Pro)

The difference between the maximum depths provided by EFDC+ model and the SLOSH model was calculated (Mobile Bay EFDC model – SLOSH model), and the statistics of the differences are summarized in the Table 4.84 and Table 4.85.

Table 4.84 Statistics of the difference in flooding depth between Mobile Bay EFDC model and SLOSH model.

All coastal cells	Cat1	Cat2	Cat3	Cat4	Cat5
Average of difference in depth (m)	0.28	0.58	1.00	1.27	2.69
Max of difference in depth (m)	3.83	5.29	7.29	9.12	10.54
Std. dev. of difference (m)	1.23	2.02	2.38	3.28	3.97

Table 4.85 Statistics of the difference in flooding depth between Mobile Bay EFDC model and SLOSH model (If top wetland part is not included).

All coastal cells	Cat1	Cat2	Cat3	Cat4	Cat5
Average of difference in depth (m)	-0.36	-0.53	-0.32	-0.49	0.34
Max of difference in depth (m)	4.16	6.01	7.76	10.36	13.19
Std. dev. of difference (m)	0.76	1.20	1.52	2.23	2.56

4.6.2 DISCUSSION

If we divide the Mobile Bay into three regions: Top, middle, and bottom, we can see certain variations in water depths for SLOSH model and EFDC+ model for those three regions. On the bottom and middle regions of the bay, we can see that water depths are higher for SLOSH model (with similar magnitude of difference between SLOSH model and Mobile Bay EFDC model of around 0.4 m for all 5 hurricane category as seen in Table 4.85) as compared to the EFDC+ model. However, if we looked at the top region of the bay, which mostly consists of wetlands, we can see that water depths are higher for the EFDC+ model than the SLOSH model. These variations can also be seen in the data from the Table 4.84 and Table 4.85. When all the regions were included in calculations, the EFDC+ model provided higher average and maximum depths with increasing values for higher hurricane categories. However, when the top region was not included in the calculations, the SLOSH model provided higher average depths and maximum depths than EFDC+ model.

This might have been due to different approaches used in model simulation. SLOSH model uses three different hurricane forward speeds: 5 mph, 15 mph, and 25 mph (~2.2 m/s, ~6.7 m/s, and 11.1 m/s) and it also accounts for weakening phenomena of hurricanes after making landfall (by increasing central pressure and radius of maximum winds). For EFDC+ model, we have assumed forward speed of 5 m/s and weakening of hurricane was represented by reducing the wind speed after it reaches peak intensity at the center of the bay instead of during the landfall. As slow-moving hurricanes produce higher storm surge than fast moving hurricanes which is discussed in Chapter 2.2 and Chapter 4.5, the SLOSH model (which considers much slower moving hurricane) has higher water depths compared to the EFDC+ model in the bottom to central region of the bay. Since hurricane strength is reduced after the landfall in SLOSH model (which considers weakening phenomena of a hurricane after a landfall), it might have produced lower water depths compared to EFDC+ model on the top region of the bay.

CHAPTER 5.SUMMARY AND CONCLUSIONS

5.1 SUMMARY

This thesis presents the study of impact of hurricanes in terms of flooding in the coastal region of Mobile Bay, AL. A 3D hydrodynamic model using EFDC+ was developed and calibrated to simulate the hurricanes and their impact on the coast. EFDC+ is a comprehensive modeling tool which is used by researchers all over the globe and has been widely used for the study of many water bodies such as rivers, lakes, reservoirs, estuaries, wetlands, and coastal regions. The basic input data required for the simulation of the hydrodynamic of the Mobile Bay EFDC model is the model grid, bathymetric data, initial and boundary conditions. The required data were obtained from various sources such as NOAA, USGS, and NOAA NHC.

Model development starts with the development of the model grid. As the major focus of this study is to determine which part of the coastal land in Mobile Bay could be flooded under different hurricane scenarios, the curvilinear grid was developed in such a way that the grid resolution is higher along the coastal areas (both shallow water and normal dry lands along shorelines) and lower on the remaining open-water areas. This curvilinear grid with varying resolution was able to accurately represent the elevation changes along coastal shorelines which ultimately enhanced the analysis/simulation of flooding water/wave movement in the coastal shoreline areas. Normal EFDC hydrodynamic models typically do not include coastal lands as a part of simulation domain. This process involved in the generation of the curvilinear grid for the Mobile Bay is discussed in detail in section 3.4. As compared to the SLOSH model grid, Mobile Bay EFDC model grid cells are much finer which can represent the flooding pattern with higher spatial resolution. This thesis also discusses the data sources for the DEM and GIS method to develop the input bathymetric data, which also includes the elevation data for the coastal lands along shorelines, for the EFDC+ model. This process is discussed in section 3.5. The curvilinear grid and bathymetry data of the Mobile Bay region was then used to develop the hydrodynamic model using EFDC+ that was later used for investigating and analyzing hurricane flooding patterns in the study area.

This thesis also discusses the calibration and verification process of the Mobile Bay EFDC model. Water level calibration was performed using two historical hurricane events: Hurricane Ivan 2004 and Hurricane Sally 2020. Hurricane parameters were obtained from the NOAA NHC and loaded

into the tropical cyclone module in EFDC+. The simulated water surface elevations (WSEL) were compared against the observed data at different monitoring stations within the bay with good agreement (coefficient of determination, $R^2 = 0.96$ and 0.92 between the observed WSEL and the modeled results at Dauphin Island station for 2004 and 2020 respectively).

This thesis also presents the response of the bay under different hurricane scenarios based on two different approaches: one was based on the storm events provided by Hazus application, and another was based on hypothetical worst-case approach with three different hurricane track directions. These modeling scenarios provide general information on coastal flooding under different hurricane intensities and directions.

Based on the result of the modeling scenarios, the most flooded coastal region was identified which was common for most of the hurricane events. This region was used for testing the ability of different NNBFs to reduce the impacts of the hurricane events. The different NNBFs that are tested are vegetations with three different plant densities (#/m^2), artificial reefs modeled as partially blocking fixed masks, artificial sand dunes modeled by increasing the bottom elevation, and also the combination of NNBFs such as artificial sand dunes with vegetation with different plant densities.

This thesis also compares the coastal flooding due to different forward moving speed of a hurricane. Two forward moving speeds of 5 m/s and 10 m/s were used for the comparison. Finally, the results from this study were compared against the SLOSH model results for Mobile Bay. MOM maps were developed based on modeling scenario 2 for each of the five hurricane categories for this comparison.

5.2 CONCLUSIONS

This study compares the impact of hurricane events with different tracks and intensities to identify the vulnerable regions, in terms of flooding, on the coastal region of the Mobile Bay. The following conclusions are developed for the study:

1. The northern coastal area in Baldwin County (coastal region of the Daphne-Fairhope cities of Baldwin County) sits at relatively higher elevation as compared to the other coastal regions in Mobile and Baldwin Counties which makes it the least impacted region for all the hurricane scenarios.

2. Hurricanes were modeled in such a way that the peak windspeed was achieved along the top half of the bay, which was the reason low lying northern coastal region of Mobile County was mostly flooded for all major hurricanes (Categories 3 and above).
3. For Hurricane categories 2 and below, the flooding occurred along the track of the hurricanes whereas for major hurricanes (Categories 3 and above), the flooding occurred along the path as well as other low-lying areas away from the track.
4. The coastal highways: Dauphin Island Parkway 193 in Mobile County and Scenic Highway 98 and Fort Morgan Road in Baldwin County are heavily affected by category 4 and 5 with highest impact by hurricane moving north and northeast followed by northwest. Therefore, hurricane intensity, hurricane track, and the ground elevation determine the most vulnerable areas to flooding on the coast of Mobile Bay according to this study.
5. The NNBFs test evaluated the benefits of three different NNBFs in mitigating hurricane flooding. Among the three tested NNBFs, construction of artificial sand dunes was seen to be much more effective, followed by vegetation with higher plant density. The artificial reef was the least effective in reducing flooding according to the model.
6. Different combinations of NNBFs were also compared, among which the use of combination of NNBFs such as sand dunes with high density vegetations was even more effective at reducing the storm impacts.
7. The results from the comparison of slow-moving hurricanes with the fast-moving hurricane showed that the slow-moving hurricane caused higher flooding depths as compared to the flooding depths by fast moving hurricanes at various regions of the bay. This suggests that slow-moving hurricanes are more dangerous compared to fast-moving hurricanes.
8. The MOM results from the SLOSH model have higher flooding depth as compared to the Mobile Bay EFDC+ model on the middle and bottom half of the bay whereas on the top half of the bay, Mobile Bay EFDC+ model has the higher flooding depth with increasing magnitude with higher hurricane intensity. These variations might have resulted due to different modeling approaches such as forward speeds, weakening phenomena, number of tracks and directions that were followed for modeling hurricanes.
9. SLOSH's MEOW and MOM results for Mobile Bay are for more conservative planning from 1815 hypothetical hurricane model runs. The SLOSH flooding depths along shorelines of Mobile Bay do not occur at the same time during a particular hurricane. The EFDC+

modeling can identify specific flooding shoreline areas in Mobile Bay for a specific hurricane if its forward speed, track, and potential maximum wind speed are given or predicted.

5.2.1 LIMITATION OF THE STUDY AND FUTURE STUDIES

The primary focus of this study is to understand the ability of NNBFs in reducing the impacts of hurricanes in the coastal region of Mobile Bay. Therefore, this study starts with the modeling of hurricanes followed by testing of different NNBFs. As hurricanes being a complex weather phenomenon, it is very hard to predict. Thus, we have tested various hurricanes based on the probabilistic approach from the HAZUS as well as some hypothetical cases. However, there are still many things to be considered for better understanding of a hurricane impacts and NNBFs such as hurricane moving speeds, directions, different types of vegetation parameters and many more which will help to improve the accuracy of this study.

Some of the limitations and improvements for future studies are discussed below.

- For all the hurricane scenarios in this study, we have assumed the same forward moving speed. Therefore, multiple possible forward moving speeds should be tested for better understanding of the hurricane flooding.
- We have assumed three hurricane direction following a straight track which is a rare thing to happen in nature as hurricanes change their direction based on the wind direction. To account for this phenomenon, many other possible directions should be studied, and hurricane tracks should be adjusted accordingly.
- We have modeled the hurricane in such a way that it reaches its maximum intensity near the center of the bay. But most hurricanes weaken after making landfall because the central pressure and radius of maximum winds increase. These phenomena should be addressed for future studies.
- For all the hurricane scenarios in this study, flow data from Hurricane Sally 2020 was used as the upstream flow boundary. However, flow in a river gets directly affected by hurricane intensity, hurricane track, windspeed and other parameters. Thus, upstream flow data should be adjusted according to the hurricane parameters to improve the model results. Another alternative is to use water level that varies in a smaller range and may have less impact on the simulation results.

- The rainfall event during hurricane is not considered in this study whereas heavy rainfall is one of the characteristics of a hurricane. This phenomenon should be incorporated into the model in future for better knowledge of the hurricane impacts on the coastal areas.
- We have not included wave component in this study. During a severe storm, waves can have a significant impact on the storm surge by contributing to the water level near the coast. Thus, wave models should be included to study wave impacts on storm surge and flooding.
- For this study, we have considered a single type of vegetation with different plant densities. Other vegetation parameters should be tested to identify the most effective vegetation in reducing hurricane impacts.
- We have selected the NNBFs test region based on the most inundated area for most of the tested hurricanes. For future studies, vulnerable coastal areas should be identified based on the economic analysis to study the NNBFs.

REFERENCES

Abdelhafez, M. A., Ellingwood, B., & Mahmoud, H. (2021). Vulnerability of seaports to hurricanes and sea level rise in a changing climate: A case study for mobile, AL. *Coastal Engineering*, *167*, 103884. https://doi.org/10.1016/j.coastaleng.2021.103884

Adhikari, P., Abdelhafez, M. A., Dong, Y., Guo, Y., Mahmoud, H. N., & Ellingwood, B. R. (2021). Achieving Residential Coastal Communities Resilient to Tropical Cyclones and Climate Change. *Frontiers in Built Environment*, *6*, 576403. https://doi.org/10.3389/fbuil.2020.576403

Alarcon, V. J., & McAnally, W. H. (2012). Using Hydrodynamic Modeling for Estimating Flooding and Water Depths in Grand Bay, Alabama. In B. Murgante, O. Gervasi, S. Misra, N. Nedjah, A. M. A. C. Rocha, D. Taniar, & B. O. Apduhan (Eds.), *Computational Science and Its Applications – ICCSA 2012* (Vol. 7334, pp. 578–588). Springer Berlin Heidelberg. https://doi.org/10.1007/978-3-642-31075-1_43

Athikalam, P. T., & Karur Vaideeswaran, A. (2022). Vegetation bioshield for coastal protection in South Asia: Status and way forward. *Journal of Coastal Conservation*, *26*(1), 3. https://doi.org/10.1007/s11852-022-00850-x

Barnes, H. H., Callaway, C., Davis, H. R., Kraft, B., Griggs, M. J., King, M. T., Perry, M. S., Swann, D. L., Wright, D. R., Bender, D., Crozier, D. G., Quackenbush, D. S., Fogarty, M. B., Hinesley, M. P., Mahoney, M. S., Struthers, M. E., & Valentine, D. J. (2008). *State of Mobile Bay*. https://www.mobilebaynep.com/images/uploads/library/State-of-Mobile-Bay-Final.pdf

Bates, P. D., Dawson, R. J., Hall, J. W., Horritt, M. S., Nicholls, R. J., Wicks, J., & Mohamed Ahmed Ali Mohamed Hassan. (2005). Simplified two-dimensional numerical modelling of coastal flooding and example applications. *Coastal Engineering*, *52*(9), 793–810. https://doi.org/10.1016/j.coastaleng.2005.06.001

Berg, R., & Brad, J. R. (2021). Tropical Cyclone Report Hurricane Sally. *National Hurricane Center*.

Bhusal, A., Parajuli, U., Regmi, S., & Kalra, A. (2022). Application of Machine Learning and Process-Based Models for Rainfall-Runoff Simulation in DuPage River Basin, Illinois. *Hydrology*, *9*(7), 117. https://doi.org/10.3390/hydrology9070117

Bilkovic, D. M., & Mitchell, M. M. (2013). Ecological tradeoffs of stabilized salt marshes as a shoreline protection strategy: Effects of artificial structures on macrobenthic assemblages. *Ecological Engineering*, *61*, 469–481. https://doi.org/10.1016/j.ecoleng.2013.10.011

Borsje, B. W., Van Wesenbeeck, B. K., Dekker, F., Paalvast, P., Bouma, T. J., Van Katwijk, M. M., & De Vries, M. B. (2011). How ecological engineering can serve in coastal protection. *Ecological Engineering*, *37*(2), 113–122. https://doi.org/10.1016/j.ecoleng.2010.11.027

Bouwer, L. M. (2019). Observed and Projected Impacts from Extreme Weather Events: Implications for Loss and Damage. In R. Mechler, L. M. Bouwer, T. Schinko, S. Surminski, & J. Linnerooth-Bayer (Eds.), *Loss and Damage from Climate Change* (pp. 63–82). Springer International Publishing. https://doi.org/10.1007/978-3-319-72026-5_3

Bridges, T. S., Wagner, P. W., Burks-Copes, K. A., Bates, M. E., Collier, Z. A., Fischenich, C. J., Gailani, J. Z., Leuck, L. D., Piercy, C. D., Rosati, J. D., Russo, E. J., Shafer, D. J., Suedel, B. C., Vuxton, E. A., & Wamsley, T. V. (2015). *Use of Natural and Nature-Based Features (NNBF) for Coastal Resilience*.

Bruun, P. (1998). Dunes—Their Function and Design. *Journal of Coastal Research*, *26*.

Byron, D., & Heck, K. L. (2006). Hurricane effects on seagrasses along Alabama's Gulf Coast. *Estuaries and Coasts*, *29*(6), 939–942. https://doi.org/10.1007/BF02798654

Chen, G., Fang, X., & Devkota, J. (2016). Understanding flow dynamics and density currents in a river-reservoir system under upstream reservoir releases. *Hydrological Sciences Journal*, *61*(13), 2411–2426. https://doi.org/10.1080/02626667.2015.1112902

Chen, Q., Wang, L., & Tawes, R. (2008). Hydrodynamic Response of Northeastern Gulf of Mexico to Hurricanes. *Estuaries and Coasts*, *31*(6), 1098–1116. https://doi.org/10.1007/s12237-008-9089-9

Chen, Zhu, L., Ding, Y., Jafari, N. H., Rosati, J. D., & Johnson, B. D. (2022). *Evaluation of vegetated shoreline capacity using CSHORE-VEG*. Engineer Research and Development Center (U.S.).

Cheung, K. F., Phadke, A. C., Wei, Y., Rojas, R., Douyere, Y. J.-M., Martino, C. D., Houston, S. H., Liu, P. L.-F., Lynett, P. J., Dodd, N., Liao, S., & Nakazaki, E. (2003). Modeling of storm-induced coastal flooding for emergency management. *Ocean Engineering*, *30*(11), 1353–1386. https://doi.org/10.1016/S0029-8018(02)00133-6

Craig, P. M., Chung, D. H., Lam, N. T., Son, P. H., & Tinh, N. X. (2014). *Sigma-zed: A computationally efficient approach to reduce the horizontal gradient error in the EFDC's vertical sigma grid*.

Darayi, M., Barker, K., & Nicholson, C. D. (2019). A multi-industry economic impact perspective on adaptive capacity planning in a freight transportation network. *International Journal of Production Economics*, *208*, 356–368. https://doi.org/10.1016/j.ijpe.2018.12.008

Devkota, J., & Fang, X. (2015). Numerical simulation of flow dynamics in a tidal river under various upstream hydrologic conditions. *Hydrological Sciences Journal*, *60*(10), 1666–1689. https://doi.org/10.1080/02626667.2014.947989

Devkota, J., Fang, X., & Fang, V. Z. (2013). Response Characteristics of the Perdido and Wolf Bay System to Inflows and Sea Level Rise. *British Journal of Environment and Climate Change*, 229–256. https://doi.org/10.9734/BJECC/2013/3516

Ding, Y., Chen, Q., Zhu, L., Rosati, J., & Johnson, B. (2022). *Implementation of flexible vegetation into CSHORE for modeling wave attenuation*. Engineer Research and Development Center (U.S.). https://doi.org/10.21079/11681/43220

DSI LLC. (2023). *EFDC+ Theory, Version 11*. DSI LLC, Edmonds WA. https://www.eemodelingsystem.com/wp-content/Download/Documentation/EFDC Theory Document Ver 11.pdf

Ellis, J. T., Spruce, J. P., Swann, R. A., Smoot, J. C., & Hilbert, K. W. (2011). An assessment of coastal land-use and land-cover change from 1974–2008 in the vicinity of Mobile Bay,

Alabama. *Journal of Coastal Conservation*, *15*(1), 139–149. https://doi.org/10.1007/s11852-010-0127-y

Emanuel, K. (2005). Increasing destructiveness of tropical cyclones over the past 30 years. *Nature*, *436*(7051), 686–688. https://doi.org/10.1038/nature03906

Environmental Fluid Dynamics Code (EFDC) | US EPA. (2023, October 24). *Environmental Fluid Dynamics Code (EFDC)* [US EPA]. US EPA. https://www.epa.gov/ceam/environmental-fluid-dynamics-code-efdc

Frey, A. E., Olivera, F., Irish, J. L., Dunkin, L. M., Kaihatu, J. M., Ferreira, C. M., & Edge, B. L. (2010). Potential Impact of Climate Change on Hurricane Flooding Inundation, Population Affected and Property Damages in Corpus Christi1: Potential Impact of Climate Change on Hurricane Flooding Inundation, Population Affected and Property Damages in Corpus Christi. *JAWRA Journal of the American Water Resources Association*, *46*(5), 1049–1059. https://doi.org/10.1111/j.1752-1688.2010.00475.x

Galperin, B., Kantha, L., Hassid, S., & Rosati, A. (1988). *A quasi-equilibrium turbulent energy model for geophysical flows.* Journal of the atmospheric sciences.

Ghisalberti, M., & Nepf, H. M. (2004). The limited growth of vegetated shear layers: Limited growth of vegetated shear layers. *Water Resources Research*, *40*(7). https://doi.org/10.1029/2003WR002776

Glahn, B., Taylor, A., Kurkowski, N., & Shaffer, W. A. (2009). *The role of the slosh model in national weather service storm surge forecasting*.

Hamrick, J. M. (1992). *Three-Dimensional Environmental Fluid Dynamics Computer Code: Theoretical and computational aspects*. https://doi.org/10.21220/V5TT6C

Hamrick, J. M. (1996). *User's Manual for the Environmental Fluid Dynamics Computer Code*. https://doi.org/10.21220/V5M74W

Hazus 6.0 Inventory Technical Manual. (2022).

Holland, G. J. (1980). *An Analytic Model of the Wind and Pressure Profiles in Hurricanes Holland(1980)*.

Jadhav, R. S., Chen, Q., & Smith, J. M. (2013). Spectral distribution of wave energy dissipation by salt marsh vegetation. *Coastal Engineering*, *77*, 99–107. https://doi.org/10.1016/j.coastaleng.2013.02.013

James, S. C., & O'Donncha, F. (2019). Drag coefficient parameter estimation for aquaculture systems. *Environmental Fluid Mechanics*, *19*(4), 989–1003. https://doi.org/10.1007/s10652-019-09697-7

Jelesnianski, C. P. (1972). *SPLASH : (Special Program to List Amplitudes of Surges from Hurricanes). I, Landfall storms*. NOAA technical memorandum NWS TDL ; 46. https://repository.library.noaa.gov/view/noaa/13509

Jelesnianski, C. P., Chen, J., & Shaffer, W. A. (1992). *SLOSH : Sea, Lake, and Overland Surges from Hurricanes*. NOAA technical report NWS ; 48. https://repository.library.noaa.gov/view/noaa/7235

Ji, Z.-G. (2008). *Hydrodynamics and water quality: Modeling rivers, lakes, and estuaries*. John Wiley & Sons.

Kim, C.-K., & Park, K. (2012). A modeling study of water and salt exchange for a micro-tidal, stratified northern Gulf of Mexico estuary. *Journal of Marine Systems*, *96–97*, 103–115. https://doi.org/10.1016/j.jmarsys.2012.02.008

Knutson, P. L., Brochu, R. A., Seelig, W. N., & Inskeep, M. (1982). Wave damping inSpartina alterniflora marshes. *Wetlands*, *2*(1), 87–104. https://doi.org/10.1007/BF03160548

Knutson, T. R., McBride, J. L., Chan, J., Emanuel, K., Holland, G., Landsea, C., Held, I., Kossin, J. P., Srivastava, A. K., & Sugi, M. (2010). Tropical cyclones and climate change. *Nature Geoscience*, *3*(3), 157–163. https://doi.org/10.1038/ngeo779

Liu, Z., Hashim, N. B., Kingery, W. L., Huddleston, D. H., & Xia, M. (2008). Hydrodynamic Modeling of St. Louis Bay Estuary and Watershed Using EFDC and HSPF. *Journal of Coastal Research*, *10052*, 107–116. https://doi.org/10.2112/1551-5036-52.sp1.107

Matias, A., Ferreira, Ó., Mendes, I., Dias, J. A., & Vila-Concejo, A. (2005). Artificial Construction of Dunes in the South of Portugal. *Journal of Coastal Research*, *213*, 472–481. https://doi.org/10.2112/03-0047.1

Mei, C. C., Chan, I.-C., Liu, P. L.-F., Huang, Z., & Zhang, W. (2011). Long waves through emergent coastal vegetation. *Journal of Fluid Mechanics*, *687*, 461–491. https://doi.org/10.1017/jfm.2011.373

Mellor, G. L., Ezer, T., & Oey, L.-Y. (1994). *The Pressure Gradient Conundrum of Sigma Coordinate Ocean Models*. Journal of atmospheric and oceanic technology. https://doi.org/10.1175/1520-0426(1994)011%3C1126:TPGCOS%3E2.0.CO;2

Mellor, G. L., & Yamada, T. (1982). Development of a turbulence closure model for geophysical fluid problems. *Reviews of Geophysics*, *20*(4), 851. https://doi.org/10.1029/RG020i004p00851

Misachi, J. (2021). Mobile Bay. *WorldAtlas*. https://www.worldatlas.com/bays/mobile-bay.html

Moore, R. A., & Torres, M. (2020). *Characterization of Seasonal Variability in Tides*.

Nezu, I. (1993). *Turbulence in Open-Channel Flows*.

NOAA's National Weather Service. (n.d.). *Hurricane Ivan—September 16, 2004*. NOAA's National Weather Service. https://www.weather.gov/mob/ivan

Palinkas, C. M., Orton, P., Hummel, M. A., Nardin, W., Sutton-Grier, A. E., Harris, L., Gray, M., Li, M., Ball, D., Burks-Copes, K., Davlasheridze, M., De Schipper, M., George, D. A., Halsing, D., Maglio, C., Marrone, J., McKay, S. K., Nutters, H., Orff, K., … Williams, T. (2022). Innovations in Coastline Management With Natural and Nature-Based Features (NNBF): Lessons Learned From Three Case Studies. *Frontiers in Built Environment*, *8*, 814180. https://doi.org/10.3389/fbuil.2022.814180

Parajuli, U., Bhusal, A., Babu Ghimire, A., & Shin, S. (2023). Comparing HEC-HMS, PCSWMM, and Random Forest Models for Rainfall-Runoff Evaluation to Extreme Flooding Events. *World Environmental and Water Resources Congress 2023*, 1250–1262. https://doi.org/10.1061/9780784484852.114

Park, K., Valentine, J. F., Sklenar, S., Weis, K. R., & Dardeau, M. R. (2007). The Effects of Hurricane Ivan in the Inner Part of Mobile Bay, Alabama. *Journal of Coastal Research*, *23*(5), 1332. https://doi.org/10.2112/06-0686.1

Parker, D. W. (1979). *Hurricane Frederic Post Disaster Report*.

Plew, D. R. (2011). Depth-Averaged Drag Coefficient for Modeling Flow through Suspended Canopies. *Journal of Hydraulic Engineering*, *137*(2), 234–247. https://doi.org/10.1061/(ASCE)HY.1943-7900.0000300

Qin, Z., He, Z., Wu, G., Tang, G., & Wang, Q. (2022). Developing Water-Quality Model for Jingpo Lake Based on EFDC. *Water*, *14*(17), 2596. https://doi.org/10.3390/w14172596

Saffir-Simpson Hurricane Wind Scale. (n.d.). https://www.nhc.noaa.gov/aboutsshws.php

Schrass, K., & Mehta, A. V. (2017). *Improved Use and Understanding of NNBF in the Mid-Atlantic*. North Atlantic Landscape Conservation Cooperative.

Sea, Lake, and Overland Surges from Hurricanes (SLOSH). (n.d.). https://www.nhc.noaa.gov/surge/slosh.php

Sheng, Y. P., Zhang, Y., & Paramygin, V. A. (2010). Simulation of storm surge, wave, and coastal inundation in the Northeastern Gulf of Mexico region during Hurricane Ivan in 2004. *Ocean Modelling*, *35*(4), 314–331. https://doi.org/10.1016/j.ocemod.2010.09.004

Sigren, J. M., Figlus, J., & Armitage, A. R. (2014). *Coastal sand dunes and dune vegetation: Restoration, erosion, and storm protection*. *82*(4).

Simpson, & Saffir. (2007). Tropical Cyclone Destructive Potential by Integrated Kinetic Energy. *Bulletin of the American Meteorological Society*, *88*(4), 513–526. https://doi.org/10.1175/BAMS-88-4-513

Smagorinsky, J. (1963). General circulation experiments with the primitive equations: I. The basic experiment*. *Monthly Weather Review*, *91*(3), 99–164. https://doi.org/10.1175/1520-0493(1963)091<0099:GCEWTP>2.3.CO;2

Smith, J. M., Bryant, M. A., & Wamsley, T. V. (2016). Wetland buffers: Numerical modeling of wave dissipation by vegetation: Jane McKee Smith, Mary Anderson Bryant, and Ty V. Wamsley. *Earth Surface Processes and Landforms*, *41*(6), 847–854. https://doi.org/10.1002/esp.3904

Stewart, S. (2011). Tropical Cyclone Report Hurricane Ivan. *National Hurricane Center*.

StormSmart Coasts Program CZM. (2013). StormSmart Properties Fact Sheet 1: Artificial Dunes and Dune Nourishment. *Massachusetts Office of Coastal Management (CZM)*.

Sutton-Grier, A. E., Wowk, K., & Bamford, H. (2015). Future of our coasts: The potential for natural and hybrid infrastructure to enhance the resilience of our coastal communities, economies and ecosystems. *Environmental Science & Policy*, *51*, 137–148. https://doi.org/10.1016/j.envsci.2015.04.006

Sweet, W., Dusek, G., Obeysekera, J. T. B., & Marra, J. J. (2018). Patterns and Projections of High Tide Flooding Along the U.S. Coastline Using a Common Impact Threshold. *NOAA Technical Report NOS CO-OPS ; 086*. https://doi.org/10.7289/V5/TR-NOS-COOPS-086

Takagi, H., Thao, N. D., Esteban, M., Tam, T. T., Knaepen, H. L., & Mikami, T. (2012). *Vulnerability of coastal areas in Southern Vietnam against tropical cyclones and storm surges*.

Takagi, H., & Wu, W. (2015). *Maximum wind radius estimated by the 50 kt radius: Improvement of storm surge forecasting over the Western North Pacific* [Preprint]. Sea, Ocean and Coastal Hazards. https://doi.org/10.5194/nhessd-3-6431-2015

Temmerman, S., Meire, P., Bouma, T. J., Herman, P. M. J., Ysebaert, T., & De Vriend, H. J. (2013). Ecosystem-based coastal defence in the face of global change. *Nature*, *504*(7478), 79–83. https://doi.org/10.1038/nature12859

TNC. (2023). *Alabama's living shorelines*. Living Shorelines. (n.d.). The Nature Conservancy. https://www.nature.org/en-us/about-us/where-we-work/united-states/alabama/stories-in-alabama/living-shorelines/

Tropical Cyclone Climatology. (n.d.). https://www.nhc.noaa.gov/climo/index.php

Turan, C. K., Kinfu, Y. P., Samad, M. A., Farhadzadeh, A., & Ng, K. (2018). Comparison of ADCIRC and SLOSH Model Simulations for Hurricanes Andrew and Irma near Miami, Florida. *World Environmental and Water Resources Congress 2018*, 176–187. https://doi.org/10.1061/9780784481424.019

Wamsley, T. V., Cialone, M. A., Smith, J. M., Ebersole, B. A., & Grzegorzewski, A. S. (2009). Influence of landscape restoration and degradation on storm surge and waves in southern Louisiana. *Natural Hazards*, *51*(1), 207–224. https://doi.org/10.1007/s11069-009-9378-z

Webster, P. J., Holland, G. J., Curry, J. A., & Chang, H.-R. (2005). Changes in Tropical Cyclone Number, Duration, and Intensity in a Warming Environment. *Science*, *309*(5742), 1844–1846. https://doi.org/10.1126/science.1116448

Weisberg, R. H., & Zheng, L. (2006). Hurricane storm surge simulations for Tampa Bay. *Estuaries and Coasts*, *29*(6), 899–913. https://doi.org/10.1007/BF02798649

Wikipedia contributors. (2023a). Mobile Bay. *Wikipedia*. https://en.wikipedia.org/wiki/Mobile_Bay

Wikipedia contributors. (2023b). Sporobolus alterniflorus. *Wikipedia*. https://en.wikipedia.org/wiki/Sporobolus_alterniflorus#/media/File:Spartina_alterniflora.jpg

Wikipedia contributors. (2023c). Tropical cyclone. *Wikipedia*. https://en.wikipedia.org/wiki/Tropical_cyclone

Woodruff, J. D., Irish, J. L., & Camargo, S. J. (2013). Coastal flooding by tropical cyclones and sea-level rise. *Nature*, *504*(7478), 44–52. https://doi.org/10.1038/nature12855

Xia, M., Craig, P. M., Wallen, C. M., STODDARD, A., MANDRUP-POULSEN, J., Peng, M., SCHAEFFER, B., & Liu, Z. (2011). Numerical Simulation of Salinity and Dissolved Oxygen at Perdido Bay and Adjacent Coastal Ocean. *Journal of Coastal Research*, *27*(1), 73. https://doi.org/10.2112/JCOASTRES-D-09-00044.1

Ysebaert, T., Yang, S.-L., Zhang, L., He, Q., Bouma, T. J., & Herman, P. M. J. (2011). Wave Attenuation by Two Contrasting Ecosystem Engineering Salt Marsh Macrophytes in the Intertidal Pioneer Zone. *Wetlands*, *31*(6), 1043–1054. https://doi.org/10.1007/s13157-011-0240-1

Zhang, X., Lin, P., Gong, Z., Li, B., & Chen, X. (2020). Wave Attenuation by Spartina alterniflora under Macro-Tidal and Storm Surge Conditions. *Wetlands*, *40*(6), 2151–2162. https://doi.org/10.1007/s13157-020-01346-w

Zhao, Y., Peng, Z., He, Q., & Ma, Y. (2023). Wave attenuation over combined salt marsh vegetation. *Ocean Engineering*, *267*, 113234. https://doi.org/10.1016/j.oceaneng.2022.113234

Zhong, L., Li, M., & Zhang, D.-L. (2010). How do uncertainties in hurricane model forecasts affect storm surge predictions in a semi-enclosed bay? *Estuarine, Coastal and Shelf Science*, *90*(2), 61–72. https://doi.org/10.1016/j.ecss.2010.07.001

Zou, R., Bai, S., & Parker, A. (2008). Hydrodynamic and Eutrophication Modeling for a Tidal Marsh Impacted Estuarine System Using EFDC. *Estuarine and Coastal Modeling (2007)*, 561–589. https://doi.org/10.1061/40990(324)31